Development of New Materials for Solar Cells Application

The University Of Sheffield.

Solyamn Al faifi

A thesis submitted to
The University of Sheffield
as partial fulfilment for the degree of Doctor of Philosophy

Department of Chemistry
May 2015

Dedication

I dedicate this thesis to the loving memory of my father and brother, whose words of encouragement and push for tenacity ring in my ears and for instilling the importance of hard work and higher education.

This dissertation is lovingly dedicated with a special feeling of gratitude to my loving mother for her support, encouragement, and constant love which have sustained me throughout my life.

To my dear wife, a very special thank you for your practical and emotional support as I added the roles of wife and then mother.

I also dedicate this dissertation to my brothers and sisters who have supported me throughout my study.

Declaration

This thesis is submitted for the degree of doctorate of philosophy (PhD) at the University of Sheffield, having been submitted for no other degree. It records the research carried out at the University of Sheffield from February 2010 to October . It is entirely my original work, unless where referenced.

Signed .....

Date .....

Abstract

Conjugated polymers have attracted much attention and academic research as a result of their potential use in the area of organic photovoltaic. In this project, series of copolymers have been synthesised successfully via Suzuki cross-coupling. Furthermore, these copolymers are designed taking in account some parameters that effect the opto-electronic properties of polymers.This project reports the synthesis of three low band gap copolymers **(P1), (P2)** and **(P3)** which have similar chemical structure to PCDTBT. In **(P2)**, the carbazole repeat units have been substituted with fluoride group in the positions 3 and 6 . Also, the carbazole repeat units have been replaced with fluorene in **(P3)**. The results indicate that **P3** has the lowest band gap energy compared to the carbazole analogous polymers . **P3** provided a power conversion efficiency of 5.41 % and 4.22 % for **P1**. The effective conjugation length also has been investigated in this project through design and prepare **(P4)** , **(P5)** which have two extra unsubstituted thiophene rings attached to the ends of the 4,7-dithien-2-yl-2,1,3-benzothiadiazole **(DTBT-8)**. The results shows that **P4** achieved 4.12 % when blended with PCBM in a bulk heterojunction solar cell device.

This thesis also covers the synthesis of a series of low band gap 2,6- and 2,7-based anthracene copolymers **(P6)** , **(P7)**. The results indicate that the 2,6-anthracene based copolymer has a lower band gap 4.17 % compared to the 2,7-anthacene copolymer as a result of its symmetrical structure of **P6** .

A block copolymer **(P8)** using blocks of **(P1)** and **(P3)** is also reported in this project**.** The physical and electrochemical properties of this block copolymer indicate good electronic properties. In addition , this project focuses on attempts to prepare poly-(3-hexylthiophene) (P3HT) **(P9)** with high yield of H/Br end groups to be used as an electron donor with different series of polymers .

Acknowledgements

First of all , I would like to express the deepest appreciation to my supervisor Dr. Ahmed Iraqi, for his guidance, support and advice during my PhD. Also, I would like to thank all members of Iraqi group in the past and present for their invaluable help and all members of the F-floor.

I would like to thank Professor David Lidzey and the Lidzey group from the department of Physics and Astronomy at The University of Sheffield for studing photovoltaic properties of the polymers.

I would like to thank Rob Hanson, Simon Thorpe, Sue Bradshow, Mel Hannah for their help with various measurements. In addition, I would like to thank Nick Smith and Peter Farran in the chemistry store and everyone in the department of Chemistry who has helped me.

Last but not least I would like to thank the Royal Embassy of Saudi Arabian, Culture Bureau in London for their services and help, and King Abdulaziz University for their financial support.

List of Publication

1- Yi, H.; Al-Faifi, S.; Iraqi, A.; Watters, D. C.; Kingsley, J.; Lidzey, D. G. *Journal of Materials Chemistry* **2011**, *21*, 13649.

2- Almeataq, M. S.; Yi, H.; Al-Faifi, S.; Alghamdi, A. A. B.; Iraqi, A.; Scarratt, N. W.; Wang, T.; Lidzey, D. G. **2013**.

3- Alghamdi, A. A. B.; Watters, D. C.; Yi, H.; Al-Faifi, S.; Almeataq, M. S.; Coles, D.; Kingsley, J.; Lidzey, D. G.; Iraqi, A. *Journal of Materials Chemistry A* **2013**, *1*, 5165.

Table of Contents

Table of Figures

Table of Schemes

Table of Tables

Glossary of Abbreviations and Terms

A

Acetone-d_6 : Deuterated acetone

AFM : Atomic force microscopy

B

bs : Broad singlet (NMR)

^{t}BuLi : *Tertiery*-butyllithium

BHJ : Bulk heterojunction organic solar cells

C

$CDCl_3$-d_1 : Deuterated Chloroform

$CHCl_3$: Chloroform

CV : Cyclic voltammetry

CB : Conduction band

D

d : Doublet (NMR)

dd : Double doublet (NMR)

DCM : Dichloromethane

DMF : *N*,*N*-dimethylformamide

dppf : 1,1'-Bis(diphenylphosphino)-ferrocene

E

E_g : Band gap

E_g^{opt} : Obtical band gap

E_g^{elc} : Electrochemical band gap

E_{Bla} : Bond Length alternation.

E_{Sub} : Substituent Effects

E_{Res} : Aromatic resonance energy

E_{Int} : The intermolecular Interactions

E_θ : The planarity

EtOAc : Ethyl Acetate

F

FETs : Field-effect transistors

FT-IR : Fourier Transform Infra-Red spectroscopy

FF : Fill factor

G

GPC : Gel Permeation Chromatography

H

HOMO : Highest Occupied Molecular Orbital

HPLC : High Performance Liquid chromatography

I

IR : Infrared spectroscopy

ITO : Indium Tin Oxide

J

J_{SC} : short circuit current

K

KOAc : Potassium acetate

L

LED : Light Emitting Diode

LUMO : Lowest Unoccupied Molecular Orbital

λ : Wavelength/ nm

M

m : Multiplet (NMR)

M_n : Number average molecular weight

M.p. : Melting point

M_w : Weight average molecular weight

M_w/M_n : Polydispersity

MO : Molecular orbital theory

MDMO-PPV :Poly[2-methoxy-5-(3′,7′-dimethyloctyloxy)-1,4-phenylene vinylene]

N

NBS : *N*-Bromosuccinide

NEt_4OH : Tetra ethylammonium hydroxide

NMR : Nuclear Magnetic Resonance

P

PA : Polyacetylene

PAn : Poly(aniline)

PCBM or C60 : 1-(3(Methoxy carbonyl) propyl-1-phenyl [6,6]-methono-fullerene

Pd : Polydispersity: Pd = M_w/M_n

$Pd(dppf)Cl_2$: [1,1'-Bis(diphenylphosphino) ferrocene] dichloro-palladium (II)

$Pd(OAc)_2$: Palladium(II) acetate

$Pd(PPh_3)_4$: Palladium-tetrakis(triphenylphospine)

PF : Poly(fluorene)

$PhB(OH)_2$: Phenylboronic acid

PhBr : Bromobenzene

P3HT : Poly(3-hexylthiophene)

PPh_3 : Tri-*para*-tolylphospine

PPP : Poly(*para*-phenylene)

PPV : Poly(*para*-phenylenevinylene)

PPy : Polypyrrole

PT : Poly(thiophene)

PV : Photovoltaic

PVK : Poly(*N*-vinylcarbazole)

P_{out} : Output power

P_{in} : Input power

R

R_f : Release factor

S

s : Singlet (NMR)

T

t : Triplet (NMR)

TFA : Trifluoroacetic acid

TFAA : Trifluoroacetic anhydrate

TGA : Thermo-gravimetric analysis

THF : Tetrahydrofuran

TLC : Thin layer chromatography

TMS : Tetramethylsilane

TEM : Transmission electron microscopy

U

UV-vis : Ultra Violet-visible spectroscopy

V

VB : Valence bond theory

V_{OC} : Open circuit voltage

Chapter 1: Introduction

1.1 Motivation

The identification of sustainable, low-cost and environmentally friendly energy sources is of paramount importance. Fossil fuel resources (oil, coal and gas) are finite, and at some point they will not be sufficient to meet the global demand for energy, which is ever increasing. Furthermore, these classic energy sources have a harmful effect upon the natural ecological balance of the earth. Carbon dioxide, which is the final product of burning fossil fuels, is known to cause air pollution and climate problems. According to Prof. John Smol from the Canadian Centre for Environmental Change, in 2011 the carbon dioxide emissions resulting from world energy consumption reached 31.8 billion tonnes [1]. Such a huge amount of carbon dioxide cannot be absorbed by plants. Thus it remains in the atmosphere, where it has reached high levels, leading to global warming. This causes climate change, which leads to changes in the weather and thus natural disasters, such as tornados, and an increase in sea levels [2]. Climate change is widely expected to have a destructive effect on humans and organisms on the earth in the future. Thus, a great deal of effort has been put into finding and developing alternative energy sources that are economically viable and environmentally friendly. Solar energy is a promising contender and the most ideal alternative source since it is reliable, cheap, invariable and environmentally friendly [3]. In 1954, Chapin and colleagues of Bell Laboratories discovered that it was possible to generate electricity from sunlight using photovoltaic cells [4]. Monocrystalline silicon based solar cells with an efficiency of 6 % were reported [4]. Later, these cells exceeded 24 % of energy conversion [5]. Since then, the search for materials with a high conversion efficiency that are cheaper than silicon has been a priority. Such organic

materials are cheap, flexible and light weight [6]. Organic photovoltaic solar cells with an efficiency of almost 10% have been reported [7]. However, the development of these cells is still in the early stages, and they are not yet ready to compete commercially with silicon cells.

1.1.1 Conjugated Polymers

Since the creation of polyacetylene in 1970 by Hideki Shirakawa, much attention has been paid to conjugated polymers in an attempt to reach a better understanding of this promising branch of polymer science [8]. Conjugated polymers have a unique structure that differs from non-conjugated polymers; therefore, their applications are different, as illustrated in Figure **1**. Non - conjugated polymers are currently widely used in the electronics industry as heat insulating materials to coat electrical wires and the casings of electrical equipment.

A B

Figure 1: Conjugated polymers (A), non - conjugated polymers (B)

By contrast, conjugated polymers have electrical properties which resemble those of semiconductors metals. These polymers have a special structure which consists of alternating single and double bonds between carbon-carbon atoms [9]. In addition to the carbon atoms, this system contains other atoms, such as nitrogen, sulphur or oxygen, alternating with carbon double bonds as shown in Figure 2.

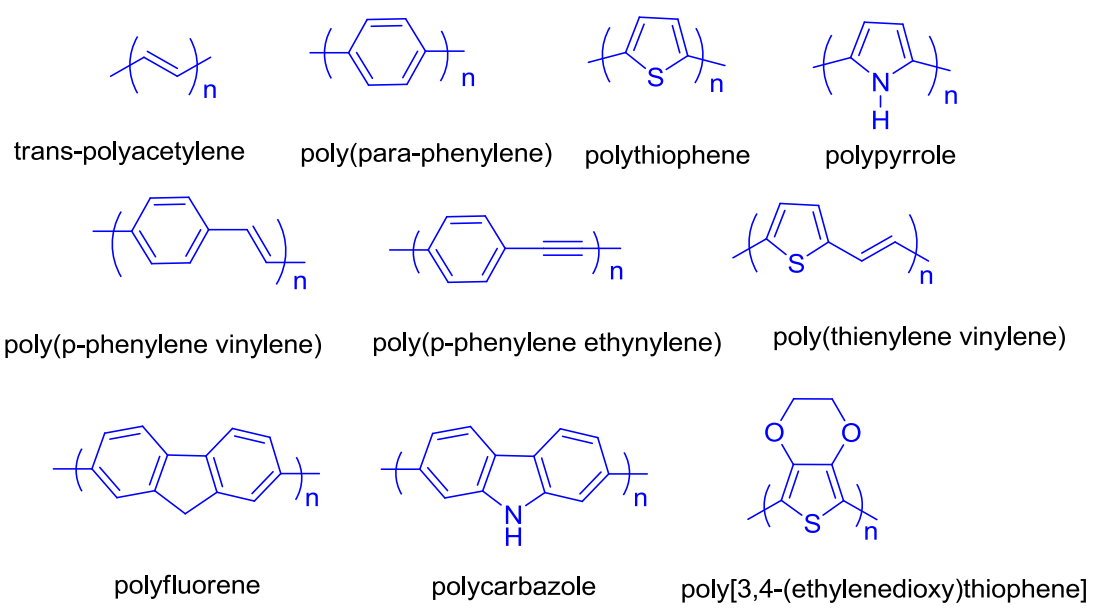

Figure 2: Chemical structure of some conjugated polymers [10]

Although conjugated polymers have been known about for a long time, their unique properties were not identified until the end of the seventies [8]. In 1977, Heeger, MacDiarmid and Shirakawa synthesized and doped polyacetylene by reaction with Br_2 or I_2 vapours. This doped polymer exhibited a conductivity of about 10^3 S cm^{-1} [11]. Despite the high electrical conductivity of doped PA, it exhibits undesirable properties, such as poor solubility and low thermal and environmental stability [10]. All the previously undesirable properties directly affected conductivity, which led to it having limited applications. This resulted in efforts being made to discover many aromatic conjugated polymers with conducting properties comparable to those of PA in Figure 2.

1.1.2 Chemistry of Conjugated Polymers

Conjugated polymers have a fundamental structural property that distinguishes them from classical polymers. This property gives these polymers a conductivity comparable to semiconducting materials [11]. The π- system in conjugated polymers displays physical and chemical properties that do not exist in the traditional polymers.

1.1.3 Bonding in Conjugated Polymers

The alternation of single and double carbon-carbon bonds in conjugated polymers are responsible for the unique characteristics of these polymers, such as electronic and optical properties. Several theories have been put forward to account for bonding in organic molecules. One of the most important basic theories is valence bond theory (VB), which is based upon quantum mechanics [9b]. In this theory, the concept of hybridization is used to understand and explain the bonding and structure of molecules. This approach describes the formation of a bond based upon the mixing of atomic orbitals to create new hybrid orbitals [12]. This approach can also be applied to conjugated systems with alternating single and double bonds. The prototype example of these conjugated systems is polyacetylene, which is the simplest conjugated polymer [8]. Polyacetylene is chemically synthesized by breaking one of the $\boldsymbol{\pi}$ bonds of acetylene to form a bond with a new carbon [13], so as to form a long chain of conjugated polyacetylene as shown in Figure 3 [14].

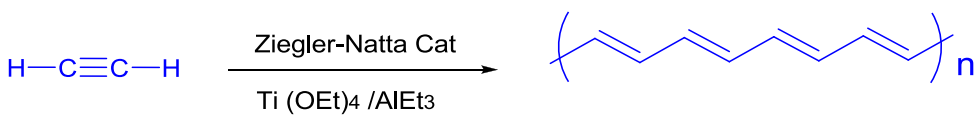

Figure 3: Synthesis of polyacetylene

Polyacetylene is formed of a chain of sp^2 hybridized carbon atoms bonded by alternating single and double bonds. Another theory to describe the bonding in conjugated polymers is molecular orbital theory (MO). In this theory the combination of p_z atomic orbital in each carbon atom forms two molecular orbitals, one a low-energy π bonding orbital (occupied orbital) and the other one is a high-energy π^* anti-bonding orbital (unoccupied orbital),

.

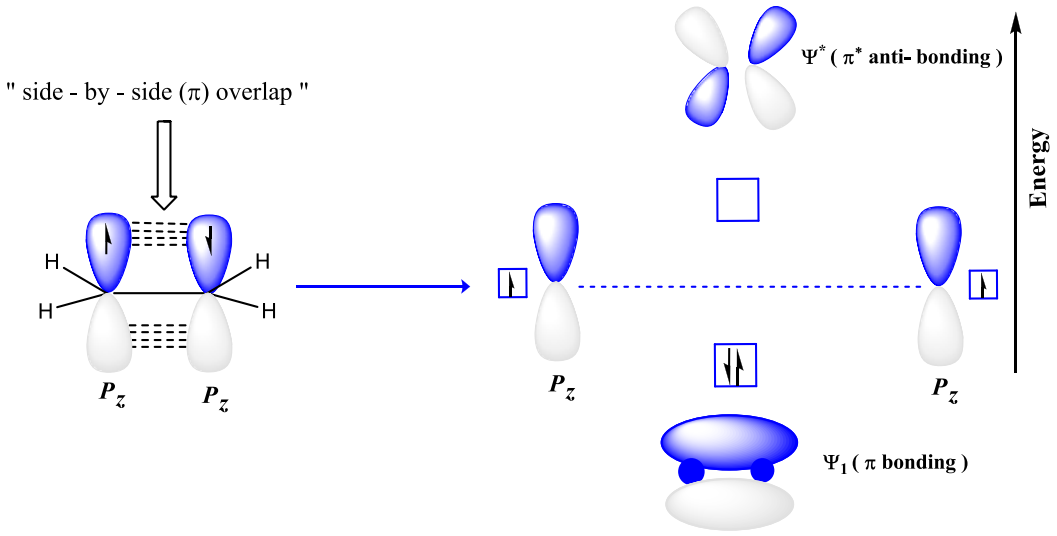

Figure 4: Formation of π bond by overlap the pz atomic orbitals in ethylene.

In molecular orbital theory, the occupied π orbital refers to the highest occupied molecular orbital (HOMO) and the unoccupied π^* orbital refers to the lowest unoccupied molecular orbital (LUMO). In conjugated polymers, the double bonds are delocalised along the entire molecule, which means that the number of molecular orbitals increases

forming energy bands. Meanwhile, the energy difference between the between the HOMO levels and LUMO levels decreases as conjugation increases. The existence of an infinite number of atoms will form an infinite number of molecular orbitals very close together, and these molecular orbitals merge with each other to form bands rather than discrete energy levels as indicated in Figure 5.

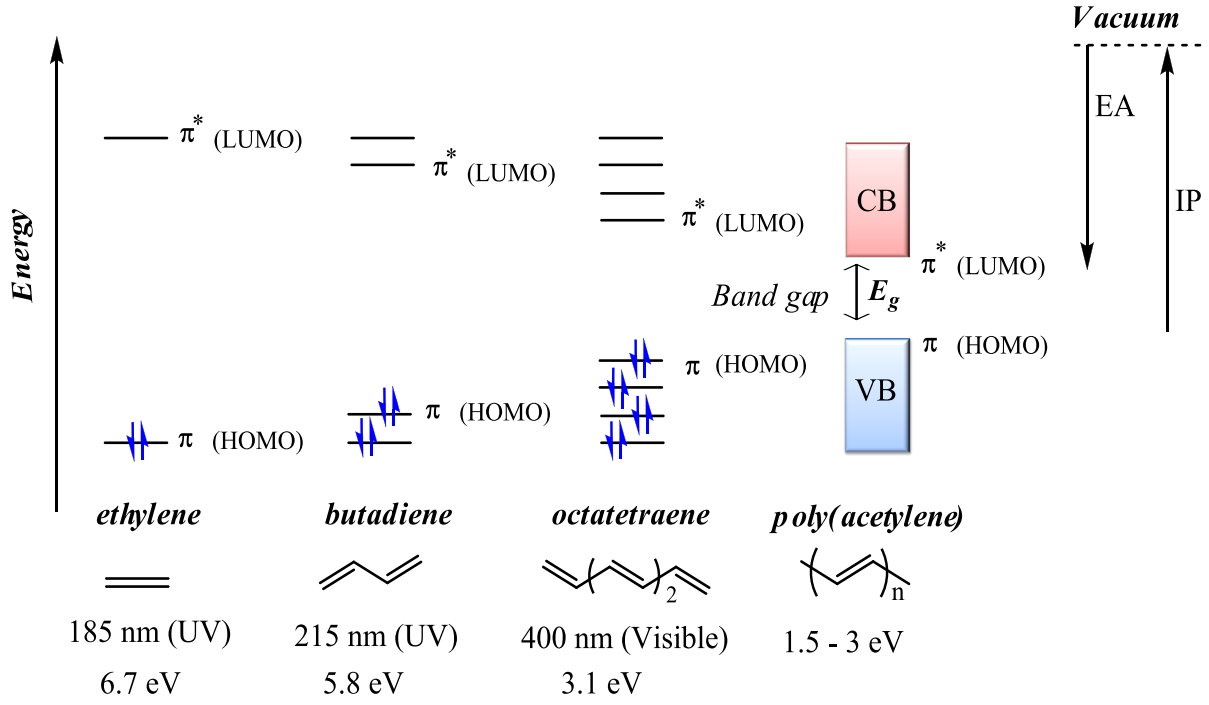

Figure 5: Evolution of the molecular orbital theory to describe the bonding in a conjugated system (Adapted from ref [10] , License Number : 3585501362005)

1.1.3.1 Electronic Structure of Conjugated Polymers

A common feature of all conjugated polymers is that they have a delocalized ***π*** system that spreads over the polymer backbone [15]. In polyacetylene, each carbon atom has an atomic orbital p_z that overlaps with the p_z of the adjacent atoms to form an ***π*** bond that stretches along the polymer [16], Figure 6 .

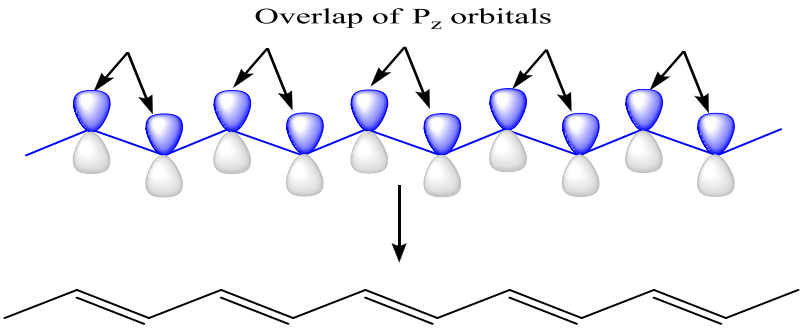

Figure 6: Overlapping of Pz orbitals to form polyacetylene .

In an ideal conjugated structure, one would expect electronic delocalisation along the whole polymer backbone with no bond length alternation. From this point of view, all of the p_z orbitals in the $\boldsymbol{\pi}$ system of the polymer chain tend to be entirely overlapping. Therefore, the polymer would behave as a one – dimensional system, where the energy gap between the valence band (HOMO) and the conduction band (LUMO) would be zero , Figure 7 [17] .

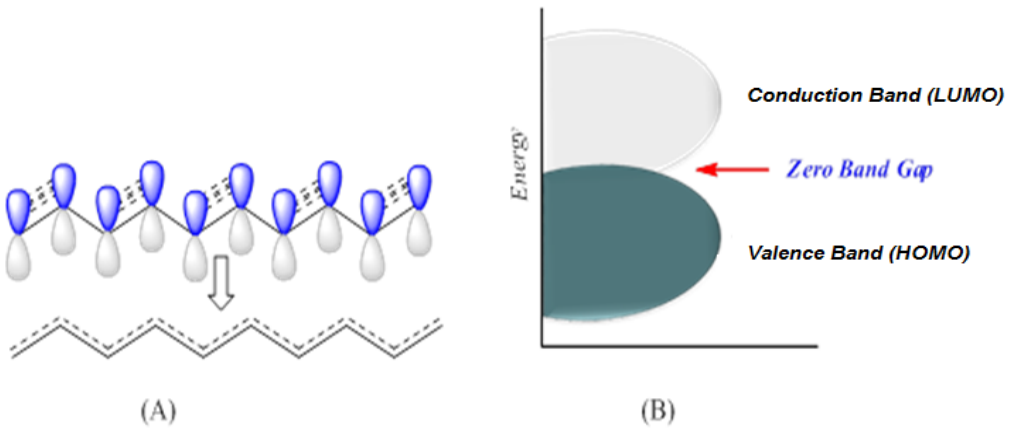

Figure 7:Hypothetical polyacetylene (A), behaviour of polyacetylene as a one – dimensional metal (B).

In reality, conjugated polymers do not behave as a one – dimensional system, as metals do. The conductivity of polyacetylene is between 7 x 10^{-10} and 7 x 10^{-3} Sm^{-1} compared to copper, which has a conductivity of over 10^{5} Sm^{-1} [17a-d],figure 8.

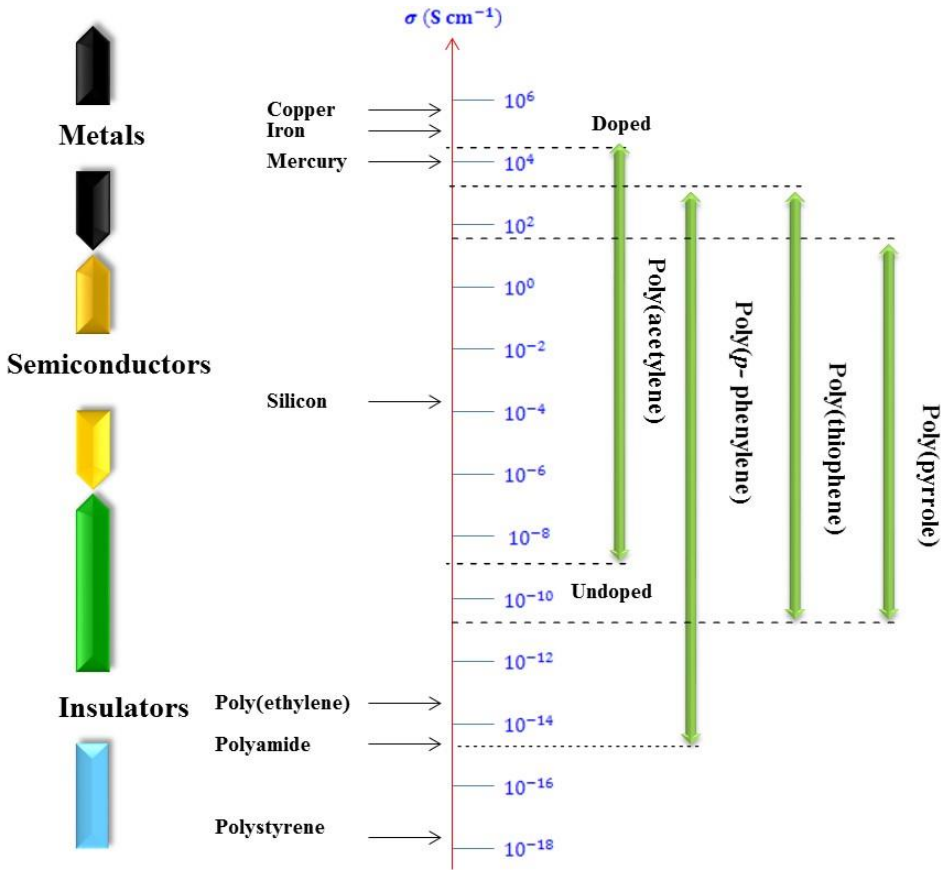

Figure 8: The conductivities of doped poly(acetylene) in comparison with other materials.

This means that the structure of conjugated polymers does not render them able to behave as one -dimensional metals. In addition, in order to exhibit the metallic behaviour of polyacetylene, all the carbon bonds must be of equal length [18]. In this case, the double

bonds are delocalized along the polymer chain, as is depicted in the left hand side of Figure 7 - A [18b]. However, this cannot be applied in the case of conjugated polymers, which are known as semiconductors in their undoped state [18a].

Consequently, an approach has been adopted to elucidate this behaviour and understand the electronic structure of conjugated polymers. Due to the difference in the length of single and double bonds, the electron delocalisation would be broken along the polymer chain [18b]. As a result, the energy of the HOMO and the LUMO is affected, leading to a band gap developing between these levels as shown in - C [9b].

Therefore, polyacetylene cannot be correctly treated as a one dimensional metal. Peierls explains the structural deformation of polyacetylene, stating that a one dimensional metal or any similar system having equivalent bonds would be generally unstable [8]. Therefore, a polyacetylene chain tends to lower its energy in two ways: either the bonds in the adjacent atoms are alternately elongated and shortened, with the single bonds being slightly longer than the double bonds, or the chain is twisted while the length of the bonds remains the same , figure 9 A - B [17e,19].

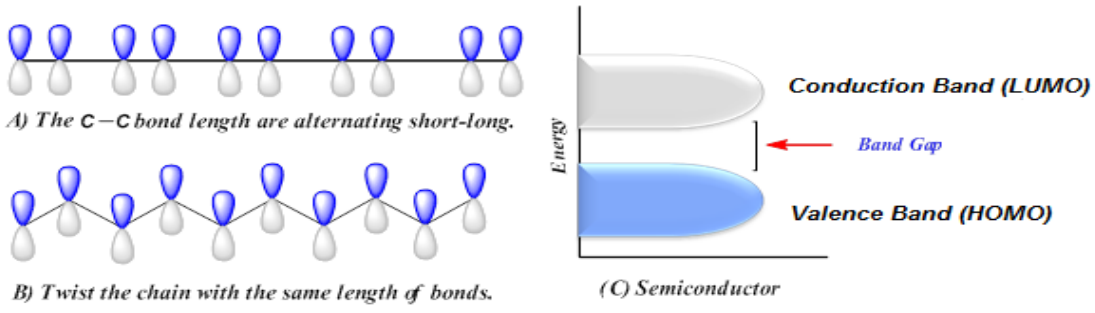

Figure 9: Peierls distortion in Polyacetylene (A) and (B), the structure of the band gap (C).

1.1.3.2 Band Theory and Conductivity of Conjugated Polymers

Molecular orbital theory describes how atoms in a conjugated system interact in order to form an infinite number of bonding and anti-bonding molecular orbitals. These molecular orbitals merge with each other to appear as bands. These bands are known as the valence band (VB) and the conduction band (CB), and they are referred to as the HOMO and the LUMO, respectively [10]. The electrical properties in materials are attributed to these bands. Band theory describes the electrical behaviour of conductors, insulators and semiconductors [17e]. The energy difference between these bands is called the energy gap; the size of this gap and whether the band is filled or not determines whether the material is a conductor, a semiconductor or an insulator [10] as depicted in Figure 10

.

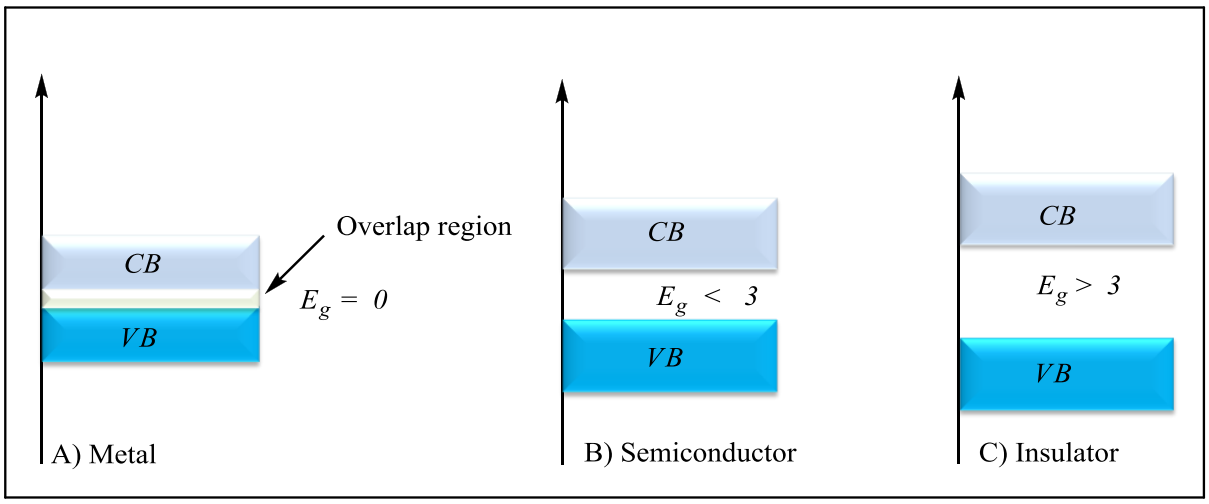

Figure 10: Band theory diagram showing the difference between A) Metals B) Semiconductors and C) Insulators.

In conductors such as copper, silver and aluminium, the VB is partially filled and the conducting band is empty. In addition, there is considerable overlap between these bands

and therefore a zero energy gap. The electrons in the VB are fully able to move between these bands under thermal excitation without more energy consumption [20].

In semiconductors, the lower band (VB) is completely filled and there is no degree of overlap between the bands and indeed a small distance separates them. Hence, there is a small energy gap between them, and the electrons in the lower band (VB) need energy to bridge the gap to the higher band (CB) [20].

In insulators, the lower band (VB) is completely filled and there is a large degree of separation between the bands. So the band gap is larger than 3 eV, and the electrons in VB are not promoted to the higher band. Therefore, these materials do not conduct electricity [20]. Owing to the $\boldsymbol{\pi}$ system in conjugated polymers, they have unique electrical and optical properties. Polyacetylene is the classic example of a conducting polymer and represents the first generation of semiconductor polymers. It is found in two forms, known as trans-polyacetylene and cis-polyacetylene [14] . The cisorm is less stable and can be thermally transformed to the trans form [9a]. The conductivity of undoped polyacetylene is 1.7×10^{-9} S cm^{-1} for the cis form with a band gap of 2 eV and 4.4×10^{-5} S cm^{-1} for the trans form with a band gap of 1.8 eV [21].

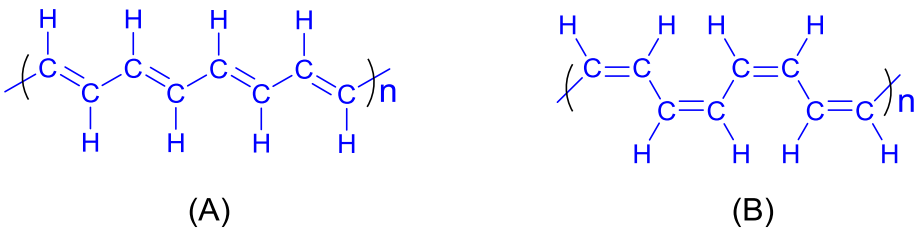

Figure 11: Trans – polyacetylene (A), cis – polyacetylene (B) [14].

In their natural state, conjugated polymers are extrinsic semiconductors with a finite band gap. The conductivity of an undoped conjugated systems is between 10^{-3} S cm^{-1} and

10^{-10} S cm^{-1} with a band gap between 0.8 and 4 eV [10,20]. Therefore, conjugated polymers are considered to possess electrical properties between semiconductors and insulators [20]. The low values of electrical conductivity in the first generation of conducting polymers is attributed to morphological and structural disorder in the polymer chains [20]. These factors reduce the charge carrier mobility along the polymer chains and thereby minimize the conductivity [22].

Several studies have been done over the past few decades to improve the mobility and conductivity in conjugated polymers. The Hall mobility of polyacetylene was measured in 1978 by Seeger, who found it to be 2×10^{-2} cm^{-2} / Vs with conductivity of 1080 S/cm upon doping with 17% AsF_5 [23]. This low value of mobility stems from the fibril structure of polyacetylene [24]. In 1993, Reichenbach estimated the mobility of neutral polyacetylene to be 1.3 cm^{-2} / Vs, and this value was somewhat compatible with the value of $1 - 10$ cm^{-2} / Vs predicted by Jeyadev and Conwell [25]. The conductivity associated with this value reached 10^3 S/ cm using a doping level of 6×10^{-2} per CH unit [24]. Later, Naarmann found that mobility and conductivity are directly proportional to one another using highly oriented polyacetylene doped with iodine, and these values were 10^3 cm^2/Vs and 1.5^5 S/cm, respectively [24]. The variation in mobility values for doped and undoped polyacetylene can be attributed to the effect of doping on the conformations and structural disorder in the polymer chains [24]. The polymer chains in the undoped polyacetylene suffer from structural disorders, such as flexibility and twisting, leading to electron localization over some units and reduce the effective conjugated for π- electrons, as shown in Figure12 - A [24].

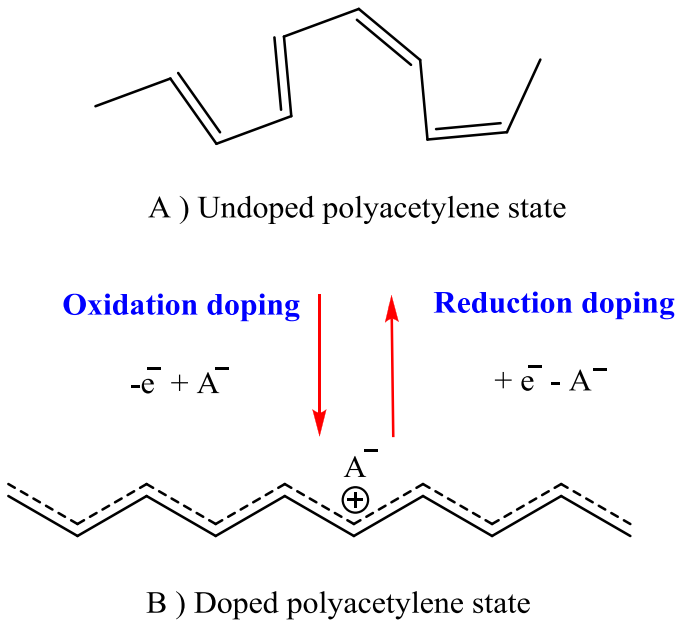

Figure 12: Structural change of the polyacetylene chain in undoped state (reduced form) and doped state (oxidized form) using oxidation and reduction doping process [24] .

By contrast, in the oxidized form or doped state shown in Figure 12 – B, the polymer chain is straightened to be more orderly and planar as a result of the presence of delocalized and extended π- electrons along the polymer chain [24]. This extension in the polymer structure eventually leads to an increase in the charge carrier mobility.

1.1.4 Doping

The conjugated polymers do not possess effective intrinsic charge carriers and therefore do not conduct electricity. Creating charge carriers in the electronic structure of the polymer requires the introduction of agents that have the ability to meet this requirement [20,22]. This process is called doping, and it is found to be an effective way to increase the conductivity of semi conductor materials [26].

Doping in conjugated polymers was first accomplished in 1977 by Shirakawa [8]. He found that the conductivity of polyacetylene can be altered and increased using doping by 9 to 13

orders of magnitude [26]. He converted polyacetylene into a polymeric conductor through direct exposure to bromine or iodine vapours [8]. The nature of the doping process is mainly based on a charge transfer redox reaction [10]. This chemical doping involves an oxidation process (*P*-type doping) or a reduction process (*N*-type doping). The neutral polymer chains can be converted into a poly(cation) or poly(anion) using (*P*-type doping) or (*N*-type doping), respectively [10]. These processes are carried out with the simultaneous insertion of counter ions to neutralize the polymer chains, figure 13 [8].

*** (*P*-type doping) – Oxidation process** :

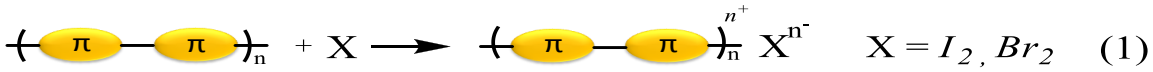

*** (*N*-type doping) – Reduction process**:

Figure 13: The doping processes in conjugated polymers.

The doping process used to dope conjugated polymers depends on the type of atoms involved in the formation of a polymer chain [8]. Conjugated polymers which do not have strong basic centres, such as poly(acetylene), poly(*p*-phenylene), polyheterocyclic systems and their derivatives, can be doped under the redox doping process [8].Conversely, conjugated polymers which have strong basic centres are subject to both the redox process and acid – based doping [8].

1.1.5 Low Band Gap Polymers

In the early nineties, research into conducting polymers and their applications led to remarkable developments, such as field effect transistors (FETs) and light emitting diodes (LEDs) as well as organic photovoltaics (OPVs) [27]. These promising applications can be ascribed to the optical and electronic properties of these polymers due to the presence of a π conjugated system. This π system creates a band gap between the valance band and conduction band, which gives these materials their electronic and optical properties.

The band gap (Eg) of conjugated polymers can be defined in two ways:

The optical band gap (E_g^{opt}), which can be calculated from (UV) spectroscopy[7]. Electrochemical band gap (E_g^{el}) which is the difference between the HOMO and the LUMO levels and can be determined by cyclic voltammetry (CV), as determined from their onsets of oxidation and reduction respectively as depicted in figure 14[28]. Normally, the (E_g^{el}) is larger than (E_g^{opt}) about 0.3 – 0.6 eV, this variation can be attributed to the exciton binding energy of conjugated polymers which is believed to be in the range of ~0.4-1.0 eV[29].

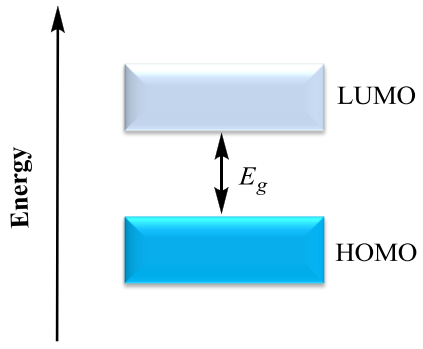

Figure 14: Definition of band gap (Eg).

Generally, low band gap polymers are defined as materials that absorb light at wavelengths that are longer than 620 nm in the electromagnetic spectrum with a band gap below 2 eV. All organic semiconductors are restricted to absorbing specific regions of the solar spectrum. Extending their absorbance to the near IR region is a decisive factor that requires materials with low band gaps and leads to attaining effective overlap between the solar spectrum and the absorption spectra of the polymers [7]. Such an overlap leads to more efficient photon harvesting and improved efficiency [30].

When sun irradiance and photon flux are plotted as a function of the wavelength, the maximum of photon flux is shifted in the direction of the IR wavelength , Figure 15. From this point of view, efficient photon harvesting requires materials that absorb light at higher wavelengths.

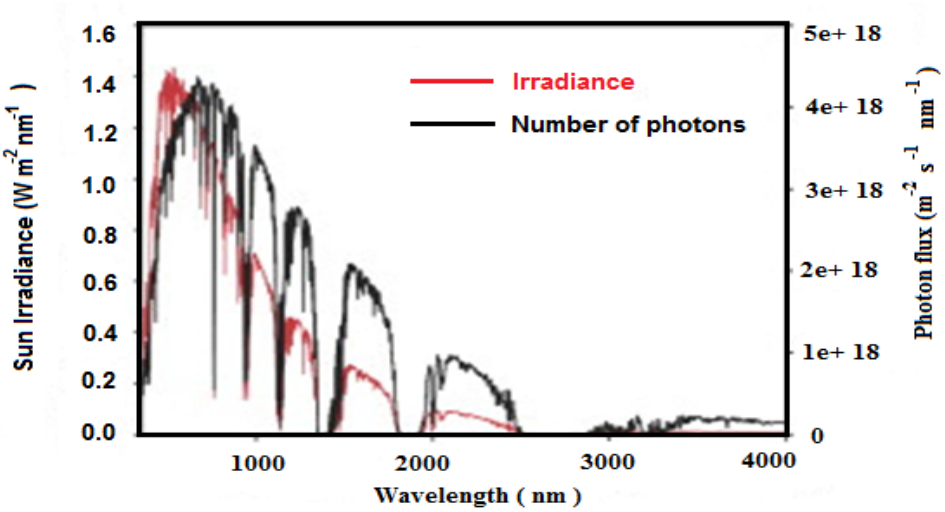

Figure 15: Sun irradiance (red) and photon flux (black) as a function of wavelength .

1.1.6 Designing and Controlling the Band Gap in Conjugated Polymers

The control of energy levels (HOMO) and (LUMO) and the band gap of conjugated polymers is one of the most important parameters for high PCE [31]. They have been studied in recent decades since they are crucial in terms of attaining good electronic and optical properties [32]. Both experimental and theoretical studies on tuning the band gap of conjugated polymers indicate that several factors have a significant effect on the band gap as illustrated in Figure 16 [32-33].These parameters have an energetic effect on the magnitude of the band gap; therefore, the band gap can be expressed by the sum of these contributions [27] :

$$E_g = E_{Bla} + E_{Sub} + E_{Res} + E_{Int} + E_{\theta} \quad \ldots$$

Where these factors can be defined as follow:

E_{Bla} = Bond Length alternation.

E_{Sub} = Substituent Effects.

E_{Res} = Aromatic resonance energy.

E_{Int} = The intermolecular Interactions .

E_{θ} = The planarity.

When designing and synthesising polymers with low band gaps, these factors should be taken into account to reduce their energetic contributions in the band gap equation [32] .

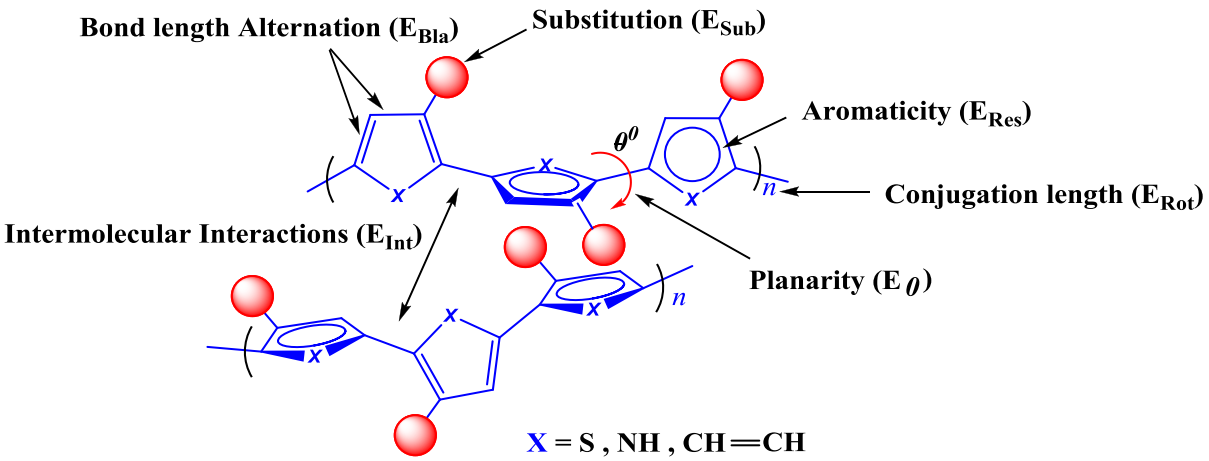

Figure 16:Contribution of structural factors determining the band gap of polymers *(Modified with permission from [31-32] License Number : 3586030549820) .*

The effect of these factors will be investigated individually in the following discussion as well as how to minimize and manipulate their impact on the design and synthesis of low band gap polymers [34].

1.1.6.1 Bond Length alternation *(E_{Bla})*

The existence of the band gap in conjugated systems is essentially a result of the alternation of single and double bonds. In a hypothetical polyacetylene, the equal length of the single and double bonds makes electrons delocalize along the polymer backbone to form a degeneracy state [18b] , Figure17. Such an ideal model would make polyacetylene a metallic conductor with a zero band gap [18b].

Figure 17: Degeneracy state of polyacetylene.

However, as has been pointed out in many theoretical and experimental studies, such a structure would be unstable as a result of alternating shorter double bonds and longer single bonds, leading to a structural deformation with a band gap ≈ 1.5 eV [18b]. Therefore, the degree of bond length alternation in linear π-conjugated systems (LCSs) has a major effect on the existence of a finite band gap [32]. Bond length alternation (BLA) can be defined as the average of the difference in length between adjacent carbon-carbon bonds in a polyene chain [35]. Moreover, this geometrical parameter represents the ratio of the aromatic to quinoid population in a polyaromatic conjugated system [35].

In polyaromatic polymers, such as poly(p-phenylene), poly(pyrrole) and poly(thiophene), they vary according to their non-degenerate ground state, where their two forms are not energetically equivalent , Figure 18 [32]

.

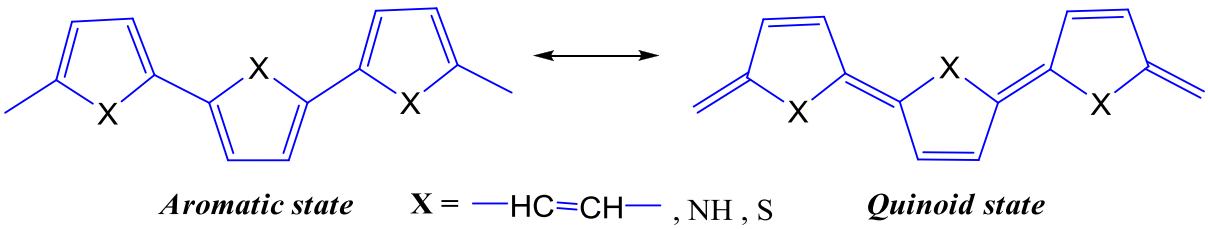

Figure 18: Two energetically inequivalent structures of non-degenerate polyaromatic system *(adopted from [32] License Number : 3586030549820).*

The bond length alternation (BLA) will become large when the aromatic form is prevalent, leading to a wide band gap [35]. The existence of such aromatic cycles linked by single bonds will lead to a departure from co-planarity as a result of the rotational disorder around these single bonds [36]. Therefore, the overlap between orbitals can be influenced by this rotation, which leads to an increase in the band gap. To overcome this issue, it has been found that the contribution of the quinoid form transforms the carbon-carbon single

bond between two adjacent rings to double bond character, which leads to a decrease in the (BLA) [35]. The quinoid form enhances the planarization between adjacent aromatic units, enriches parallel p-orbital interactions to extend conjugation and facilitates delocalization. This in turn leads to a decrease in the BLA and a reduction in the band gap. Generally, the HOMO-LUMO band gap decreases linearly as a function of the increasing quinoid character with a concomitant decreasing BLA value [35]. The aromatic state is energetically more stable and of lower energy than the quinoid state, and the quinoid form in most cases has a smaller band gap as illustrated in Figure 19 [10,32].

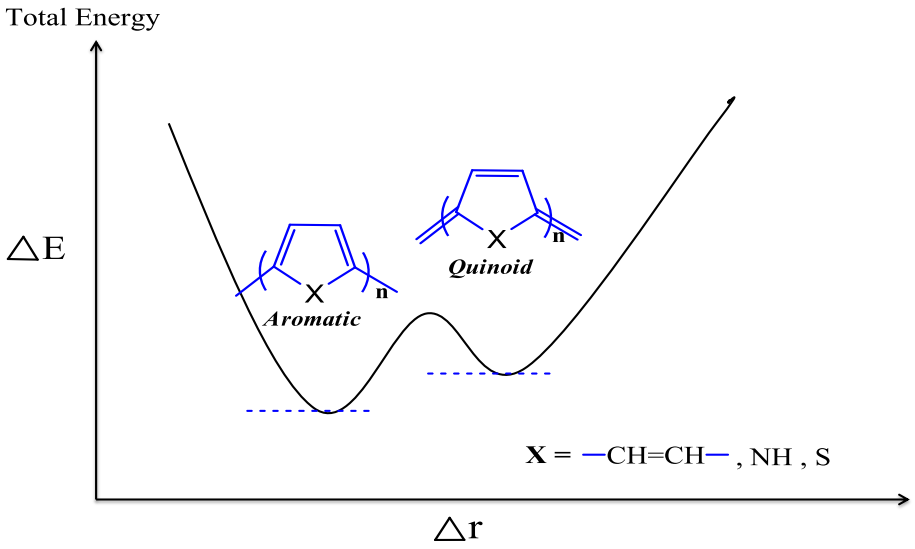

Figure 19: Potential energy as a function of bond length alternation for non-degenerate polyaromatic system (Adapted from ref [10] , License Number : 3585501362005).

1.1.6.2 Substituent Effects *(E_{Sub})*

An important approach that has been used to lower the band gap of conjugated polymers is the introduction of electron releasing or electron withdrawing groups into the donor – acceptor system [36]. This has been found to be the most immediate method of not only

reducing the band gap of polymers but also controlling the HOMO and LUMO energy levels of conjugated systems [27]. The effective interaction between the donor and acceptor enriches the double bond character among the repeat units and makes the HOMO and LUMO levels much closer , Figure 20.

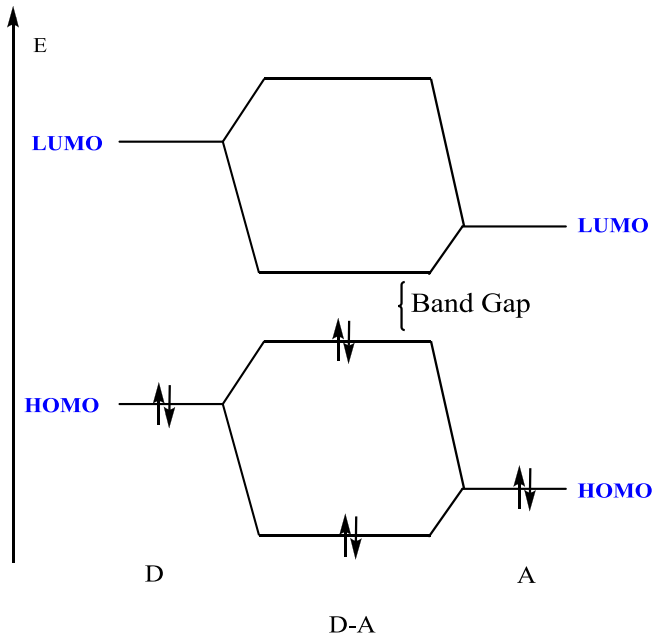

Figure 20: The interaction between the alternating donor and acceptor units .

The existence of substitution groups on the repeating units has been found to enhance the strength of the donor and acceptor units and thus reduce the band gap of polymers [36]. Electron releasing groups lead to a reduction in the band gap by increasing the HOMO level [27]. Moreover, the releasing group facilitates the solubility of the polymer and makes it easier to process.

On the other hand, electron withdrawing groups contribute to a reduction in the band gap by reducing the LUMO level [37]. In 1990, Ferraris and Lambert reported that electron withdrawing groups, such as keto or dicyano pending on poly(cyclopentabithiophene)s,

showed low band gap values of 1.20 eV for keto and 0.80 eV for dicyano groups [38], Figure 21.

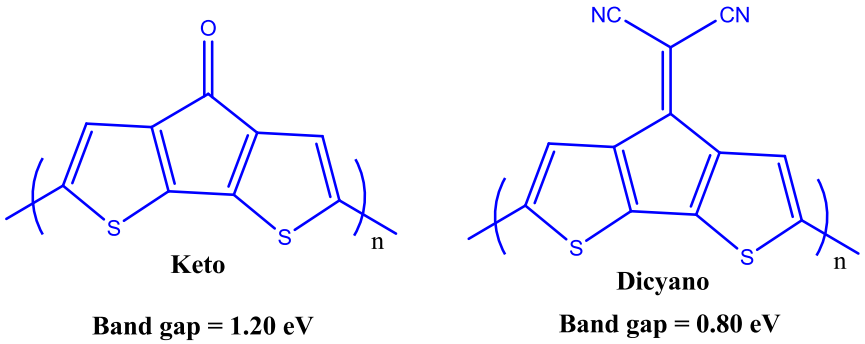

Figure 21: Electron withdrawing groups and reducing the band gap energy[27].

Theoretical studies carried out on this approach attribute these low band gap values to an increase in the quinoid character [27].

1.1.6.3 Aromatic resonance energy (E_{Res})

Aromaticity is a decisive factor in relation to enlarging the band gap in polyaromatic conjugated polymers. It has been found that the monomers containing aromatic rings in their structure usually widen the band gap of the corresponding polymers [39]. The reason for this negative contribution lies essentially in conjugation. To elucidate this behaviour, the conjugation in the polyaromatic conjugated system is affected by the competition between delocalization along the chain and π- electron confinement within the rings [39]. To surpass this issue and achieve low band gap polymers, the quinonoid character must be dominant [35]. Theoretical calculations and experimental evidences reveal the contribution of both

forms (aromatic and quinoid) in polyaromatic conjugated systems as illustrated in , Figure 22.

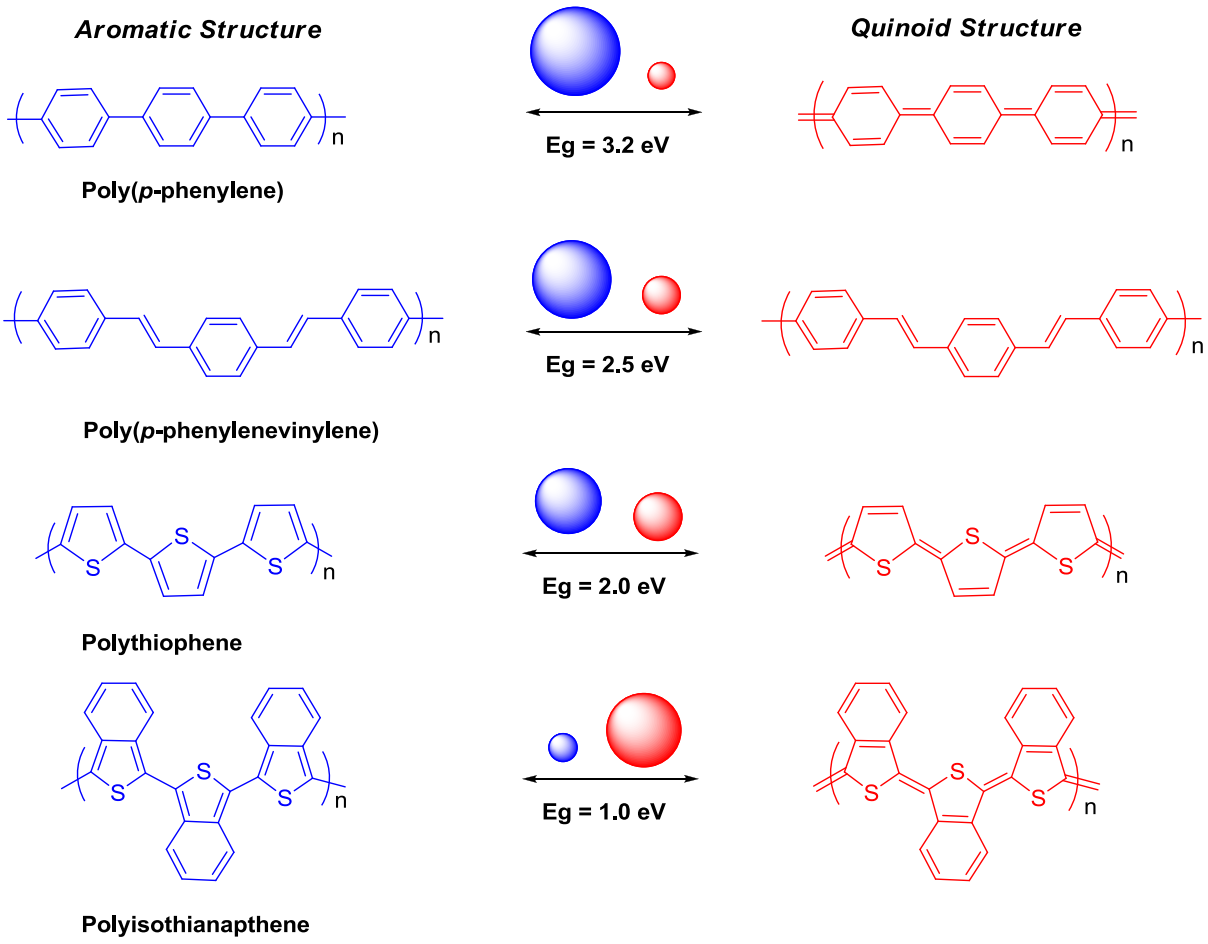

Figure 22: The contribution of aromatic and quinoid forms on the band gap for some polyaromatic conjugated systems. The large size makes the greater contribution to the band gap [35].

As illustrated in Figures 19 and 22, polyaromatic conjugated polymers have two resonance forms for the ground state with non-degenerate energy. It is apparent from Figure 22 that thiophene and benzene units in aromatic form maintain their aromaticity are still dominant with confined π- electrons [35]. One the other hand, the destruction of the aromaticity of the

aromatic units in these polymers enhances the formation of the quinoid form through π-electron delocalization [35]. As seen from Figure 22, transformation from the aromatic form to the quinoid form leads to destruction of the aromaticity and a decrease in the band gaps. The high degree of aromaticity in benzene rings gives poly(*p*-phenylene) a high band gap of 3.2 eV with the most contribution coming from the aromatic form [40]. Enhancing the quinoid form by inserting ethylenic linkages between the benzene rings reduces the aromaticity of the benzene rings, leading to a lower band gap of 2.5 eV [27]. Furthermore, polythiophene shows a reduction in the band gap to 2 eV due to its lower aromaticity [35]. In 1984, Wudl and co-workers reported an approach to increasing the quinoid character of polythiophene and reducing its band gap [41]. This approach was based on involving a fused thiophene ring with an aromatic system, such as benzene [27]. Polyisothianaphthene (PITN) represents this creative way of making the contribution of the quinoid character dominant [41]. The thiophene ring has a smaller aromatic resonance energy than the benzene ring (1.26 eV *vs* 1.56 eV), so the thiophene ring de-aromatizes to espouse a quinoid character while maintaining the benzene aromaticity , figure 23. [27,35,39,42]. This direct way makes polyisothianaphthene (PITN) an unprecedented polymer with a narrow band gap 1.0 eV [27,35,42].

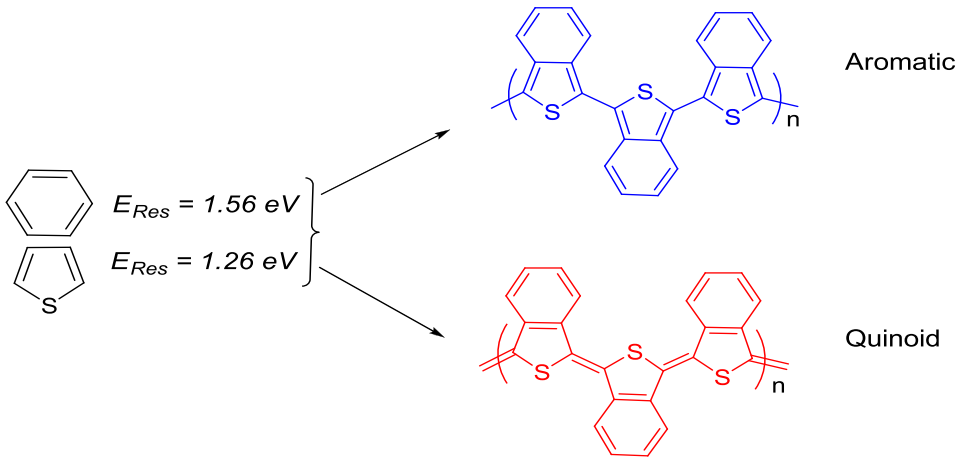

Figure 23: Dearomatization of thiophene to adoption a quinoid structure [27].

1.1.6.4 The Intermolecular Interactions (E_{Int})

The intermolecular interaction force between polymer chains is crucial in determining a polymer's properties. This force is large in the solid state, while in a solution or in amorphous polymer it is very small. In conjugated polymers, the band gap is much smaller in the solid state when compared with the solution phase [34]. This difference can be attributed to the increased interaction between the chains in a solid state [34]. Furthermore, the conjugated polymers in a solid state undergo a mesoscopically ordered phase, which has been shown to cause a considerable decrease in the band gap when compared with the disordered phase [34]. Despite the decrease in the band gap, the drawback of this force lies essentially in the absence of solubility [27]. A simple and straightforward way to enhance the solubility is to involve bulky side groups in the polymer backbone that hinder intermolecular interactions between the polymer chains , Figure 24 [27].

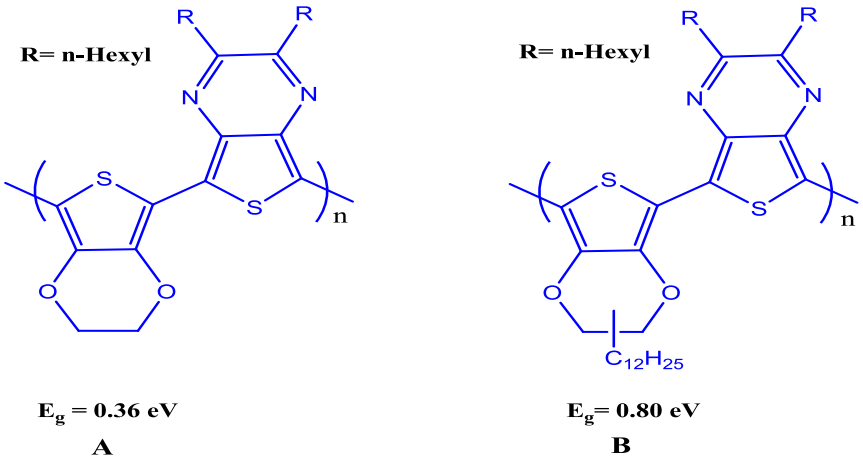

Figure 24: Effect of bulky side groups on band gap and solubility [27].

In polymer A (Figure 24), the polymer chains show a high degree of order produced by π-stacking and the folding of the polymer chains, leading to a low band gap of 0.36 eV [27].

This polymer is quite insoluble in solvents, despite the existence of two hexyl chains as a result of the intermolecular D-A interactions in the solid state [27,31]. The solubility issue is surpassed by introducing an alkyl substituent into polymer **B** (Figure 24), where the π-stacking between the neighbouring chains is suppressed [27]. However, enhancing the solubility in polymer **B** leads to an increase in the band gap of 0.80 eV, making it roughly twice as large as that of polymer **A** [27]. These obtained results provide an experimental evaluation of the contribution of intermolecular interactions to the band gap [27].

1.1.6.5 The Planarity (E_θ)

The planarity of conjugated polymers is one of the important parameters used to determine the band gap. The existence of torsion between neighbouring aromatic rings leads to the occurrence of intermolecular rotations and partially interrupts the conjugation length. Any deviation from co-planarity results in an effective increase in the bandgap (E_g). This planarity is represented by (E_θ), which is related to the torsion angle between the rings of adjacent units [33]. The existence of steric hindrance in the molecule plays a major role in the torsion angle. Some strategies enhance the backbone planarity, such as reducing the tilt angle of the molecule by adding smaller side groups, bridging via H-bonds [33]. Roncali and coworkers demonstrated that the rotational disorder due to steric hindrance can be counteracted by using covalent chemical bonding via linking and rigidifying the neighbouring aromatic units , Figure 25[33,35,43].

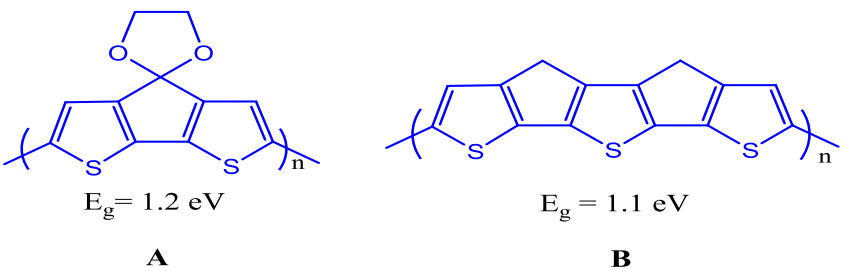

E_g= 1.2 eV

A

E_g = 1.1 eV

B

Figure 25: Control the planarity through covalent bonding[35] .

In Figure 25, the polymer A has sp^3 carbon of a ketal group which is employed to bridge and rigidify the bithiophene repeating units to exhibit a low band gap of 1.2 eV [32,35]. Further bridging in polymer B leads to a reduction in the band gap to 1.1 eV [32,35]. The quinoid form contributes to improving the planarity between adjacent aromatic units, which enriches parallel p-orbitals interactions to facilitate delocalization and extend conjugation. This reinforcement in turn leads to a decrease in the band gap [35]. All these parameters discussed above not only affect the bandgap but also affect each other and the chemical and physical properties [31]. Therefore, they need to be fulfilled to attain reasonable band gap and high value of power conversion efficiency. In addition to the previous factors, the type of heteroatom could affect the mechanical and physical properties of the polymer leading to a further decrease in the band gap [44].

1.1.7 Preparation routes of Conjugated polymers

Since the advent of high conductivity doped polyacetylene, research efforts have focused upon creating materials with a high degree of stability and novel electronic properties [45]. Polyarylenes, such as polythiophene, polyfluorene and poly(p-phenylene vinylene) are prototypes of the second generation of conjugated systems Figure 2 [14]. These materials can be used in numerous electronic applications. The direct link between the aromatic repeat units by C-C bonds is the key feature of these materials [46]. This thesis will focus on two common and important methods to create these conjugated systems, which are Suzuki and Stille cross coupling.

1.1.7.1 Suzuki Coupling

The Suzuki cross-coupling reaction is a highly effective methodology used for the creation of carbon carbon bonds. It is a powerful tool for building new C-C bonds through linking

two sp^2 hybridized orbitals of C atoms [46]. This worldwide methodology is called Suzuki polycondensation (SPC) [46]. The Suzuki reaction is the coupling of a vinyl or an aryl boronic acid with a vinyl or an aryl halide in the presence of a palladium catalyst , Figure 26 [47].

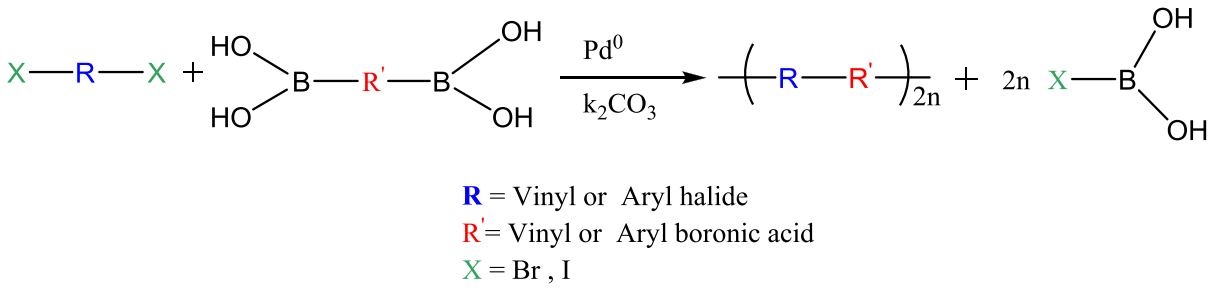

Figure 26: Suzuki cross-coupling.

The Suzuki cross-coupling reaction mechanism and its steps, as shown in scheme 1.

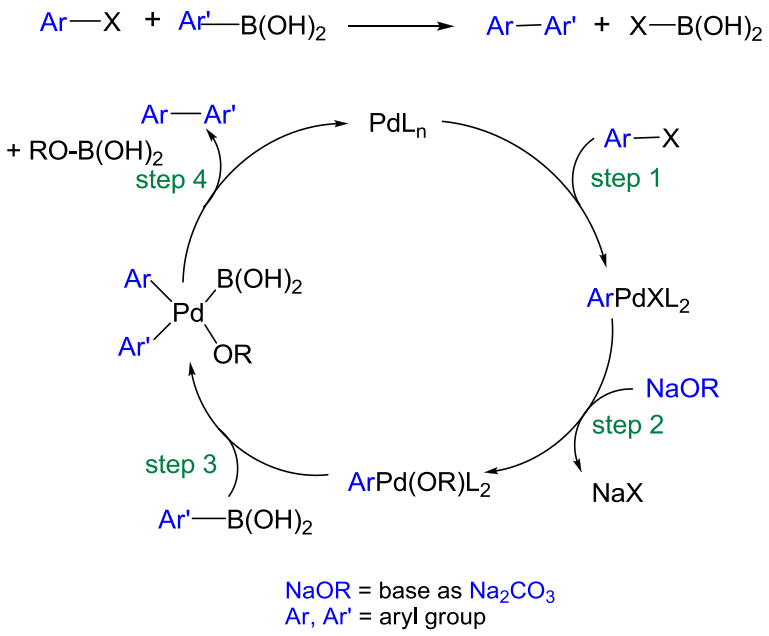

Scheme 1: Suzuki cross-coupling reaction mechanism.

1.1.7.2 Stille Coupling

The Stille cross-coupling reaction is an extremely versatile way to form C-C bonds. This reaction is classified as a polycondensation reaction used to form conjugated polymers. This reaction occurs in the presence of a palladium catalyst between arylstannanes and aryl halides Figure 27 [48].

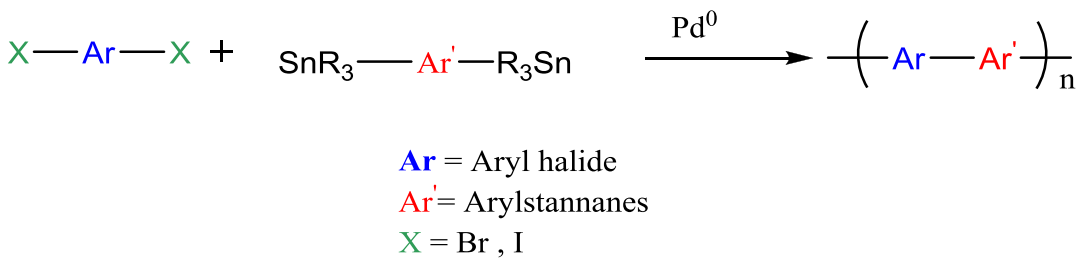

Figure 27: Stille cross-coupling.

The Stille cross-coupling mechanism, as shown in scheme 2.

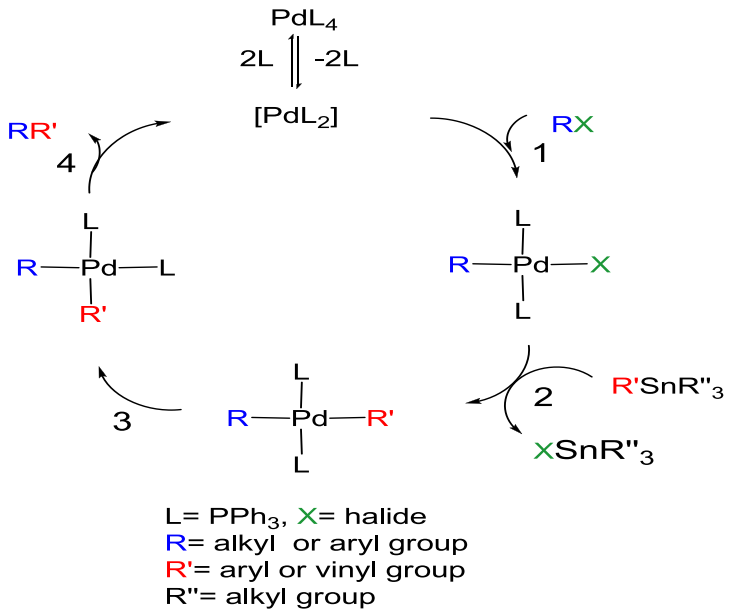

Scheme 2:Mechanism of Stille cross-coupling reaction.

1.2 Organic Photovoltaics

1.2.1 Background

Since Becquerel discovered the photocurrent in inorganic materials, they have been widely used for solar cells. Inorganic semiconductors like silicon are used in solar cells with an efficiency of nearly 25% [49]. Recently, organic solar cells have emerged as a new competitor in this field due to their unique properties. However, organic solar cells are still in the early stages of development and may not yet have reached their full potential. They do though have many appealing advantages, such as low weight, low cost, solubility, flexibility and tunability. The simple production process of organic semiconductors at much lower temperatures (20-200^0 C) than inorganic cells make them a promising alternative to conventional cells [50]. Semiconducting polymers are another interesting alternative materials due to their unique opto-electronic properties and good mechanical and processing properties.

1.2.2 Operating Principles

The general principles of organic solar cells resemble those of inorganic solar cells, but the difference is that the photon absorption process in organic semiconductors leads to the formation of bound electron hole pairs (excitons) [50]. Six important processes have to be improved to achieve a high conversion efficiency and generate electrical energy, Figure 28 :

1. Absorption of light.

2. Excitons creation.

3. Excitons diffusion.

4. Charge separation.

5. Charge transport.

6. Charge collection.

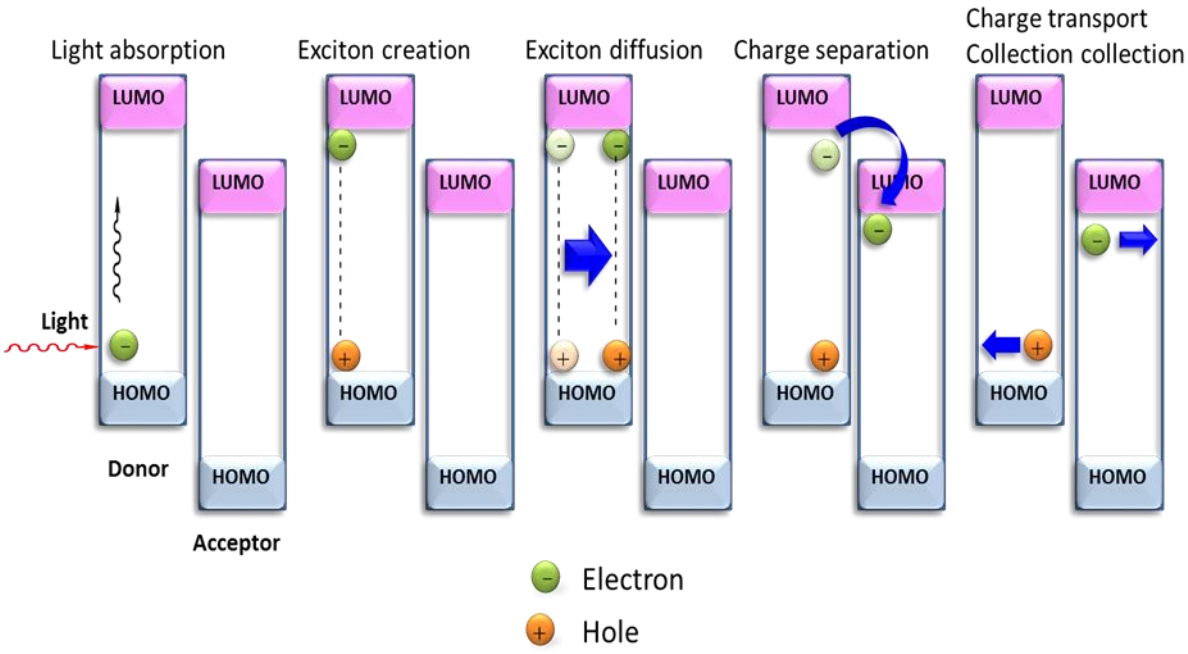

Figure 28: Working of organic solar cell [35]

1.2.2.1 Absorption of light

The proportion of incident light absorbed in organic materials is very small. This problem can be attributed to their large energy gap. This gap is very small 1.1 eV (1100 nm) in traditional silicon solar cells, where 77 % of the solar irradiation can be absorbed [8]. However, the band gap of most semiconducting polymers is higher than 2 eV (620 nm) [8]. Therefore, the harvesting of the solar photons of these materials is about 30% of solar

irradiation [8,36]. Moreover, the absorption coefficients of organic semiconductor are above 10^7 $m^{-1,}$ meaning that 100 nm thickness of the active layer is sufficient to absorb photons in organic photovoltaic devices [51], Figure 29. By contrast, inorganic polycrystalline semiconductor materials, such as $CuInSe_2$ and crystalline silicon solar cells, need a few micrometres thick active layer of up to 100µm for good absorption [51]. In organic solar cells , the energy of absorbed photon to excite electron from HOMO to LUMO must be greater than the band gap energy :

$$E_{photon} = \frac{C \cdot h}{\lambda photon} \geq Eg$$

This excitation of an electron from the HOMO level to the LUMO level leaves behind a hole in the valence band (VB).

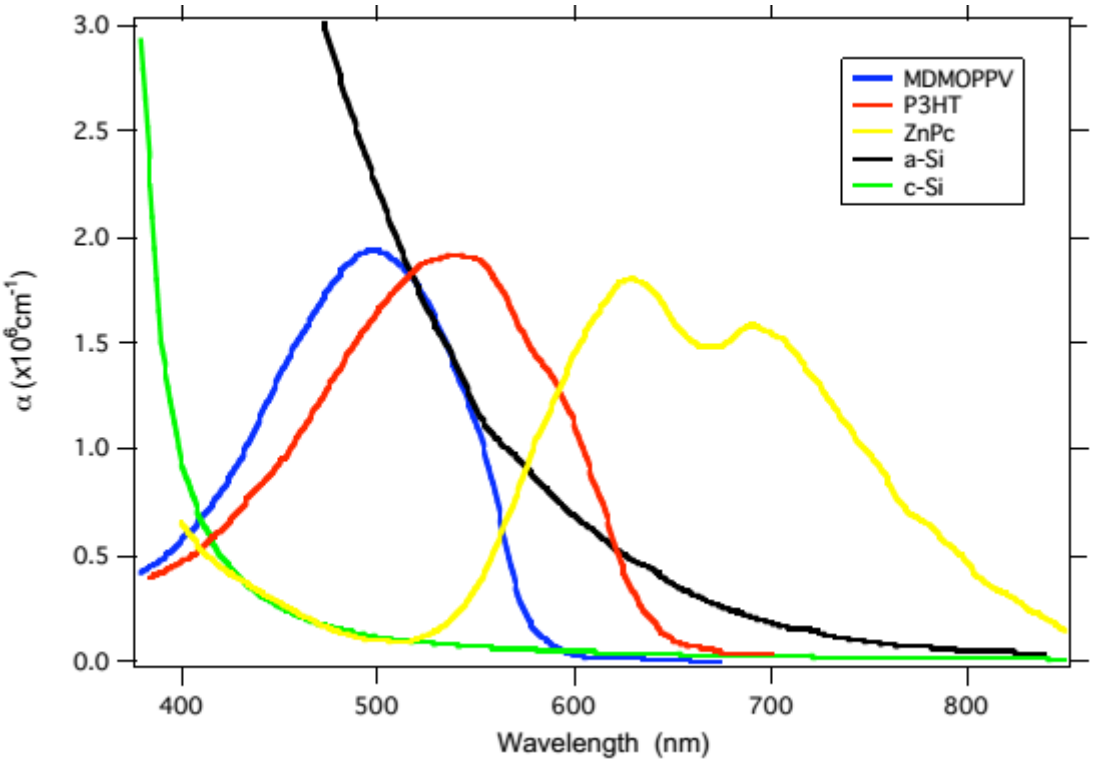

Figure 29: Absorption coefficients of different materials : MDMOPPV and P3HT (polymers), ZnPc (organic dye), crystalline and multicrystalline silicon Si (inorganic materials).

1.2.2.2 Excitons Creation

The absorption of photons in organic semiconductors leads to the formation of bound electron-hole pairs called excitons rather than free charge carriers [8]. It has been found that in conjugated polymers 10% of photoexcitations leads to free charge carriers [34,52]. Exciting electrons requires light with an energy larger than the band gap energy [53]. In organic semiconductor materials these excitations are the HOMO-LUMO excitations that occur in the HOMO-LUMO of the donor.

1.2.2.3 Excitons Diffusion

Ideally, the formed excitons should reach an interface area and diffuse there. This area is between the organic absorbing material (donor) and the next organic layer (acceptor). The diffusion length of the excitons and the thickness of the active layer play a critical role in light harvesting and increasing efficiency. In general, the diffusion length of the excitons in conducting polymer materials is in the range of 5 - 20 nm [16,19,54]. Therefore, the excitons should be created in the range of the diffusion length of the interface. In other words, it is better that the domain size of the active layer, and the diffusion length should be in the same range. The domain size in ideal morphology of the active layer should be in the range of 10 ~ 30 nm to match the diffusion length [19,54]. This compatibility between the domain size of the active layer and the diffusion length of the excitons will lead to a good charge separation.

1.2.2.4 Charge Separation

The charge separation process occurs at the interface area between the donor and acceptor by electron transfer. The electron and hole (excitons) in the interface area are not separated, but they are still held together by Coulomb interaction Figure 30[55]. This Coulomb interaction remains dominant as long as the distance between the electron-hole is

close , Figure 30. To overcome this Coulomb force, an energy larger than a binding energy is required, which is typically 0.25 - 1 eV [55-56]. This can be supplied by an externally applied electrical field.

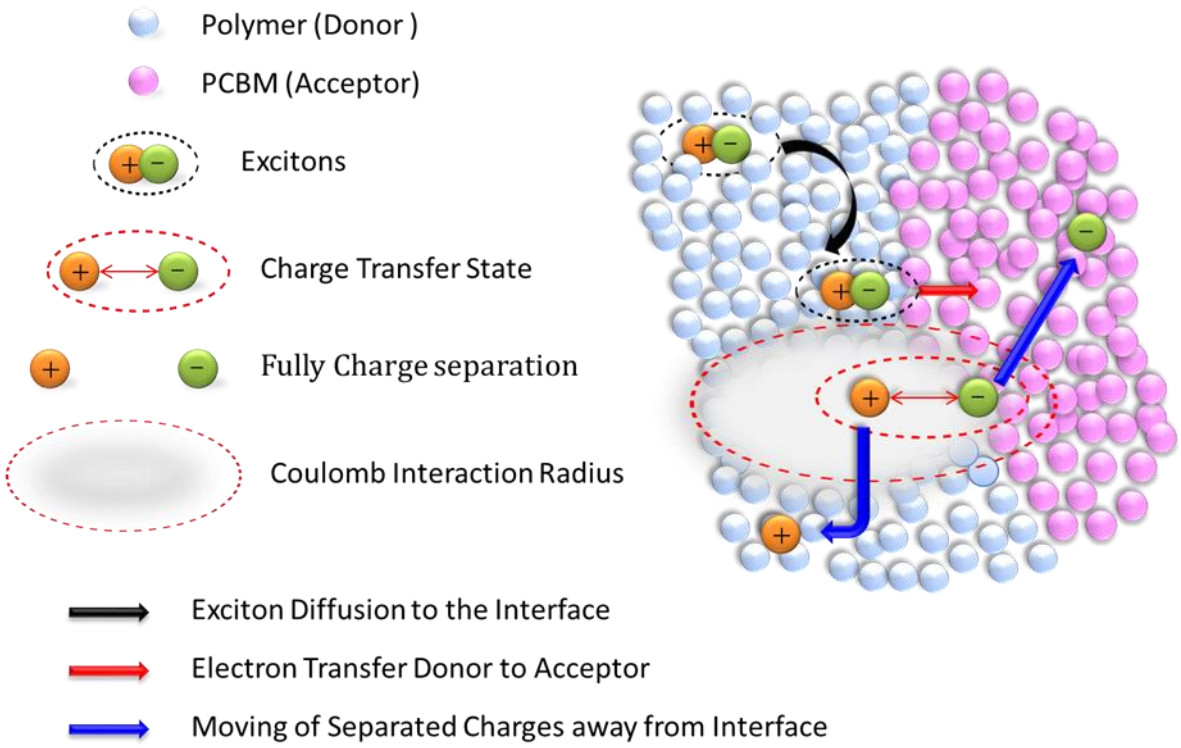

Figure 30:Schematic of charge separation at the Donor – Acceptor interface cell [57].

1.2.2.5 Charge Transport

Following charge separation, the separated charges travel towards the donor and acceptor phases respectively. The electrons travel to the anode (Al) and the hole to the cathode (ITO) [51].

1.2.2.6 Charge Collection

The transported charges are collected at two electrodes to generate current, and this process is commonly accomplished by a transparent material (ITO) as the cathode and a metal contact as the anode (Al, Ca, etc.) on the other side of the cell device.

1.3 Organic solar cell architectures

1.3.1 Single Layer Devices

This device consists of one layer sandwiched between two electrodes [58]. The anode is normally indium tin oxide (ITO), which is a transparent layer placed between a glass substrate and the organic layer Figure 31, [58]. The cathode is a layer of metal, such as Ca, Al and Mg, evaporated on the organic layer. Although single layer devices produce a sensible value of V_{OC}, the results obtained from this type of device are not satisfactory [58]. The external quantum efficiencies (EQE) obtained from this cell are only 0.1 - 1%, and the power conversion efficiencies are low at roughly (< 0.1 %) [59]. Also, the main problem is that the generated photocurrent is very low.

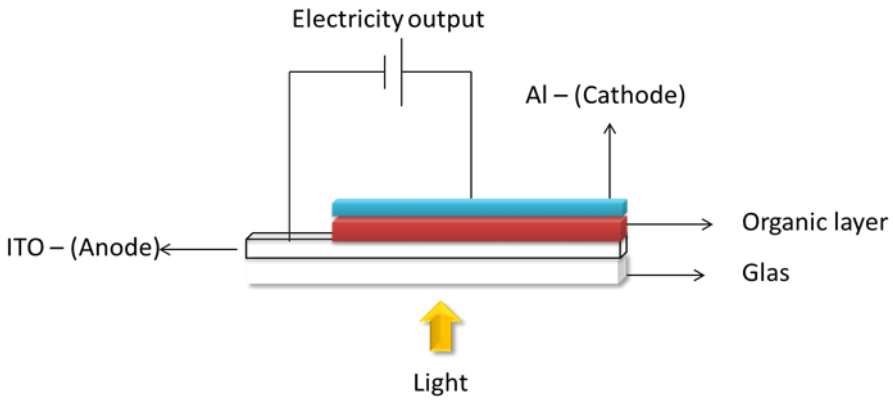

Figure 31: Single Layer Organic Solar Cell .

1.3.2 Bilayer Heterojunction Devices

These devices are formed from two active layers (electron donor and electron acceptor) sandwiched between two electrodes Figure 32[16,19,58]. These two layers have different properties, such as electron affinities and ionization potentials [7]. This design promotes the dissociation of charges at the interface between the two active layers. Thus, the electron is accepted by the acceptor layer (larger electron affinity), and the hole is accepted by the donor layer (lower ionization potential) [7]. In this device, the excitons are created at a distance of 10-20 nm from the interface, so a small proportion of the excitons can reach the interface [60]. Therefore, the absorbed photons will be far from the interface, which in turn leads to a decrease in the quantum efficiencies [60]. Generally, in organic electronic materials, the diffusion length of the excitons is typically in the range of 10 nm. Therefore, to achieve efficient light harvesting, the excitons should be created in the same range as the diffusion length of the interface [7]. In other words, it is best if the thickness of the layer and the diffusion length are in the same range.

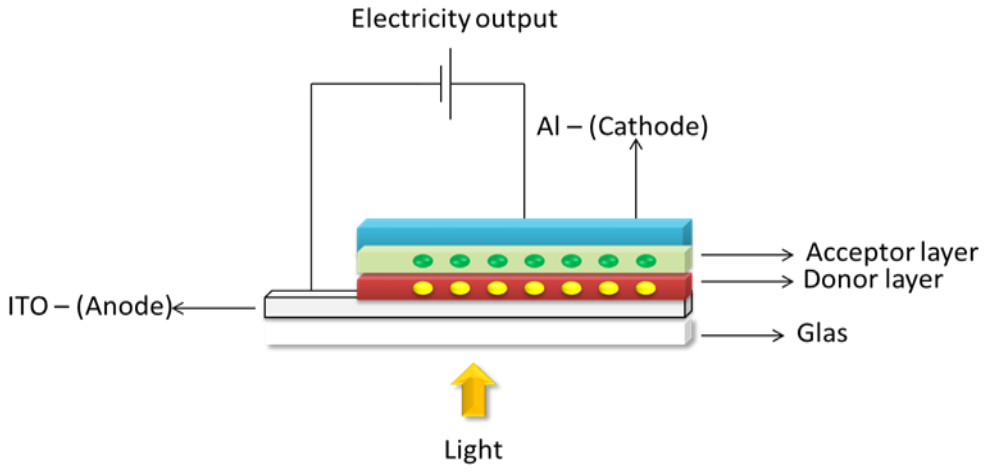

Figure 32: Bilayer Organic Solar Cells.

1.3.3 Bulk Heterojunction Devices

To ensure the efficient harvesting of light, the thickness of the film has to be more than 100 nm, and the thicker the film the more light it will absorb. But the main problem here is that a small number of the formed excitons will reach the interface area and dissociate [17a]. This problem can be overcome by designing a bulk heterojunction device. Unlike bilayer heterojunction devices, where the donor and acceptor layers are entirely isolated from each other, in the dispersed heterojunction, both layers are completely blended in one layer , Figure 33 [61]. This design helps to achieve good contact between the donor and acceptor and at the same time increases the interface area through making nanoscale size domains [62].

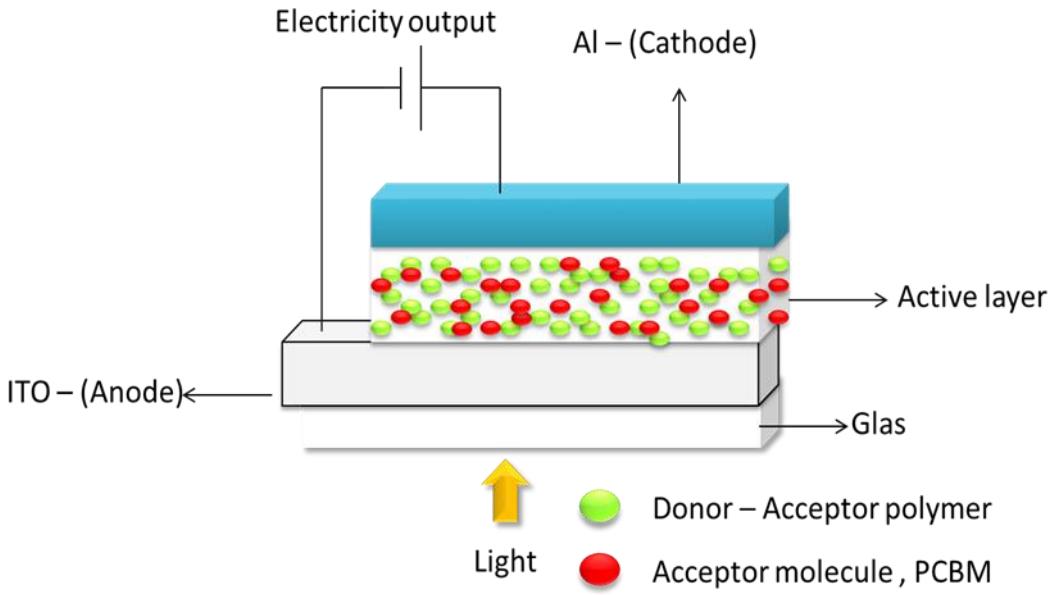

Figure 33: Bulk Heterojunction Solar cell.

1.3.4 Molecular Heterojunction Devices

The morphology in bulk heterojunction cells allows good contact between the donor and acceptor. However, the limited miscibility between the acceptor and donor within the

organic active layer leads to formation of aggregates and phase separation. This degree of domain size and phase separation depends on the solvent chosen to cast films from and also the miscibility of the donor and acceptor molecules [17a]. Increased phase separation in the active layer may prevent the continuity of the phases and reduce the charge transport properties of the material [17a].

The strategy for controlling the bicontinuous phase separation and increasing the interfacial area between the donor and acceptor uses block copolymers [17a]. Block copolymers can self-assemble and are known to form ordered domains [17a] as shown in Figure 34.

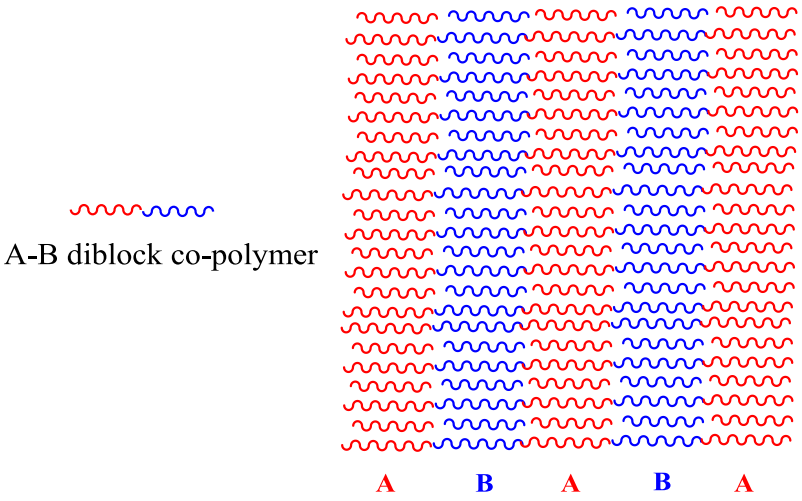

Figure 34: Self-assembled configuration of diblock copolymer.

1.4 Characteristics of Organic Solar Cells

1.4.1 Efficiency of Organic Photovoltaic Devices

Preparation of polymers with low band gaps that are able to absorb a large portion of the electromagnetic radiation from sunlight and with suitable energy level alignment can lead an increase in the efficiency of devices. The efficiency of the organic photovoltaic solar cell device can be described and characterized using some important parameters [63]. These parameters are the open circuit voltage (V_{OC}), the short circuit current (J_{SC}) and the fill factor (FF) [63].

The efficiency (PCE) of solar cell can be defined as the percentage of output power compared to input power [64]. That is to say that (PCE) measures the amount of power created by a solar cell relative to the power available in the incident solar radiation [64]. The power conversion efficiency (PCE) is mathematically represented as follows:

$$\mathbf{PCE} = \frac{P_{out}}{P_{in}} = \frac{V_{OC} \cdot J_{SC} \cdot FF}{P_{in}} \cdot 100\%$$

Where:

P_{out} is the output power , P_{in} is the input power.

V_{OC} is the maximum voltage that the device can produce under an open circuit. It is in general proportional to the difference between the HOMO of the donor (polymer) and the LUMO of the acceptor [63].

(J_{SC}) is the maximum current that flows in the device under illumination when no voltage is applied. It has been found that the (J_{SC}) is dependent on the morphology of the active layer and the mobility of the charge carriers [65].

Fill factor (FF) is a parameter that in conjunction with (J_{SC}) and V_{OC} .It is the value that determines the maximum power output from a solar cell and can be defined as the ratio of the maximum power output from the solar cell to the power output of (J_{SC}) and V_{OC} . [64].

1.5 Morphology of active layers in Devices

All previous parameters require a harmonious intermixing of donor and acceptor phases in the active layer to achieve high efficiency [61]. Therefore, the morphology of the active layer has to be optimised to attain an intimate intermixing between donor and acceptor phases. The ideal morphology is defined as the bicontinuous composite of donor and acceptor with a large interface area for exciton dissociation and a mean domain size commensurate with the exciton diffusion length (5–10 nm)[66]. Donor and acceptor materials should form co-continuous networks with nanoscale phase separation to be able to effectively dissociate excitons into free electrons and holes and to guarantee fast charge carrier transport from any place in the active layer to the corresponding electrodes [67]. In this respect, controlling the morphology using A-B diblock-copolymers is recognised as a very useful strategy for attaining a bicontinuous composite with nanoscale phase separation [61]. It is an alternative method for controlling domain spacing and modifying morphology. A-B diblock-copolymers exhibit self organized structures depending on the fractions of A and B blocks as illustrated in Figure 35. The contact surface between this block is minimized by aggregating into domains, which are close in size to the length of each block [10].

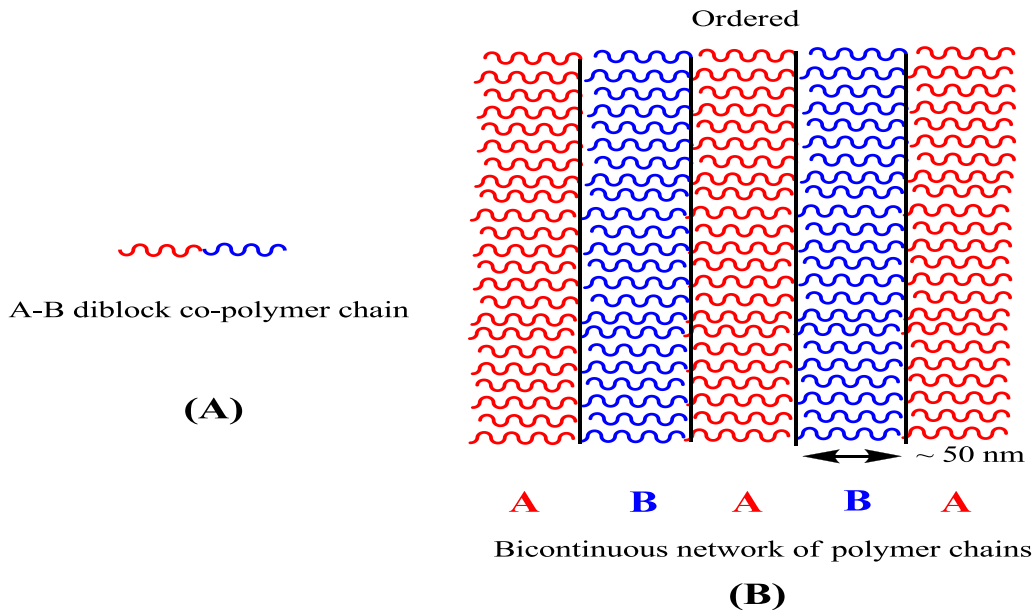

Figure 35: A chain of A-B diblock co-polymer (A), Ordered network of polymer chains (B).

1.5.1 Factors Affecting Morphology

The morphology of the active layer can be affected by several factors during the film formation or treatments afterwards [68], and this has to be taken into account when making devices. These factors are the spin casting solvent, the ratio between the polymer donor and fullerene which use as acceptor molecule and the annealing temperature [68].

1.5.1.1 Solvent

Preparation techniques for devices require the materials for solution processing to be soluble. The first study of the solubility of polymer/fullerene D/A solar cells was performed by the Heeger group [68]. They found that the solubility of pure C_{60} in organic solvents is limited and that, moreover, C_{60} tends to crystallize during film formation. This limited solubility of C_{60} prevents the use of high concentration blends. This issue was overcome by attaching solubilizing groups on $C_{60,}$ such as (PCBM) [61,68]. The study by Shaheen on a device based on MDMO-PPV/PCBM (1 : 4 by weight) showed that a

dramatic efficiency (PCE) increase occurs upon changing the active layer blend from toluene to chlorobenzene [65a]. It was found that casting the active layer blend from toluene gave power conversion efficiencies of about 0.9 %, while the efficiency dramatically improved to 2.5 % when the solvent was changed to chlorobenzene [65a]. This change in efficiency can be attributed to the domain sizes in the thin film nanomorphology, demonstrated by atomic force microscopy (AFM) [65a,68-69] Figure 36.

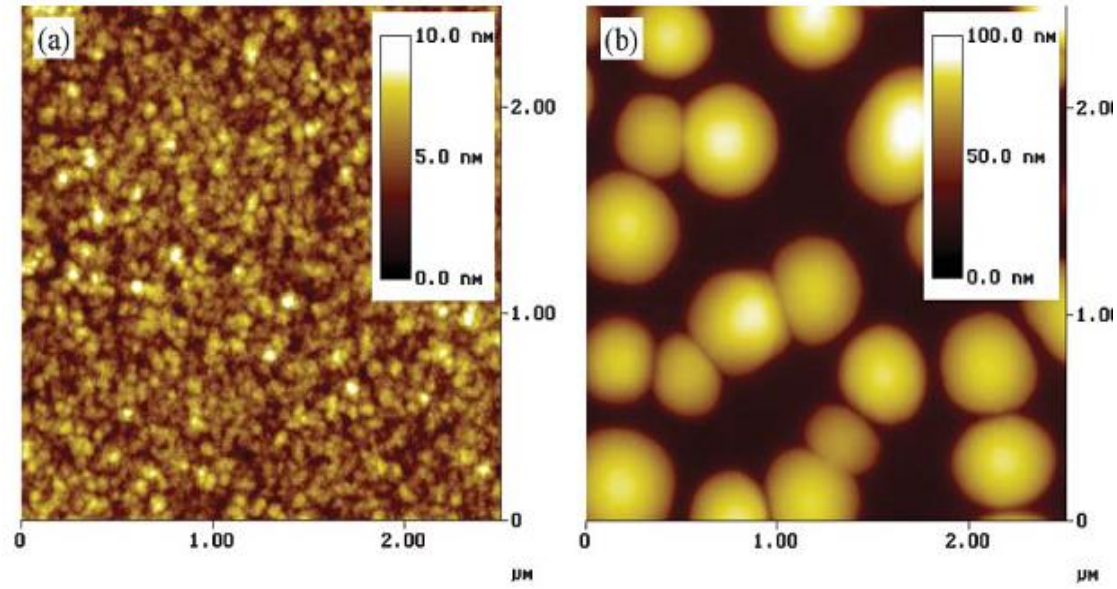

Figure 36: Tapping mode AFM topography scans of MDMO-PPV : PCBM 1 : 4 (by weight) blended films, spin cast from (a) chlorobenzene and (b) toluene solution. The toluene cast film exhibits height variations that are one order of magnitude larger than those on chlorobenzene cast films. Features of a few hundred nanometers in width are visible in (b), while features in (a) are around 50 nm [68]

The images in Figure 36 confirm very different surface morphologies. In the toluene blend (image b), a large scale of phase separation is formed where the surface includes domains with horizontal dimensions in the order of 500 nm [69]. It has been found that these large domains lead to macroscale phase segregation in the system [70]. Moreover, these domains are much larger than the thickness of the film (100 nm) [69]. The solubility of PCBM in toluene is much lower than that of chlorobenzene, leading to the formation of phase-segregated regions that contain higher concentrations of fullerenes [70].

In contrast, the film cast of the chlorobenzene blend (image a) shows domains in the order of only 100nm [70]. The film surface is smooth and shows homogenous and bicontinuous composite, which facilitates the charge transport and increases the efficiency to 2.5 [70]. It is clear that the choice of solvent is a decisive factor in generating homogenous morphology and improving efficiency [70].

1.5.1.2 Ratio between polymer and fullerene in active layer blends.

The first study of the blend ratio in bulk heterojunction solar cells investigated the blend of MEH-PPV : PCBM and was conducted by Yu et al. [68,71]. They found that the device achieved the best performance with a blending ratio of 1 : 4 between polymer and fullerene, respectively [68]. Further studies on the blend of MDMO-PPV : PCBM revealed that the best performance was when the blend ratio was 1 : 4 between polymer and PCBM. However, in the case of the blend for P3HT : PCBM, the ratio was 1:1 between P3HT and PCBM. These results can be attributed to the inherent miscibility between P3HT and PCBM than is observed for MDMO-PPV and PCBM [70].

1.5.1.3 Annealing Temperature

Thermal post treatment or annealing is recognised as a useful tool for influencing the morphology of the active layer of polymer solar cells [67]. This thermal treatment has a twofold action: it forces the film morphology to self organize through the transition from amorphous to crystalline and it enhances the stability of the morphology long-term. The latter action is currently still a challenge for scientists [67]. The influence of annealing the system P3HT/PCBM was investigated by Padinger et al., who found that annealing leads to stabilizing the morphology and improving the power conversion efficiency [67]. Further studies were done on the morphology-driven high performance of P3HT/PCBM, and in all the studies an increase in performance and an improvement in the power conversion

efficiencies as high as 5.2% after annealing was observed [67]. The morphology studied by Yang et al. based on TEM illustrates that a nanoscale network with a crystalline order is formed for P3HT and PCBM through thermal annealing [67]. The TEM images show that the length of the fibrillar P3HT crystals is extended and nanocrystalline PCBM domains are developed due to the annealing , Figure 37.

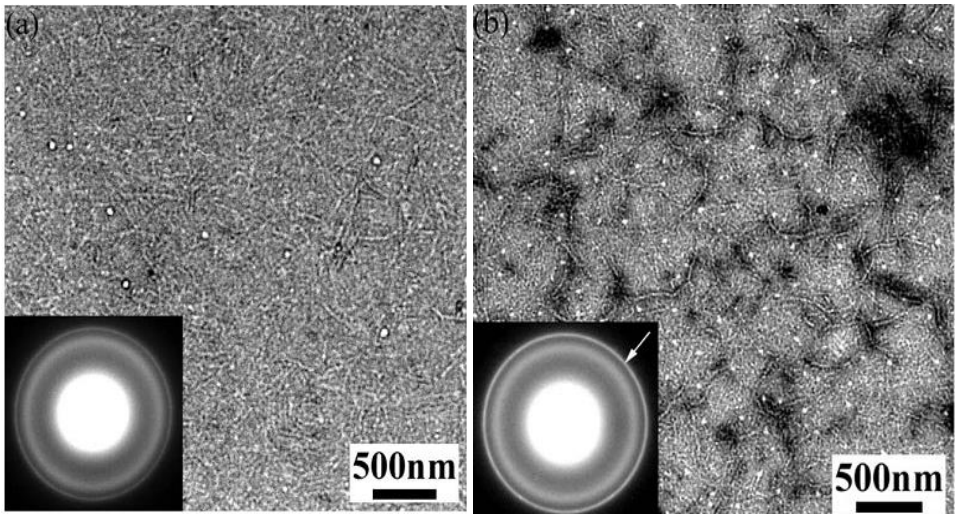

Figure 37: TEM images patterns of untreated (Left) and thermally annealed (Right) P3HT : PCBM blend films [81].

Clearly, the formation and improvement in the nanocrystalline nature of the film after annealing is pivotal to controlling the morphology and increasing the power conversion efficiency [67-68].

1.6 Organic Solar Cells Materials

During the past few decades, organic materials have attracted particular attention as opto-electroactive materials. Carbazole and fluorene based low energy gap polymers are of special interest for use in BHJ solar cells. The optoelectronic properties of anthracene-based systems have been investigated for solar cell applications. These molecules have been studied as electron donating units and copolymerized along with electron accepting repeat units, such as benzothiadiazole units. Their performance in solar cell devices has been investigated, and they have shown great promise.

1.6.1 Carbazole-Based Conjugated Comonomers

In recent years, carbazole-based conjugated polymers have attracted considerable attention due to their valuable applications as photorefractive materials in BHJ solar cells [72]. Indeed, carbazole has many advantages as an aromatic organic molecule [73]. 9H- carbazole is available, a cheap starting material and a co-planar molecule [74]. It has good chemical and environmental stabilities due to its fully aromatic configuration , Figure 38 [75].

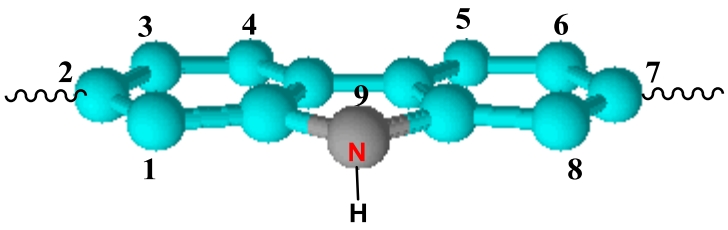

Figure 38: 2,7-linked carbazole Structure and numeration.

A variety of alkyl and aryl chains can be added through easy substitution on the nitrogen atom, which can modulate the properties of carbazole [76]. These substitution groups provide polymer solubility without increasing the steric interactions near the backbone and tuning the optical and electrical properties [74-75]. Owing to the structure of carbazole, it can be linked at different positions to form carbazole derivatives with different properties and potential applications. These positions are 3, 6-positions and 2, 7-positions to yield poly(3,6-carbazole)s and poly(2,7-carbazole)s, respectively [74-75].

In addition to the above features of poly-carbazole derivatives, the better hole transporting properties and the versatility to fine tune the band gap make them a promising material for photovoltaic applications [76]. Owing to their low (HOMO) energy levels, poly(2,7-carbazole) derivatives show great potential, present excellent air-stability and possibly a high open circuit voltage (V_{OC}) in BHJ solar cells [76]. The first study based on a poly(2,7-carbazole) to investigate its performance in solar cells was done by Mullen [77]. They used perylene tetracarboxydiimide (PDI) as the electron acceptor [77]. The performance of the prepared device was low at (PCE) = 0.6% even though the (V_{OC}) = 0.71V was relatively high. This obtained result was attributed to the poor solar spectrum match [76]. Leclerc and co-workers synthesized 2,7-carbazole-based copolymers with low band gaps in the range of 1.7 to 2.3 eV, but the devices performed very poorly (up to 0.8%) [76]. The low molecular weight as well as the poor solubility were behind the poor performances [76]. The high molecular weight polymers were obtained through optimized Suzuki cross-coupling polymerization. New copolymers were reported by Iraqi and co-workers based on 6,7-diphenyl-4,9-bis-(thiophen-2-yl)-[1,2,5]thiadiazolo[3,4-g]quinoxaline and 2,7-carbazole [78]. They were prepared following Suzuki polymerization procedures, and their absorbed light was extended up to 1200 nm [78]. The efficiency achieved by these polymers was PCE (0.61%), even though their band gaps were low (1.1 to 1.3 eV) [76,78]. The low value of the

efficiency PCE (0.61%) can be attributed to the small value of the V_{OC} (0.4 V), which arises from the difference between the HOMO of the copolymers (4.8 eV) and the LUMO of the PCBM (3.8 to 4.3 eV) [76].

1.6.2 Fluorene-Based Conjugated Comonomers

Fluorene molecules have been studied extensively in photovoltaic applications due to their unique photophysical properties [35]. The fluorene's monomer is rigid and consists of planar biphenyl units bridged at carbon 9 - position by a carbon atom , [79].

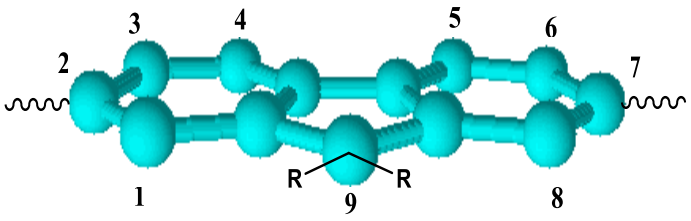

Figure 39: Fluorene monomer with ring numbering [79].

Fluorene's monomer can be easily functionalized at the 9- position with a variety of alkyl or aryl groups [79]. Such alkyl groups are found to improve the solubility of fluorene in common organic solvents [79]. Owing to the low lying HOMO levels of fluorene derivative units and their high hole mobility, they are expected to attain higher open circuit voltages and short-circuit currents [35]. The previous features make them highly promising materials for photovoltaic applications [35]. Nevertheless, they exhibit a wide band gap for efficient sunlight harvesting where it is found that the band gap for poly(9,9-dialkylfluorene) is 3.0 eV [35]. The strategy used to overcome their low band gap includes the incorporation of an electron accepting unit into the polymer chain, thereby reducing the band gaps of the resulting copolymers through formation of donor-acceptor alternating arrangement [35]. The

first work using a low band gap polyfluorene derivative (PFDTBT) as an efficient and promising BHJ solar cell was done by Andersson in 2003, Figure 40 [80] .

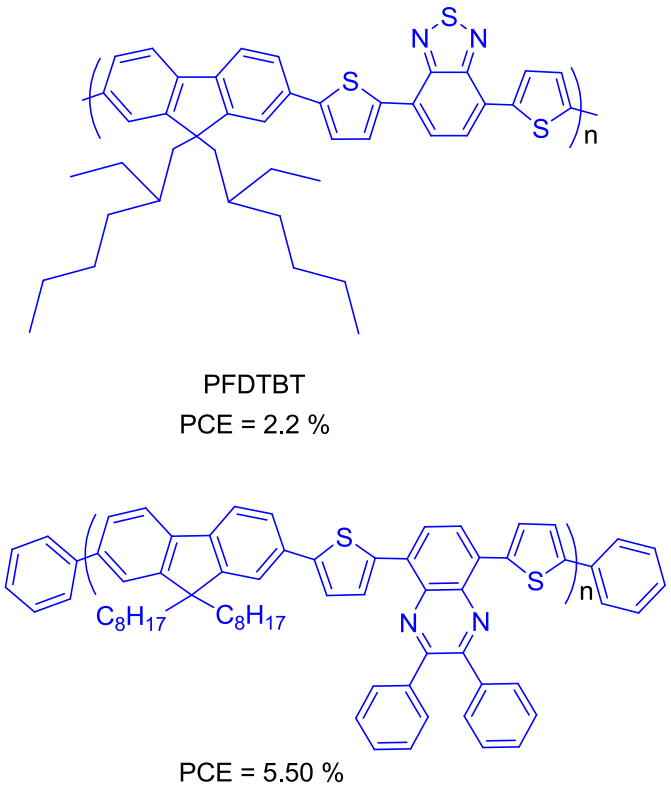

Figure 40: Polyfluorene derivatives for BHJ solar cells.

The performance of that polymer in BHJ solar cells was moderate to the extent that a PCE of 2.2% was exhibited [80]. The best solar cell based on polyfluorene derivatives so far was reported by Tsukamoto et al. with a PCE of 5.50 % , figure 40 [80-81] .

1.6.3 Thiophene -Based Conjugated Comonomers

The study of thiophene based polymers in electronic applications has significantly increased in the last decades. Such polymers have features that other materials do not, which makes them promising candidates for photovoltaic applications [82]. Thiophene rings contain sulphur atoms which have high polarizability leading not also to stabilize the conjugated chain but also to enhance the charge transport properties [83] . They have been developed enormously in the last decade to be one of the most important classes of conjugated polymers and ideal building blocks in cross - coupling reactions [84] . The fusibility and solubility of these polymers allow the formation of thin films with good optical properties [82]. Moreover, their optical properties such as band gap can be altered at least for varying from 1 to 3 eV by introducing small substitution groups on the main chain [82]. These materials exhibit an environmental stability [83].

The conductivity of PTs was studied in the early 1980s by Glenis et al. using polythiophene and poly(3-methylthiophene) (P3MT) [85], but the efficiency achieved was still poor. Poly(3-hexylthiophenes) (P3HT) belongs to this group and is among the leading polymer semiconductors for solar cells applications Figure 41.The devices based on a blend of P3HT and PCBM displayed a power conversion efficiency of 5.2% with a band gap of around 1.9 eV. P3HT is the most commonly used material for PSC studies at present [82].

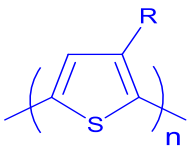

R= n-Hexyl

Figure 41: Structure of Poly(3-alkylthiophenes) (P3HT).

1.6.4 Anthracene -Based Conjugated Comonomers

Anthracene molecule is a planar cyclic aromatic system , consisting of three fused benzene rings , Figure 42. The chemical structure of anthracene makes it a promising material in solar cell application . The photovoltaic properties of anthracene units were investigated in 1950 by Kallmann and Pope [86].The anthracene units and their derivatives have been extensively investigated in optoelectronic applications due to their good hole mobilities , high chemical and environmental stability [87]. Among anthracene and its derivatives, 2,6- anthracene based polymers have been investigated in (BHJ) solar cells with efficiencies (PCEs) of up to 1.7% [88].

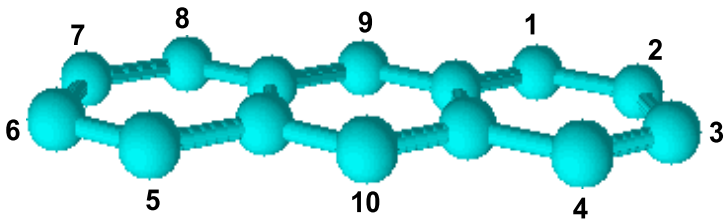

Figure 42: Anthracene Monomer with Ring Numbering.

Chapter 2: Aims and Objectives

In the past years, solar cells based on bulk heterojunction (BHJ) conjugated polymers have attracted a great deal of attention as a potential renewable energy technology. To fully exploit the sun's energy, the absorption spectra of organic materials should cover a wide range of the solar radiation to achieve desired efficiency. However, improving the power conversion efficiency (PCE) of these polymers towards commercialization is still in its early stages [89] . Developing polymers with low band gaps and suitable electronic energy levels is an effective way to overcome the low values of efficiency [89] . This way will enhance the generation, separation, transport, and collection of charge carriers [89]. Therefore, the promising approach for obtaining low band polymers and high absorption can be achieved by incorporation of donor (electron-rich) and acceptor (electron-deficient) units alternatively in a conjugated polymer chain [90]. Studies done on BHJ devices have proposed several models to estimate the polymer performance. These studies illustrate that the ideal conjugated polymer for BHJ devices using (PCBM) as the electron acceptor should exhibit an optical band gap between 1.2 and 1.9 eV with a HOMO energy level ranging between -5.2 and -5.8 eV to allow air stability, a LUMO energy level near -3.8 to -4.0 eV to allow electron transfer to (PCBM)[91] .These electronic properties are highly desirable and should be taken into consideration when designing and preparing polymeric materials for effective bulk heterojunction solar cells .Taking the previous considerations into account, this project is aimed at designing and developing polymeric materials for solar cell applications. Therefore, besides these synthetic methods, the electronic and physical properties, band gap, HOMO and LUMO energy levels, electron transport, morphology, solubility and environmental stability are modified through manipulating the

polymers structures. Leclerc [92], have reported that the polymer PCDTBT exhibit a high efficiency when used as an electron donor polymer in bulk heterojunction solar cells using PCBM as an acceptor , Figure 43. This polymer contains carbazole unit as electron donor segment comprising 4,7-dithien-2-yl-2,1,3-benzothiadiazole **(DTBT)** unit as electron acceptor. Even though the PCDTBT exhibits a high glass transition temperature, good air-stability and high efficiency , it is firmly expected that further improvements in solubility , molecular weights, device fabrication (e.g., film thickness, annealing, solvent) should lead to even better performances [92].

HXS-1 , is another polymer which was prepared by Qin, R., *et al* [93].This polymer is similar to PCDTBT but the acceptor unit is 5,6-dioctyl-4,7-di(thiophen-2-yl)benzo[c][1,2,5]thiadiazole **(DTBT- 8)** unit , which contains two octyloxy substituents at the 5, 6-positions of benzothiadiazole **(BT)** unit. Moreover, the carbazole unit contains only one linear N-octyl substituent as shown in Figure 43. This polymer was found to be highly planar with a narrow band gap and a high efficiency (PCE of 5.4%) [94]. While it exhibited high efficiency, it had low solubility and could only be processed from hot solutions [95].

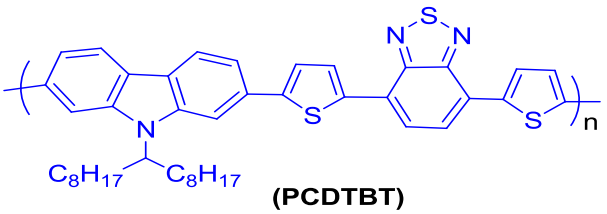

(PCDTBT)

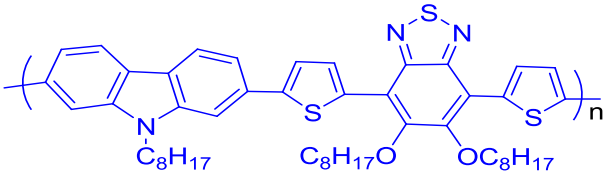

(HXS-1)

Figure 43: Chemical structures of PCDTBT and HXS – 1 .

Along these lines, the project is aimed at synthesising a series of novel copolymers which resemble PCDTBT with 5,6-dioctyl-4,7-di(thiophen-2-yl)benzo[c][1,2,5]thiadiazole **(DTBT- 8)** as acceptor units rather than **(DTBT)** unit . The first target copolymer is poly[9-(heptadecan-9-yl)-9H-carbazole-2,7-diyl-alt-(5,6-bis(octyloxy)-4,7-di(thiophen-2-yl)benzo[c][1,2,5]thiadiazole) -5,5-diyl**] (P1)**, Figure 44 . The carbazole unit in this polymer does not have any substetuents at the 3- and 6-positions. The second target copolymer is poly[3,6-difluoro-9-(1-octyl-nonyl)-9H-carbazole-2,7-diyl-alt- 5,6-bis(octyloxy)-4,7-di(thiophen-2-yl)benzo[c][1,2,5]thiadiazole **(P2)** which has 3,6-difluoro substituted carbazole as donor unit , Figure 44. The electronic properties of **P1** and **P2** polymers and the effect of the octyloxy or fluorine substituents are to be investigated and compared with those of PCDTBT.

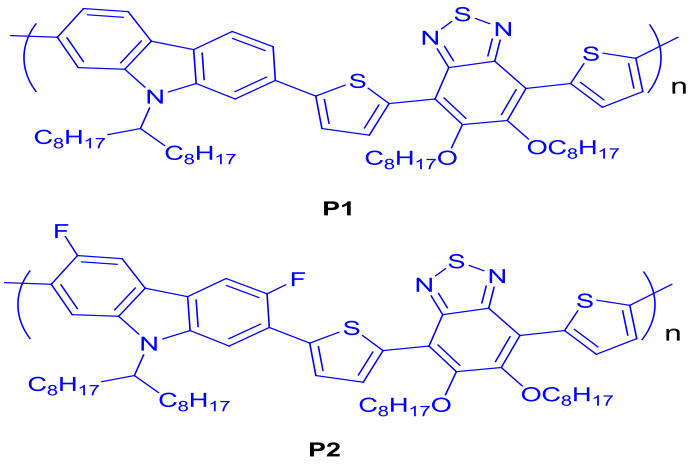

Figure 44: Chemical structures of P1 and P2 .

Polyfluorene based copolymers have been studied extensively in photovoltaic applications due to their unique photophysical properties. Therefore, one of the aims of

this project is to synthesise a polyfluorene based co-polymer 9,9-dioctyl-9H-fluorene as donor unit and 4,7-dithien-2-yl-2,1,3-benzothiadiazole **(DTBT)** as acceptor unit. The target polymer poly[9,9-dioctyl-9H-fluorene-2,7-diyl-alt-(4,7-di-2thiophen-2-yl)-2',1',3'-benzothiadiazole-5,5-diyl] **(P3)** has been synthesised and its properties compared with those of PCDTBT , Figure 45.

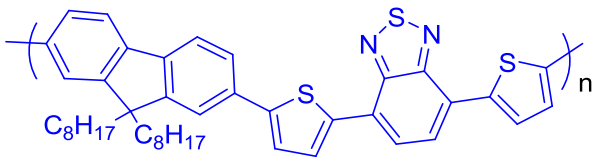

P3

Figure 45: Chemical structures of P3 containing fluorene unit .

Extension of the conjugation length in the polymer chains would be a promising strategy to improve the absorption and electronic properties of polymers for solar cells applications (PSCs). The aim of this project is to prepare novel highly processable donor–acceptor polymers comprising alternating carbazole repeat unit as donor units and 4,7-di(2,2'-bithiophen-5-yl)-5,6-bis(octyloxy)benzo[c][1,2,5]thiadiazole **(DT2BT-8)** unit as acceptor unit. This acceptor has been extended with two extra unsubstituted thiophene rings attached to the ends of the 4,7-dithien-2-yl-2,1,3-benzothiadiazole **(DTBT-8)**. The targets polymers are poly[9-(heptadecan-9-yl)-9H-carbazole-2,7-diyl-alt-(5,6-bis(octyloxy)-4,7-di(2,2'-bithiophen-5-yl)benzo[c][1,2,5] thiadiazole)-5,5-diyl] **(P4**) and poly[3,6-difluoro-9-(1-octyl-nonyl)-9H-carbazole-2,7-diyl-alt-4,7-di(2,2'-bithiophen-5-yl)-5,6-bis(octyloxy)benzo[c][1,2,5]thiadiazole **(P5)** respectively , Figure 46 . These polymers are similar, but the difference is that **(P5)** has 3,6-difluoro substituted carbazole as donor units. Moreover, these polymers are similar to **(P1)** and **(P2)** respectively, but the difference is that the acceptor segment in **(P4)** and **(P5)** is 4,7-di(2,2'-bithiophen-5-yl)-5,6-

bis(octyloxy)benzo[c][1,2,5]thiadiazole **(DT2BT-8)** unit.The electronic, photophysical and photovoltaic properties of these new polymers are to be analyzed and contrasted to those of PCDTBT.

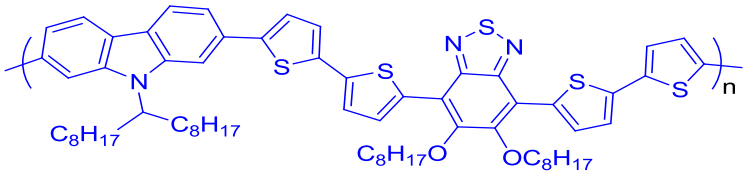

P4

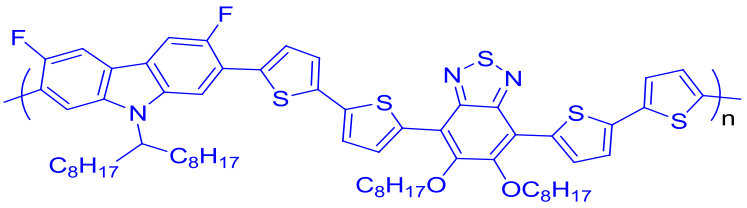

P5

Figure 46: The target polymers P4 and P5 .

Acquiring good charge transport characteristics and hole mobilities in conjugated copolymers could result by enhancing the π – π stacking and close packing of the polymer chains and is a crucial factor for the further improvement of device performance [87,96]. Those parameters can be enhanced by increasing the molecular coplanarity and rigidity[96]. Anthracene and its derivatives are been extensively investigated in view of their good hole mobilities as a result of π – π stacking of adjacent molecules in films [87]. This project is aimed at preparing of low band gap polymers with alternating 2,6 and 2,7 linked anthracene units as donor segments and 4,7-di(2,2'-bithiophen-5-yl)-5,6-bis(octyloxy)benzo[c][1,2,5]thiadiazole **(DT2BT-8)** as acceptor units. These targets polymers are poly(9,10-bis(4-(dodecyloxy)phenyl)-anthracene-2,6-diyl-alt-(5,6-

bis(octyloxy)-4,7-di(2,2'-bithiophen-5-yl)benzo[c][1,2,5] thiadiazole)-5,5-diyl](P6) and poly(9,10-bis(4-(dodecyloxy)phenyl)-anthracene-2,6-diyl-alt-(5,6-bis(octyloxy)-4,7-di(2,2'-bithiophen-5-yl)benzo[c][1,2,5] thiadiazole)-5,5-diyl] **(P7)** were identified for preparation ,Figure 47 . The electronic, photophysical and photovoltaic properties of these polymers are to be investigated and compared to each other.

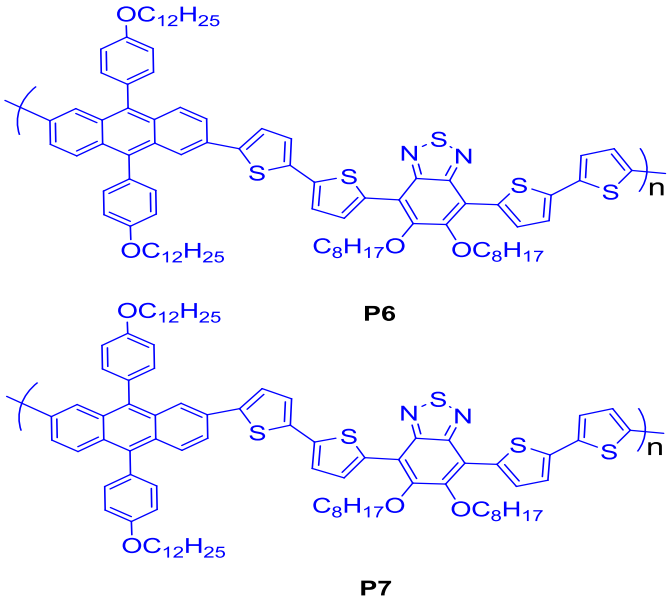

Figure 47: The target polymers P6 and P7.

Attaining an intimate intermixing between donor and acceptor phases and optimizing the domain sizes and the nanoscale donor–acceptor morphology plays a crucial role for the efficiency of BHJ solar cells[61,97]. A very useful strategy to achieve such an ideal morphology is by using the A-B di-block-copolymers concept. It is an alternative method for controlling domain spacing , self organized structures , and modifying morphology [10]. This project is aimed at synthesising and characterizing a di-block co-polymer and investigate its performance in solar cells. The target polymer poly [4-(5-(9,9-dioctyl-7-(5-(7-(thiophen-2-yl)benzo[c][1,2,5]thiadiazol-4-yl)thiophen-2-yl)-9H-fluoren-2-yl)thiophen-2-yl)-7-(5-(9-(heptadecan-9-yl)-9H-carbazol-2-yl)thiophen-2-yl)-

5,6bis(octyloxy)benzo[c][1,2,5]thiadiazole] **(P8)** is a di-block co-polymer comprising blocks of **(P1)** and **(P3)** respectively , Figure 48 .

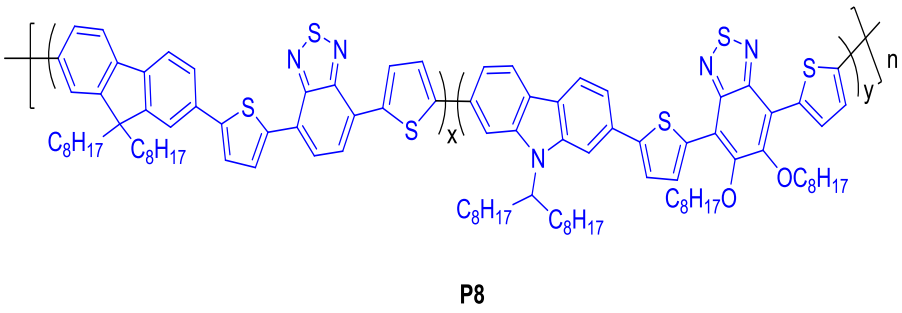

P8

Figure 48: The target di-block co-polymer P8.

Polythiophene and its derivatives are popular heterocyclic conjugated polymers used in electronic devices. The blend of donor poly(3-hexylthiophene) P3HT with the electron acceptor (6,6)-phenyl-C61-butyric acid (PCBM) was one of the most studied efficient polymer blends in solar cell devices with power conversion efficiencies of 5 .2% [14]. Even though a good efficiency can be obtained from this class of polymers with PCBM , there are some issues with PCBM as electron acceptor . It was found that its deep LUMO level reduce not only the efficient charge separation but also the open-circuit voltage [98]. Therefore, using a polymer/polymer blend was an alternative method to overcome this issue [99]. This approach of polymer/polymer blends has some unique potential advantages over polymer/fullerene blends. It is considered that such blends will have more efficient light absorption materials than PCBM blends due to their high absorption coefficients [99-100]. Moreover, they have relatively higher open-circuit voltages which is crucial for the achievement of high power conversion efficiencies [99-100]. Another advantage is having a

large potential for fine tuning of energy levels, due to their structural variety [100]. The earliest studies on block copolymers was done by McNeill, C.R., et al. They synthesized a diblock copolymer based on poly(3-hexylthiophene) (P3HT) as electron donor blocks (p-type) and poly((9,9-dioctylfluorene)-2,7-diyl-alt-[4,7-bis(3-hexylthiophen-5-yl)-2,1,3-benzothiadiazole]-2',2''-diyl) (F8TBT) as electron acceptor blocks (n-type) with power conversion efficiency of 1.8% Figure 49 [98] .

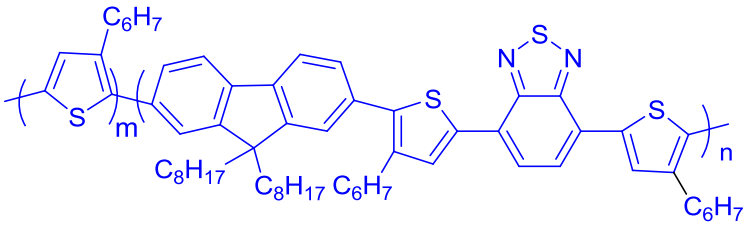

PCE = 1.8 %

Figure 49: The structure of P3HT / F8TBT blend .

Another research study based on block copolymers was done by Mori, D., et al using poly-(3-hexylthiophene) (P3HT) as the electron donor and poly{2,7-(9,9-didodecylfluorene)-alt-5,5-[4',7'-bis(2-thienyl)-2',1',3' -benzothiadiazole]} (PF12TBT) as the acceptor [99] , Figure 50 . The power conversion efficiency obtained from this diblock copolymer based on P3HT / PF12TBT was 2% [99].

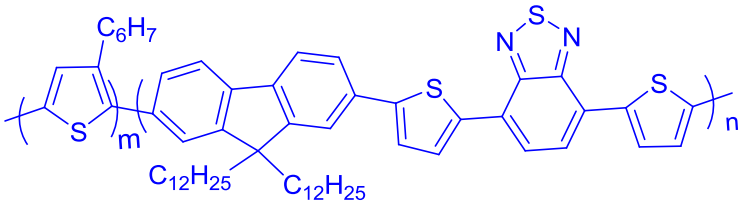

PCE = 2 %

Figure 50: The structure of P3HT / PF12TBT blend.

This part of the project is aimed at synthesising and characterizing poly-(3-hexylthiophene) (P3HT) **(P9)** with high yield of H/Br end group to be used as electron donor with different series of polymers Figure 51 .

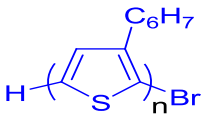

P9

Figure 51: The target polymer P9.

The aim is to synthesis and characteriz di-block co-polymers using (**P9)** as the electron donor blocks and investigate their performance in solar cell. In this project the P3HT is to be used as electron donor with blocks of **P1** , **P3** , **P4** as electron acceptor blocks to afford **P10** - **P12** , Figure 52.

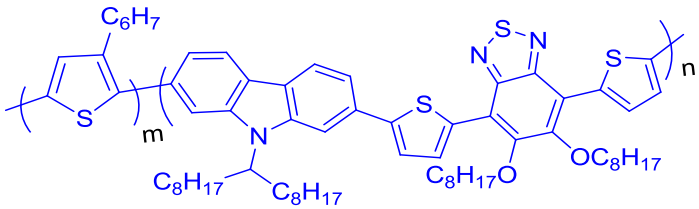

P10

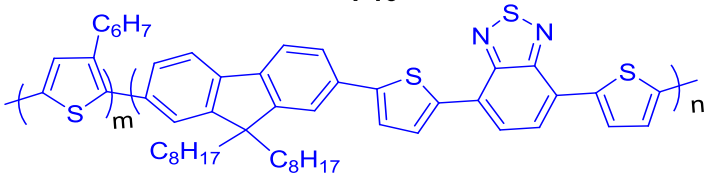

P11

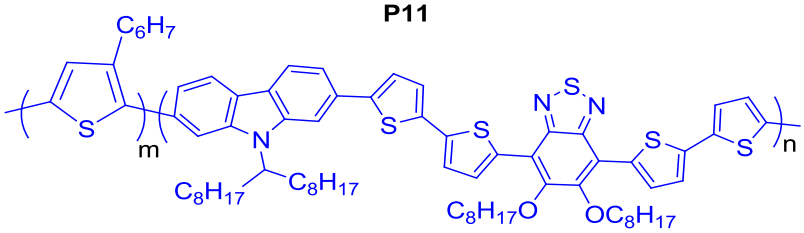

P12

Figure 52: The structure of the target di-block co-polymers P10 , P11 and P12.

Chapter 3: Experimental

3.1 Materials

All chemicals were ordered from commercial suppliers (Sigma-Aldrich, Fisher, Alfa Aesar and Acros Organics) and used as received unless stated otherwise. Dry solvents were used for reactions unless stated otherwise, most of them were obtained from the Grubbs solvent purification system such as hexane, DCM, chloroform, THF, DMF, toluene and acetonitrile. Reagent grade solvents were obtained from internal stores and used for extraction, chromatography and some reactions. Most of the reagents, acids, bases, salts and drying agents were obtained from internal stores. All the reactions and polymerizations were carried out under an inert atmosphere of nitrogen or argon, using Schlenk line techniques.

3.2 Analysis techniques

3.2.1 Thin layer chromatography (TLC)

TLCs were run on silica-coated aluminium plates. The chromphores were visualised by UV light.

3.2.2 Nuclear magnetic resonance spectra (NMR)

NMR spectroscopy was recorded on Bruker Avance 250 (250 MHz), Avance 400 (400 MHz) and Bruker DRX-500 (500 MHz) NMR spectrometers at 22 ˚C in acetone - d_6 chloroform-d_6 for monomers and intermediate products. The NMR spectroscopy of the copolymers were reported on Bruker 500 (500 MHz) NMR spectrometer at 80 ^{o}C and 100 ^{o}C in1,1,2,2-tetrachloroethane.

3.2.3 Infra-red absorption spectroscopy (IR)

IR absorption spectra were recorded on the PerkinElmer Spectrum 100 FT-IR spectrometer.

3.2.4 UV-visible absorption spectroscopy

UV-visible absorption spectra were measured by Hitachi U-2010 Double Beam UV / Visible Spectrophotometer. The absorbance of copolymers were measured in a solution of chloroform at ambient temperature using rectangular quartz cuvettes (light path = 10 mm) . In addition, UV-visible absorption spectra analysis of the copolymers were done in thin films which were performed by dip coating quartz plates into approximately 1 mg cm^3 solutions of chloroform., These plates were then dried in the air at room temperature.

3.2.5 Elemental analysis

Elemental analyses for both monomers and copolymers were performed using the Perkin Elmer 2400 CHN Elemental analyser for CHN analysis while sulphur and halides (anions) were analyzed by the Schoniger oxygen flask combustion method. The weights submitted for analysis were 5 mg for both CHN and anion analysis.

3.2.6 Mass spectrometry

Matrix Assisted Laser Desorption / Ionisation, Time of Flight (MALDI-ToF) spectra were recorded on a Bruker Reflex III in reflection positive-ion mode and with using trans-2-[3-(4-tert-butylphenyl)-2-methyl-2-propenylidene]malononitrile (DCTB) as a matrix. Mass spectroscopy were recorded on Perkin Elmer Turbomass Mass Spectrometer equipped with autosystem XL GC and autosampler. It can operate in both electron ionisation (EI) and chemical ionisation (CI) modes.

3.2.7 Melting points

Melting points were measured using Gallenkamp Melting Point Apparatus with mercury thermometer.

3.2.8 Gel permeation chromatography analysis (GPC)

GPC data was collected from a system which consisted of a Hewlet-Packard 1090 HPLC, a Hewlett Packard Model 1037 Differential Refractive Detector, two Polymer Labs PLgel 5 µm Mixed-C (300 mm × 7.5 mm) column and a guard (50 mm × 7.5 mm), using $CHCl_3$ and 1,2,4-trichlorobenzene as the eluents at rate of 1 cm^3 $minute^{-1}$. The oven was adjusted to 100 ˚C for runs using 1,2,4-trichlorobenzene and the polymer samples were prepared as solutions in 1,2,4-trichlorobenzene (2.5 mg cm^{-3}) then spiked with toluene as a reference. The GPC curves were calibrated with a series of polystyrene narrow standards and obtained by the RI- detection method. The polydispersity index (PD) was calculated as shown in the equation below.

$$PD = \frac{M_w}{M_n}$$

Where Mw is the weight-average molecular weight of the polymer and Mn is the number-average molecular weight of the polymer.

3.2.9 Cyclic voltammetry (CV)

Cyclic voltammograms were performed using a Princeton Applied Research Model 263A Potentiostat/Galvanostat. All measurements were performed under an inert argon atmosphere at approximately 25 ˚C. The electrolyte solution was 10 ml of tetrabutylammonium perchlorate in dry acetonitrile solution (0.1 M). The system consists of a three electrodes immersed in an electrochemical cell containing electrolyte solution under an inert atmosphere of argon. The first electrode is the reference electrode Ag/Ag^+

which is a wire of silver in silver nitrate solution in the electrolyte solution (0.01 mol L-1). The second one is the working electrode which is a metal of platinum with 2 mm-diameter, and the counter electrode which is a platinum wire. The sample measurement was performed by drop casting of 1.0 mm^3 of polymer solution onto the working electrode to form a polymer solid state thin film which is left to dry in the air at room temperature.

3.2.10 Thermo-gravimetric analysis (TGA)

TGA curves were obtained by Perkin Elmer TGA-7 Thermogravimetric Analyser at a scan rate of 10 ˚C/ minute under an inert atmosphere of nitrogen. Sample weights were about 10 mg.

3.3 Preparation of Monomers

3.3.1 Synthesis of 1,2-Bis(octyloxy)benzene (1)

1,2-Bis(octyloxy)benzene **(1)** was obtained using a procedure by Zhang [101].

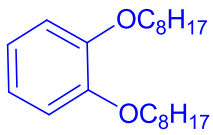

(1)

To a mixture of catechol (20.00 g, 181.64 mmol), 1-bromooctane (65.64 ml, 1.118 g/ml, 379.97 mmol) and potassium carbonate K_2CO_3 (76.00 g, 549.80 mmol) was added dry DMF (100 ml). Then the mixture was stirred under N_2 overnight at 100 °C. Water (200 ml) was added and the organic layer was separated. The aqueous layer was extracted with DCM (3 x 100 ml) and the combined organic phases were washed with water (5 x 200 ml) to remove DMF. Then it was dried over $MgSO_4$ and the solvent was removed in vacuum. The product was recrystallized twice from ethanol to obtain 1,2-bis(octyloxy)benzene **(1)** as white needle crystals (41.00 g, 90% yield). The product showed a single spot on TLC (R_f = 0.55) (silica-gel plates - petroleum ether : ethyl acetate (8: 2)). M.p. = 24 .5 - 25 °C. ^{1}HNMR($CDCl_3$):(δ_H/ppm) 6.91 (s, 4 H), 4.01 (t, 4 H, J = 6.8 Hz),1.95–1.20 (m, 24H), 0.91 (t, 6H, J = 6.7Hz). ^{13}C NMR ($CDCl_3$): δ = 149.23, 121.00, 114.03, 69.24, 31.89, 29.46, 29.38, 29.35, 26.10, 22.73, 14.15. FT-IR (ATR): (cm^{-1}) 2922, 2848,1593, 1507, 1466, 1451, 1389, 1331, 1253, 1222, 1129, 1060, 963, 732. Mass (EI+): (m/z) 334 (M^+); (calculated for $C_{22}H_{38}O_2$: 334.54). Elemental Analysis (%) calculated for $C_{22}H_{38}O_2$: C, 79.02; H, 11.82 .Found: C, 79.14; H, 12.46.

3.3.2 Synthesis of 1,2-dinitro-4,5-bis(octyloxy)benzene (2).

1,2-Dinitro-4,5-bis(octyloxy)benzene **(2)** was prepared according to procedure by Sessler [102].

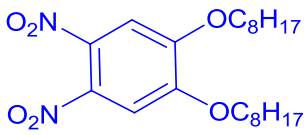

(2)

To a two neck round-bottom flask containing dichloromethane (240 ml), acetic acid (240 ml), and 1,2-bis(octyloxy)benzene **(1)** (20.06 g, 59.96 mmol) cooled to 10 °C was added dropwise 65% nitric acid (40 ml). The reaction was left to warm at ambient temperature and stirred for 1 hour. The mixture was again cooled to 10 °C and nitric acid (80 ml) was added dropwise. The mixture was again left to warm at room temperature and the mixture was stirred for 40 hours. After completion of the reaction, the reaction mixture was poured into ice-water and the dichloromethane layer separated. The aqueous phase was extracted with DCM (3× 200 ml). The combined organic phase was washed with water (3×200 ml), sat. $NaHCO_3$ (aq) , brine NaCl (aq) and dried over $MgSO_4$.The crude product **(2)** was recrystallized from ethanol as yellow crystals (22.00 g, 87% yield). M.p. = 87 – 88 °C. ^{1}HNMR ($CDCl_3$) : (δ_H/ppm) 7.30 (s, 2H), 4.12 (t, 4H, J = 6.6 Hz), 1.94–1.82 (m,4H), 1.54–1.23(m, 20H), 0.90 (t, 6H , J = 6.5 Hz). ^{13}C NMR ($CDCl_3$) : (δ_C/ppm)151.78, 136.40, 107.84, 70.19, 31.77, 29.20, 28.69, 25.82, 25.66, 14.11. FT-IR (ATR): (cm^{-1}) 3071, 2956, 2921, 2853, 1587, 1526, 1464, 1371, 1354, 1335, 1290, 1225, 1035, 993, 955, 909, 828, 811, 751, 720, 665, 618. Mass (EI+): (m/z) 424 (M^+); (calculated for $C_{22}H_{36}N_2O_6$: 424.53). Elemental Analysis (%) calculated for $C_{22}H_{36}N_2O_6$: C, 62.24; H, 8.55; N, 6.60. Found: C, 62.37; H, 8.75; N, 6.37.

3.3.3 Synthesis of 4, 5-Bis(octyloxy)benzene-1,2-diaminium chloride (3)

4,5-Bisoctaoxybenzene-1,2-diaminium chloride **(3)** was performed according to procedure by Martin [103] .

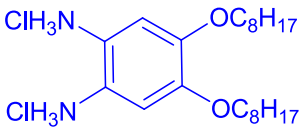

(3)

A mixture of 1,2-dinitro-4,5-bis(octyloxy)benzene **(2)** (2.00 g, 3.37 mmol) and $SnCl_2$ (5.10 g , 26.9 mmol) in ethanol (50 ml) and conc. HCl (20 ml) was heated to 85 ^oC overnight. After cooling to room temperature the product was filtered and washed with water and methanol. Then, it was dried at room temperature under an inert atmosphere of argon which is used directly in next reaction without further analysis. The obtained product **(3)** was an off-white powder (1.80 g, 88% yield).

3.3.4 Synthesis of 5,6 – Bis-octyloxy-benzo[1,2,5]thiadiazole (4)

5,6 – Bis-octyloxy-benzo[1,2,5]thiadiazole **(4)** was perpared according to a procedure by Bouffard and Swager [104].

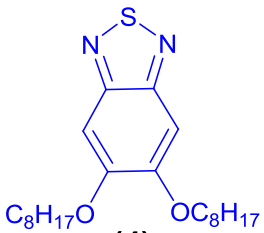

(4)

To a mixture of 4,5-bis(octyloxy)benzene-1,2-diaminium chloride **(3)** (7.20 g, 16.45 mmol) and triethylamine (16 ml , 25.1 mmol) in DCM (188 mL) was slowly added a solution of thionyl chloride (2.26 ml , 31.25 mmol) in DCM (24 mL) . After addition the mixture was heated to reflux for 6 hours. The cooled solution was concentrated in vacuum

followed by trituration in water. After stirring for 30 min, the product was filtered and recrystallized from ethanol to obtain **(4)** as an off-white solid (5.05 g, 88 % yield). M.p. = 97 – 98 °C. ^{1}HNMR($CDCl_3$):(δ_H/ppm) 7.15 (s,2H), 4.11 (t, *J* = 6.5 Hz, 4H), 1.98 – 1.85 (m, 4H), 1.59–1.23 (m, 20H), 0.91 (t, 6H , *J* = 6.7). ^{13}C NMR ($CDCl_3$):(δ_C/ppm) 154.12, 151.39, 98.38, 69.13, 31.81, 29.33, 29.28, 28.74, 26.03, 22.69, 14.13. FT-IR (ATR): (cm^{-1}) 3116, 3081, 3053, 2956, 2917, 2872, 2849, 1700, 1614, 1528, 1497, 1460, 1403, 1378, 1308, 1257, 1213, 1194, 1179, 1126, 1063, 1013, 998, 958, 937, 909, 851, 823, 753, 784, 723, 663, 604. Mass (EI+): (m/z) 392 (M^+); (calculated for $C_{22}H_{36}N_2O_2S$: 392.60). Elemental Analysis (%) calculated for $C_{22}H_{36}N_2O_2S$: C, 67.30; H, 9.24; N, 7.14; S, 8.17 Found: C, 67.09; H, 9.54; N, 6.92.

3.3.5 Synthesis of 4,7-Dibromo-5,6-bis-octyloxy-benzo[1,2,5]thiadiazole (5)

4,7-Dibromo-5,6-bis-octyloxy-benzo[1,2,5]thiadiazole **(5)** was synthesized according to a procedure by Bouffard and Swager [104].

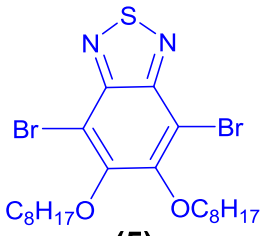

(5)

To a solution of 5,6 – bis-octyloxy-benzo[1,2,5]thiadiazole **(4)** (2.61 g, 6.64 mmol) in a mixture of dichloromethane (130 ml) and acetic acid (57 ml) was added bromine (2 ml , 40.55 mmol), and the resulting mixture was stirred in the dark for 48 h at room temperature. The mixture was then poured in water (300 ml), extracted with DCM (3×200 ml), sequentially washed with water, saturated $NaHCO_3$ (aq), 1M Na_2SO_3 (aq) and the solvents were evaporated under reduced pressure. The crude product was purified by

recrystallization from ethanol twice to give the product as a white powder (3.00 g, 82% yield). M.p. = 45 - 46 °C. ^{1}HNMR($CDCl_3$):(δ_H/ppm) 4.18 (t, *J* = 6.6 Hz, 4H), 1.96–1.85 (m, 4H), 1.59 – 1.28 (m, 20H), 0.91 (t, *J* = 6.6 Hz, 6H). ^{13}C NMR ($CDCl_3$) : (δ_C/ppm) 154.50, 150.37, 106.28, 75.16, 31.85, 30.28, 29.41, 29.29, 26.00, 22.68, 14.13. FT-IR (ATR): (cm^{-1}) 2955, 2922, 2873, 2848, 2160, 2023, 1590, 1468, 1431, 1385, 1284, 1267, 1214, 1169, 1057, 1028, 992, 942, 891, 881, 847, 738, 709, 625. Mass (EI+); (m/z): 548, 550, 552 (M^+) ; (calculated for $C_{22}H_{34}Br_2N_2O_2$ S: 550.39). Elemental Analysis (%) calculated for $C_{22}H_{34}Br_2N_2O_2S$: C, 48.01 ; H, 6.23; N, 5.09 ; Br , 29.04 ;S , 5.83. Found: C, 48.01 ; H, 6.28; N, 4.86 .Br , 29.0; S , 5.92.

3.3.6 Synthesis of 2,2'-bithiophen-5-ylributylstannane (6)

2,2'-Bithiophen-5-ylributylstannane **(6)** was synthesized according to procedure by Jousselme [60].

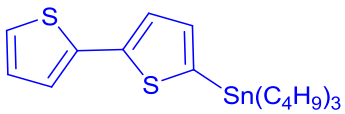

(6)

Bithiophene (2.56 g , 16 mmol) in THF (50 ml) was treated dropwise with t-BuLi (1.6 M in hexane , 10 ml , 16 mmol) and stirred for 0.5 h at -78 ^{0}C under an argon atmosphere. To this solution Bu_3SnCl (5ml , 16 mmol) was added. The reaction mixture was left to warm to room temperature and further stirred for 6 hours then ethanol (2 ml) was added to remove unreacted n-BuLi. The solution was evaporated and the residue was dissolved in hexane (100 ml) and filtered . The obtained oil was purified by column chromatography (98% petroleum ether / 2% triethylamine) to give the crude product as a colourless oil (7.77 g, 90% yield). ^{1}HNMR($CDCl_3$):(δ_H/ppm) 7.31 (d, 1H, *J* = 3.28 Hz), 7.21 – 7.19 (m, 2H), 7.08 (d, 1H, *J* = 3.36 Hz) , 7.02 (t , IH, *J* = 4.36 Hz

), 1.78 – 1.51 (m, 6H), 1.46 – 1.07 (m, 12H), 0.92 (t, 9H, *J* = 7.3 Hz). ^{13}C NMR ($CDCl_3$):(δ_C/ppm): 136.08, 127.77, 127.73, 124.98, 124.35, 123.96, 123.76, 123.45, 28.86, 27.28, 16.39, 13.70. FT-IR (ATR): (cm^{-1}) 3437, 3105, 3070, 2981, 2914, 1413, 773, 797, 692. :Mass (EI+); (m/z): 455 (M^+) ;(calculated for $C_{20}H_{32}S_2Sn$: 455.31). Elemental Analysis (%) calculated for $C_{20}H_{32}S_2Sn$: C, 52.76 ; H, 7.08; S, 14.08. Found : C, 52.60; H, 7.01; S, 13.98.

3.3.7 Synthesis of 4,7-di(2,2'-bithiophen-5-yl)-5,6-bis(octyloxy)benzo[c][1,2,5]thiadiazole (7)

Synthesis of 4,7-di(2,2'-bithiophen-5-yl)-5,6-bis(octyloxy)benzo[c][1,2,5]thiadiazole **(7)** was undertaken via a modified procedure by Zhou [90].

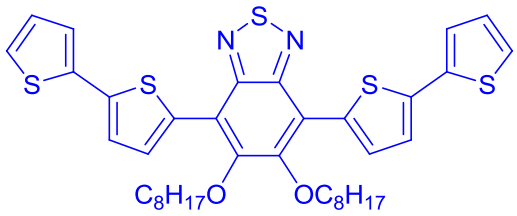

(7)

To 4,7-dibromo-5,6-bis-octyloxy-benzo[1,2,5] thiadiazole **(5)** (3.00g , 5.45 mmol) was added $Pd(OAc)_2$ (20.00 mg , 8.91×10^{-2} mmol) and tri(*o*-tolyl)phosphine (54.23 mg , 0.178 mmol) in toluene (100 ml) then 5,5'-bis(tri-n-butylstannyl)-2,2'-bithiophene **(6)** (6.30 g, 13.84 mmol) was added under argon and the mixture was heated to 95 ^{0}C for 24 hours. The mixture was cooled to room temperature and water (100 ml) was added. The organic phase was separated and the water phase was washed with toluene (2 ×150 ml). The combined organic phases were washed with brine and then water, dried over $MgSO_4$ and the solvent evaporated to afford the crude product. The crude product was purified by using column chromatography (silica gel 15 40 μm, eluted with petroleum ether (40 -60) / chloroform, gradient 5 : 1 to obtain **(7)** as orange solid crystals (912.00 mg ,92 % yield).

mp = 89 °C.^{1}HNMR($CDCl_3$):(δ_H/ppm) 8.52 (d, *J* = 4.08 Hz, 2H), 7.31 (d, *J* = 4.08 Hz, 4H), 7.28 (d, *J* = 4.08 Hz, 2H), 7.09 (dd, *J* = 5.32, 4.08 Hz, 2H), 4.19 (t, *J* = 7.20 Hz 4H), 2.01 (m, 4H), 1.53-1.31 (br, 20H), 0.91 (t, *J* = 6.88 Hz , 6H).^{13}C NMR ($CDCl_3$):(δ_C/ppm)151.60, 150.79, 138.86, 137.59, 133.16, 131.64, 127.96, 124.65, 123.74, 123.58, 117.29, 74.55, 31.86, 30.47, 29.60, 29.35, 26.09, 22.72, 14.14. FT-IR (ATR): (cm^{-1}) 2954, 2851, 2921,1556, 1494, 1466, 1437, 1426, 1392, 1375, 1347, 1281, 1213, 1176, 1090, 1056, 1016, 953, 938, 920, 894, 883, 855,830, 757, 745, 722, 675, 650, 633. Mass (EI+); (m/z): 720 (M^+) ;(calculated for $C_{38}H_{44}N_2O_2S_5$: 720.20). Elemental Analysis (%) calculated for $C_{38}H_{44}N_2O_5S_5$: C, 63.29; H, 6.15; N 3.88. Found: C, 63.07; H, 6.11; N 3.72.

3.3.8 Synthesis of 4,7-bis(5'-bromo-2,2'-bithiophen-5, 6-bis(octyloxy)benzo[c][1,2,5]thiadiazole (8).

4,7-Bis(5'-bromo-2,2'-bithiophen-5-yl)-5,6-bis(octyloxy)benzo[c][1,2,5]thiadiazole **(8)** was performed via a modified procedure by Zhou [90].

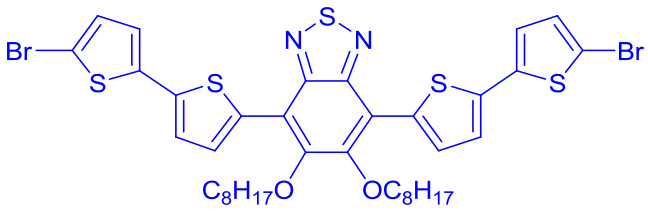

(8)

A two-necked flask under argon containing 4,7-di(2,2'-bithiophen-5-yl)-5,6-bis(octyloxy)benzo[c][1,2,5]thiadiazole **(7)** (1.00 g , 1.387 mmol) and N-bromosuccinimide (0.48 mg, 2.697 mmol) was degassed. To the mixture was added chlorobenzene (30 ml), the flask was degassed, the mixture was heated to 55 ^{o} C for 3 h in the dark and then heated to 100 ^{o} C for 15 min. The solvent was evaporated and the crude product was purified by column chromatography using petroleum ether (40 - 60) / chloroform (4: 1) . The resulting product was precipitated in hot methanol affording the

product **(8)** as dark red crystals (0.98 g, 80% yield). mp = 93 °C. ^{1}HNMR ($CDCl_3$):(δ_H/ppm) 8.51 (d, *J* = 4.08 Hz, 2H), 7.25 (d, *J* = 4.08 Hz, 2H), 7.04 (m, 4H), 4.17 (t, *J* = 6.95 Hz, 4H), 1.99 (m, 4H), 1.53-1.20 (br, 20H), 0.91 (t, *J* = 6.95 Hz, 6H). ^{13}C NMR ($CDCl_3$) : (δ_C/ppm)151.67, 150.70, 139.10, 137.80, 133.59, 131.70, 130.79, 123.78, 117.25, 111.27, 74.61, 31.85, 31.87, 30.45, 29.59, 29.36, 26.09, 22.37, 14.14. FT-IR (ATR): (cm^{-1}) 2950, 2920, 2870, 2851, 1723, 1555, 1462, 1262, 1281,1256, 1214, 1194, 1179, 1126, 1062, 1024, 793, 782, 773, 677.. Mass (EI+); (m/z): 876 , 878, 880 (M^+) ;(calculated for $C_{38}H_{42}Br_2N_2O_2S_5$: 878.89).Elemental Analysis (%) calculated for $C_{38}H_{42}Br_2N_2O_5S_5$: C,51.93; H, 4,82; N, 3.19. Found: C52.59; H, 4.94; N, 2.76.

3.3.9 Synthesis of 1,4-Dibromo-2-fluoro-5-nitrobenzene (9)

1,4-Dibromo-2-fluoro-5-nitrobenzene **(9)** was synthesized according to Chen [105].

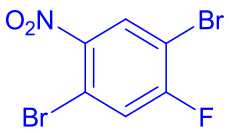

(9)

1,4-Dibromo-2-fluorobenzene (100.00 g, 394 mmol) was dissolved in a 2:2:1 mixture of DCM (300 ml), trifluoroacetic acid (300 ml), trifluoroacetic anhydride (150 ml). The solution was cooled down to 0 °C in an ice bath, and then ammonium nitrate (38.80 g, 484 mmol) was added slowly with stirring. The mixture was allowed to warm to room temperature and left stirring overnight. Then the reaction mixture was poured onto ice (500 g) and the product was extracted with DCM (3 x 300 mL). The organic phase was dried over $MgSO_4$ and the solvent removed in vacuo to give the crude product as a yellow solid. The product was recrystallised from ethanol to obtain 1,4-dibromo-2-fluoro-5-nitrobenzene **(9)** as yellow crystals (101.60 g, 86% yield). The product showed a single spot on TLC (R_f = 0.66) in DCM/Hexane (1:1). m.P = 60- 62.5 °C. ^{1}HNMR

($CDCl_3$):(δ_H/ppm) 8.20 (d, J_{H-F} = 6.4 Hz); 7.55 (d, J_{H-F} = 7.4 Hz). ^{13}C NMR ($CDCl_3$) δ_C/ppm: 159.31 (d, J_{C-F} = 258.5 Hz), 130.93, 123.01 (d, J_{C-F} = 26.5 Hz), 122.74, 115.00, 108.76 (d , J_{C-F} = 22.7 Hz). FT-IR (ATR): (cm^{-1}) 3091, 3022, 2158, 2029, 1975, 1760, 1585, 1567, 1526, 1344, 1283, 1250, 1223, 1131, 1065, 933, 891, 869, 829, 752, 695, 643, 623. Mass (EI+); (m/z): 297, 299, 301 (M^+); (calculated for $C_6H_2Br_2FNO_2$: 298.89). Elemental Analysis (%) calculated for $C_6H_2N_2OBr_2F_2$: C, 24.11; H, 0.67; N, 4.96; Br, 53.47. Found: C, 24.10; H, 0.37; N, 4.58; Br, 53.42.

3.3.10 Synthesis of 4,4'-Dibromo-5,5'-difluoro-2,2'-dinitrobiphenyl (10)

4,4'-Dibromo-5,5'-difluoro-2,2'-dinitrobiphenyl **(10)** was obtained by a modified procedure of Yamato [106].

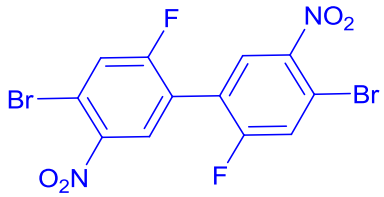

(10)

To 1,4-dibromo-2-fluoro-5-nitrobenzene **(9)** (50.89 g, 170.20 mmol) in dry DMF (250 ml) was added Cu powder (14.42 g, 226.90 mmol) and the mixture was refluxed for 3 hours. The reaction mixture was cooled to room temperature and toluene was added (250 mL) and the mixture stirred for a further 1 hour. The unreacted Cu powder was filtered off and the filtrate washed with a saturated NaCl solution. The organic layer was dried over $MgSO_4$ and the solvent removed in vacuo to give the crude product. The product was recrystallised from ethanol and dried in vacuo to give 4,4'-dibromo-2,2'-difluoro-5,5'-dinitrobiphenyl **(10)** as yellow crystals (26.00 g, 70% yield) . The product gave a single spot on TLC (R_f = 0.78) in petroleum ether (40-60) /ethyl acetate (8:2).m.p. = 114.5-115.2 °C. ^{1}HNMR ($CDCl_3$):(δ_H/ppm) 8.57 (d, 2H, J_{H-F} = 6.1 Hz) , 7.09 (d, 2H J_{H-F} = 7.7

Hz).^{13}C NMR ($CDCl_3$) δ_C/ppm: 162.99 (d, J_{C-F} = 258.4 Hz); 160.40; 134.12 ; 131.14 ; 118.41(d, 2C , J_{C-F} = 25.5 Hz) ; 110.25 (d, J_{C-F} = 22.6 Hz). FT-IR (ATR): (cm^{-1}) 3061, 2159, 2031, 1611, 1563, 1524, 1489, 1471, 1394, 1339, 1292, 1227, 1184, 1113, 1065, 994, 902, 876, 846, 821, 760.758, 692, 657. Mass (EI+); (m/z) : 436, 438, 440 (M^+); (calculated for $C_{12}H_4Br_2F_2N_2O_4$: 437.98).Elemental Analysis (%) calculated for $C_{12}H_4N_2O_4\ F_2Br_2$: C, 32.91; H, 0.92; N, 6.40; Br, 36.49. Found: C, 33.07; H, 0.65; N, 6.19; Br, 36.45.

3.3.11 Synthesis of 2,2'-Diamino-4,4'-dibromo-5,5'-difluorobiphenyl (11)

2,2'-Diamino-4,4'-dibromo-5,5'-difluorobiphenyl (11) was obtained by a modified procedure of Yamato [106].

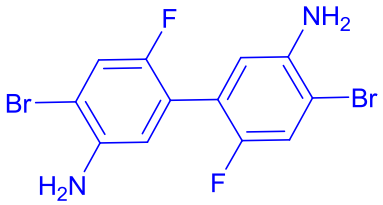

(11)

4,4'-Dibromo-5,5'-difluoro-2,2'-dinitrobiphenyl **(10)** (11.60 g, 26.50 mmol) was added to ethanol (200 ml) and HCl (60 ml , 32 % wt), then tin powder (12.45 g, 104.80 mmol) was added. The reaction was taken to reflux for 1.5 hour and then cooled to room temperature and a further portion of tin powder (12.45 g, 104.80 mmol) was added and the mixture refluxed for 1 hour. The reaction was again cooled to room temperature and the unreacted tin powder was filtered off. The filtrate was poured onto ice and a 10 wt % solution of NaOH (1000 ml). The filtrate was then extracted with diethyl ether (4 x 300 ml) and the resulting fine white suspension was filtered off using Celite filter gel and washed with diethyl ether. The organic layer was washed with distilled H_2O (3 x 250 ml), dried over $MgSO_4$ and the solvent removed in vacuo to give a brown solid. The product was then

recrystallised from ethanol to obtain pale brown crystals and dried in vacuo to give 4,4'-dibromo-6,6'-difluorobiphenyl-3,3'-diamine **(11)** as pale brown crystals (9.40 g, 89 % yield). The product gave a single spot on TLC (R_f = 0.40) in petroleum ether (40-60) / ethyl acetate (8:2).M.P.= 162.1-168 °C.^{1}HNMR ($CDCl_3$):(δ_H/ppm) 7.11 (d, 2H, J_{H-F} = 5.7 Hz) , 6.95 (d, 2H, J_{H-F} = 9.18 Hz), 4.66 (b, 4H). ^{13}C NMR ($CDCl_3$) δ_C/ppm: 152.3 (d, J_{C-F} = 237.6 Hz); 140.9; 122.8; 119.7; 117.9(d, J_{C-F} = 22.9 Hz); 109.4 (d, J_{C-F} = 21.5 Hz). FT-IR (ATR): (cm^{-1}) 3309, 3191, 2358, 2193, 1622, 1483, 1406, 1297, 1274, 1241, 1196, 1163, 1056, 992, 889, 867, 815, 757, 702. Mass (EI+); (m/z): 376, 378, 380 (M^+); (calculated for $C_{12}H_8Br_2F_2N_2$: 378.01). Elemental analysis (%) calculated for $C_{12}H_8Br_2F_2N_2$: C, 38.13; H, 2.13; N, 7.41; Br, 42.28. Found: C, 38.72; H, 2.04; N, 7.47; Br, 42.34.

3.3.12 Synthesis of 2,7-dibromo-3,6-difluoro-*9H*-carbazole (12)

2,7-Dibromo-3,6-difluoro-*9H*-carbazole **(12)** was prepared according to the procedure by Sonntag [107] .

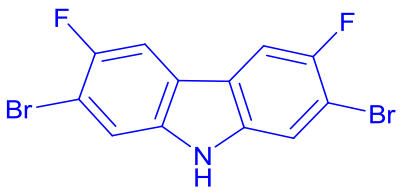

(12)

To 4,4'-dibromo-6,6'-difluorobiphenyl-3,3'-diamine **(11)** (4.00 g, 10.58 mmol) was added concentrated phosphoric acid (85%) (90 ml) and the mixture heated at 190 °C for 24 hours. The crude product was filtered and washed with water. The crude product was then solubilised in hot toluene and the solution filtered through a silica gel plug and then washed with hot toluene, then dried over $MgSO_4$. The solvent was removed in vacuo to give a pale orange solid. The crude product was recrystalised from toluene/hexane (10:1)

to give the product **(12)** as an ivory powder (2.90 g, 76 % yield). The product gave a single spot on TLC (R_f = 0.41) in petroleum ether (40-60) /ethyl acetate (8:2). m.p. = 348 – 350 °C. ^{1}H NMR (Acetone-d_6) :(δH/ppm) 10.63 (br, 1H) , 8.10 (d, 2H, J_{H-F} = 8.9 Hz),7.83 (d, 2H, J_{H-F} = 5.8 Hz). ^{13}C NMR (Acetone-d_6) δC/ppm: 153.9 (d, J_{C-F} = 234.0 Hz); 138.6; 123.1; 116.3; 108.1; 107.8 (d, J_{C-F} = 21.0 Hz). FT-IR (ATR): (cm^{-1}) 3451, 3042, 1944, 1704, 1615, 1572, 1477, 1442, 1350, 1279, 1257, 1205, 1177, 1151, 1039, 991, 909, 857, 836, 788, 719, 676, 626. Mass (EI+); (m/z): 359, 361, 363 (M^{+}); (calculated for $C_{12}H_5NF_2Br_2$: 360.98). Elemental Analysis (%) calculated for $C_{12}H_5NF_2Br_2$: C, 39.93; H, 1.40; N, 3.88; Br, 44.27. Found: C, 39.24; H, 1.07; N, 3.96; Br, 44.44.

3.3.13 Synthesis of heptadecan-9-ol (13)

Heptadecan-9-ol **(13)** was synthesized according to the procedure by Leclerc et al [92].

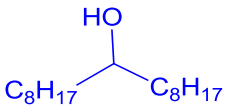

(13)

In a 1L 3-necked flask containing Mg (13.37 g, 549.9 mmol) was added dry THF (270 ml). Then a solution of 1-bromooctane (96.57 g, 500 mmol) in THF (160 ml) was added drop-wise to the Mg suspension. An ice bath was used to maintain the temperature below 25°C. The mixture was then heated to reflux for 2 hours to obtain octylmagnesium bromide as a grey solution (Grignard solution). Another 1L 2-necked flask containing a solution of ethyl formate (12.35 g, 166.7 mmol) in THF (285 ml) was cooled to -78 °C before the octylmagnesium bromide solution was added dropwise and the resulting mixture stirred overnight at room temperature. Methanol and a saturated NH_4Cl solution were then added to quench the reaction. The mixture was extracted with diethyl ether (3 x 350 ml) and

the organic phase washed with a saturated NaCl solution. The organic layer was dried over $MgSO_4$ and the solvent removed in vacuo to give the product as colourless oil which turns into solid at room temperature. The product gave a single spot on TLC (R_f = 0.52) using petroleum ether (40-60) /ethyl acetate 10:1 to obtain **(13)** as colourless oil (42.00 g, 98 % yield) which used directly in the next step without further purification. M.p. = 29 - 31 °C. ^{1}HNMR($CDCl_3$):(δH/ppm) 3.67-3.57 (br m, H), 1.46 (m, 8H) ,1.29 (m, 21H) , 0.89 (t, 6H, *J* = 6.9 Hz).^{13}C NMR ($CDCl_3$) δC/ppm: 72.0, 37.4, 31.9, 29.7, 29.6, 29.3, 25.7, 22.7, 14.1. FT-IR (ATR): (cm^{-1}) 3315, 2996, 2916, 2872, 2848, 1465, 1375, 1352, 1241, 1135, 1124, 1089, 1065, 1054, 1026, 1008, 986, 894, 846, 796, 720. Mass (EI+); (m/z); 256 (M^+); (calculated for $C_{17}H_{36}O$: 256.47). Elemental Analysis (%) calculated for $C_{17}H_{36}O$: C, 79.61; H, 14.15 Found: C, 80.07; H, 14.90.

3.3.14 Synthesis of heptadecan-9-yl 4-methylbenzenesulfonate (14)

Heptadecan-9-yl 4-methylbenzenesulfonate **(14)** was prepared according to the procedure by Leclerc [92].

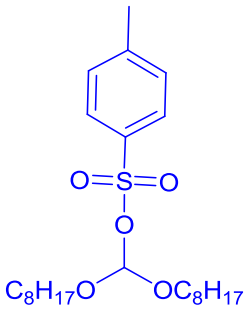

(14)

p-Toluenesulfonyl chloride (65.00 g, 340.00 mmol) in DCM (235 ml) was added to heptadecan-9-ol **(13)** (48g, 190.00 mmol), Et_3N (68 ml, 49.00 mmol) and Me_3N.HCl (10.00 g, 22.00 mmol) in DCM (200 ml) at 0 °C. The solution was stirred for 90 mins after

which H_2O was added and the product extracted with DCM (3 x 250 mL). The organic phase was then washed with H_2O , brine NaCl then dried over Na_2SO_4 .The solvent was removed in vacuo to give the product as a low melting point white solid. The product was purified via silica gel column chromatography, eluting with (89 % hexane, 9 % ethylacetate, 2 % Et_3N) to obtain 9-heptadecane p-toluenesulfonate **(14)** as white solid (75.00 g, 96 % yield). The product gave a single spot on TLC (R_f = 0.49) in hexane/ethyl acetate (9:1).M.p.= 31–32.5 °C.^{1}HNMR($CDCl_3$):(δH/ppm) 7.80 (d, 2H, *J* = 8.2 Hz), 7.34 (d, 2H, *J* = 8.2 Hz),4.50 (m, H), 2.46 (s, 3H), 1.62-1.48 (m, 4H), 1.35-1.10 (m, 24H), 0.89 (t, 6H, *J* = 6.8 Hz). ^{13}C NMR ($CDCl_3$) δC/ppm: 144.2, 134.7, 129.6, 127.7, 84.6, 34.1, 31.8, 29.7, 29.6, 29.3, 24.6, 22.6, 21.6, 14.1. FT-IR (ATR): (cm^{-1}) 2955, 2923, 2873, 2851, 1598, 1466, 1353, 1353, 1305, 1185, 1172, 1150, 1096, 1021, 964, 895, 881, 816, 766, 719, 661.Mass (EI+): (m/z) 410 (M^+); (calculated for $C_{24}H_{42}O_3S$: 410.65).Elemental Analysis (%) calculated for $C_{24}H_{42}O_3S$: C, 70.19; H, 10.31; S, 7.81. Found: C, 71.11; H, 10.98; S, 7.87.

3.3.15 Synthesis of 2,7-dibromo-3,6-difluoro-9-(1-octyl-nonyl)-*9H*-carbazole (15)

2,7-Dibromo-3,6-difluoro-9-(1-octyl-nonyl)-9H-carbazole **(15)** was synthesized using a modified procedure by Leclerc [92]

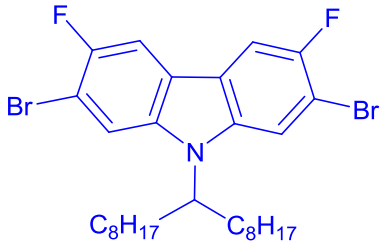

(15)

2,7-Dibromo-3,6-difluoro-*9H*- carbazole **(12)** (11.00 g, 30.47 mmol) and KOH (8.55 g, 11.00 mmol) were dissolved in dried DMSO (50 ml). Heptadecan-9-yl-4-

methylbenzenesulfonate (14) (18.07 g, 45.53 mmol) was dissolved in dried DMSO (35 ml) and was added dropwise over 2 hours at room temperature and the reaction was allowed to stir for 6 hours. The reaction was poured onto distilled H_2O (300 ml), and the product extracted with hexane (3 x 250 ml). The combined organic fractions were dried over $MgSO_4$ and the solvent removed in vacuo. The product was purified via silica gel column chromatography, eluting with hexane. Then the product was recrystallised from methanol to obtain pure product as a brown solid (8.93 g, 67.22 % yield). The product gave a single spot on TLC (R_f = 0.50) in 100 % hexane. m.p. = 78 – 79.5 °C. ^{1}HNMR ($CDCl_3$):(δ_H/ppm) 7.79-7.68 (br m , 2H), 7.57 (d, 2H, J = 4.11 Hz), 4.45-4.34 (m, 1H), 2.26-2.12 (m, 2H), 1.97-1.86 (m, 2H), 1.29-1.09 (b , 20H), 1.02-0.89 (bm, 4H), 0.85 (t, 6H, J = 7.14Hz).^{13}C NMR ($CDCl_3$), δ_C/ppm: 153.0 (d, J_{C-F} = 237 Hz), 139.4, 135.8, 122.7, 121.1, 115.5, 113.3, 107.5 (bm), 106.7 (d, J_{C-F} = 26 Hz), 57.3, 33.5, 31.7, 29.2, 29.0, 26.6, 22.6, 14.0. FT-IR (ATR): (cm^{-1}) 2953, 2920, 2852, 1601, 1571, 1466, 1449, 1425, 1333, 1296, 1277, 1246, 1192, 1177, 1159, 1042, 980, 937, 854, 809, 796, 720, 692, 639, 619. Mass (EI +); (m/z): 597, 599, 601 (M^+) ; (calculated for $C_{29}H_{39}NF_2Br_2$: 599.43). Elemental Analysis (%) calculated for $C_{29}H_{39}NF_2Br_2$: C, 58.11; H, 6.56; N, 2.34; Br, 26.66. Found: C, 58.29; H, 6.54; N, 2.18; Br, 26.53.

3.3.16 Synthesis of 3,6-difluoro-9-(1-octyl-nonyl)-2,7-bis(4,4,5,5-tetramethyl-1,3,2- dioxaborolan-2-yl)-*9H*-carbazole (16)

3,6-Difluoro-9-(1-octyl-nonyl)-2,7-bis(4,4,5,5-tetramethyl-1,3,2-dioxaborolan-2-yl)-9H-carbazole **(16)** was synthesized using a modified procedure by Brunner [108].

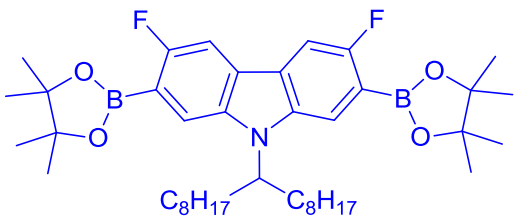

(16)

2,7-Dibromo-3,6-difluoro-9-(1-octyl-nonyl)-9*H*-carbazole **(15)** (5.00 g, 8.34 mmol), bis(pinacolato)diboron (7.42 g, 29.21 mmol), potassium acetate (4.90 g, 49.93 mmol) and Pd(dppf)Cl_2 (0.4 g, 49.00 mmol) in DMF (100 ml) were heated to 100 °C for 36 hours. The reaction mixture was cooled to room temperature, then poured into H_2O (100 ml) and extracted with diethyl ether (3 × 150 ml). The organic phases were combined, then washed with H_2O (2 × 150 mL) and dried over $MgSO_4$. The crude product was dissolved in the minimum amount of acetone and then precipitated in hot methanol (400 ml) which had been ran through a basic column. The product **(16)** was obtained as a light brown solid (4.91 g, 84.8 % yield). m.p. = 140 – 141 °C. ^{1}HNMR ($CDCl_3$):(δ_H/ppm) 7.97-7.83 (b, 1H), 7.82-7.72 (br, 1H), 7.71-7.61 (b, 2H),4.68-4.56 (m, 1H), 2.37-2.23 (bm, 2H), 2.0 - 1.87 (m, 2H), 1.43 (s, 24H), 1.29 -1.08 (b, 20H), 1.04 - 0.89 (m, 4H), 0.84(t, 6H, J = 7.06 Hz). ^{13}C NMR ($CDCl_3$) δ_C/ppm: 160.8 (d, J_{C-F} = 239.0 Hz), 139.4, 136.0, 126.2, 124.8, 119.0, 116.5, 114.8 (b), 106.2 (d, J_{C-F} = 30 Hz), 83.8, 56.5, 33.8, 31.7, 29.3, 29.2, 29.1, 26.6, 24.8, 22.6, 14.0. FT-IR (ATR): (cm^{-1}) 2924, 2854, 1611, 1568, 1442, 1391, 1331, 1291, 1270, 1246, 1213, 1168, 1137, 1067, 968, 881, 853, 808, 735, 720, 698, 665. mass (EI +); (m/z): 693 (M^+) ; (calculated for $C_{41}H_{63}B_2NO_4F_2$: 693.56). Elemental Analysis (%) calculated for $C_{41}H_{63}B_2NO_4F_2$: C, 71.0, H, 9.16, N, 2.02. Found: C, 71.72, H, 9.15, N, 2.00.

3.3.17 Synthesis of 5,6-dioctyl-4,7-di(thiophen-2-yl)benzo[c][1,2,5]thiadiazole (17)

5,6-Dioctyl-4,7-di(thiophen-2-yl)benzo[c][1,2,5]thiadiazole **(17)** was prepared according to the procedure by Helgesen [103].

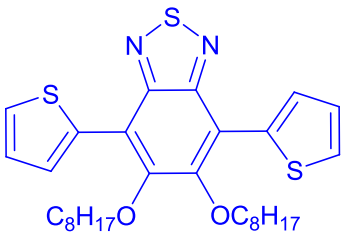

(17)

To a solution of **(5)** (4.00g, 4.17 mmol), $Pd(OAc)_2$ (46 mg , 0.05 mmol) and tri-o-tolylphosphine (122.00 mg , 10.40 mmol) in dry toluene (10 ml) was added 2-tributylstannylthiophene (1.16 g , 3.13 mmol) and the reaction mixture was heated to reflux for 16 hours under argon. The solvent was removed under reduced pressure, the residue was chromatographically purified on silica gel column eluting with hexane/ethyl acetate , gradient 10: 1 % to obtain **(17)** as orange solid crystals (3.82 g , 95.5 % yield). The product gave a single spot on TLC (R_f = 0.47) in hexane/ethyl acetate (10:1) .m.p. = 75- 76 °C.^{1}HNMR ($CDCl_3$): (δ_H/ppm) 8.49 (d, *J* = 3.7 Hz, 2H), 7.53 (d, *J* = 4.5 Hz, 2H), 7.26 (t, *J* = 4.47 Hz, 2H), 4.13 (t, *J* = 7.1 Hz, 4H), 1.99 – 1.89 (m, 4H), 1.51 – 1.42 (m, 4H), 1.41 – 1.24 (m, 16H), 0.92 (t, *J* = 6.9 , 6H). ^{13}C NMR ($CDCl_3$) δ_C/ppm: 151.46, 150.39, 135.69, 131.05, 129.70, 117.00, 115.47, 74.58, 31.84, 30.30, 29.49, 29.31, 25.94, 22.72, 14.16. FT-IR (ATR): (cm^{-1}) 2952, 2922, 2852, 1494, 1464, 1417, 1378, 1343, 1279, 1213, 1175, 1090, 1026, 1016, 953, 938, 920, 894, 883, 855,830, 757, 745, 722, 696. Mass (EI+): (m/z) 556 (M^+); (calculated for $C_{30}H_{40}N_2O_2S_3$: 556.85). Elemental Analysis (%) calculated for $C_{30}H_{40}N_2O_2S_3$: C, 64.71; H, 7.24; N, 5.03 S, 17.27. Found : C, 64.65; H, 7.15; N, 4.96 S, 17.07.

3.3.18 Synthesis of 4,7-bis(5-bromothiophen-2-yl)-5, 6-bis(octyloxy)benzo-[c][1,2,5]-thiadiazole (18)

4,7-Bis(5-bromothiophen-2-yl)-5,6-bis(octyloxy)benzo-[c][1,2,5]-thiadiazole **(18)** was synthesized according to Ruiping [93].

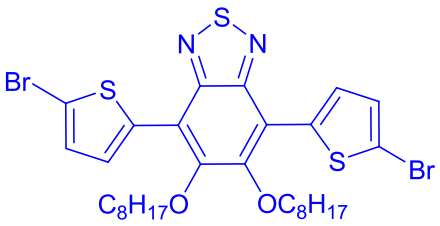

(18)

A mixture of 5,6-dioctyl-4,7-di(thiophen-2-yl)benzo[c][1,2,5]thiadiazole **(17)** (1.04 g, 1,867 mmol), N-bromosuccimide (NBS) (664.8 mg, 3.734 mmol), and chloroform (26 ml) was stirred at room temperature in dark for 24 hours. The solvent was removed under reduced pressure, the residue was chromatographically purified on silica gel column eluting with DCM / hexane (1 : 10) to afford **(18)** as orange crystals (1.29 g, 97%). The product gave a single spot on TLC (R_f = 0.43) in DCM / hexane (1 : 10). m.p. = 74- 76 °C.^{1}HNMR ($CDCl_3$):(δH/ppm) 8.39 (d, 2H, *J* = 4.1 Hz), 7.19 (d, 2H, *J* = 4.0 Hz), 4.14 (t, 4H, *J* = 7.22 Hz), 2.0-1.91 (m, 4H), 1.52-1.44 (m, 4H), 1.43-1.26 (16, H), 0.92 (t, 6H, *J* = 6.8 Hz). ^{13}C NMR ($CDCl_3$), (δ_C/ppm) 151.50, 150.41, 135.70, 131.01, 129.69, 117.01, 115.46, 74.59, 31.83, 30.28, 29.47, 29.29, 25.93, 22.69, 14.13. FT-IR (ATR): (cm^{-1}) 2953, 2850, 2922, 1494, 1465, 1437, 1427, 1392, 1375, 1347, 1283, 1209, 1178, 1090, 1056, 1030, 966, 948, 920, 894, 883, 855,830, 789, 750, 745, 722, 677. mass (EI+): (m/z) 712, 714, 716 (M^+); (calculated for $C_{30}H_{38}Br_2N_2O_2S_3$: 714.64). Elemental Analysis (%) calculated for $C_{30}H_{38}Br_2N_2O_2S_3$: C, 50.42, H, 5.36, N, 3.92, Br , 22.36 , S, 13.46 Found: C, 50.60, H, 5.41, N, 3.94, Br, 22.57, S, 12.52.

3.3.19 Synthesis of 3-hexylthiophene (19)

3-Hexylthiophene **(19)** was synthesized following a procedure developed by Urien [109].

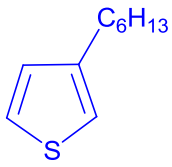

(19)

1-bromohexane (22.9 ml , 163 mmol) was added dropwise under inert atmosphere to a mixture of magnesium turnings (4.73 g , 195 mmol) and dry diethyl ether (250 ml) at 0 °C over an hour. The resulting mixture was refluxed overnight, allowed to cool to room temperature , then added dropwise over 1 hour to a solution containing 3-bromothiophene (14.5 ml , 155 mmol), [1,3-bis(diphenyphosphino)propane] nickel dichloride (131.00 mg ,150 mmol) and dry diethyl ether 150 ml at 0 °C under an inert atmosphere. The reaction mixture was refluxed overnight and then allowed to cool to room temperature, and the resulting two-phase solution was poured over distilled water (450 mL of ice and water and 50 ml of 1 M HCl). The aqueous phase was extracted with diethyl ether (2 × 150 ml) and the organic phase washed with saturated $NaHCO_3$ solution (100 ml) and distilled water (100 ml). The organic fraction was dried over $MgSO_4$, and the diethyl ether was removed in *vacuo*. High vacuum distillation (b.p. 65°C) gave the desired product **(19)** as a clear oil (6.00 g, 23 % yield). ^{1}HNMR ($CDCl_3$) : (δ_H/ppm) 7.3 (m, 1H), 7(m, 2H), 2.7 (t, 2H , J = 7.5Hz), 1.70 (m, 2H), 1.42 (m, 6H), 0.93 (t, 3H).^{13}C NMR ($CDCl_3$), δ_C/ppm): 143.20, 128.21, 124.95, 119.68, 31.53, 30.37, 30.13, 28.86, 22.45, 13.91. mass (EI+): (m/z) 168.10 (M^+); (calculated for $C_{10}H_{16}S$: 168.30). Elemental Analysis (%) calculated for $C_{10}H_{16}S$: C, 71.37, H, 9.58, S, 19.05.Found: C, 71.20, H, 9.40, S, 18.95.

3.3.20 Synthesis of 2, 5-dibromo-3-hexylthiophene (20)

2, 5-Dibromo-3-hexylthiophene **(20)** was synthesized following a procedure by Hammer [110].

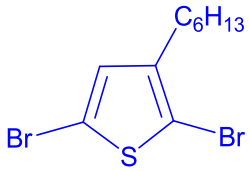

(20)

Crude 3-hexylthiophene **(19)** (6.00 g, 35.6 mmol) and THF (44 ml) were added to a 100 ml flask that was degassed for 15 min . NBS (11.60 g, 65.00 mmol) was added and the reaction was run at room temperature for 4 h. The resulting mixture was run through a plug of Celite 545 filter powder and the solvent was removed by rotary evaporation. The crude product was distilled and collected at 135 ^{0}C to obtain **(20)** as a colourless oil with (8.50 g, 88% yield). ^{1}HNMR ($CDCl_3$):(δ_H/ppm) 6.80 (s, H), 2.65 (t, 2H , J = 7.7Hz); 1.55 (m, 2H), 1.40 – 1.23 (m, 6H), 0.91 (t, 3H, J = 7Hz).^{13}C NMR ($CDCl_3$), δ_C/ppm) 143.18, 131.16, 110.60, 108.21, 31.87, 30.00, 29.76, 29.09, 22.88, 14.40. Mass (EI+): (m/z) 323.92 , 325.92 , 327.91 (M^+); (calculated for $C_{10}H_{14}Br_2S$: 326.09). Elemental Analysis (%) calculated for $C_{10}H_{14}Br_2S$: C, 36.83; H, 4.33; S, 9.83, Br, 49.01.Found: C, 36.40, H, 3.99, S, 9.01, Br, 48.90.

3.3.21 Synthesis of 2-bromo-3-hexylthiophene (21)

2-Bromo-3-hexylthiophene **(21)** was synthesized following a procedure by Li [111].

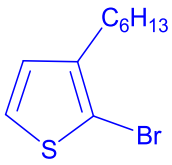

(21)

To a 200 ml flask , 3-hexylthiophene **(19)** (5.00 g, 5.30 ml , 29.7 mmol) was dissolved in 100 ml of THF. The resulting colourless solution was cooled in an ice bath and NBS (5.28 g, 29.7 mmol) was added in one portion. Stirring was continued in the ice bath for 1 h and the mixture was poured into water. The aqueous phase was extracted twice with hexanes (2×100 ml) and the combined organic layer was dried over $MgSO_4$. The solvent was removed in *vacuo* to leave a crude oil, which was purified by column chromatography (hexane) on silica gel to afford **(21)** as colourless oil (7.00 g, 82% yield). ^{1}HNMR ($CDCl_3$):(δ_H/ppm) 7.19 (d, 1H, *J*= 5.4 Hz) , 6.80 (d, 1H , *J*= 5.4 Hz), 2.57 (t, 2H, *J*= 7.5 Hz), 1.56-1.61 (m, 2H), 1.28-1.37 (m, 6H), 0.90 (t, 3H , *J*= 6.6 Hz).^{13}C NMR ($CDCl_{za}$), (δ_C/ppm) 141.19. 128.20, 125.11, 108.08, 31.61, 29.72, 29.64, 28.19, 22.16, 14.10. FT-IR (ATR): (cm^{-1}) 2980, 2928, 2857, 1541, 1509, 992, 714, 635. mass (EI+): (m/z) 247.01, 249.01 (M^+); (calculated for $C_{10}H_{15}BrS$: 247.20). Elemental Analysis (%) calculated for $C_{10}H_{15}BrS$: C, 48.59, H, 6.12, S, 12.97, Br, 32.32. Found: C, 48.40, H, 6.01, S, 11.99, Br, 31.98.

3.4 Other Compounds Used

3.4.1 Synthesis 9-(Heptadecan-9-yl)-2,7-bis(4,4,5,5-tetramethyl-1,3,2-dioxaborolan-2-yl)-*9H*-carbazole (22)

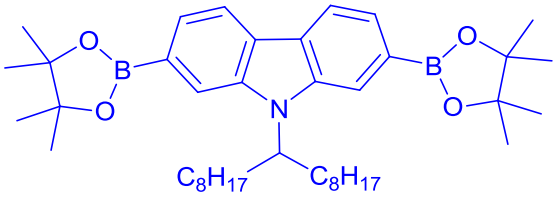

(22)

9-(Heptadecan-9-yl)-2,7-bis(4,4,5,5-tetramethyl-1,3,2-dioxaborolan-2-yl)-*9H*-carbazole **(22)** was prepared by the Iraqi group according to the procedures by Blouin et al Yamato el al and Sonnata.

3.4.2 2,2'-(9,9-Dioctyl-9H-fluorene-2,7-diyl)bis(4,4,5,5-tetramethyl-1,3,2-dioxaborolane (23).

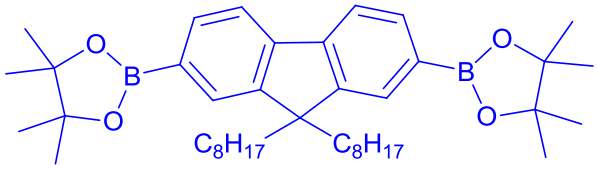

(23)

2,2'-(9,9-Dioctyl-9H-fluorene-2,7-diyl)bis(4,4,5,5-tetramethyl-1,3,2-dioxaborolane) **(23)** was supplied by Sigma Aldrich.

3.4.3 4,7-Bis(5-bromothiophen-2-yl)benzo[c][1,2,5]thiadiazole (24)

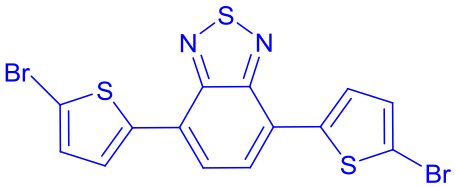

(24)

4,7-Bis(5-bromothiophen-2-yl)benzo[c][1,2,5]thiadiazole **(24)** was prepared by the Iraqi group.

3.4.4 2,6-Bis-(4,4,5,5-tetramethyl-[1,3,2]dioxaborolan-2-yl)-9,10-bis(4(dodecyloxy)phenyl) anthracene (25).

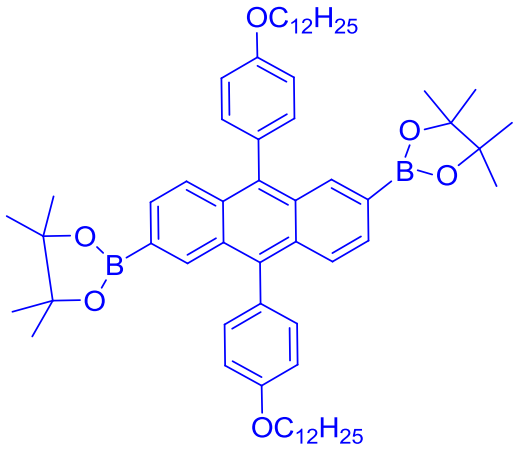

(25)

2,6-Bis-(4,4,5,5-tetramethyl-[1,3,2]dioxaborolan-2-yl)-9,10-bis(4-(dodecyloxy)phenyl) anthracene **(25)** was prepared by the Iraqi group .

3.4.5 2,2'-(9,10-bis(4-(dodecyloxy)phenyl)anthracene-2,7-diyl)bis(4,4,5,5-tetramethyl-1,3,2-dioxaborolane) (26)

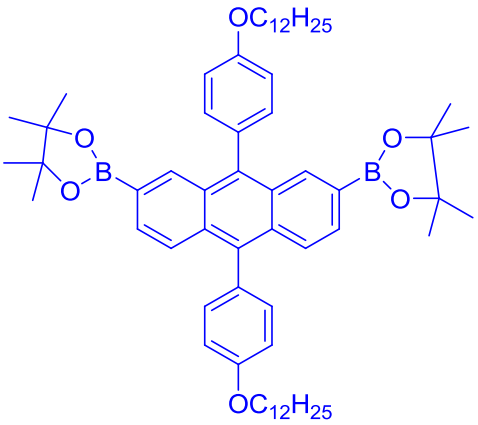

(26)

2,2'-(9,10-bis(4-(dodecyloxy)phenyl)anthracene-2,7-diyl)bis(4,4,5,5-tetramethyl-1,3,2-dioxaborolane(26)2,6-Bis-(4,4,5,5-tetramethyl-[1,3,2]dioxaborolan-2-yl)-9,10-bis(4-(dodecyloxy)phenyl) anthracene **(26)** was prepared by the Iraqi group .

3.5 Preparation of the Polymers

3.5.1 Poly[9-(heptadecan-9-yl)-9H-carbazole-2,7-diyl-alt-(5,6-bis(octyloxy)-4,7-di(thiophen-2-yl)benzo[c][1,2,5]thiadiazole) -5,5-diyl] (P1).

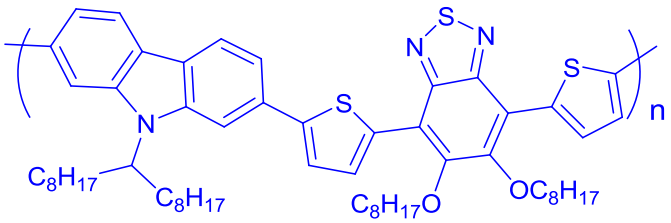

P1

9-(Heptadecan-9-yl)-2,7-bis-(4,4,5,5-tetramethyl-[1,3,2]dioxaborolan-2-yl)-*9H*-carbazole **(22)** (249.0 mg, 378.0 mmol) and 4,7-bis(5-bromothiophen-2-yl)-5, 6-bis(octyloxy)benzo-[c][1,2,5]-thiadiazole **(18)** (270.0 mg, 378.0 mmol) were introduced to a two-necked flask under argon. To the mixture was added toluene (10 ml). Then 20 wt% tetraethylammonium hydroxide (2.5 ml, 3.39 mmol, previously degassed) was added. To this mixture was added $Pd(OAc)_2$ (3.0 mg, 1.34×10^{-2} mmol), tri(*o*-tolyl)phosphine (8.3 mg, 2.73×10^{-2} mmol) under an inert argon atmosphere and it was heated to 95 °C for 48 h. The mixture was cooled to room temperature and bromobenzene (0.1 ml, 0.147 g; 0.936 mmol) was added. It was then degassed and heated to 90 °C for 1 h. The mixture was cooled to room temperature and phenylboronic acid (0.120 g; 0.984 mmol) was added. The mixture was degassed and heated to 90 °C for 1 h. After cooling to room temperature, $CHCl_3$ (200 ml) was added to solubilise the polymer. An ammonium hydroxide solution (28% in H_2O, 50 ml) was then added and the mixture was stirred overnight. The organic phase was separated and washed with distilled water (2 × 100 ml). It was then concentrated to about 50 ml in volume and poured into a degassed methanol/water mixture (10:1, v;v, 300 ml). The resulting mixture was then stirred overnight and filtered through a membrane filter. The collected solid was cleaned using a Soxhlet extraction under an inert argon atmosphere with methanol, acetone, hexane then toluene. The toluene fraction was concentrated to about 50 ml and then poured into degassed methanol (200 ml). The resulting mixture was stirred overnight and the solid collected by filtration to afford polymer **P1** as a red powder (369.0 mg, yield 99.2%). GPC (trichlorobenzene at 100 ˚C): Mw= 78.600 , Mn = 32.800 , PD = 2.37. ^{1}HNMR($CDCl_3$):(δ_H/ppm) 8.65 (d, 2H), 8.16 (br, 2H), 7.95 (s, 1H), 7.72 (s, 1H), 7.69 (br, 2H), 7.60 (br, 2H), 4.71 (br, 1H), 4.26 (br, 4H), 2.50 (br, 2H), 2.11 (br, 6H), 1.50-1.12 (br, 44H), 0.91 (t, 6H), 0.89 (t, 6H). Elemental

Analysis calculated for $(C_{59}H_{79}N_3O_2S_3)_n$: C, 73.93, H, 8.31, N, 4.38. Found: C, 72.64, H, 8.29, N, 4.17. no detectable Br.

3.5.2 Poly[3,6-difluoro-9-(1-octyl-nonyl)-9H-carbazole-2,7-diyl-alt- 5,6-bis(octyloxy)-4,7-di(thiophen-2-yl)benzo[c][1,2,5]thiadiazole (P2).

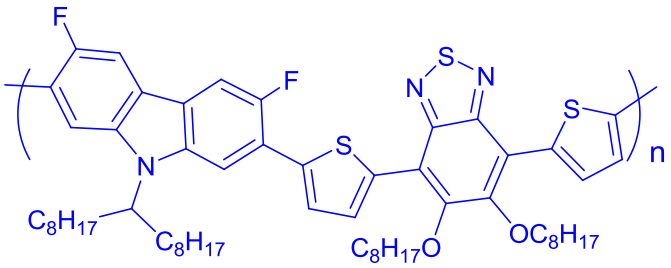

P2

3,6-Difluoro-9-(1-octyl-nonyl)-2,7-bis(4,4,5,5-tetramethyl-1,3,2-dioxaborolan-2-yl)-9H-carbazole **(16)** (262.2 mg , 378.0 mmol) and 4,7-bis(5-bromothiophen-2-yl)-5, 6-bis(octyloxy)benzo-[c][1,2,5]-thiadiazole **(18)** (270.0 mg , 378.0 mmol) were introduced to a two-necked flask under argon. To the mixture was added THF (10 ml) and the mixture was degassed. Then a saturated solution of $NaHCO_3$ (2.0 ml , previously degassed) was added. To this mixture was added $Pd(OAc)_2$ (3.0 mg, 1.34×10^{-2} mmol), tri(*o*-tolyl)phosphine (8.3 mg, 2.73×10^{-2} mmol) under an inert argon atmosphere and it was heated to 95 °C for 4 h. The mixture was cooled to room temperature and bromobenzene (0.1 ml, 0.147 g; 0.936 mmol) was added. It was then degassed and heated to 90 °C for 1 h. The mixture was cooled to room temperature and phenylboronic acid (0.120 g; 0.984

mmol) was added. The mixture was degassed and heated to 90 °C for 1 h. After cooling to room temperature, $CHCl_3$ (200 ml) was added to solubilise the polymer. An ammonium hydroxide solution (28% in H_2O, 50 ml) was then added and the mixture was stirred overnight. The organic phase was separated and washed with distilled water (2 × 100 ml). It was then concentrated to about 50 ml in volume and poured into a degassed methanol/water mixture (10:1, v;v, 300 ml). The resulting mixture was then stirred overnight and filtered through a membrane filter. The collected solid was cleaned using a Soxhlet extraction under an inert argon atmosphere with methanol, acetone, hexane then toluene. The toluene fraction was concentrated to about 50 ml and then poured into degassed methanol (200 ml). The resulting mixture was stirred overnight and the solid collected by filtration to afford polymer **P2** as a red powder (376.0 mg , yield 82.4 %) .GPC (trichlorobenzene at 100 ˚C): Mw= 21.000 , Mn = 12.500 , PD = 1.68 . ^{1}HNMR($CDCl_3$):(δ_H/ppm) 8.55 (bs, 2H), 7.75 (bm, 4H), 7.65 (bs, 2H), 4.60 (bm, 1H), 4.35 (bm, 4H), 2.43 (bm, 2H), 2.11 (bm, 4H), 1.62 (bm, 4H), 1.40-1.51 (bm, 24H), 1.28 (bm, 18H), 0.90 (t, 6H), 0.80 (t, 6H). Elemental Analysis calculated for $(C_{59}H_{79}F_2N_3O_2S_3)_n$: C, 71.11, H, 7.99, N, 4.22, Br, 0. Found: C, 71.0, H, 7.90, N, 4.10. no detectable Br.

3.5.3 Poly[9,9-dioctyl-9H-fluorene-2,7-diyl-alt-(4,7-di-2thiophen-2-yl)-2',1',3'-benzothiadiazole-5,5-diyl] (P3)

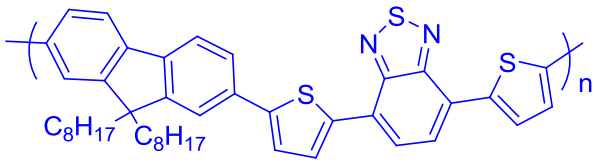

P3

9,9-Dioctylfluorene-2,7-diboronic acid bis(1,3-propanediol) ester **(23)** (152.4 mg, 273.0 mmol) and 4,7-bis(5-bromothiophen-2-yl)-benzo[c][1,2,5]thiadiazole **(24)** (125 mg, 273.0 mmol) were introduced to a two -necked flask under argon. To the mixture was added toluene (5 ml) and the mixture was degassed. Then 20 wt% tetraethylammonium hydroxide (1.3 ml, 1.76mmol), previously degassed was added. To this mixture was added $Pd(OAc)_2$ (1.5 mg, 6.6×10^{-3} mmol), tri(o-tolyl) phosphine (4 mg, 1.3×10^{-2} mmol) under an inert argon atmosphere and it was heated to 95 °C overnight. The mixture was cooled to room temperature and bromobenzene (0.1 ml , 0.147 g; 0.936 mmol) was added. It was then degassed and heated to 90 °C for 1 h. The mixture was cooled to room temperature and phenylboronic acid (0.120 g; 0.984 mmol) was added. The mixture was degassed and heated to 90 °C for 3 h. After cooling to room temperature, $CHCl_3$(200 ml) was added to solubilise the polymer. An ammonium hydroxide solution (28% in H_2O, 50 ml) was then added and the mixture was stirred overnight. The organic phase was separated and washed with distilled water (2 × 100 mL). It was then concentrated to about (50 ml) in volume and poured into a degassed methanol/water mixture (10:1, v;v, 300 ml). The resulting mixture was then stirred overnight. The collected solid was cleaned using a Soxhlet extraction under an inert atmosphere with methanol, acetone, hexane , toluene and chloroform. The toluene and chloroform fractions were concentrated to about 50 ml and then poured into methanol (200 ml). The resulting mixtures were stirred overnight and the solids collected by filtration to afford the two polymer fractions as purple powders. Toluene fraction (37 mg, 19 % yield), Chloroform fraction (71 mg, 37 % yield). GPC (1,2,4-trichlorobenzene at 100 ˚C) for toluene fraction: Mw = 7.300 , Mn = 5.300 , PD=1.38. GPC (1,2,4-trichlorobenzene at 100 ˚C) for chloroform fraction: Mw = 23.800, Mn= 15.100, PD = 1.57. ^{1}HNMR($C_2D_2Cl_4$ at 100 °C δ_H/ppm) 8.20 (bs, 2H), 8.01 (bs, 2H), 7.80 (m, 6H), 7.60 (bs, 2H), 2.12 (bm, 4H), 1.52 (bm, 4H), 1.24–1.28 (bm,

16H), 0.97 (bm, 4H), 0.91 (t, 6H). Elemental Analysis calculated for ($C_{43}H_{46}N_2S_3$): C, 75.17; H, 6.75; N, 4.08. Found: C, 73.50, H, 6.06, N, 4.44.

3.5.4 Poly[9-(heptadecan-9-yl)-9H-carbazole-2,7-diyl-alt-(5,6-bis(octyloxy)-4,7-di(2,2'-bithiophen-5-yl)benzo[c][1,2,5] thiadiazole)-5,5-diyl](P4).

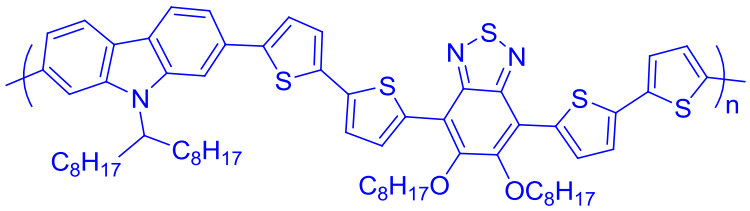

P4

9-(Heptadecan-9-yl)-2,7-bis-(4,4,5,5-tetramethyl-[1,3,2]dioxaborolan-2-yl)-*9H*-carbazole (0.303g,0.461mmol)**(22)** and 4,7-bis(5'-bromo-2,2'-bithiophen-5-yl)-5,6-bis(octyloxy)benzo[c][1,2,5]thiadiazole **(8)** (405.00 Mg, 461.00 mmol) were introduced to a two-necked flask under argon. To the mixture was added toluene (10 ml) and the mixture was degassed. Then 20 wt% tetraethyl ammonium hydroxide (2.5 ml, 3.39 mmol, previously degassed) was added. To this mixture was added $Pd(OAc)_2$ (3.00 mg, 1.34×10^{-2} mmol), tri(*o*-tolyl)phosphine (8.3 mg, 2.73×10^{-2} mmol) under an inert argon atmosphere and it was heated to 95 °C for 4 h. The mixture was cooled to room temperature and bromobenzene (0.1 ml, 0.147 g; 0.936 mmol) was added. It was then degassed and heated to 90 °C for 1 h. The mixture was cooled to room temperature and phenylboronic acid (0.120 g; 0.984 mmol) was added. The mixture was degassed and heated to 90 °C for 1 h. After cooling to room temperature, $CHCl_3$ (200 ml) was added to solubilise the polymer. An ammonium hydroxide solution (28% in H_2O, 50 ml) was then added and the mixture was stirred overnight. The organic phase was separated and washed

with distilled water (2 × 100 ml). It was then concentrated to about 50 ml in volume and poured into a degassed methanol/water mixture (10:1, v;v, 300 ml). The resulting mixture was then stirred overnight and filtered through a membrane filter. The collected solid was cleaned using a Soxhlet extraction under an inert argon atmosphere with methanol, acetone, hexane then toluene. The toluene fraction was concentrated to about 50 ml and then poured into degassed methanol (200 ml). The resulting mixture was stirred overnight and the solid collected by filtration to afford polymer **P4** as a dark red powder (310.0 mg, yield 60 %). GPC (Trichlorobenzene at 100 ˚C):Mw = 57.200 , Mn = 31.100 , PD = 1.84. ^{1}HNMR($CDCl_3$):(δ_H/ppm) 8.56 (br, 4H), 8.07 (br, 4H), 7.82 (br, 2H), 7.64-7.02 (br, 6H), 4.67 (br, 1H), 4.23 (br, 4H), 2.41 (s, 2H), 2.05 (br, 6H), 1.61 (br, 8H), 1.49-1.11 (br, 36H), 0.92 (br, 6H), 0.83 (br, 6H). Elemental Analysis calculated for $(C_{67}H_{83}N_3O_2S_5)_n$: C, 72.02; H, 7.62, N, 3.65 ; Br, 0. Found: C, 71.34, H, 7.50, N, 3.58. no detectable Br.

3.5.5 Poly[3,6-difluoro-9-(1-octyl-nonyl)-9H-carbazole-2,7-diyl-alt-4,7-di(2,2'-bithiophen-5-yl)-5,6-bis(octyloxy)benzo[c][1,2,5]thiadiazole (P5)

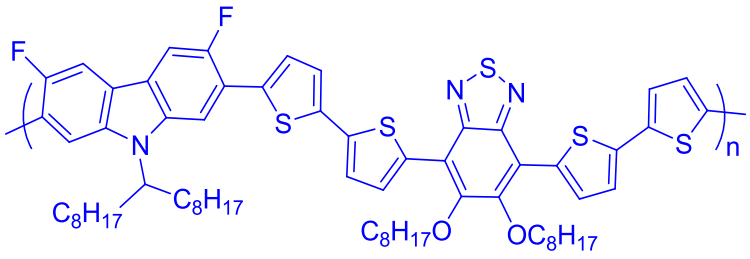

P5

3,6-Difluoro-9-(1-octyl-nonyl)-2,7-bis(4,4,5,5-tetramethyl-1,3,2-dioxaborolan-2-yl)-*9H*-carbazole**(16)** (151.9 mg , 231.0 mmol) and 4,7-bis(5'-bromo-2,2'-bithiophen-5-yl)-5,bis(octyloxy)benzo[c][1,2,5]thiadiazole **(8)** (202.9 mg, 231.0 mmol) were introduced to a two-necked flask under argon. To the mixture was added THF (10 ml) and the mixture

was degassed. Then a saturated $NaHCO_3$ (2.0 ml, previously degassed) was added. To this mixture was added $Pd(OAc)_2$ (3.0 mg, 1.34×10^{-2} mmol), tri(*o*-tolyl)phosphine (8.3 mg, 2.73×10^{-2} mmol) under an inert argon atmosphere and it was heated to 95 °C for 4 h. The mixture was cooled to room temperature and bromobenzene (0.1 ml, 0.147 g; 0.936 mmol) was added. It was then degassed and heated to 90 °C for 1 h. The mixture was cooled to room temperature and phenylboronic acid (0.120 g; 0.984 mmol) was added. The mixture was degassed and heated to 90 °C for 1 h. After cooling to room temperature, $CHCl_3$ (200 ml) was added to solubilise the polymer. An ammonium hydroxide solution (28% in H_2O, 50 ml) was then added and the mixture was stirred overnight. The organic phase was separated and washed with distilled water (2 × 100 ml). It was then concentrated to about 50 ml in volume and poured into a degassed methanol/water mixture (10:1, v;v, 300 ml). The resulting mixture was then stirred overnight and filtered through a membrane filter. The collected solid was cleaned using a Soxhlet extraction under an inert argon atmosphere with methanol, acetone, hexane then toluene. The toluene fraction was concentrated to about 50 ml and then poured into degassed methanol (200 ml). The resulting mixture was stirred overnight and the solid collected by filtration to afford polymer **P5** as a dark red powder (197.0 mg, yield 73 %). GPC (trichlorobenezene at 100 ˚C): Mw= 16.800 , Mn = 6.000 , PD = 2.81. ^{1}HNMR($CDCl_3$):(δ_H/ppm) 8.54 (bs, 2H), 7.75 (bm, 4H), 7.50 (brs, 2H), 7.45-7.02 (br, 4H), 4.67 (br, 1H), 4.23 (br, 4H), 2.41 (s, 2H), 2.05 (br, 6H), 1.61 (br, 8H), 1.49-1.11 (br, 36H), 0.92 (br, 6H), 0.83 (br, 6H). Elemental Analysis calculated for $(C_{67}H_{81}F_2N_3O_2S_5)_n$: C, 69.45, H, 7.05, N, 3.63, Br, 0. Found: C, 69.01, H, 6.99, N, 3.10. no detectable Br.

3.5.6 Poly(9,10-bis(4-(dodecyloxy)phenyl)-anthracene-2,6-diyl-alt-(5,6-bis(octyloxy)-4,7-di(2,2'-bithiophen-5-yl)benzo[c][1,2,5] thiadiazole)-5,5-diyl] (P6).

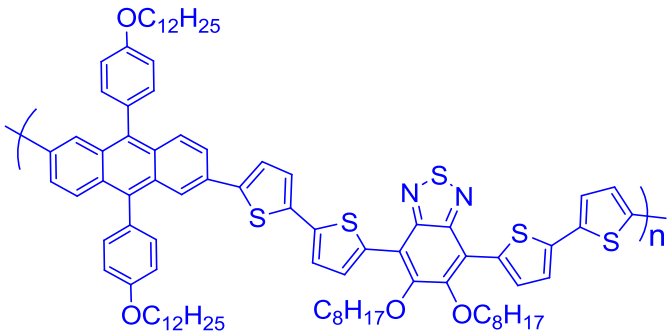

P6

To a solution of 2,6-bis-(4,4,5,5-tetramethyl-[1,3,2]dioxaborolan-2-yl)-9,10-bis(4-(dodecyloxy)phenyl)anthracene **(25)** (200.0 mg, 210.0 mmol) and 4,7-bis-(5'-bromo-[2,2']bithiophenyl-5-yl)-5,6-bis-octyloxy-benzo[1,2,5]thiadiazole **(8)** (185.0 mg, 210.0 mmol) in dry toluene (8 ml) was added a 20 % w/w aqueous solution of tetraethyl ammonium hydroxide (1.3 ml , 1.76 mmol) and the mixture was degassed. To this mixture was added $Pd(AcO)_2$ (3.3 mg, 0.015 mmol) and tri-o-tolylphosphine (9 mg, 0.0295 mmol) and the mixture was degassed then heated to 95 °C for 3 h. After cooling, the polymer was end-capped with the addition of 1-bromobenzene (0.1 ml , 0.94 mmol) and heated to 90 °C for 1 h. After cooling to room temperature, phenyl boronic acid (0.120 g; 0.984 mmol) was added and again the reaction was heated to 90 °C for 3 h. The reaction mixture was cooled to room temperature, then dissolved in $CHCl_3$ (200 ml) and to this solution was added an ammonium hydroxide solution (28% in H_2O, 50 ml) followed by stirring overnight. Then, the organic layer was separated and washed with distilled water. The organic layer was concentrated to about (50 ml) and poured into methanol (300 ml). The resulting mixture was stirred overnight and filtered through a membrane filter. The solid obtained was cleaned using Soxhlet extraction with solvents in order: methanol, acetone, hexane,

toluene and chloroform. The chloroform fraction was concentrated to about (50 ml) and then poured into methanol (200 ml). The resulting mixture was stirred overnight and the solid collected by filtration to afford the product as a dark purple (0.044 g,15%). GPC (trichlorobenzene at 100 ˚C) for chloroform fraction: Mw = 19.100 , Mn= 15.400, PD = 1.23. ^{1}H NMR ($C_2D_2Cl_4$, 100 °C) (δ_H/ppm) ; 8.47 (s, 2H), 7.95 (bs, 2H), 7.80 (m, 2H), 7.65 (m, 2H), 7.55 (m, 2H), 7.40 (m, 4H), 7.3 – 7,05 (m, 8H), 4.05 (bm, 8H), 1.99-1.81 (m, 8H), 1.60-1.20 (m, 56H), 0.93-0.80 (m, 12H). Elemental Analysis calculated for ($C_{88}H_{106}N_2O_4S_5$): C, 74.64, H, 7.54, N, 1.98, S, 11.32. Found: C, 72.85, H, 7.20, N, 1.60, S, 9.10.

3.5.7 Poly(9,10-bis(4-(dodecyloxy)phenyl)-anthracene-2,7-diyl-alt-(5,6-bis(octyloxy)-4,7-di(2,2'-bithiophen-5-yl)benzo[c][1,2,5] thiadiazole)-5,5-diyl] (P7).

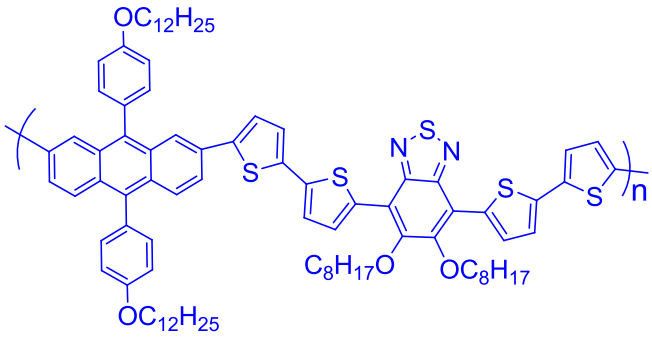

P7

To a solution of 2,7-bis(4,4,5,5-tetramethyl-1,3,2-dioxaborolane(9,10-bis(4-(dodecyloxy)phenyl)anthracene **(26)** (200.0 mg , 210.0 mmol) and 4,7-bis-(5'-bromo-[2,2']bithiophenyl-5-yl)-5,6-bis-octyloxy-benzo[1,2,5]thiadiazole **(8)** (185.0 mg, 210.0 mmol) in dry toluene (8 ml) was added a 20 % w/w aqueous solution of tetraethyl ammonium hydroxide (1.3 ml , 1.76 mmol) and the mixture was degassed. To this mixture was added $Pd(OAc)_2$ (3.3 mg, 0.015 mmol) and tri-o-tolylphosphine (9 mg , 0.0295 mmol) and the mixture was degassed then heated to 95 °C for 3 h. After cooling, the polymer was

end-capped with the addition of 1-bromobenzene (0.1 ml , 0.94 mmol) and heated to 90 °C for 1 h. After cooling to room temperature, phenylboronic acid (0.120 g ; 0.984 mmol) was added and again the reaction was heated to 90 °C for 3 h. The reaction mixture was cooled to room temperature, then dissolved in $CHCl_3$ (200 ml) and to this solution was added an ammonium hydroxide solution (28% in H_2O, 50 ml) followed by stirring overnight. Then, the organic layer was separated and washed with distilled water. The organic layer was concentrated to about 50 ml and poured into methanol (300 ml). The resulting mixture was stirred overnight and filtered through a membrane filter. The solid obtained was cleaned using Soxhlet extraction with solvents in order: methanol, acetone, hexane, toluene and chloroform. The toluene fraction was concentrated to about (50 ml) and then poured into methanol (200 ml). The resulting mixture was stirred overnight and the solid collected by filtration to afford the product as dark purple (295.0 mg , 97%). GPC (trichlorobenzene at 100 ˚C) for toluene fraction: Mw = 69.000 , Mn= 33.000, PD = 2.09. ^{1}H NMR ($C_2D_2Cl_4$, 100 °C) (δ_H/ppm) ; 8.42 (s, 2H), 8.0 (s, 2H), 7.77 (m, 2H), 7.60 (m, 2H), 7.50 – 7.36 (m, 4H), 7.28 (m, 2H), 7.23 – 7,10 (m, 8H), 4.16 (bm, 8H), 2.04 -1.74 (m, 8H), 1.71-1.20 (m, 56H), 0.92-0.80 (m, 12H). Elemental Analysis calculated for ($C_{88}H_{106}N_2O_4S_5$): C, 74.64, H, 7.54, N, 1.98, S, 11.32. Found: C, 73.29, H, 7.44, N, 1.70, S, 10.46.

3.5.8 Poly [9-(heptadecan-9-yl)-9H- carbazole -2-7-diyl-alt-(5,6-bis(octyloxy)-4,7-di(thiophen-2-yl)benzo[c][1,2,5]thiadiazole)-5,5-diyl-b-poly[9,9-dioctyl- fluorene-2,7-diyl-alt-(4,7-di(thiophen -2 .[1.0 : 1.0 : 1.0 : 1.0][23:24:22:18] (P8).

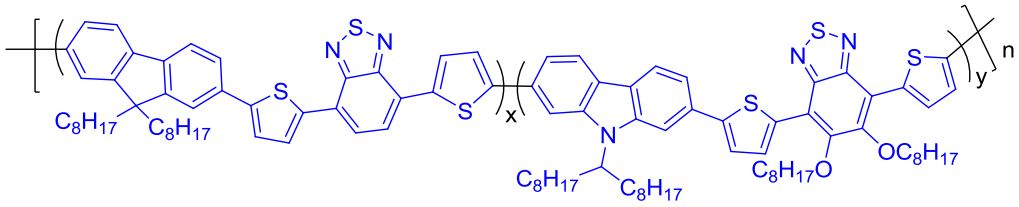

P8

9,9-Dioctylfluorene-2,7-diboronic acid bis(1,3-propanediol) ester **(23)** (125. mg, 224.0 mmol) and 4,7-bis(5-bromothiophen-2-yl)-benzo[c][1,2,5]thiadiazole **(24)** (102.6 mg, 224.0 mmol) were introduced to a two -necked flask under argon. To the mixture was added toluene (10 ml) and the mixture was degassed. Then 20 wt% tetraethyl ammonium hydroxide (2.5 ml , 3.4 mmol), previously degassed was added. To this mixture was added $Pd(OAc)_2$ (3.4 mg, 0.015 mmol), tri(o-tolyl) phosphine (9.1 mg, 0.03 mmol) under an inert argon atmosphere and it was heated to 95 °C for 3 h. The The mixture was cooled to room temperature and 9-(heptadecan-9-yl)-2,7-bis-(4,4,5,5-tetramethyl-[1,3,2]dioxaborolan-2-yl)-*9H*-carbazole (147.0 mg, 224.0 mmol) **(22)** and 4,7-bis(5-bromothiophen-2-yl)-5, 6-bis(octyloxy)benzo-[c][1,2,5]-thiadiazole **(18)** (160.0 mg , 224.0 mmol) were added and heated to 90 °C for 48 h. The mixture was cooled to room temperature and bromobenzene (0.1 mL, 0.147 g; 0.936 mmol) was added. It was then degassed and heated to 90 °C for 1 h. The mixture was cooled to room temperature and phenylboronic acid (0.120 g; 0.984 mmol) was added. The mixture was degassed and heated to 90 °C for 3 h. After cooling to room temperature, $CHCl_3$(200 ml) was added to solubilise the polymer. An ammonium hydroxide solution (28% in H_2O, 50 ml) was then added and the mixture was stirred overnight. The organic phase was separated and washed with distilled water (2 × 100 ml). It was then concentrated to about (50 ml) in volume and

poured into a degassed methanol/water mixture (10:1, v;v, 300 ml). The resulting mixture was then stirred overnight. The collected solid was cleaned using a Soxhlet extraction under an inert atmosphere with methanol, acetone, hexane , toluene and chloroform. The toluene and chloroform fractions were concentrated to about 50 ml and then poured into methanol (200 ml). The resulting mixtures were stirred overnight and the solids collected by filtration to afford the two polymer fractions as purple powders. Toluene fraction (160 mg, 43 % yield), Chloroform fraction (77 mg, 20 % yield). GPC (Chloroform at RT) for toluene fraction: Mw = 14.600 , Mn= 8.700, PD=1.68. GPC (Chloroform at RT) for chloroform fraction: Mw= 30.100 , Mn= 18.800, PD = 1.59. ^{1}HNMR($CDCl_3$):(δ_H/ppm) 8.60 (b , 2H), 8.10 (m, 3H), 7.90 (bs, 2H), 7.5-7.8 (m, 10H), 4.75 (bm, IH), 4.30 (bm, 4H), 2.49 (bm, 2H), 2.15 (bm, 10H), 1.55 (bm, 6H), 1.24–1.45 (bm, 67H), 0.95 (t, 8H), 0.89 (t, 10H). Elemental Analysis calculated for ($C_{102}H_{125}N_5O_2S_6$): C, 74.45, H, 7.66, N, 4.26. Found: C, 74.30, H, 7.40, N, 4.01.

3.5.9 Ploy (3-hexylthiophene) (Br – P3HT) (P9).

3.5.9.1 Method 1: Time of Polymerization is 2h.

Poly(3-hexylthiophene) (Br-P3HT) **(P9)** was prepared according to the procedure by Antoun, et al [112].

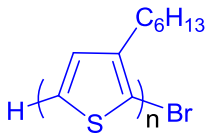

P9

To a solution of 2,5-dibromo-3-hexylthiophene **(20)** (1.80 g, 5.51 mmol) and THF (80 ml), was added i-PrMgCl.LiCl (4.42 ml , 5.75 mmol) in tetrahydrofuran (1.3M) via a syringe. The reaction mixture was refluxed for 2 h. The reaction mixture was then cooled to room temperature then Ni(dppp)Cl_2 (10.0 mg, 0.018 mmol) was added. The polymerization was allowed to proceed for 2 h at room temperature. Afterwards the mixture was poured into methanol (800 ml) to precipitate the polymer . The polymer was separated using a centrifuge and subjected to Soxhlet extraction with methanol, hexane and toluene. The toluene fraction was concentrated to about (50 ml) and then poured into methanol (200 ml). The resulting mixture was stirred overnight and the solid collected by filtration to afford **(9)** as dark red powder (300 mg , yield 40 %). GPC (Chloroform at 40 ˚C) : Mw = 32.500 , Mn= 24.900 , PD = 1.30. MALDI-MS: M_n = 3650 of H/H end groups , H/H end groups = 75 % .M_n = 3568 of H/Br end groups, H/Br end groups = 25 % .

3.5.9.2 Method 2: Time of Polymerization is 24h.

To a solution of 2,5-dibromo-3-hexylthiophene **(20)** (2.50 g, 7.65 mmol) and THF (111 ml), was added i-PrMgCl.LiCl(6.13 ml , 7.98 mmol) in tetrahydrofuran (1.3M) via a syringe. The reaction mixture was refluxed for 2 h. The reaction mixture was then cooled to room temperature then Ni(dppp)Cl_2 (13.8 mg, 0.025 mmol) was added. The polymerization was allowed to proceed for 24 h at room temperature. After the polymerization was complete the mixture was poured into methanol (800 ml) to precipitate the polymer. The polymer was separated using a centrifuge and subjected to Soxhlet

extraction with methanol, hexane, toluene and chloroform . The toluene and chloroform fractions were concentrated to about (50 ml) and then poured into methanol (200 ml). The resulting mixture was stirred overnight and the solid collected by filtration to afford **(9)** as dark red powder fractions were evaporated to afford (9) as dark red powders. Toluene fraction (100 mg, 6 % yield), Chloroform fraction (130 mg, 7 % yield). GPC (Chloroform at 40 ˚C) for toluene fraction: Mw = 28.200 , Mn= 20.500, PD=1.37 .GPC (Chloroform at 40 ˚C) for chloroform fraction: Mw = 46.000 , Mn= 35.000, PD = 1.31. MALDI-MS for toluene fraction: M_n = 4570 of H/H end groups, H/H end groups = 75 %. M_n = 4490 of H/Br end groups, H/Br end groups = 25 % .

3.5.9.3 Method 3: via the McCullough method.

Poly(3-hexylthiophene) (Br-P3HT) **(9)** was prepared according to the procedure by *McCullough* [113].

Distilled diisopropylamine (DIPA) (1.4 ml , 10 mmol) and (3.7 ml , 9.5 mmol) of *n*-BuLi 2.58 M were dissolved in dry THF (50 ml) at -78 ^{0} C. The mixture was then warmed to room temperature over 5 min and then cooled to -78 ^{0} C. The monomer 2-bromo-3-hexylthiophene (21) (2.5 g, 10 mmol) was added to the freshly generated lithium diisopropylamide (LDA)and the reaction stirred at -70 ^{0} C for 1 h. Anhydrous $ZnCl_2$ (1.43 g,10.5 mmol) was then added at -70 ^{0} C and the reaction was stirred for 1 h. The reaction was warmed to 0 ^{0} C and [Ni(dppp)Cl_2] (35 mg, 0.065 mmol) was added. The mixture was warmed to room temperature and then stirred for an additional 30 min.The polymer was precipitated with methanol, then washed and fractionated by Soxhlet extraction with methanol, hexane, dichloromethane, and tetrahydrofuran. The THF fraction afforded a red powders (430 mg, 18 % yield).). GPC (Chloroform at 40 ˚C) for THF fraction: Mw =

25.200 , Mn= 17.500, PD=1.44 MALDI-MS : M_n = 4980 of H/H end groups , H/H end groups = 48 % . M_n = 4902 of H/Br end groups, H/Br end groups = 52 %

3.5.9.4 Method 4: via the McCullough method.

In this method an excess of diisopropylamine was used (1.7 ml , 12mmol) following the same procedure in method 3 to afford DCM and THF fractions . DCM fraction (100 mg, 4 % yield), GPC (Chloroform at 40 ˚C) for DCM fraction: Mw = 38.000 , Mn= 28.000, PD = 1.35, MALDI-MS for DCM fraction: M_w = 3651 of H/H end groups , H/H end groups = 65 % . M_w = 3731 of H/Br end groups, H/Br end groups = 35 %.

3.5.9.5 Method 5

Poly(3-hexylthiophene) (Br-P3HT) **(9)** was prepared according to the procedure by Lohwasser [114].

(1.5 g, 4.6 mmol) 2,5-Dibromo-3-hexylthiophene **(20)** was dissolved in THF (9 ml) and (3.6 mL, 4.41 mmol) of t-BuMgCl were added with a syringe and stirred for 20 h. After complete active Grignard monomer formation the solution was diluted with dry THF (33 ml) and the reaction was initiated with Ni(dppp)Cl_2 (96 mg, 0.18 mmol) and the polymerization was left for 165 min .The polymerization was stopped by adding 5N HCl (5 ml). After precipitation in methanol the polymer was filtered into a Soxhlet thimble and extracted with methanol over night. The pure polymer was obtained in chloroform (15 mg, 1.3 % yield). MALDI-MS for chloroform fraction: M_n = 1574 , end groups : H/H = 98 % , H/Br = 2 % .

Chapter 4 : Result and Discussion - Monomers

4.1 Synthesis of Monomers for the bithiophene-benzothiadiazole based Copolymers : (P4) (P5) (P6) (P7).

Figure 53 shows the required monomers to prepare polymers **P4** , **P5** , **P6** and **P7** . 4,7-Bis(5'-bromo-2,2'-bithiophen-5-bis(octyloxy)benzo[c][1,2,5]thiadiazole **(8)** and 3,6-difluoro-9-(1-octyl-nonyl)-2,7-bis(4,4,5,5-tetramethyl-1,3,2-dioxaborolan-2-yl)-9H-carbazole **(16)** were synthesised successfully in good yields and their purities and

structures were confirmed by ^{1}H NMR , ^{13}C NMR , CHN elemental analysis , FT-IR and mass spectrometry analysis. 3,6-Difluoro-9-(1-octyl-nonyl)-2,7-bis(4,4,5,5-tetramethyl-1,3,2-dioxaborolan-2-yl)-9H-carbazole**(16)** and 4,7-bis(5'-bromo-2,2'-bithiophen-5-bis(octyloxy)benzo[c][1,2,5]thiadiazole **(8)** were used respectively as donor and acceptor units to prepare polymer **P5**. The synthetic route for preparing 4,7-bis(5'-bromo-2,2'-bithiophen-5-bis(octyloxy)benzo[c][1,2,5]thiadiazole **(8)** and 3,6-difluoro-9-(1-octyl-nonyl)-2,7-bis(4,4,5,5-tetramethyl-1,3,2-dioxaborolan-2-yl)-9H-carbazole **(16)** are shown in Scheme 3 and Scheme 4 respectively.

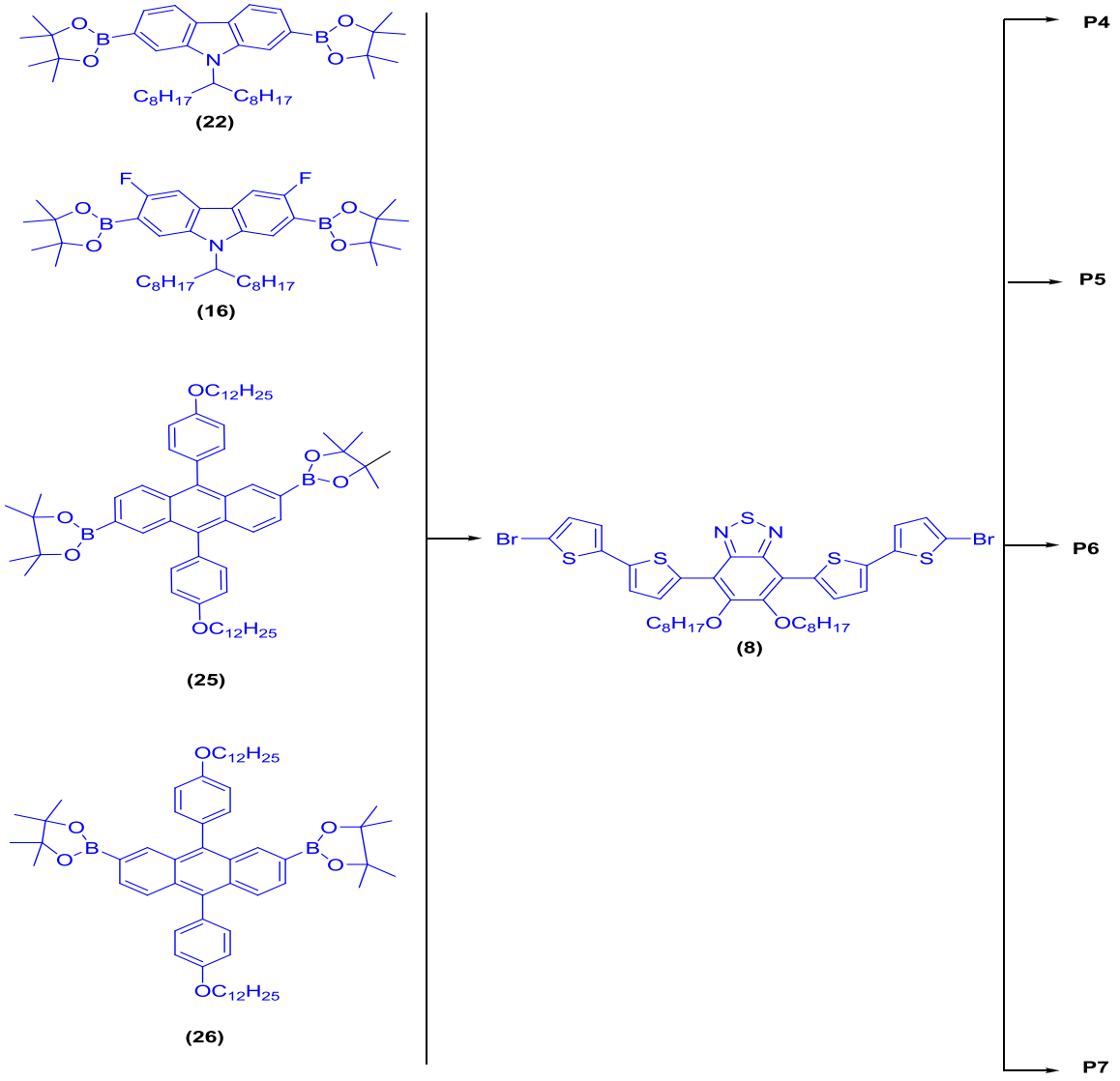

Figure 53: The monomers used to prepare P4 , P5 , P6 and P7

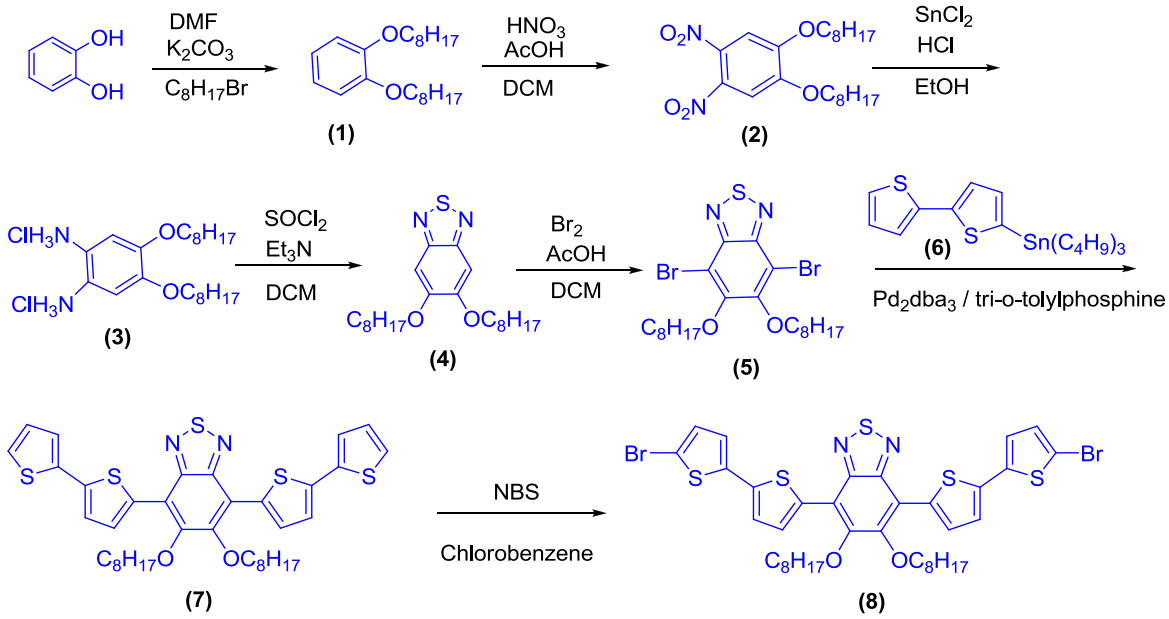

Scheme 3:The synthetic route for monomer 4,7-bis(5'-bromo-2,2'-bithiophen-5-bis(octyloxy)benzo[c][1,2,5]thiadiazole (8)

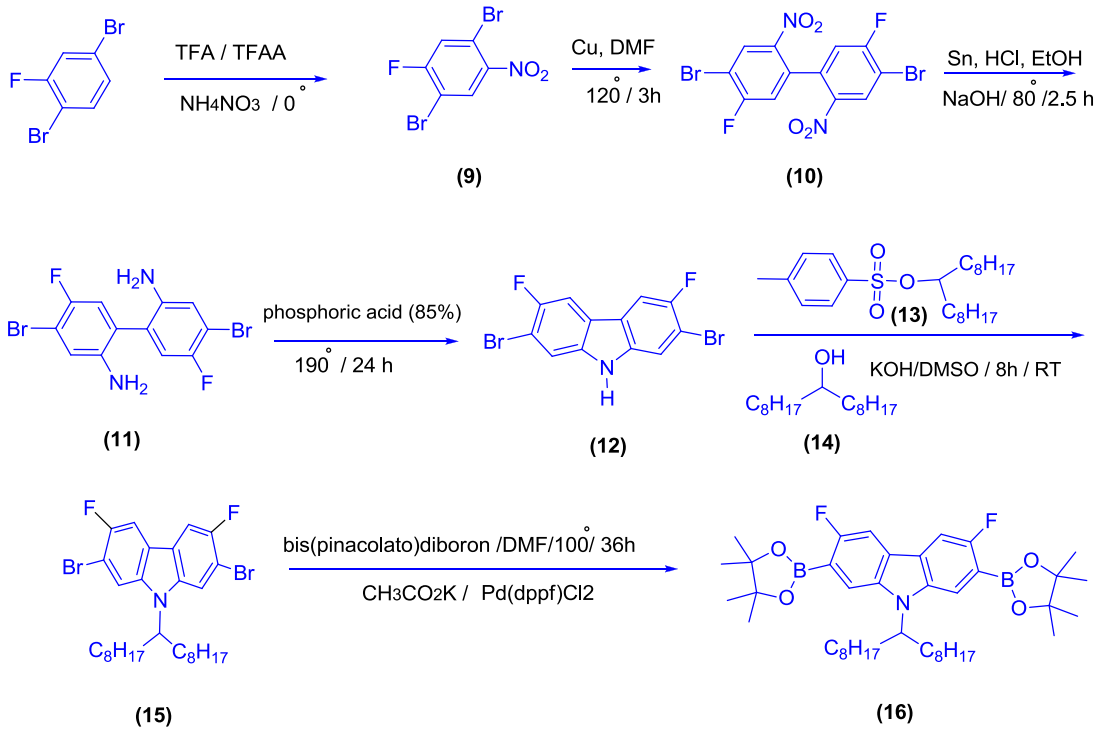

Scheme 4:The synthetic route for monomer 3,6-Difluoro-9-(1-octyl-nonyl)-2,7-bis(4,4,5,5-tetramethyl-1,3,2-dioxaborolan-2-yl)-9H-carbazole (16)

4.1.1 1,2-Bis(octyloxy)benzene (1)

1,2-Bis(octyloxy)benzene **(1)** was obtained using a procedure by Zhang [115]. This reaction was done according to the Williamson reaction as shown in scheme 5.

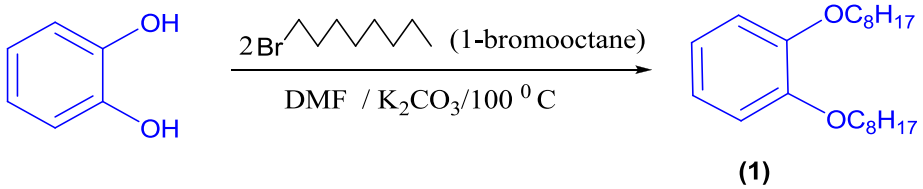

Scheme 5:Synthesis of 1,2-bis(octyloxy)benzene (1) .

The product was obtained in a good yield (90%) as white needle like crystals. The purification of the product was performed using recrystallisation from ethanol. The product gave a single spot on TLC using petroleum ether : ethyl acetate (8: 2). The reaction mechanism follows the bimolecular nucleophilic substitution (S_N2). This mechanism consists of two steps as shown in scheme 6.

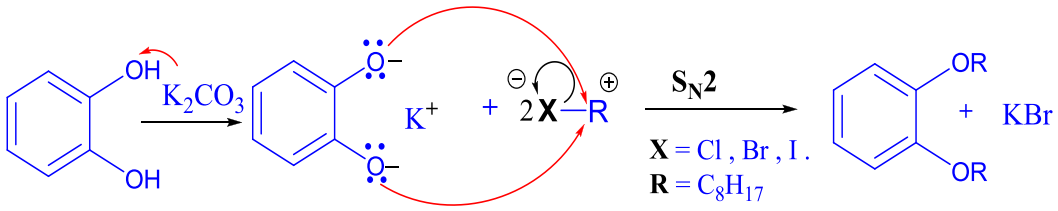

Scheme 6: SN2 mechanism for preparation of 1,2-bis(octyloxy)benzene.

The first step is a deprotonation of the hydroxyl groups by the base K_2CO_3 to form the phenoxide ion which attacks the 1-bromooctane as nucleophile to form the desired product. The purity and the structure of the product **(1)** was confirmed by TLC, ^{1}H NMR, ^{13}C NMR, elemental analysis, mass spectrometry, melting point and FT-IR. The elemental analysis confirmed the structure of the product. The mass spectrum show the main integer mass at 334 (M^+) which is in agreement with the proposed structure. The ^{1}H NMR shows a single peak at 6.91 ppm corresponding to the four hydrogens of the phenyl. The protons of (OCH_2) and (CH_3) was displayed as triplet peaks at 4.01 and 0.91 ppm respectively. The FT - IR of the product displays the C-H aliphatic asymmetrical stretching vibration bands at 2922 and 2848 cm^{-1} .The FT- IR spectra shows a strong sharp peak at 732 cm^{-1} corresponding to 1,2 disubstitution. Also there is no peak for OH groups which means that all OH groups were converted to the product. The melting point of the product was 24.5-25 ˚C in close agreement with reported value in the literature (25 – 26 ˚C)[116].

4.1.2 1,2-Dinitro-4,5-bis(octyloxy)benzene (2)

1,2-Dinitro-4,5-bis(octyloxy)benzene **(2)** was prepared according to procedure by Sessler [102] Scheme 7 .

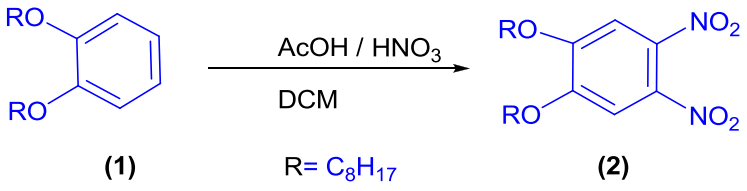

Scheme 7: Synthesis of 1,2-dinitro-4,5-bis(octyloxy)benzene (2)

This reaction follows the electrophilic aromatic substitution mechanism as shown in Scheme 8 .

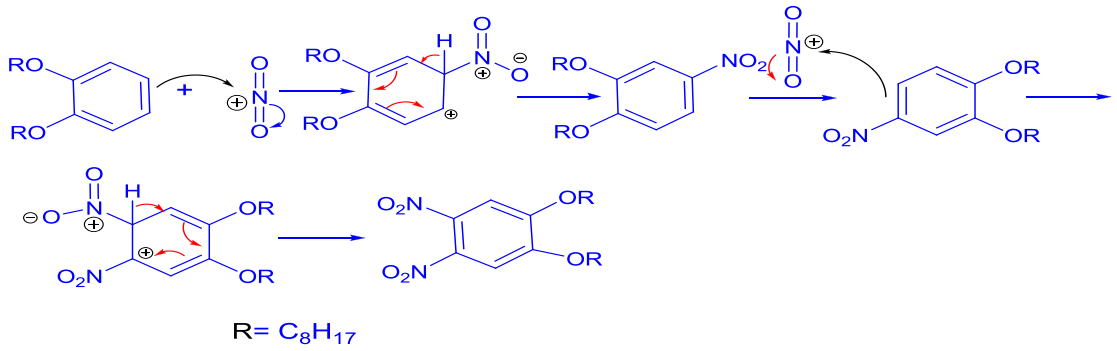

Scheme 8: Mechanism for preparation of 1,2-dinitro-4,5-bis(octyloxy)benzene.

The mechanism involves two steps where the first step is the formation of electrophile (nitronium ion) as follow in Scheme 9 :

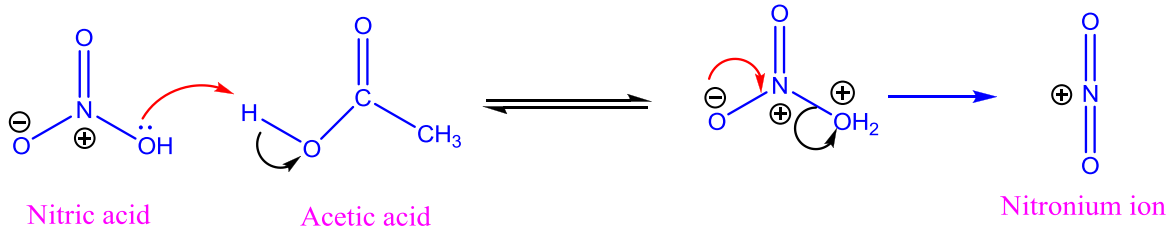

Scheme 9 : Formation of electrophile (Nitronium ion).

The second step which is the slow step is that the aromatic ring attacks the positively charged electrophile (nitronium ion) as shown in Scheme 8. The product was obtained via recrystallization from ethanol as pure yellow crystals in a yield of (87%). The chemical structure and the purity of the product were confirmed by ^{1}H NMR, ^{13}C NMR, elemental analysis, mass spectrometry, melting point and FT-IR. The ^{1}H NMR spectra illustrates that the only two aromatic protons appeared as a single peak at 7.30 ppm. The elemental analysis confirmed the structure of the product. The mass spectra show the main integer mass at 424 (M^{+}) which is in agreement with the proposed

structure. The FT-IR spectrum displayed strong absorption bands at 1526 cm^{-1} and 1464 cm^{-1} belonging to the stretching vibration of the nitro groups. The stretch vibration band of aromatic C – H bond is shown at 3071 cm^{-1}.The melting point of the product was (87- 88 ˚C) in close agreement with literature (87- 87.5 ˚C) [117] .

4.1.3 4, 5-Bis(octyloxy)benzene-1,2-diaminium chloride (3).

4, 5-Bis(octyloxy)benzene-1,2-diaminium chloride **(3)** was perpared according to procedure by Martin [103] Scheme 10 .

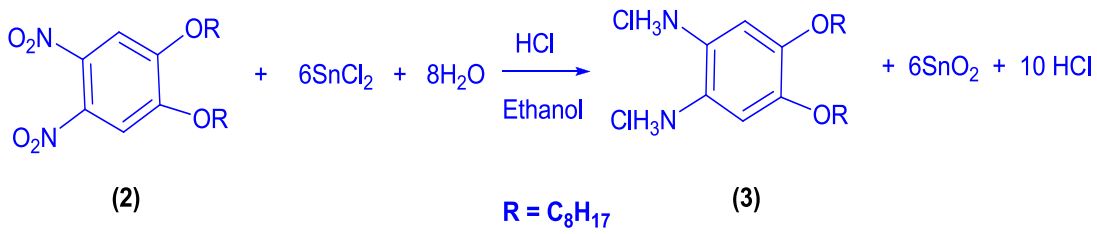

Scheme 10: Synthetic route of 4, 5-bis(octyloxy)benzene-1,2-diaminium chloride (3).

The reaction was carried out in ethanol at 85 ˚C overnight in the presence of HCl. The nitro groups on the benzene ring is reduced by $SnCl_2$ in presence of HCl. The product was obtained as a white powder in 88% yield and was used directly in the next reaction without purification, due to the instability of the product .

4.1.4 5,6 – Bis-octyloxy-benz[1,2,5]thiadiazole (4)

5,6 – Bis-octyloxy-benz[1,2,5]thiadiazole **(4)** was prepared according to the procedure by Bouffard [104]. The product was obtained via recrystallisation from ethanol as an off-white solid in 88 % yield , Scheme 11.

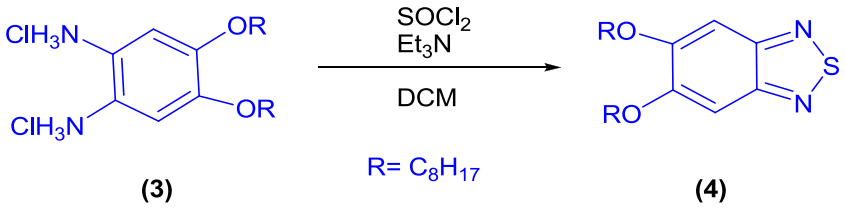

Scheme 11: Synthetic route of 5,6 – bis-octyloxy-benz[1,2,5]thiadiazol (4)

The reaction is carried out in the presence of triethylamine Et_3N under reflux for 6 hours. The HCl from compound **(3)** was removed using Et_3N to form triethylamine hydrochloride. This product follows the mechanism in Scheme 12:

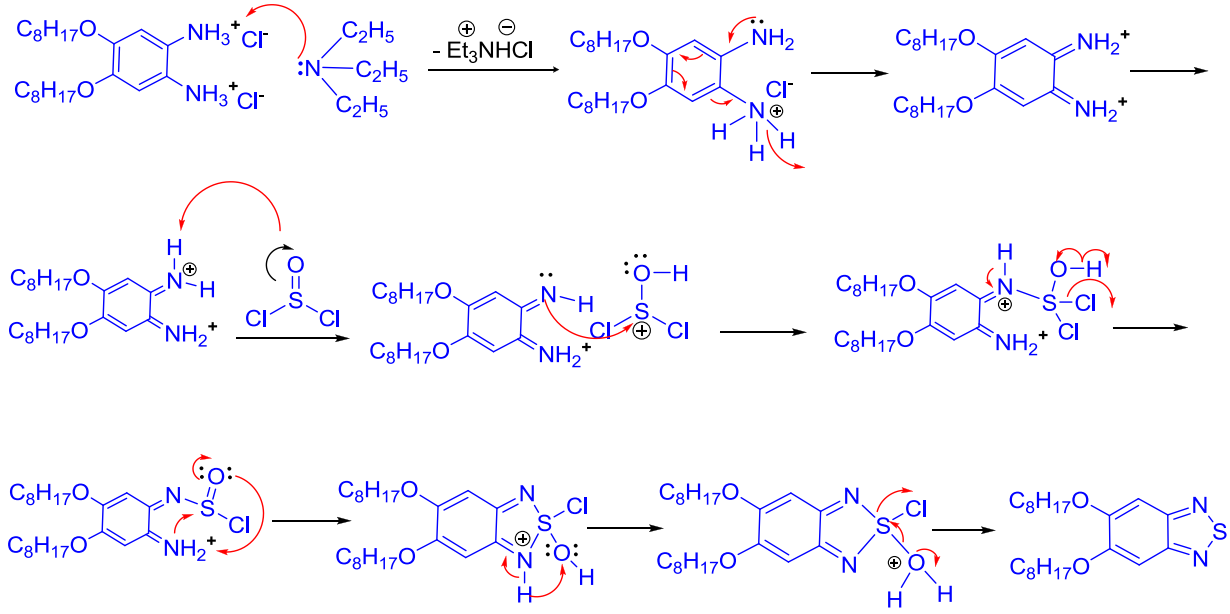

Scheme 12: Mechanism of preparation 5,6 – bis-octyloxy-benz[1,2,5]thiadiazol.

This product was purified by trituration using water then recrystallized by ethanol to provide the product as a white-solid. The structure and the purity of the product **(4)** were confirmed by ^1H NMR, ^{13}C NMR, elemental analysis, mass spectrometry, melting point and FT-IR. The ^1H NMR spectrum shows the only two aromatic protons appeared as a single peak at 7.15 ppm. The elemental analysis was in agreement with the proposed structure. The mass spectra displayed the main integer mass at 392 (M^+) which is in agreement with the proposed structure. The stretch vibration band of aromatic C – H bonds

are shown at 3116 , 3081 and 3053 cm^{-1}. The melting point of the product was 97 - 98 ˚C in agreement with the literature value (97.1 – 97.5 ˚C) [117] .

4.1.5 4,7-Dibromo-5,6-bis-octyloxy-benzo[1,2,5]thiadiazole (5)

4,7-Dibromo-5,6-bis-octyloxy-benzo[1,2,5]thiadiazole **(5)** was synthesized according to procedure by Bouffard and Swager [104]. The product was recrystallized from ethanol to give the desired product as a white solid in a good yield (82 %) , Scheme 13.

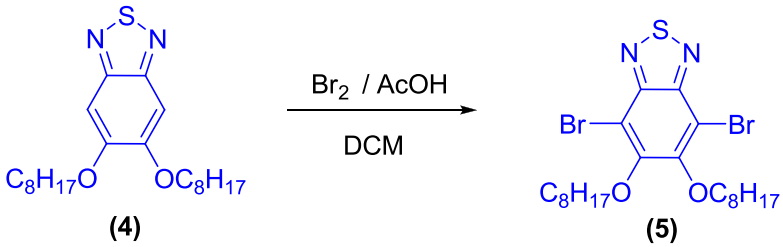

Scheme 13: Synthesis route of 4,7-Dibromo-5,6-bis-octyloxy-benzo[1,2,5]thiadiazol (5)

The reaction was done at room temperature for 48 hours in the presence of acetic acid as catalyst. The catalyst increases the electrophilic activity of the bromine.The reaction follows the electrophilic aromatic substitution mechanism as shown in Scheme 14 :

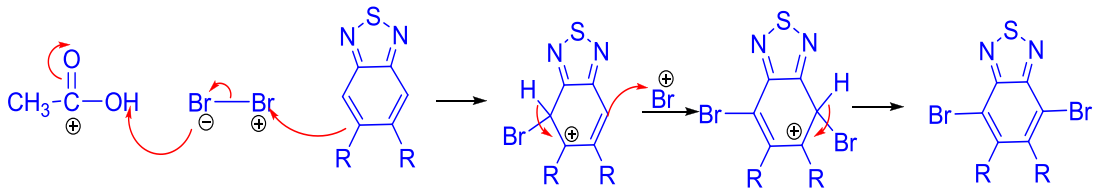

Scheme 14: Mechanism of the preparation of 4,7-dibromo-5,6-bis-octyloxy-benzo[1,2,5]thiadiazole .

The purity and the structure the product **(5)** were confirmed by ^{1}H NMR, ^{13}C NMR, elemental analysis, mass spectrometry, melting point and FT-IR. The ^{1}H NMR

spectrum shows no peaks in the aromatic region which means that all H atoms were replaced with Br. The elemental analysis for **(5)** confirmed the structure of the target product. The mass spectrum show three main integer masses at 548, 550 and 552, in 1:2:1 ratio as expected due to the presence of two bromine isotopes (^{81}Br and ^{79}Br). The FT-IR spectra showed that there are no bands over 3000 cm^{-1} , which means that all hydrogen are replaced with bromine. two absorption bands at 1057 $cm^{-1}$and 1028 cm^{-1} corresponding to the stretching vibration of the C-Br. The melting point of the product was 45 - 46 ˚C in close agreement with reported values in the literature (44.5-45.6 ˚C) [117].

4.1.6 2,2'-Bithiophen-5-yltributylstannane (6)

The preparation of **(6)** was performed according to a modified procedure by Jousselme [60] Scheme 15.

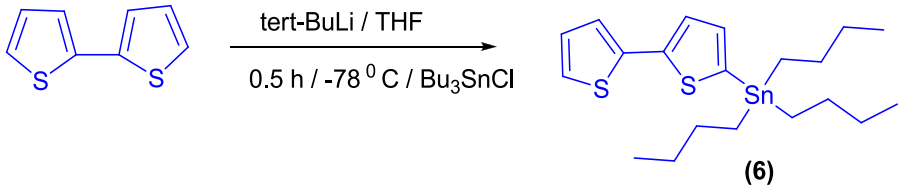

Scheme 15: Preparation of 2,2'-bithiophen-5-yltributylstannane (6)

The product was purified via silica gel column chromatography, eluting with 98% petroleum ether / triethylamine to give the crude product **(6)** as colourless oil (7.77 g, 90% yield). The reaction mechanism involves two steps as shown below in Scheme 16. The first step is deprotonation of the 5-position of 2,2'-bithiophene upon reaction with tert-BuLi. The second step is nucleophilic substitution of chlorine in Bu_3SnCl to form the desired product **(6).**

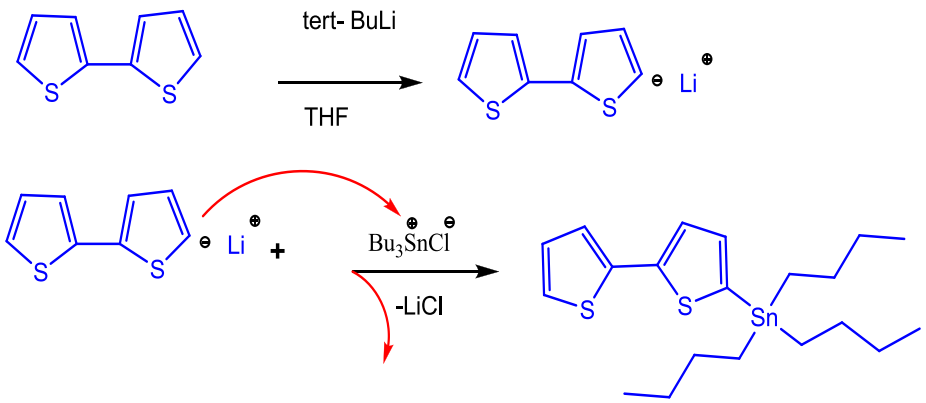

Scheme 16: Reaction mechanism for formation 2,2'-bithiophen-5-yltributylstannane

The purity and the structure the product **(6)** were confirmed by ^{1}H NMR, ^{13}C NMR, elemental analysis, mass spectrometry, and FT-IR. The ^{1}H NMR gave four expected peaks which represent five aromatic protons, a doublet at 7.31 ppm for one proton and multi peaks from 7.21 – 7.19 ppm for two protons , then another doublet at 7.08 ppm from one aromatic proton and a triplet peak at 7.02 ppm for others proton. The expected peaks for the alkyl protons of tri-butyl groups appeared as two multi peaks between 1.78 – 1.51 ppm for 6 protons and 1.46 – 1.07 ppm for 12 protons as well as the expected triplet peaks at 0.92 ppm for 9 protons. The elemental analysis for **(6)** confirmed the structure of the target product. The mass spectra show the main integer mass at 455.10 (M^{+}) which is in agreement with the proposed structure.

4.1.7 4,7-Di(2,2'-bithiophen-5-yl)-5,6-bis(octyloxy)benzo[c][1,2,5]thiadiazole (7)

4,7-Di(2,2'-bithiophen-5-yl)-5,6-bis(octyloxy)benzo[c][1,2,5]thiadiazole **(7)** was prepared via a modified procedure carried out by Zhou [90], Scheme 17.

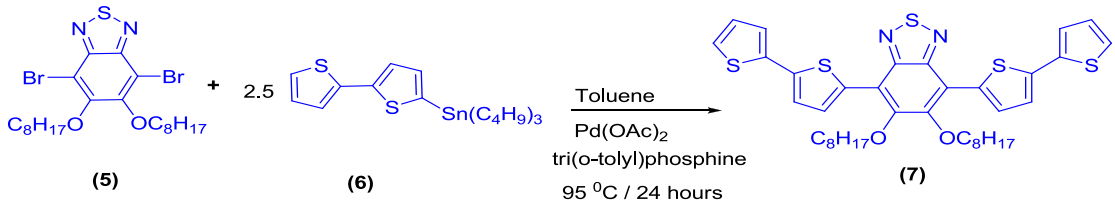

Scheme 17: Preparation of 4,7-di(2,2'-bithiophen-5-yl)-5,6-bis(octyloxy)benzo[c][1,2,5]thiadiazole (7).

The product **(7)** was synthesised using the Stille coupling reaction. This coupling is extremely versatile to form C-C bond and occurs in the presence of palladium catalyst between an arylstannanes and an aryl halides. Owing to its great tolerance towards different functional groups, Stille coupling reaction is used for transformation of highly functionalised compounds. The reaction requires 2 equivalents of the organostannyl compound to react with one equivalent of the dihalide compound. The mechanism of this coupling was introduced by Stille [48a] .The broadly accepted mechanism of Stille coupling is the catalytic cycle mechanism which involves four steps : an oxidative addition , a trans metalation, a trans / cis isomerisation and reductive elimination.The reaction was carried out in toluene 95 ^{0}C for 24 hours. The ratio of 4,7-dibromo-5,6-bis-octyloxy-benzo[1,2,5]thiadiazol **(5)** to 5,5'-bis(tri-n-butylstannyl)-2,2'-bithiophene **(6)** was 1: 2.5. The reaction was catalyzed with $Pd(OAc)_2$ and tri(*o*-tolyl)phosphine and the ratio between these two catalysis was 1 : 2 respectively. The purification was carried out by using column chromatography eluting with petroleum ether/ chloroform 5 : 1 to afford product **(7)** as red crystals in a yield 92 % . Santos have presented the most recent proposed mechanism of the reaction [118] .This mechanism is shown in Scheme 18.

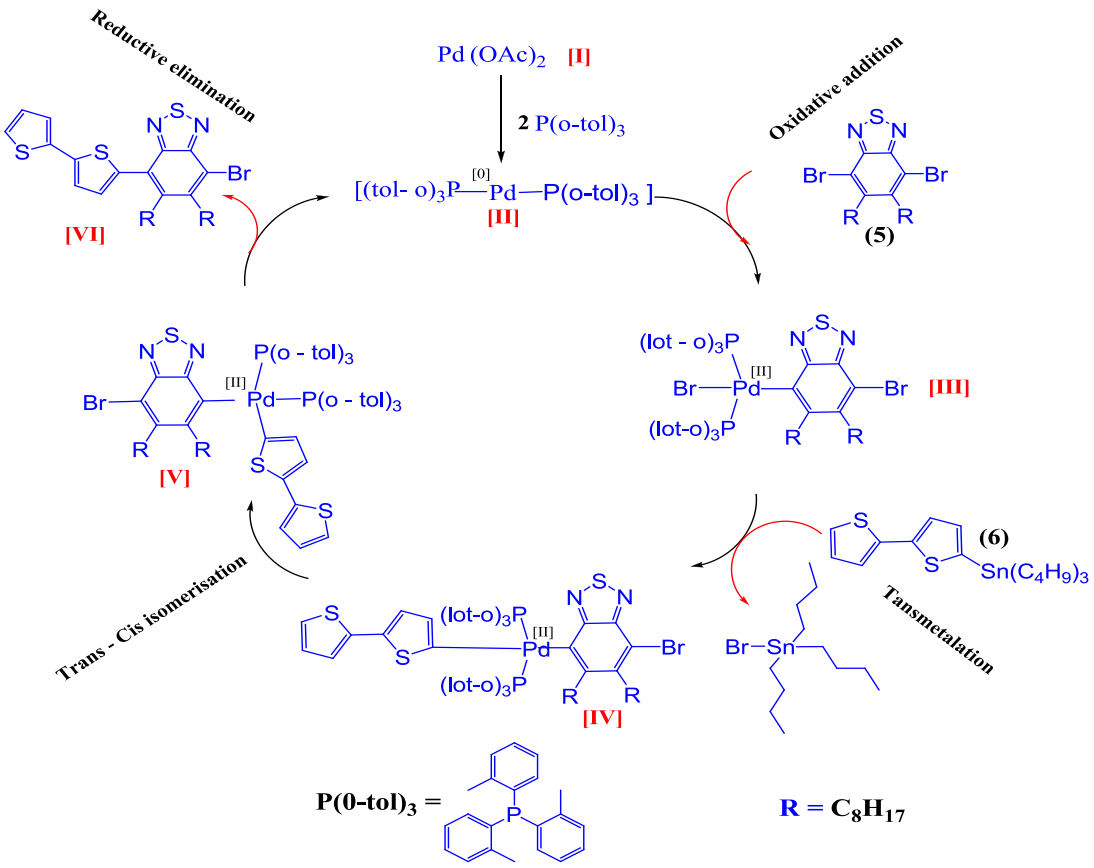

Scheme 18: The Stille coupling mechanism to prepare (7)

The purity and the structure the target product **(7)** were confirmed by ^{1}H NMR, ^{13}C NMR, elemental analysis, mass spectrometry, and FT-IR. The ^{1}H NMR gave four different environments which represent the aromatic protons. At 8.52, 7.31 and 7.28 ppm there are three doublet peaks represent 2, 4 and 2 aromatic protons respectively. At 7.09 ppm a double doublet peak comes from two aromatic protons. The alkyl protons appeared as five different peaks from 4.19 ppm to 0.91 ppm represent 34 protons. The ^{13}C NMR shows eleven expected peaks in the aromatic region between 117.3 and 151.6 ppm which show eleven different carbon environments in the structure and in agreement with the product structure. Also eight peaks for the alkyl chains between 74.5 and 14.1 ppm, those peaks

show eight different carbon environments in the product structure. The elemental analysis was in agreement with the proposed structure. The mass spectrum of the product show the main integer mass at 720 (M^+) which confirmed the proposed structure. The structure of the product was also confirmed by IR spectrum.

4.1.8 4,7-Bis(5'-bromo-2,2'-bithiophen-5-yl)-5,6-bis(octyloxy)benzo[c][1,2,5]thiadiazole (8)

4,7-Bis(5'-bromo-2,2'-bithiophen-5-yl)-5,6-bis(octyloxy)benzo[c][1,2,5]thiadiazole **(8)** was prepared via a modified procedure carried out by Zhou [90] . This reaction gave a good yield of 80 %. The reaction was carried out in chlorobenzene at 55 ^{o}C for 3 h in the dark and then heated to 100 ^{o}C for 15 min as shown in Scheme 19. The product was purified using column chromatography eluting with petroleum ether / chloroform (4 : 1) to afford the product 4,7-bis(5'-bromo-2,2'-bithiophen-5-yl)-5,6-bis(octyloxy)benzo[c][1,2,5]thiadiazole **(8)** as dark red crystals (0.98 g, 80% yield).

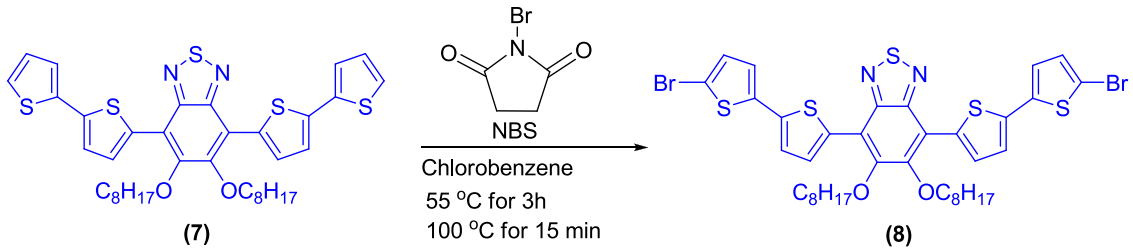

Scheme 19: Synthesisof 4,7-Bis(5'-bromo-2,2'-bithiophen-5-yl)-5,6-bis(octyloxy)benzo[c][1,2,5]thiadiazole (8)

The reaction proceeds via an electrophilic aromatic substitution mechanism as shown in Scheme 20. In this electrophilic aromatic substitution reaction, N-bromosuccinimide (NBS) was used where it can be considered a good source of cationic bromine.The ratio

used between NBS and the 4,7-di(2,2'-bithiophen-5-yl)-5,6-bis(octyloxy)benzo[c][1,2,5]thiadiazole **(7)** must not be more that 2 :1 to ensure the replacement take place on both sides of thiophene rings and to avoid formation of side products such as tri- and tetra- substituted product, which are difficult to purify and lead to undesirable network polymers. The lone pair of the sulfur atom makes the thiophene ring more active towards electrophilic substitution via the resonance effect, which makes the 5-position more nucleophilic. In the (NBS) molecule, the polarization of the carbonyl bond towards the O atom makes the bond between the N atom and the Br atom is polarized towards the N atom due to the difference in electronegativity between these atoms leaving the bromine atom slightly positive. Therefore, the thiophene ring attacks the bromine cation of NBS. The proton on the thiophene ring is attracted towards succinimide anion to produce the brominated ring. Then, this is repeated for another thiophene ring to form the desired product **(8).**

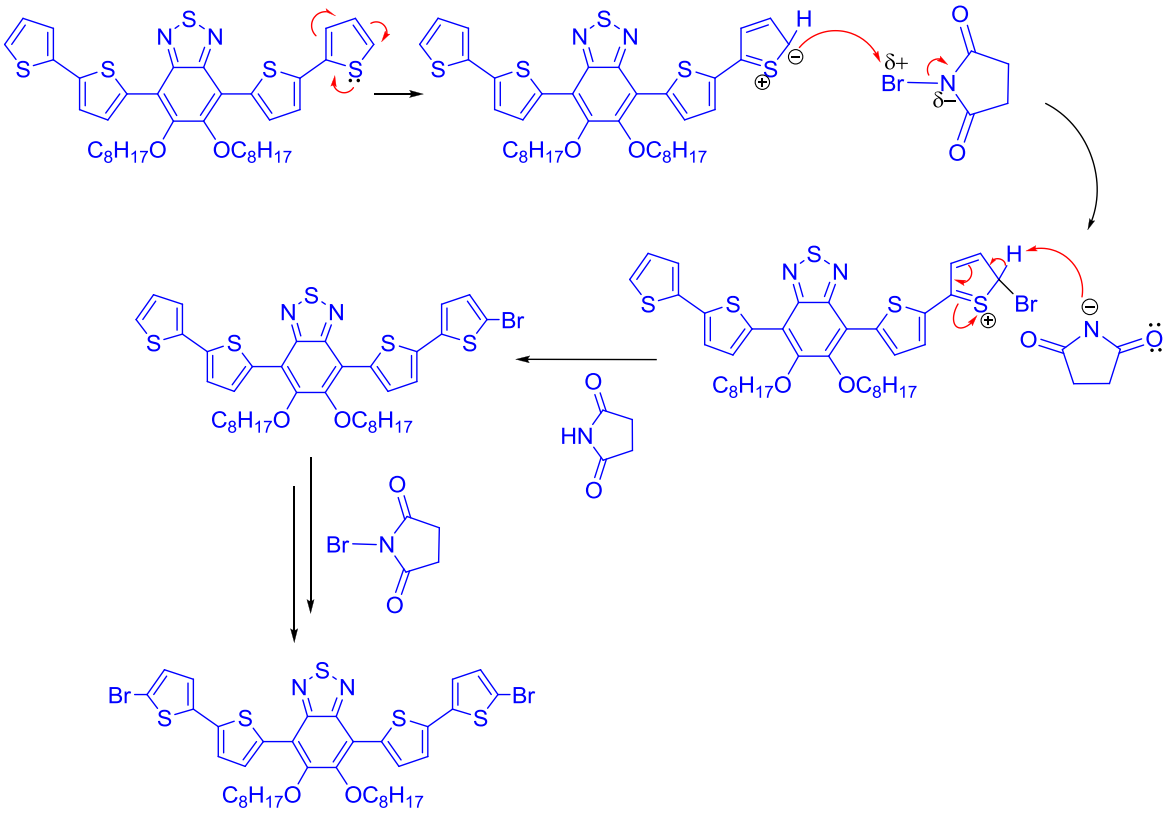

Scheme 20: The bromination mechanism of 4,7-bis(5'-bromo-2,2'-bithiophen-5-yl)-5,6-bis(octyloxy)benzo[c][1,2,5]thiadiazole (8).

The purity and the structure the target product **(8)** were confirmed by ^{1}H NMR, ^{13}C NMR, elemental analysis, mass spectrometry, and FT-IR. It can be seen from the ^{1}H NMR that there are three different environment for aromatic protons at 8.51, 7.25 and 7.04 ppm. At 8.51 and 7.25 ppm, two doublet peaks are related to the protons in the positions (a) and (b) where each one represents two aromatic protons. At 7.04 ppm a multiplet peaks can be assigned for the aromatic protons in the positions (c) and (d) respectively. The expected peaks for the alkyl protons appeared as five different peaks. At 4.17 and 0.91 ppm, two triplets peaks represent ten protons. Three multi and broad peaks at 1.99 ppm and between 1.53 – 1.20 ppm represent 24 protons, Figure 54. The mass spectrum for **(8)** showed peaks at 876, 878 and 880 due to the presence of bromine isotopes (^{81}Br and ^{79}Br). The elemental analysis of the product was in agreement with the proposed structure. The ^{13}C NMR shows eleven expected peaks in the aromatic region between 117.2 and 151.5 ppm which show eleven different carbon environments in the structure and in agreement with the product structure. Also eight peaks for the alkyl chains between 74.5 and 14.1 ppm, those peaks show eight different carbon environments in the product structure. The structure of the product was also confirmed by IR spectrum.

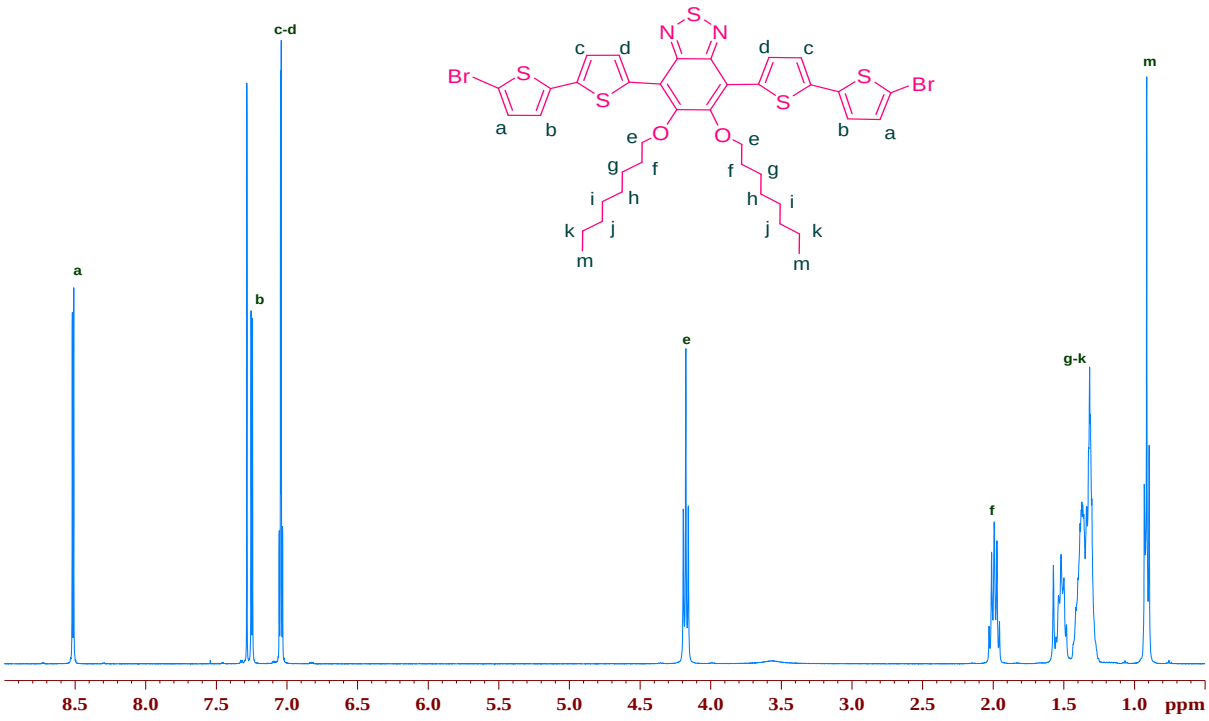

Figure 54:1H NMR of (8)

4.1.9 1,4-Dibromo-2-fluoro-5-nitrobenzene (9)

1,4-Dibromo-2-fluoro-5-nitrobenzene **(9)** was synthesized according to a procedure by Chen , Scheme 21[105]. The product was purified by recrystallisation in ethanol to give the product as a yellow solid with a relatively high yield of 86%. The reaction was carried out in the presence of trifluoroacetic acid (TFA) , trifluoroacetic anhydride (TFAA) as a catalyst, and ammonium nitrate.

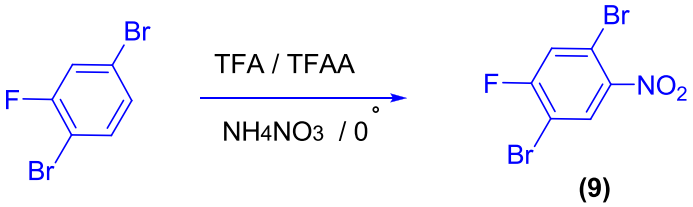

(9)

Scheme 21: Synthesis of 1,4-dibromo-2-fluoro-5-nitrobenzene (9)

The mechanism of this reaction consists of two steps: formation of electrophile (Nitronium ion) and then attack on the aromatic ring to form the desired product as shown in Scheme

22. The reaction mechanism begins by breaking the anhydride bond in trifluoroacetic anhydride (1), then after which an nucleophilic attack by NO_3 to form trifluoroacetyl nitrate (2), which dissociates later to form nitronium ion (NO_2^+) (3).

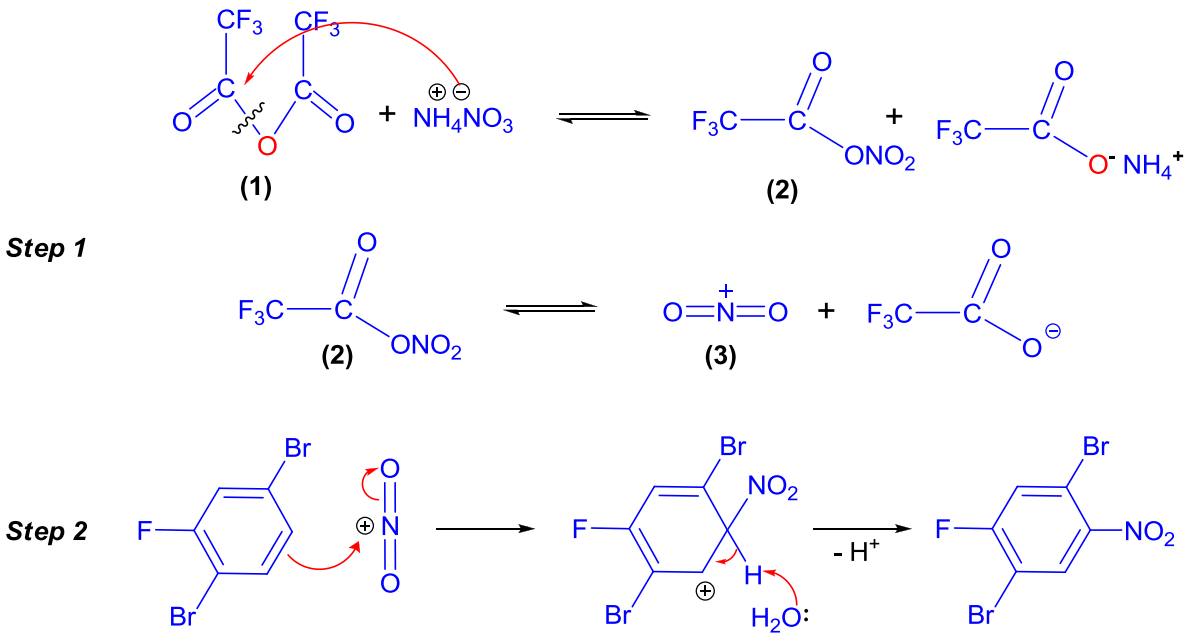

Scheme 22: Mechanism of electrophilic substitution reaction to form 1,4 -dibromo-2-fluoro-5-nitrobenzene

The structure and the purity of the product was confirmed by ^{1}H NMR, ^{13}C NMR , element analysis , mass spectra and FT-IR and TLC (R_f = 0.66). The ^{1}H NMR displays two doublet peaks at 8.20 and 7.55 ppm for aromatic proton. The ^{13}C NMR gave six peaks in the aromatic region between 159.3 and 108.7 ppm. The mass spectrum main integer masses for **(9)** were observed at 297, 299 and 301 in 1:2:1 ratio as expected due to the ^{79}Br and ^{81}Br isotopes. The structure of the product was also confirmed by elemental analysis. The FT-IR spectrum of the product **(9)** shows two sharp bands at 1526 $cm^{-1}$and 1345 cm^{-1} corresponds to the nitro group. The stretching vibration bands of the C-F and C-Br bonds are shown at 1250 cm^{-1} and 1065 cm^{-1} respectively. The stretching vibration

band of the aromatic C-H bonds appears at 3091 and 3022 cm^{-1}. The melting point was 60-62.5 °C which was in good agreement with literature values [105].

4.1.10 4,4'-Dibromo-5,5'-difluoro-2,2'-dinitrobiphenyl (10)

4,4'-Dibromo-5,5'-difluoro-2,2'-dinitrobiphenyl **(10)** was obtained by a modified procedure of Yamato [106]. The reaction was carried out in DMF at 120 °C for three hours and was purified by recrystallisation in ethanol to give the product as yellow crystals in 70 % yield Scheme 23.

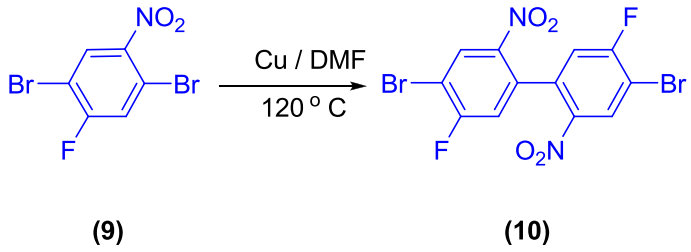

(9) **(10)**

Scheme 23: Synthesis of 4,4'-dibromo-5,5'-difluoro-2,2'-dinitrobiphenyl (10)

This reaction follows the Ullmann coupling reaction through copper catalyzed coupling as shown in Scheme 23. The reaction mechanism occurs through steps as shown in Scheme 24. In this mechanism the reactants are thought to be adsorbed on Cu surface[119] where as the reaction required using stoichiometric amounts of copper[120]. Owing to the resonance effect presented by the nitro group at the 5- position in compound (a) , the C atom at the 4-position becomes positively charged which is vulnerable to nucleophilic attack by Cu atom. The copper atom in this case undergoes oxidative addition to form organocopper intermediate (d) where the Cu atom has (II) oxidation state[120]. The next step is that the copper bromide complex formed at the 4 position of organocopper intermediate (d) reacts

as Lewis acid making the carbon at this position negatively charged as a nucleophile. While compound (e) again under resonance effect of nitro group makes the carbon at the 4- position has positive charge to be attacked by the formed nucleophile in compound (d).The previous step is thought again undergoes to oxidative addition where it coupled with another molecule of 1,4-Dibromo-2-fluoro-5-nitrobenzene (e) at position 4 to form the an unstable organocopper molecule (f) in which the copper atom has (III) oxidation state. Then, the unstable organocopper molecule (f) subjects to reductive elimination to introduce the desired product (g) and $CuBr_2$ as a side product.

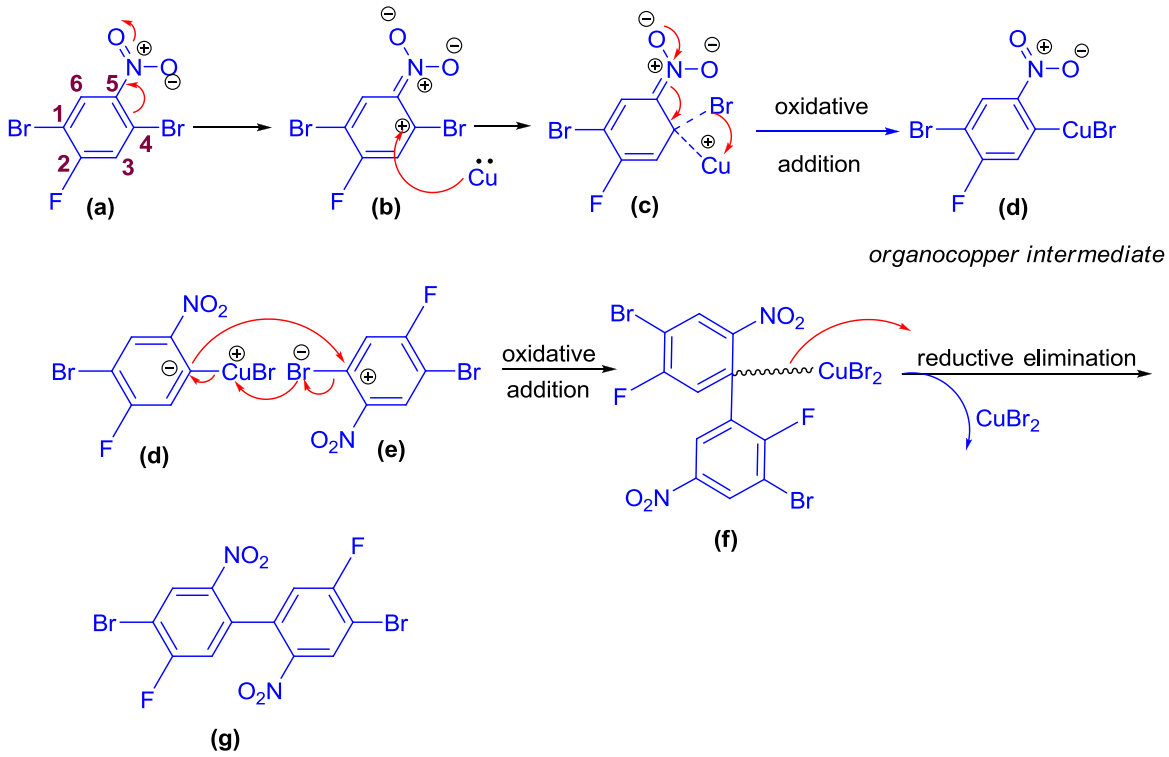

Scheme 24 : Mechanism of Ullmann reaction of 4,4'-dibromo-5,5'-difluoro-2,2'-dinitrobiphenyl

The purity and structure of the product was confirmed by ^{1}H NMR, ^{13}C NMR , mass spectrometry, melting point, elemental analysis, FT-IR and TLC (R_f = 0.78).The ^{1}H NMR shows two doublet peaks at 8.57 and 7.09 ppm for the aromatic protons. The ^{13}C NMR

displayed six peaks in the aromatic region between 162 and 110 ppm. The mass spectraum main integer masses for **(10)** are observed at 436, 438 and 440 in 1:2:1 ratio as expected due to the ^{79}Br and ^{81}Br isotopes. The structure of the product was also confirmed by elemental analysis , the melting point is in good agreement with literature values which was 114.5-115.2 ˚C [121]. The FT-IR spectra of the product **(10)** shows two sharp bands at 1524 $cm^{-1}$and 1339 cm^{-1} belongs to the nitro groups. The stretching vibration bands of the C-F and C-Br bonds are shown at 1292 cm^{-1} and 1068 cm^{-1} respectively. The stretching vibration band of the aromatic C-H bonds appears at 3061 cm^{-1}.

4.1.112,2'-Diamino-4,4'-dibromo-5,5'-difluorobiphenyl (11)

2,2'-Diamino-4,4'-dibromo-5,5'-difluorobiphenyl **(11)** was obtained by a modified procedure of Yamato [106] according to Scheme 25 in the presence of tin powder with a mixture of ethanol and HCl. The product was obtained via recrystallisation from ethanol as a pale brown powder in 89 yield %.

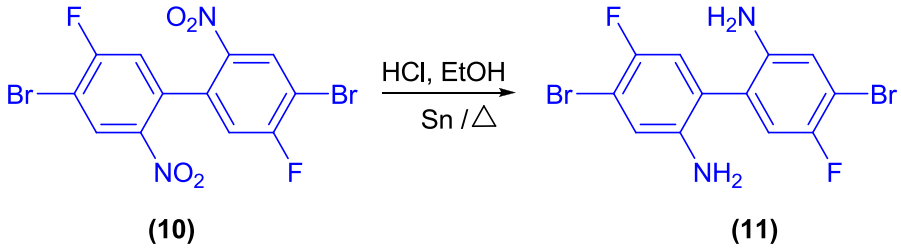

(10) **(11)**

Scheme 25 : Synthesis of 2,2'-diamino-4,4'-dibromo-5,5'-difluorobiphenyl (11)

The reaction mechanism is thought to proceeds in two steps as shown in Scheme 26. The nitro groups in **(10)** are reduced in the presence of tin powder using two equivalents of tin. Reduction process of the nitro group is done in acidic medium such as HCl. The nitro groups are protonated by the acid to introduce protonated amines and the subsequent step

is treatment with NaOH to form the desired product 2,2'-diamino-4,4'-dibromo-5,5'-difluorobiphenyl **(11).**

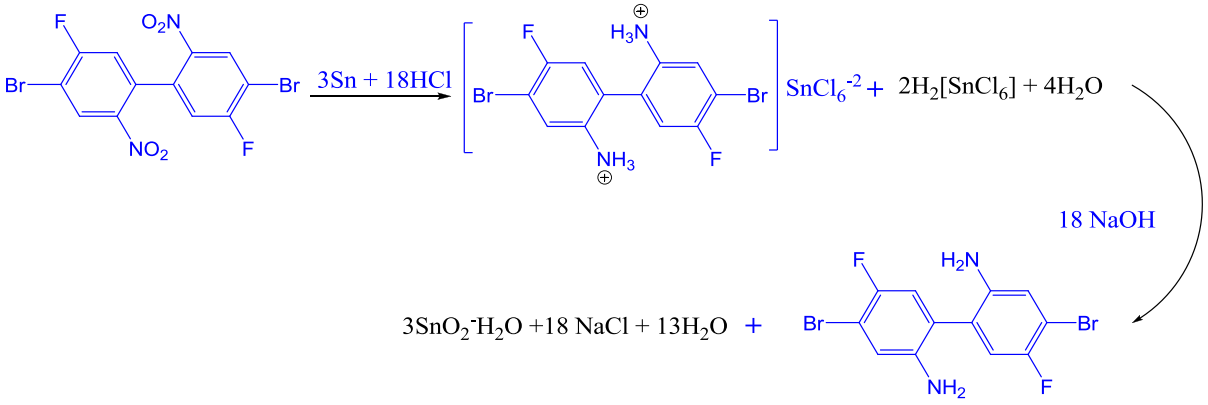

Scheme 26 : Mechanism of preparation of 2,2'-diamino-4,4'-dibromo-5,5'-difluorobiphenyl (11)

The purity and structure of the product were confirmed by ^{1}H NMR, ^{13}C NMR , mass spectrometry, elemental analysis , melting point, FT-IR and TLC (R_f = 0.40) . The ^{1}H NMR displayed three different environment peaks, two doublet peaks at 7.11 and 6.95 ppm for aromatic protons and a broad single peak at 4.66 ppm for the amine protons. The ^{13}C-NMR spectra showed six peaks, three of them are doublets at 152.4, 117.9 and 109.4 ppm , which are related to the carbons close to fluorine atom and the other three are singlet at 140.9, 122.9 and 119.8 ppm. The mass spectrums main integer masses for 4,4'-dibromo-5,5'-difluoro-biphenyl-2,2'-diamine **(11)** were observed at 376, 378 and 380 in 1:2:1 ratio as expected due to the ^{79}Br and ^{81}Br isotopes. The melting point was 162-168 °C and in good agreement with that reported in the literature [121]. The FT-IR of the product illustrates two bands at 3309 and 1622 cm^{-1} corresponds to the stretching and bending vibration of the N-H group. The stretching vibration bands of the C-N and C-Br bonds are shown at 1056 and 1163cm^{-1} respectively. The stretching vibration bands of the C-H aromatic bonds are displayed at 3191 cm^{-1} .

4.1.12 2,7-Dibromo-3,6-difluoro-9H-carbazole (12)

2,7-Dibromo-3,6-difluoro-9H-carbazole **(12)** was prepared according to the procedure by Sonntag [107]. The reaction was carried out in acidic conditions using concentrated phosphoric acid at 190 °C for 24 hour as shown in Scheme 27. The product was obtained by recrystallisation from a mixture of toluene / hexane (10:1) to remove the residual traces of the phosphoric acid, the product was washed with extra amount of water, then extraction with toluene to give the product 2,7-dibromo-3,6-difluoro-9H-carbazole **(12)** as an ivory powder in 76 % yield.

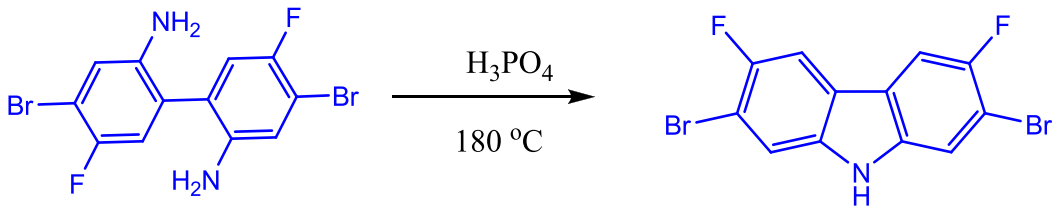

(11) **(12)**

Scheme 27 : Synthesis of of 2,7-dibromo-3,6-difluoro-9H-carbazole.

The reaction mechanism follows the intramolcular SN_2 mechanism Scheme 28. This cyclisation reaction mechanism includes two steps, where in the first step the phosphoric acid protonates one of the amino groups to form NH_3^+ group. After which the intramolecular nucleophilic attack by the amino group from the other phenyl ring leading to elimination of NH_3^+ to give product **(12).**

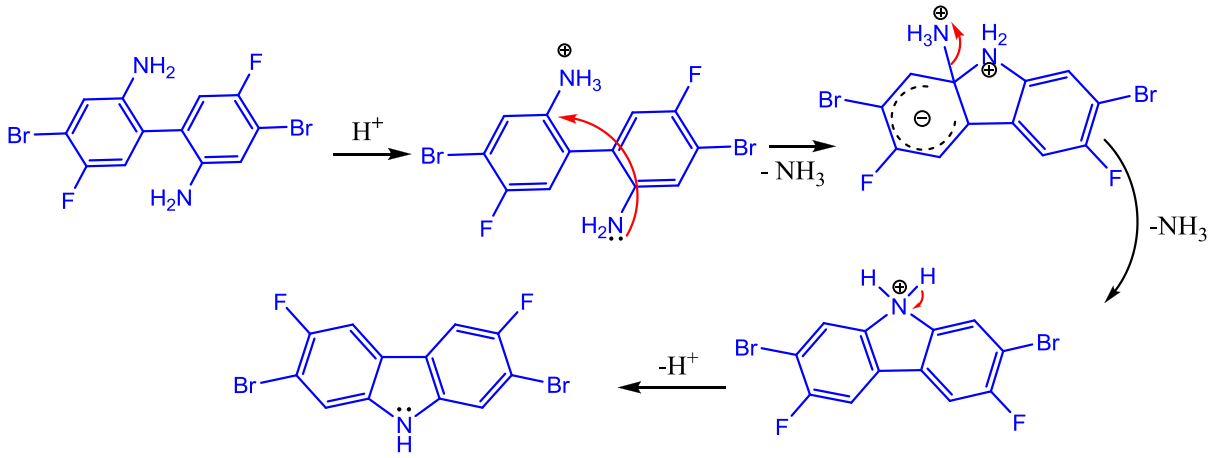

Scheme 28 : Mechanism of preparation of 2,7-Dibromo-3,6-difluoro-9H-carbazole (12)

The purity and structure of product were confirmed by ^{1}H NMR, ^{13}C NMR , mass spectrometry, melting point, elemental analysis , FT-IR and TLC. The melting point was 348 – 350°C which in agreement with that reported in the literature [78] .The product gave a single spot on TLC (R_f = 0.41) . The ^{1}H NMR gave three different environments. Two doublets peaks at 8.10 and 7.83 ppm for aromatic protons and a broad single peak at 10.63 ppm for the NH proton. The ^{13}C NMR gave six peaks in the aromatic region between 153.9 and 107.8 ppm. The two doublets at 153.9 and 107.9 ppm can be attributed to the carbons close to the fluorine atom, the other four are singlet at 138.7, 123.1, 116.4 and 108.2 ppm. The mass spectrum shows three main integer masses for 2,7-dibromo-3,6-difluoro-9H-carbazole **(12)** observed at 359, 361 and 363 in 1:2:1 ratio as expected due to the ^{79}Br and ^{81}Br isotopes. The FT-IR of the product displays the stretching vibration of the -NH group at 3451 cm^{-1} where that the peaks at 3309 and 1622 cm^{-1} that belong to – NH_2 groups in compound **(11)** have disappeared which means that the cyclisation reaction has lead to form the target product **(12)**. The stretching vibration bands of the C-N and C-Br bonds are shown at 1205 and 1151 cm^{-1} respectively. The stretching vibration band of

the aromatic C-H bond appears at 3042 cm^{-1} and 1477 cm^{-1}. The structure of the product was also confirmed by CHN element analysis.

4.1.13 Heptadecan-9-ol (13)

Heptadecan-9-ol **(13)** was synthesized according to the procedure by Leclerc et al [92]. The product was obtained as colourless oil in 98 % yield. The reaction involves two steps; the first step is the formation of (Grignard reagent) octylmagnesium bromide (b) by reacting magnesium turnings with 1- bromooctane (a) in THF. The second step is the formation of the desired product heptadecan-9-ol **(13)** through reaction of two equivalents of octylmagnesium bromide (Grignard reagent) (b) with ethyl formate (c) to obtain the target product as shown in Scheme 29 .

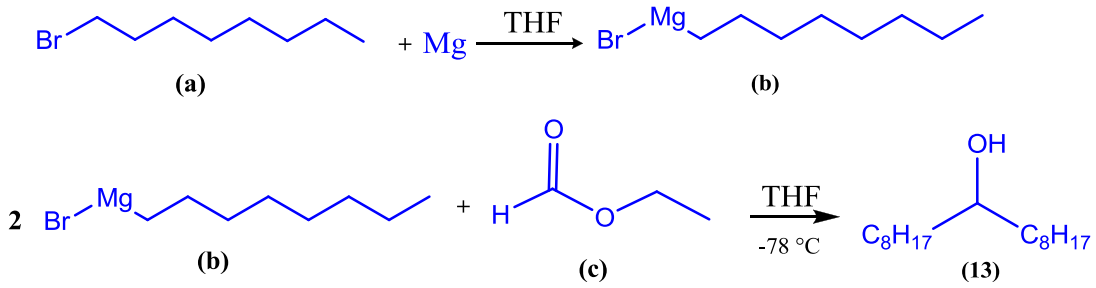

Scheme 29 : Synthesis of the Grignard reagent and the heptadecan-9-ol (13)

The reaction mechanism of adding Grignard reagent to ethyl formate to form the desired product heptadecan-9-ol **(13)** is thought to proceed through a mechanism as shown in Scheme 30.

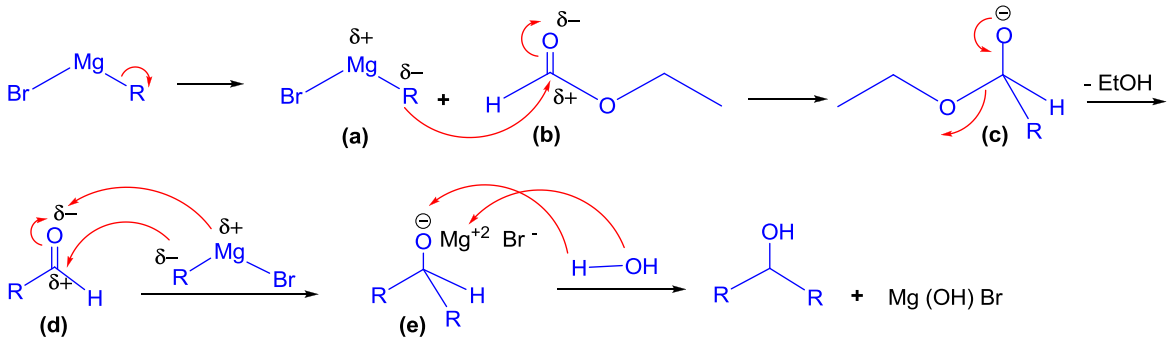

Scheme 30 : Reaction mechanism for adding Grignard reagent to ethyl formate to form Heptadecan-9-ol (13)

The purity and structure of the product was confirmed melting point , TLC , ^{1}H NMR, ^{13}C NMR , the mass spectrometry, elemental analysis and FT-IR . The melting point 29 - 31 ˚C is in agreement with that reported in the literature (28-31˚C) [122]. The product gave a single spot on TLC (R_f = 0.52). The ^{1}H NMR analysis shows a broad multi peaks at 3.60 ppm , which can be assigned to the (O – H) proton. Also another three peaks at 1.46 , 1.29 and 0.89 ppm represent the protons of alkyl chains. The ^{13}C NMR analysis gave nine peaks in the aliphatic region between 72 and 14.1 ppm. Elemental analysis of (**13)** was in agreement with its proposed structure. The mass spectrum shows the main integer mass at 255 for heptadecan-9-ol **(13)** . FT-IR displayed a peak at 3321 cm^{-1} which represents the O-H stretching of the hydroxyl group.

4.1.14 Heptadecan-9-yl 4-methylbenzenesulfonate (14)

Heptadecan-9-yl 4-methylbenzenesulfonate **(14)** was prepared according to the procedure by Leclerc [92]. The purification of the product was carried out via column chromatography eluting with ethyl acetate / hexane (1: 9) to give the desired product in a good yield (96 %) as a white solid, Scheme 31 .

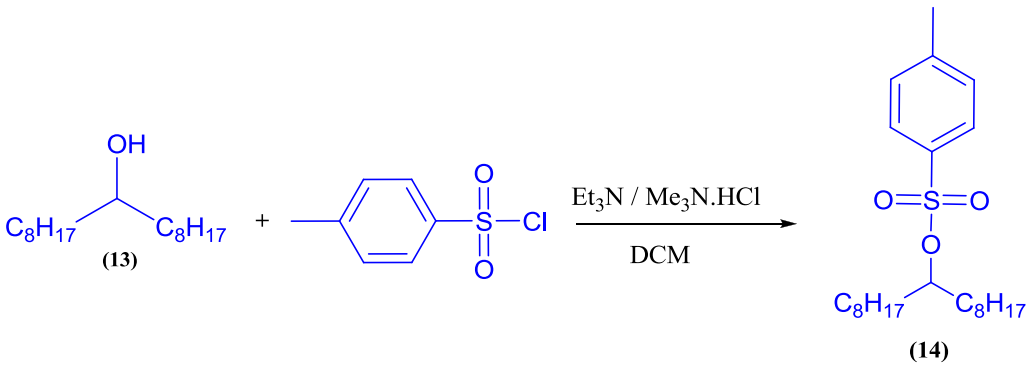

Scheme 31 : Synthesis of Heptadecan-9-yl 4-methylbenzenesulfonate (14)

The mechanism of tosylation is illustrated in Scheme 32.

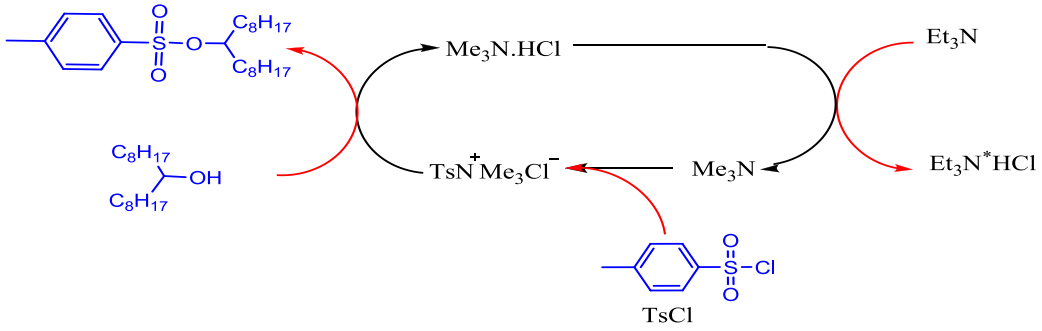

Scheme 32 : Preparation mechanism of heptadecan-9-yl 4-methylbenzenesulfonate (14)

The mechanism in Scheme 32 describes the reaction between trimethylamine hydrochloride Me_3N•HCl and triethylamine Et_3N. In this mechanism, the trimethylamine hydrochloride Me3N•HCl salt acts as a catalyst while the triethylamine Et_3N as base to form Me_3N. Then, Me_3N reacts with p-toluenesulfonyl chloride TsCl to generate the tosylate reagent (TsN^+Me_3Cl). Then, the generated tosylate reagent (TsN+Me_3Cl) reacts with hydroxyl group to obtain the desired product . The Me_3N•HCl starts a new cycle as illustrated in Scheme 32. The purity and structure of the product was confirmed by melting point, TLC, ^{1}H NMR, ^{13}C NMR , the mass spectrum, elemental analysis and FT-IR. The melting point was 31- 32.5 ˚C which was in good agreement with that reported in the literature (31-32 ˚C) [122]. The product gave a single spot on TLC (R_f = 0.49). The ^{1}H NMR

displayed two doublet peaks for aromatic protons at 7.80 and 7.34 ppm which corresponded to tosyl group. A multipeaks at 4.50 ppm represent the proton (O - C -H) close to the tosyl group. The protons of the methyl group in the para position of the tosyl group appeared at 2.46 ppm. The ^{13}C NMR gave four peaks in the aromatic region at 144.2 , 134.7 , 129.6 , 127.7 ppm. The aliphatic region between shows ten peaks between 84.6 and 14.1 ppm. The FT-IR of the product illustrates that the stretching vibration bands at 3321 cm^{-1} for the hydroxyl group (O - H) of heptadecan-9-ol **(13)** disappeared . The stretch vibration band of the aromatic C – H bond is observed at 2955 cm^{-1}. The stretching vibration of the (-SO_2) in sulfonate group is shown at 1353 cm^{-1} .The mass spectrum shows main integer mass for heptadecan-9-yl 4-methylbenzenesulfonate **(14)** at 410 (M^+), which is in agreement with the proposed structure, and the elemental analysis CHN of (14) was in agreement with its proposed structure.

4.1.15 2,7-Dibromo-3,6-difluoro-9-(1-octyl-nonyl)-9H-carbazole (15)

2,7-Dibromo-3,6-difluoro-9-(1-octyl-nonyl)-9H-carbazole **(15)** was synthesized using a modified procedure by Leclerc [92]. 2,7-Dibromo-3,6-difluoro-9-(1-octyl-nonyl)-9H-carbazole **(15)** was synthesized by the reaction between 2,7-dibromo-3,6-difluoro-9H-carbazole **(12)** and heptadecan-9-yl 4-methylbenzenesulfonate **(14)** in the presence of KOH as base. The alkylation reaction was carried out in DMSO as solvent at room temperature for 6 hours, Scheme 33.

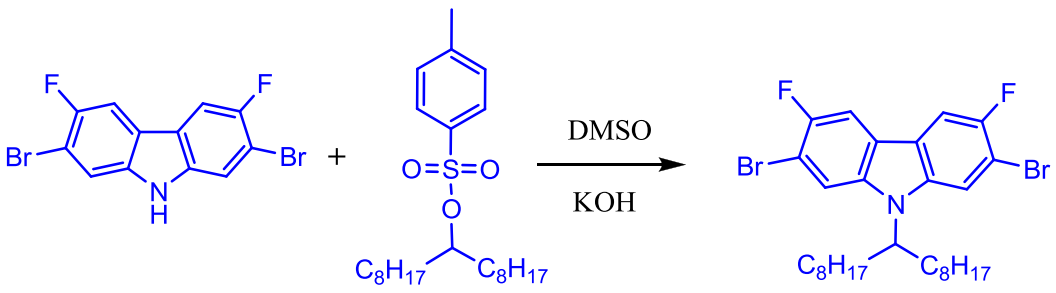

(12) **(14)** **(15)**

Scheme 33 : Synthesis of 2,7-dibromo-3,6-difluoro-9-(1-octyl-nonyl)-9H-carbazole (15)

The product was purified via silica gel column chromatography eluted with hexane to give the product **(15)** as a brown solid in 67.2 % yield.The reaction mechanism follows the bimolecular nucleophilic substitution (S_N2), which consists of two steps. The deprotonation of the N atom in carbazole by KOH followed by attack on the carbon with the toyslate group and its displacement to give the desired product (Scheme 34) .

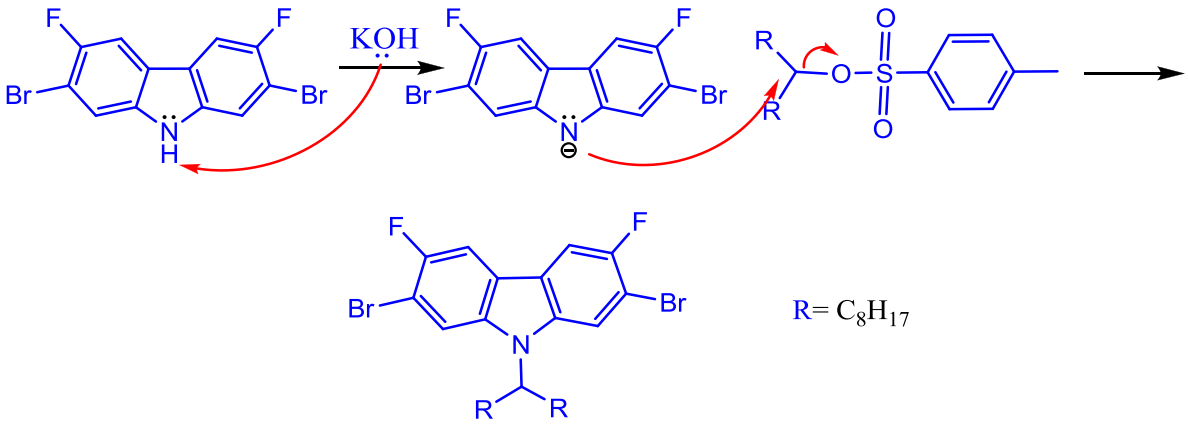

Scheme 34 : Mechanism of preparation of 2,7-dibromo-3,6-difluoro-9-(1-octyl-nonyl)-9H-carbazole (15)

The purity and structure of the product was confirmed by TLC, ^{1}H NMR, ^{13}C NMR, the mass spectrometry, elemental analysis and FT-IR. The product gave a single spot on TLC (R_f = 0.50). The ^{1}H NMR displayed broad peaks at 7.79 to 7.68 ppm and doublet peak at 7.57 ppm for aromatic protons. Also multiplet peaks at 4.45 – 4.34 ppm belongs to proton on the carbon attached to N atom. The mass spectrum show main integer masses at 597, 599 and 601 in 1:2:1 ratio as expected due to the presence of two bromine isotopes (^{81}Br and ^{79}Br). The ^{13}C NMR spectrum shows the aromatic region from 153 ppm to 106.7 ppm and the aliphatic region from 57 ppm to 14 ppm. The FT-IR of the product confirmed that peaks corresponded to (–NH) and tosyl groups of compound **(12)** and **(14)** have

disappeared , which confirm the formation of the product **(15).** Elemental analysis CHN of **(15)** was in agreement with its proposed structure.

4.1.16 3,6-Difluoro-9-(heptadecan-9-yl)-2,7-bis(4,4,5,5-tetramethyl-1,3,2-dioxaborolan-2-yl)-9*H*-carbazole (16)

3,6-Difluoro-9-(1-octyl-nonyl)-2,7-bis(4,4,5,5-tetramethyl-1,3,2-dioxaborolan-2-yl)-9H-carbazole **(16)** was synthesized using a modified procedure by Brunner [108]. The product **(16)** was obtained as a light brown solid in 84.8 % yield by the reaction between 2,7-dibromo-3,6-difluoro-9-(1-octyl-nonyl)-9H-carbazole **(15)** and bis(pinacolato)diboron in dry DMF, Scheme 35 .

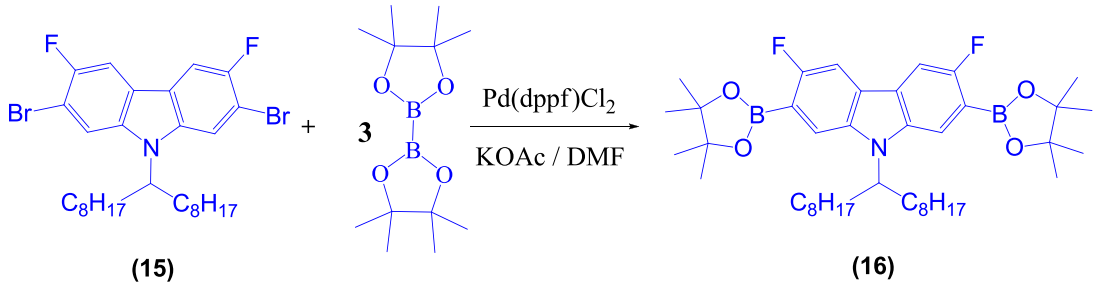

Scheme 35 : Synthesis of 3,6-difluoro-9-(1-octyl-nonyl)-2,7-bis(4,4,5,5-tetramethyl-1,3,2-dioxaborolan-2-yl)-9H-carbazole (16)

The reaction follows the Suzuki coupling reaction mechanism, which consists of three steps as shown in Scheme 36. These steps are an oxidative addition, transmetallation and reductive elimination[123].

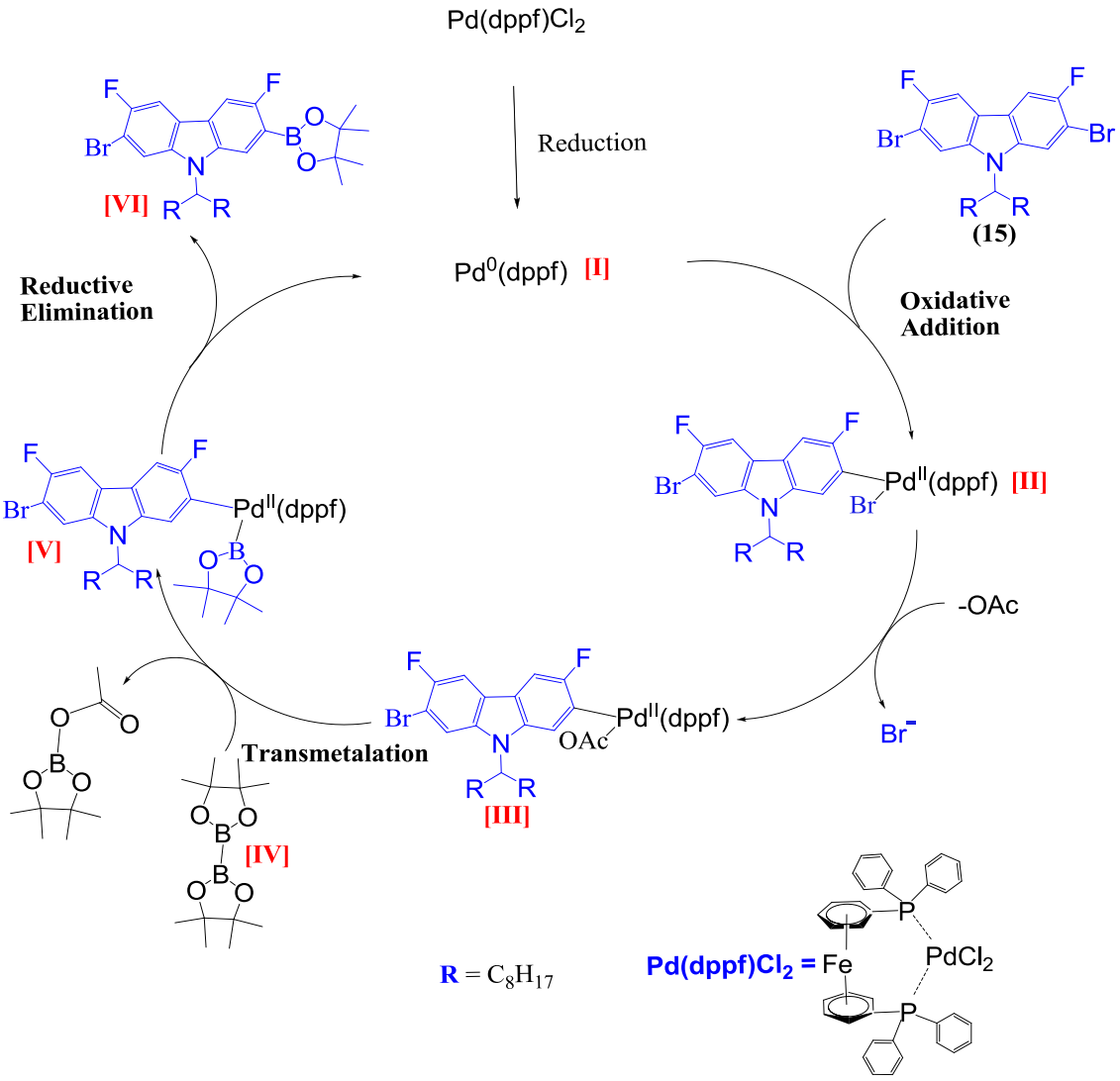

Scheme 36 : The proposed reaction mechanism for preparing 3,6-difluoro-9-(1-octyl-nonyl)-2,7-bis(4,4,5,5-tetramethyl-1,3,2-dioxaborolan-2-yl)-9H-carbazole (16)

The first step involves an oxidative addition of the 2,7-dibromo-3,6-difluoro-9-(1-octyl-nonyl)-9H-carbazole **(15)** to the catalyst Pd^{0}(dppf) [I] to form the palladium^{II} complex [II], where the bromide group in this complex is displaced by the acetate leading to the aryl palladium^{II} complex [III].A transmetalation reaction is the second step where the aryl palladium^{II} complex [III] reacts with bis(pinacolato)diboron [IV] to form an intermediate palladium^{II} [V]. The bis(pinacolato)diboron [IV] in the transmetalation reaction is activated by the reaction with base (AcO-) where this activation facilitates the transmetallation step. Using a base such as potassium acetate is an essential requirement

for transmetallation step where the absence of the base, the transmetallation reaction between the aryl palladium^{II} complex [III] and bis(pinacolato)diboron [IV] does not accrue readily due to the low nucleophilicity of the organic group on the boron atom. The final step of the catalytic cycle is the reductive elimination of the intermediate palladium^{II} [V] to yield the target coupling product [VI] where the catalytic cycle starts again with the other bromine atom to form the desired product 3,6-difluoro-9-(1-octyl-nonyl)-2,7-bis(4,4,5,5-tetramethyl-1,3,2-dioxaborolan-2-yl)-9H-carbazole **(16)** .

The purity and structure of product 3,6-difluoro-9-(1-octyl-nonyl)-2,7-bis(4,4,5,5-tetramethyl-1,3,2-dioxaborolan-2-yl)-9H-carbazole **(16)** was confirmed by ^{1}H NMR, ^{13}C NMR , the mass spectrum, elemental analysis and FT-IR. The ^{1}H NMR displayed three broad peaks at 7.89, 7.80 and 7.70 ppm which can be assigned to carbazole protons in the positions (b) and (a) . It can be seen that the carbazole protons in the position (b) are displayed in two different environments which can be attributed to the restricted rotation at the C-N bond . The multiplet peak at 4.68 ppm can be related to the ($R_2C\underline{H}N$) proton in the position (c). The multiplet peaks at 2.37, 1.87 ppm are correspond to the protons in the positions (d) and (e) respectively. The protons of the methyl group of the boronic ester in the positions (m) are shown as singlet peak observed at 1.40 ppm. The protons of the two CH_3 groups at the end of the alkyl chains are displayed at 0.84 ppm as triplet peak , Figure 55.

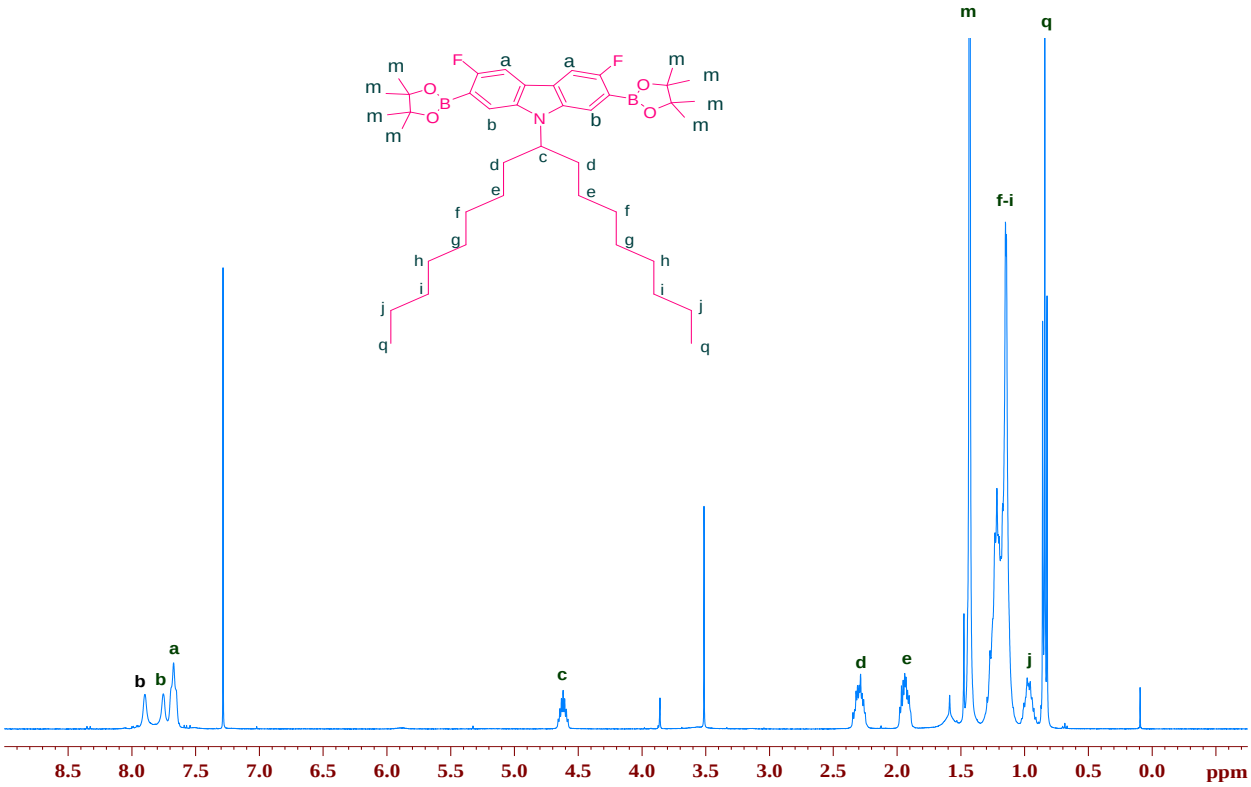

Figure 55: 1H NMR of monomer 3,6-Difluoro-9-(1-octyl-nonyl)-2,7-bis(4,4,5,5-tetramethyl-1,3,2-dioxaborolan-2-yl)-9H-carbazole (16)

The mass spectra show the main integer mass at 693 (M^+), which is in agreement with the proposed structure. The ^{13}C NMR also confirms the structure of **(16).** The FT-IR spectrum showed the stretching vibration bands of the B-O bond at 1391 cm^{-1} and 1331 cm^{-1}. Also a band at 1137 cm^{-1} corresponds to the B-C stretching.

4.2 Synthesis of the alkoxylated thiophene-benzothiadiazole based monomer for copolymers : (P1) (P2) and diblock copolymer (P8)

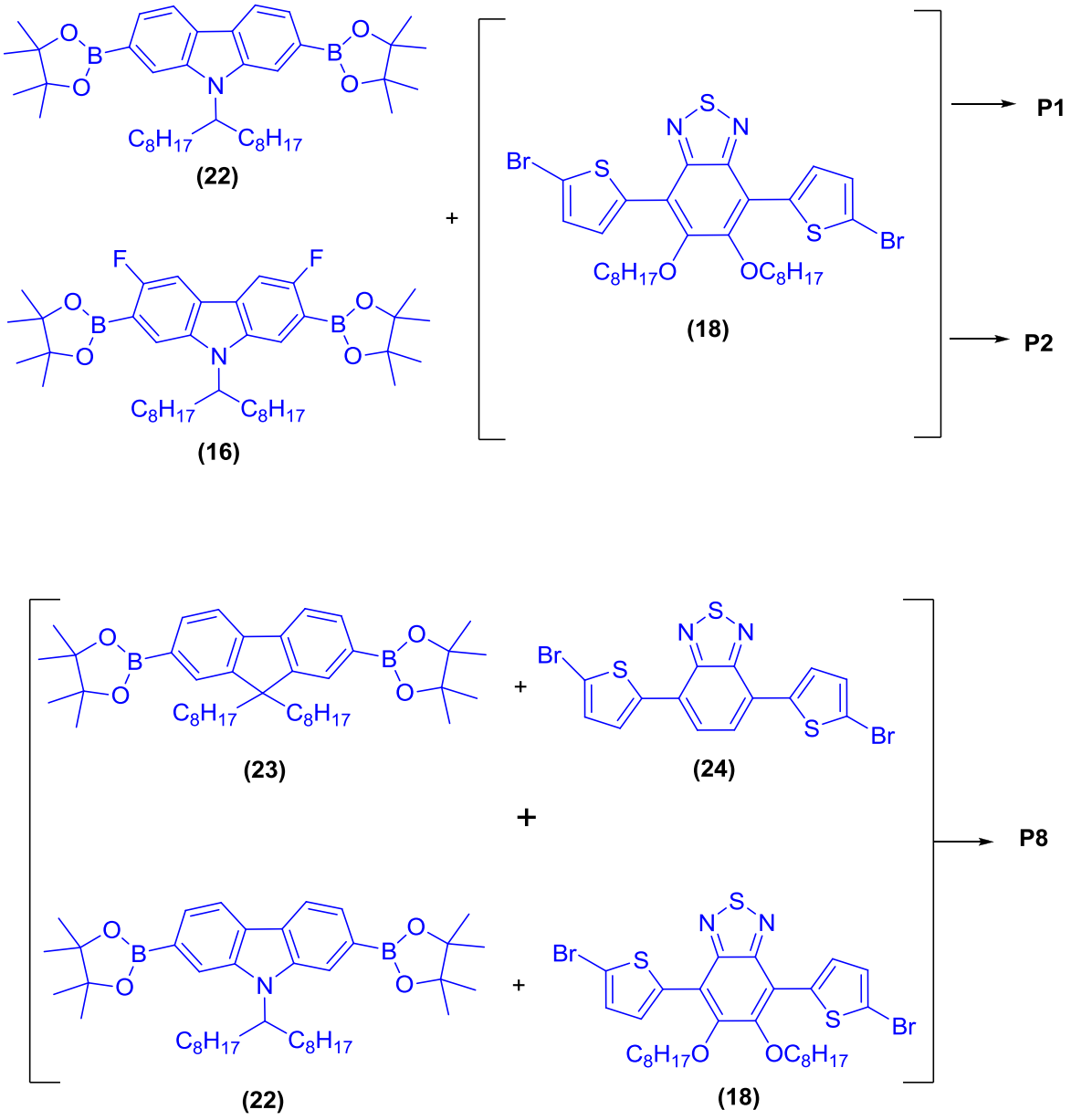

Figure 56: The monomers used to prepare P1 , P2 and P8

Figure 56 shows the required monomers to prepare the polymers **P1**, **P2** and **P8** . 4,7-Bis(5-bromothiophen-2-yl)-5, 6-bis(octyloxy)benzo-[c][1,2,5]-thiadiazole **(18)** was

synthesised successfully in a good yield and its purity and structure was confirmed by ^{1}H NMR , ^{13}C NMR, CHN elemental analysis, FT-IR and mass spectroscopy analysis. 4,7-Bis(5-bromothiophen-2-yl)-5, 6-bis(octyloxy)benzo-[c][1,2,5]-thiadiazole **(18)** was used as acceptor units to prepare polymer **P1** and **P2.** Also 4,7-bis(5-bromothiophen-2-yl)-5, 6-bis(octyloxy)benzo-[c][1,2,5]-thiadiazole **(18)** was used as co-monomer with monomers **(22) , (23)** and **(24)** to prepare block copolymer **P8.** The synthetic routes for preparing 4,7-bis(5-bromothiophen-2-yl)-5, 6-bis(octyloxy)benzo-[c][1,2,5]-thiadiazole **(18)** is shown in Scheme 37 .

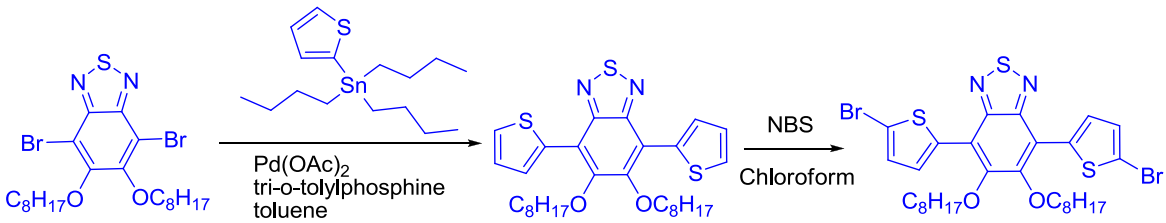

(5) **(17)** **(18)**

Scheme 37 : Synthetic route for preparing 4,7-bis(5-bromothiophen-2-yl)-5, 6-bis(octyloxy)benzo-[c][1,2,5]-thiadiazole (18)

4.2.1 4,7-Bis(5-bromothiophen-2-yl)-5,6-bis(octyloxy)benzo[c][1,2,5]thiadiazole (17)

4,7-Bis(5-bromothiophen-2-yl)-5,6 - bis(octyloxy)benzo[c][1,2,5]thiadiazole **(17)** was prepared according to the procedure by Helgesen [103], Scheme 38 . The crude product was purified via silica gel column chromatography, eluting with hexane / ethyl acetate (10:1) to obtain **(17)** as orange solid crystals in 95.5 % yield.

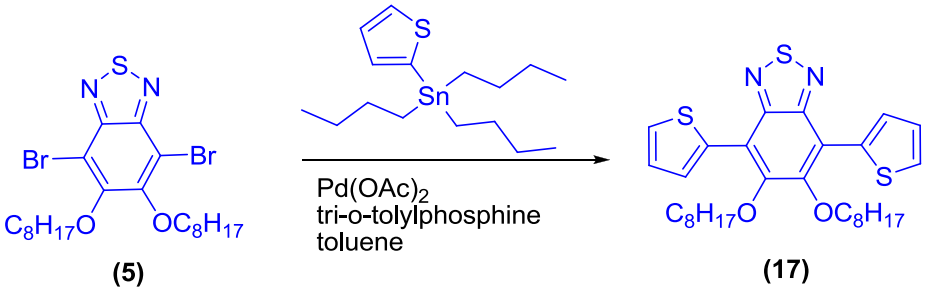

(5) **(17)**

Scheme 38 : Preparation of 4,7-bis(5-bromothiophen-2-yl)-5,6bis(octyloxy)benzo[c][1,2,5]thiadiazole (17)

The reaction was carried out in dry toluene in presence of $Pd(OAc)_2$ and tri-o-tolylphosphine as catalysts then heated to reflux for 16 hours. The ratio of 4,7-dibromo-5,6-bis-octyloxy-benzo[1,2,5]thiadiazole **(5)** and tributylstannylthiophene was 1: 2.5. The product was synthesised using the Stille coupling reaction mechanism following the same route as that described for compound **(7)** Scheme 18.

The purity and structure of product (17) was confirmed by melting point, TLC, ^{1}H NMR, ^{13}C NMR , the mass spectrometry, elemental analysis and FT-IR. The melting point was 75 - 76 ˚C which was in good agreement with that reported in the literature [103]. The product gave a single spot on TLC (R_f = 0.47). The ^{1}H NMR gave three different environments of aromatic protons, two doublets at 8.49 and 7.53 ppm and a triplet at 7.26 ppm. The ^{13}C NMR shows seven expected peaks in the aromatic region between 117.6 and 152.0 ppm and seven different carbon environments in agreement with the structure of product **(17)** . The mass spectrum of the product exhibited a peak 556 (M^{+}) which is in agreement with the proposed structure. The structure of the product was also confirmed by the IR spectrum where the two sharp bands at 1057 and 1028 cm^{-1} correspond to C-Br of the compound **(5)** no longer exist in the product **(17).**

4.2.2 4,7-Bis(5-bromothiophen-2-yl)-5, 6-bis(octyloxy)benzo-[c][1,2,5]-thiadiazole (18)

4,7-Bis(5-bromothiophen-2-yl)-5,6-bis(octyloxy)benzo-[c][1,2,5]-thiadiazole **(18)** was synthesized according to Ruiping [93], Scheme 39. The crude product was purified via silica gel column chromatography, eluting with DCM / hexane (10:1) to obtain **(18)** as orange solid crystals in 97 % yield.

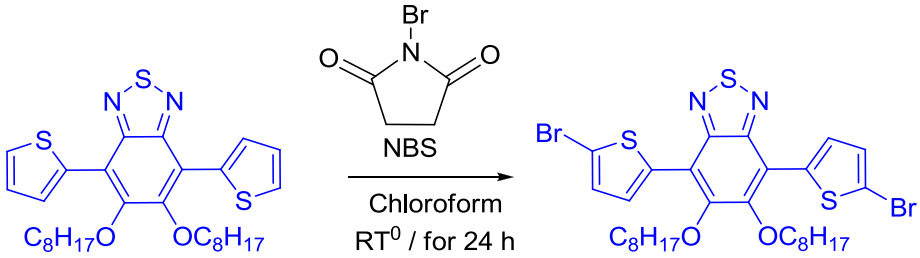

Scheme 39 : Synthesis of 4,7-Bis(5-bromothiophen-2-yl)-5, 6-bis(octyloxy)benzo-[c][1,2,5]-thiadiazole (18).

The reaction was carried out on reaction of **(17)** with NBS as shown in Scheme 39. The ratio used between NBS and the 4,7-bis(5-bromothiophen-2-yl)-5,6-bis(octyloxy)benzo[c][1,2,5]thiadiazole **(17)** must not be more that 2:1 to ensure that substitution takes place on both thiophene rings and to avoid formation of side products such as tri- and tetra- substituted product, which are difficult to purify and lead to undesirable network polymers. The reaction mechanism of **(18)** follows the same route as that described for the synthesis of 4,7-bis(5'-bromo-2,2'-bithiophen-5-yl)-5,6-bis(octyloxy)benzo[c][1,2,5]thiadiazole **(8)** Scheme 20 .

The purity and structure of the product **(18)** was confirmed by ^{1}H NMR, ^{13}C NMR , mass spectrometry, melting point, elemental analysis, FT-IR and TLC . The ^{1}H NMR gave two

different environments as expected in the aromatic region. Two doublets at 8.39 and 7.19 ppm related to the protons in positions (a) and (b) respectively. The protons in position c are shown as triplet at 4.14 ppm. The protons in position d are displayed as a multiplet at 1.90 ppm while the protons of the two methyl groups in position j are shown as a triplet at 0.92 ppm, Figure 57 .

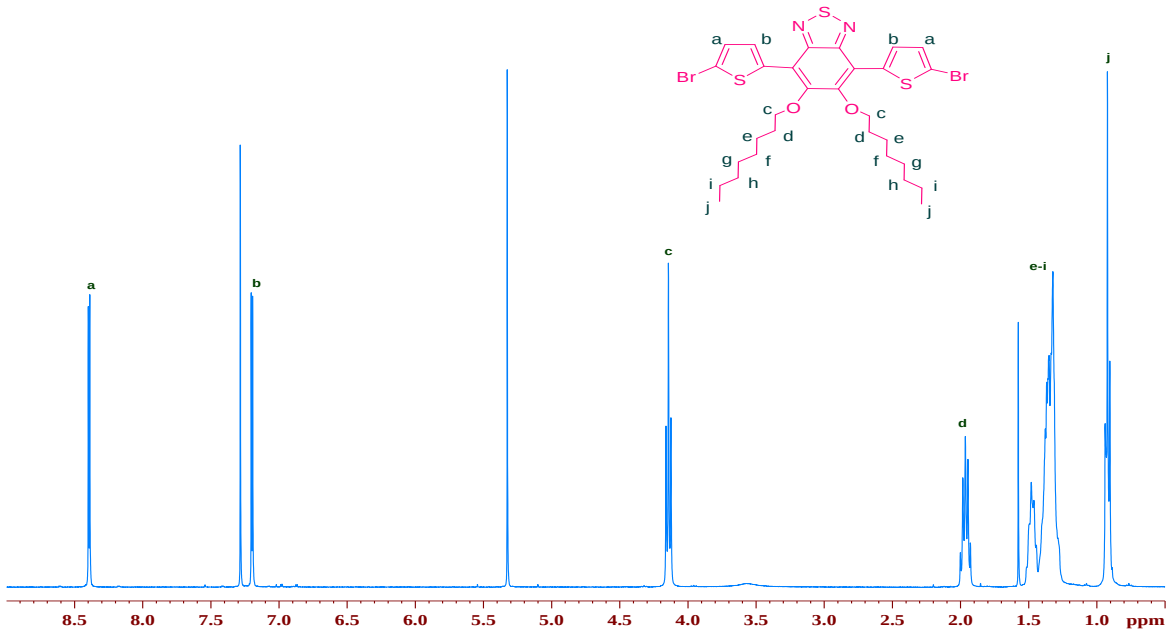

Figure 57: 1H NMR of monomer 4,7-bis(5-bromothiophen-2-yl)-5, 6-bis(octyloxy)benzo-[c][1,2,5]-thiadiazole (18)

The ^{13}C NMR shows seven expected peaks in the aromatic region between 115.4 and 151.4 ppm and in agreement with the product's structure. The mass spectrum for 4,7-bis(5-bromothiophen-2-yl)-5, 6-bis(octyloxy)benzo-[c][1,2,5]-thiadiazole **(18)** showed peaks at 712 , 714 and 716 as expected due to the presence of bromine isotopes (^{81}Br and ^{79}Br). The melting point of 74- 76 °C corresponded with that reported in the literature [103]. The structure of the product was also confirmed by IR spectra. The FT-IR spectrum showed two absorption bands at 1066 cm^{-1} and 1030 cm^{-1} related to the stretching vibration of the C-Br bonds.

4.3 Synthesis of the thiophene monomers for polymer (P9)

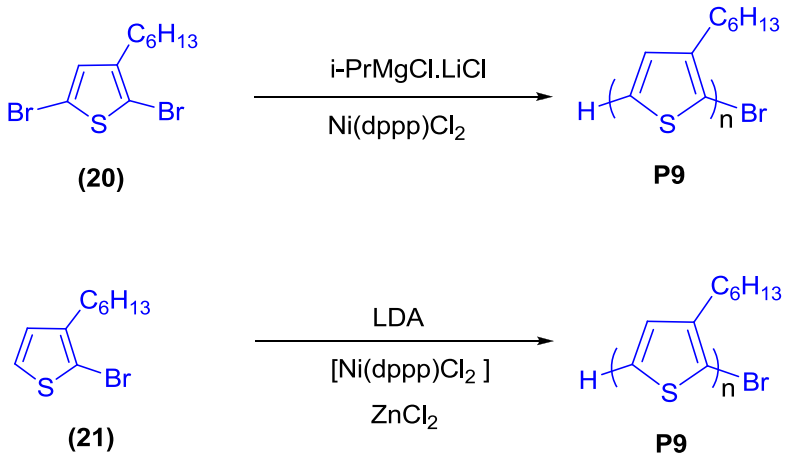

Scheme 40 : The monomers used to prepare P9

Scheme 40 shows the required monomers to prepare polymer **P9**. 2,5-Dibromo-3-hexylthiophene **(20)** and 2-bromo-3-hexylthiophene **(21)** were synthesised successfully in a good yield and their purity and structure were confirmed by ^{1}H NMR , ^{13}C NMR , CHN elemental analysis , FT-IR and mass spectrmetry. The synthetic routes for preparing 2, 5-dibromo-3-hexylthiophene **(20)** and 2-bromo-3-hexylthiophene **(21)** are shown in Scheme 41 .

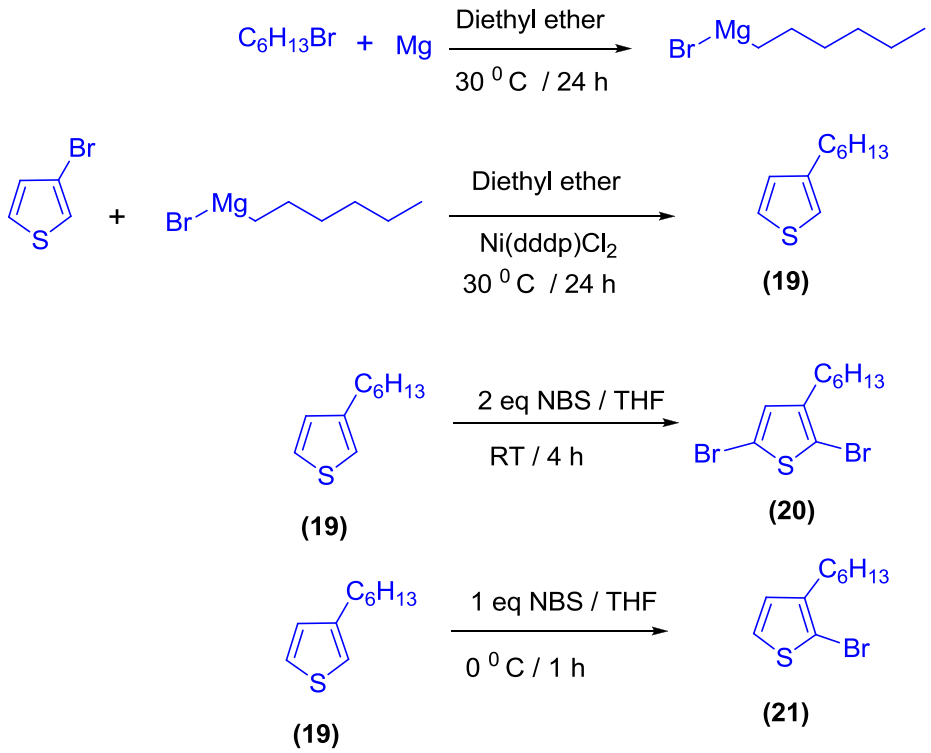

Scheme 41 : Synthetic route for preparing 2,5-dibromo-3-hexylthiophene (20) and 2-bromo-3-hexylthiophene (21)

4.3.1 3-Hexylthiophene (19)

3-Hexylthiophene **(19)** was synthesized following a procedure developed by Urien [109], Scheme 42. The crude product was purified via high vacuum distillation (b.p. 65°C) to obtain **(19)** as a clear oil in 23 % yield.

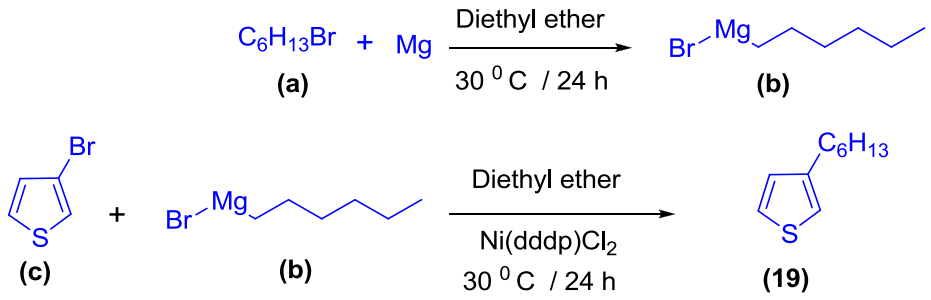

Scheme 42 : Synthesis of 3-hexylthiophene (19)

The reaction preparation of 3-hexylthiophene **(19)** involves two steps and both were carried out in dry diethyl ether ; the first step is the formation of the Grignard reagent The second step is the reaction of the Grignard reagent with 3-bromothiophene (c) in the presence of $Ni(dppp)Cl_2$ as catalyst to afford the 3-hexylthiophene **(19).**

The reaction mechanism follows the Kumada cross coupling mechanism as shown in Scheme 43. This mechanism consists of three steps [124] ; an oxidative addition, transmetallation and reductive elimination [125]. Ni and Pd catalysts are commonly used in the formation of carbon-carbon bond. Ni catalyst has advantages over Pd where the former is much lower cost and increased reactivity toward readily activated aryl halides compared to the corresponding Pd catalyst [126]. The mechanism is shown in Scheme 43.

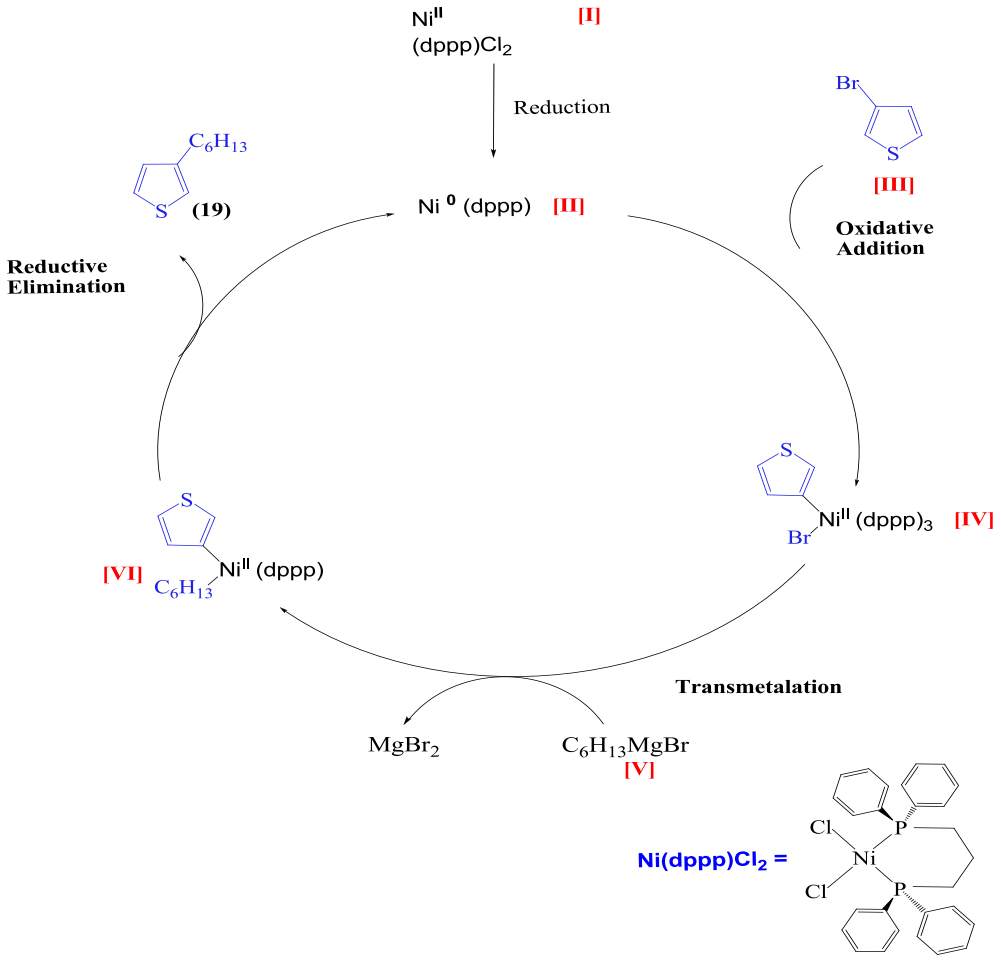

Scheme 43 : The Kumada coupling mechanism to prepare (19)

The purity and structure of the product **(19)** was confirmed by ^{1}H NMR, ^{13}C NMR, mass spectrometry, elemental analysis and FT-IR (ATR). The ^{1}H NMR gave two different environments in the aromatic region. Two multipeaks at 7.3 and 7.0 ppm represented three aromatic protons. The aliphatic protons for the hexyl chains showed from 2.7 ppm to 0.93 ppm. The ^{13}C NMR shows expected peaks between 143.2 to 13.9 ppm which show different carbon environments in the structure and in agreement with the product structure. The mass spectra for 3-hexylthiophene **(19)** were observed at 168 (M^{+}) which is in agreement with the proposed structure. The structure of the product was also confirmed by IR spectrum.

4.3.2 2, 5-Dibromo-3-hexylthiophene (20)

2,5-Dibromo-3-hexylthiophene **(20)** was synthesized following a procedure by Hammer [110]. The crude product was distilled and collected at (b.p. 135 ^{0}C) to obtain **(20)** as a colourless oil in 88% yield Scheme 44.

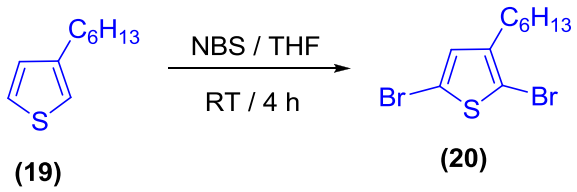

(19) **(20)**

Scheme 44 : Synthesis of 2,5-dibromo-3-hexylthiophene (20)

The reaction mechanism of **(20)** follows the same route as that described for the synthesis of compound **(8),** Scheme 20. The purity and structure of the product was confirmed by ^{1}H NMR, ^{13}C NMR, mass spectrometry, elemental analysis and FT-IR (ATR). The ^{1}H NMR gave the expected singlet peak for the aromatic proton in position (a) at 6.8 ppm. The protons in position (b) are shown as triplet at 2.5 ppm while the rest of the aliphatic protons for the hexyl chains showed between 1.55 to 0.91 ppm as shown in Figure 58.

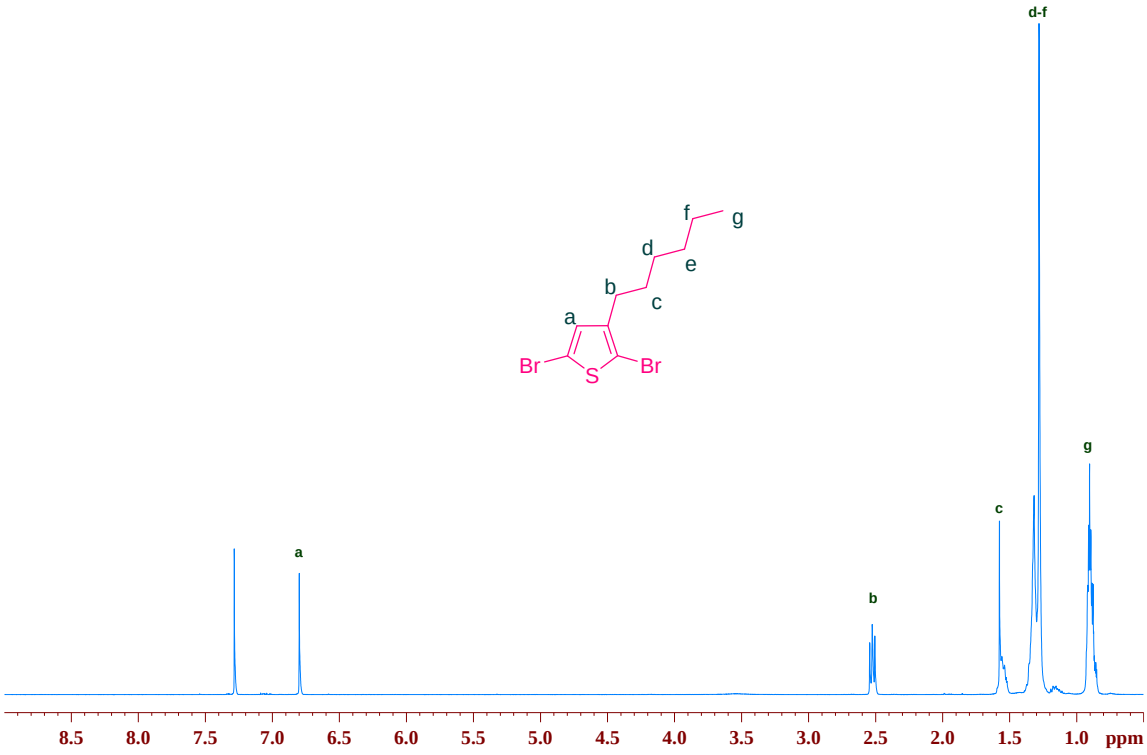

Figure 58: 1H NMR of monomer 2,5-dibromo-3-hexylthiophene (20)

The ^{13}C NMR shows expected peaks between 143.1 to 14.4 ppm which show different carbon environments in the structure and in agreement with the product structure. The mass spectra for 2,5-dibromo-3-hexylthiophene **(20)** were observed at 323, 325 and 327 (M^+) in 1:2:1 intensities because of the bromine isotopes (^{81}Br and ^{79}Br).

4.3.3 2-Bromo-3-hexylthiophene (21)

2-Bromo-3-hexylthiophene **(21)** was synthesized following a procedure by Li [111].The crude product was purified by column chromatography using hexane to afford 2-bromo-3-hexylthiophene **(21)** as colourless oil in 82% yield, Scheme 45.

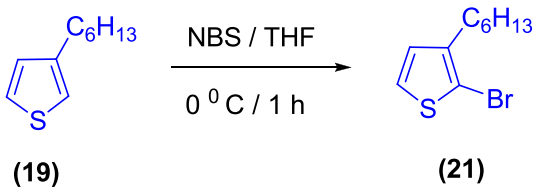

Scheme 45 : Synthesis of 2-bromo-3-hexylthiophene (21)

The reaction of was done between 3-hexylthiophene (**19)** and NBS in a ratio of 1:1 in THF as solvent for one hour. The reaction mechanism of **(21)** follows the same route as that described for the synthesis of compound **(8),** Scheme 20. The purity and structure of the product was confirmed by ^{1}H NMR, ^{13}C NMR, mass spectrometry, elemental analysis and FT-IR (ATR). The ^{1}H NMR gave two expected doublet peaks for aromatic protons in positions (a) and (b) at 7.1 and 6.8 ppm respectively. The aliphatic protons for the hexyl chain showed from 2.5 ppm to 0.90 ppm as illustrated in Figure 59.

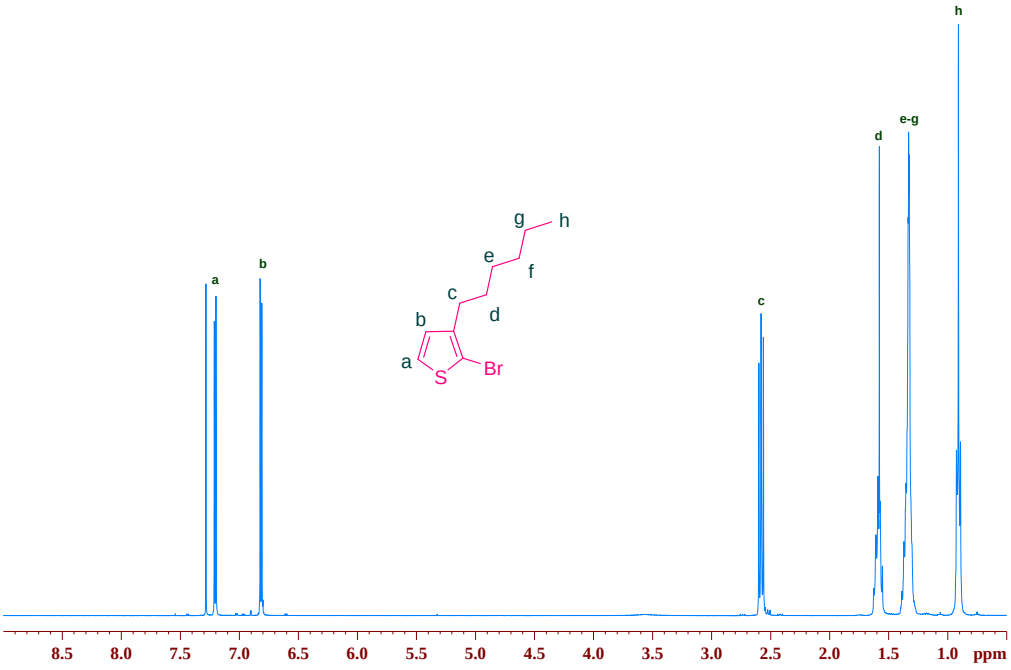

Figure 59: 1H NMR of monomer 2-bromo-3-hexylthiophene (21)

The ^{13}C NMR shows expected peaks between 141.19 to 14.10 ppm which show different carbon environments in the structure and in agreement with the product structure. The mass spectrum for 2-bromo-3-hexylthiophene **(21)** showed peaks at 247.01 and 249.01 as expected due to the presence of bromine isotopes (^{81}Br and ^{79}Br). The structure of the product was also confirmed by IR spectrum.

Chapter 5: Results and Discussion – Polymers

5.1 The Thiophene-Benzothiadiazole-based Copolymers: (P1) (P2) (P3)

Polymers **P1**-**P3** were synthesised according to Suzuki cross coupling reaction using a variety of boronic esters, solvents and bases. In polymer **P1**, the unsubstituted carbazole unit is used as donor unit , while in polymer **P2** the donor unit is 3,6-difluoro substituted carbazole. Moving from carbazole and its derivatives, the donor unit in **P3** contains a fluorene unit. In both polymers **P1** and **P2**, the acceptor unit is 5,6-dioctyl-4,7-di(thiophen-2-yl)benzo[c][1,2,5]thiadiazole **(DTBT- 8)** which contains two octyloxy substituents at the 5, 6-positions of benzothiadiazole **(BT)** units. In contrast, unsubstituted 4,7-dithien-2-yl-2,1,3-benzothiadiazole **(DTBT)** unit was used as electron acceptor unit in **P3**, which had been synthesised by the Iraqi group in a similar way to that for 5,6-dioctyl-4,7-di(thiophen-2-yl)benzo[c][1,2,5]thiadiazole **(DTBT-8)**. The structures of the monomers used in the preparation of polymers **P1**-**P3** are shown in , Figure 60**.**

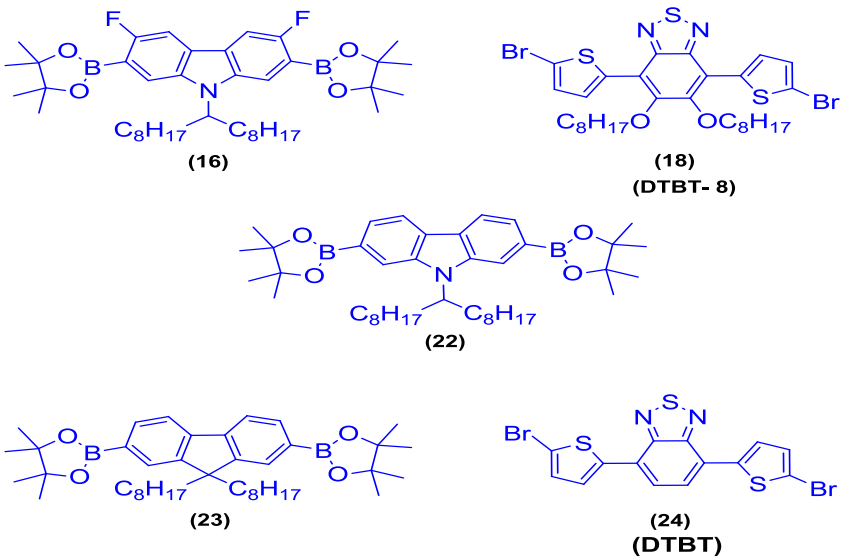

Figure 60: The structures of the monomers used in preparation polymers P1-P3

5.1.1 Synthesis and Analysis of (P1), (P2) and (P3)

The polymerisation conditions for the preparation of **P1** - **P3** are summarised in Table 1 .

Table 1 : Summary of polymerisation conditions for polymers P1-P3

Polymer	Polymerisation conditions					
	Solvent	Catalyst	Catalyst-ratio	base	Timp	Time
P1	Toluene	$Pd(OAc)_2$ +$P(o\text{-}tol)_3$	(1:2)	Et_4NOH	95 ºC	48 h
P2	THF	$Pd(OAc)_2$ +$P(o\text{-}tol)_3$	(1:2)	$NaHCO_3$	95 ºC	4 h
P3	Toluene	$Pd(OAc)_2$ +$P(o\text{-}tol)_3$	(1:2)	Et_4NOH	95 ºC	24 h

Poly[9-(heptadecan-9-yl)-9H-carbazole-2,7-diyl-alt-(5,6-bis(octyloxy)-4,7-di(thiophen-2-yl)benzo[c][1,2,5]thiadiazole) -5,5-diyl] **P1** was prepared from a Suzuki coupling reaction between 9-(heptadecan-9-yl)-2,7-bis(4,4,5,5-tetramethyl-1,3,2-dioxaborolan-2-yl)-9H-carbazole **(22)** and 4,7-bis(5-bromothiophen-2-yl)-5,6-bis(octyloxy)benzo-[c][1,2,5]-thiadiazole **(DTBT- 8) (18)** to afford **P1** as a red powder with 99 % yield . The second target polymer **P2** was carried out by the reaction between 3,6-difluoro-9-(heptadecan-9-yl)-2,7-bis(4,4,5,5-tetramethyl-1,3,2-dioxaborolan-2-yl)-9H-carbazole **(16)** and 4,7-bis(5-bromothiophen-2-yl)-5,6-bis(octyloxy)benzo-[c][1,2,5]-thiadiazole **(DTBT- 8) (18)** to afford **P2** as dark red powder with 82.5 % yield .The co-polymer based on fluorene unit **P3** was done between 2,2'-(9,9-dioctyl-9H-fluorene-2,7-diyl)bis(4,4,5,5-tetramethyl-1,3,2-dioxaborolane **(23)** as donor unit and 4,7-bis(5-bromothiophen-2-yl)benzo[c][1,2,5]thiadiazole **(DTBT) (24)** as acceptor unit to afford **P3** as purple powder . The structures of the targets polymers **P1**-**P3** are presented in Figure 61**.**

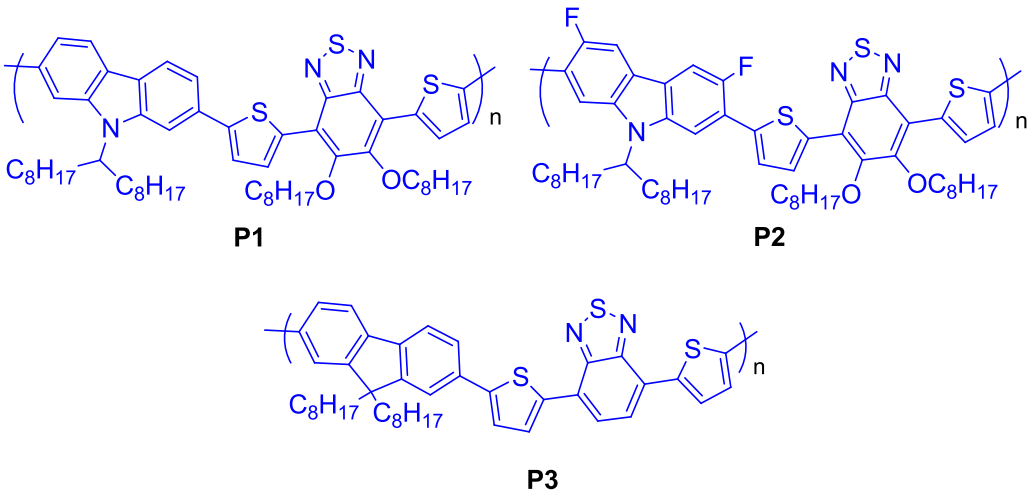

Figure 61: Structures of copolymers P1, P2 and P3

A proposed mechanism for the preparation of polymers **P1-P3** follows the Suzuki coupling reaction mechanism, which consists of three steps as shown in scheme 46 , where these steps are an oxidative addition, transmetallation and reductive elimination.

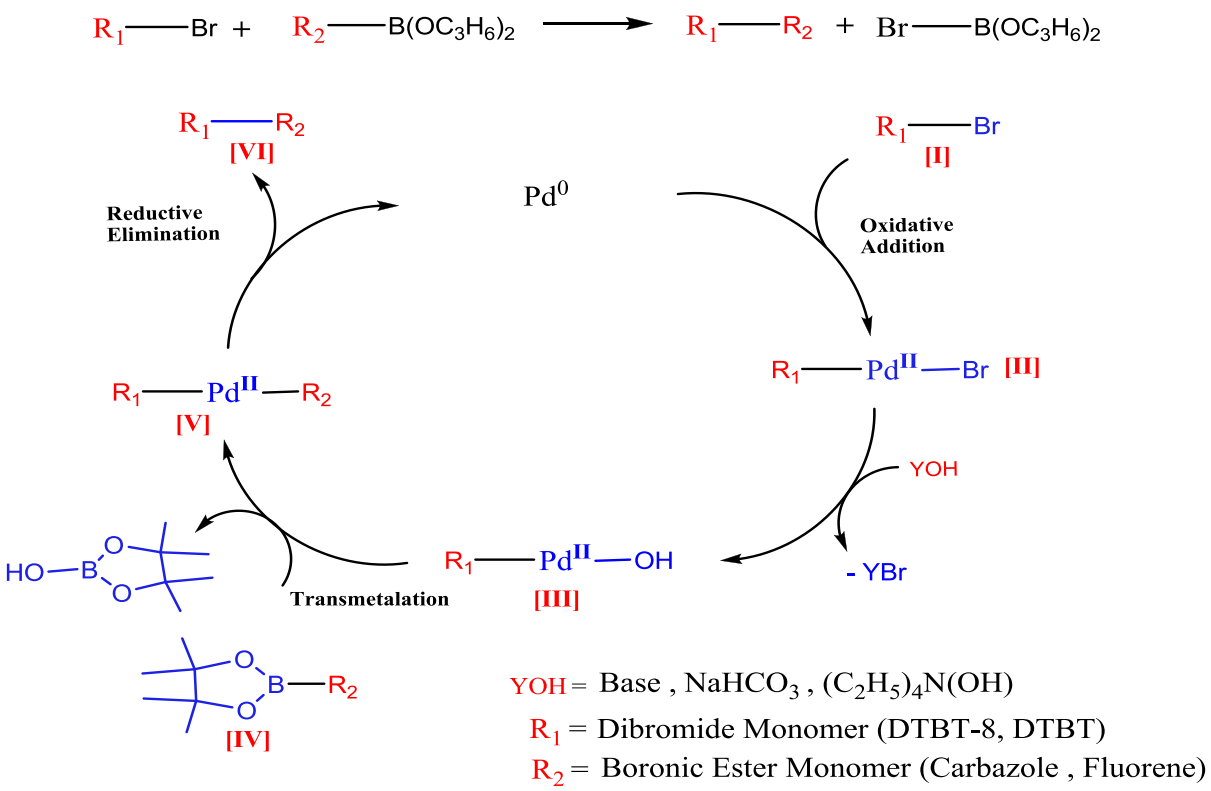

Scheme 46 : Mechanism for the polymerisation of polymers P1-P3

The first step involves an oxidative addition of the dibromide monomer **[I] (DTBT-8 , DTBT)** to the catalyst [Pd^0] to form the palladium^{II} complex **[II]**, where the bromide group in this complex is displaced by the base leading to the aryl palladium^{II} complex **[III]**.A transmetalation reaction is the second step where the aryl palladium^{II} complex **[III]** reacts with boronic ester monomer (carbazole, fluorene) **[IV]** to form an intermediate palladium^{II} **[V]**. The final step of the catalytic cycle is the reductive elimination of the intermediate palladium^{II} **[V]** to yield the target coupling polymer **[VI]**.

All polymers were prepared under argon and in a degassed system. The polymerisation process of **P1** and **P3** was performed in the same conditions with respect to the solvent , base and polymerization time , where the solvent was toluene and tetraethylammonium hydroxide (20 wt% in water) was base at 95 ^oC . The polymerization time was 48 h and 24 h for **P1** and **P3** respectively. In contrast , **P2** was prepared in different conditions using THF as solvent and $NaHCO_3$ as base. The polymerization process was run over 4 h at 95 ^oC . The polymerization process in both polymers **P1**-**P3** was stopped by adding the end-capping reagents (bromobenzene and phenyl boronic acid) to the polymer solutions, and also to increase the stability of the polymer in device operation.

The purification of the polymer solutions **P1**-**P3** of catalytic traces of palladium was done by stirring with ammonia overnight, because it is found that impurities such as Pd nano-particles impurities could affect the efficiency of the OPV devices [127]. Soxhlet extraction is another way to purify and fractionate the polymer from smaller molecules , oligomers and unreacted monomers. Polymers **P1**-**P2** were purified by Soxhlet extraction using methanol, acetone, hexane and toluene. While **P3** was purified using methanol, acetone, hexane , toluene and chloroform. All solvents from methanol to hexane removed the palladium residues, small molecules and the low molecular weight polymer fractions. Then

the purified polymers **P1**, **P2** were extracted with toluene, while **P3** was extracted in two fractions, toluene and chloroform before precipitation in methanol.

The expected structures of the polymers **P1-P3** were confirmed using elemental analysis, GPC and ^{1}H- NMR. The elemental analysis technique was used to confirm complete replacement of bromine atoms with end-capping groups. All the GPC data and physical properties of polymers **P1-P3** are summarised in Table 2 , as derived from GPC ,

Table 2 : Summary of physical analyses of polymers P1-P3 , PD is the polydispersity of the polymer.

Polymer	Soxhlet Fraction	Yield				
		Mass/mg	%	MW	Mn	PD
P1	Toluene	369	99%	78.600	32.800	2.39
P2	Toluene	376	82%	21.000	12.500	1.68
	Toluene	37	19%	7.300	5.300	1.38
P3	Chloroform	71	37%	23.800	15.100	1.57

5.1.2 Characterization of (P1), (P2) and (P3)

5.1.2.1 NMR Analysis

All the ^{1}H-NMR analyses for the polymers **P1-P3** were performed in $C_2D_2Cl_4$ at 100 ˚C to avoid polymer aggregation and peak broadening especially in the aromatic region. In Figure 62 , the ^{1}H NMR spectrum of **P1** shows doublet peak at 8.66 ppm which corresponds to the two protons at positions a on the carbazole unit, the two singlet peaks at 7.95 and 7.80 ppm corresponds to the two protons at positions b on the carbazole unit, the broad peak at 7.69 ppm is assigned to the two protons at the c positions of carbazole unit. The spectrum clearly shows two main aromatic environments for the

(DTBT-8) unit at 8.16 and 7.60 ppm.The two broad peaks at 8.16 and 7.60 ppm corresponds to the four protons at positions d and e on the thiophene rings on the **(DTBT-8)** unit .The expected peaks for the alkyl protons appeared as nine different peaks from 4.71 ppm to 0.89 ppm.The broad peak at 4.71 ppm is due to the methine at the position f directly attached to the nitrogen atom on the carbazole unit.The broad peak at 4.26 ppm corresponds to the protons on the carbon atoms (position g) attached to the oxygen atoms in the octyloxy chains of the benzothiadiazole units unit.The peaks from 2.50 ppm to 0.89 ppm represents the remaining alkyl protons of the alkyl chains connected to carbazole and benzothiadiazole units.

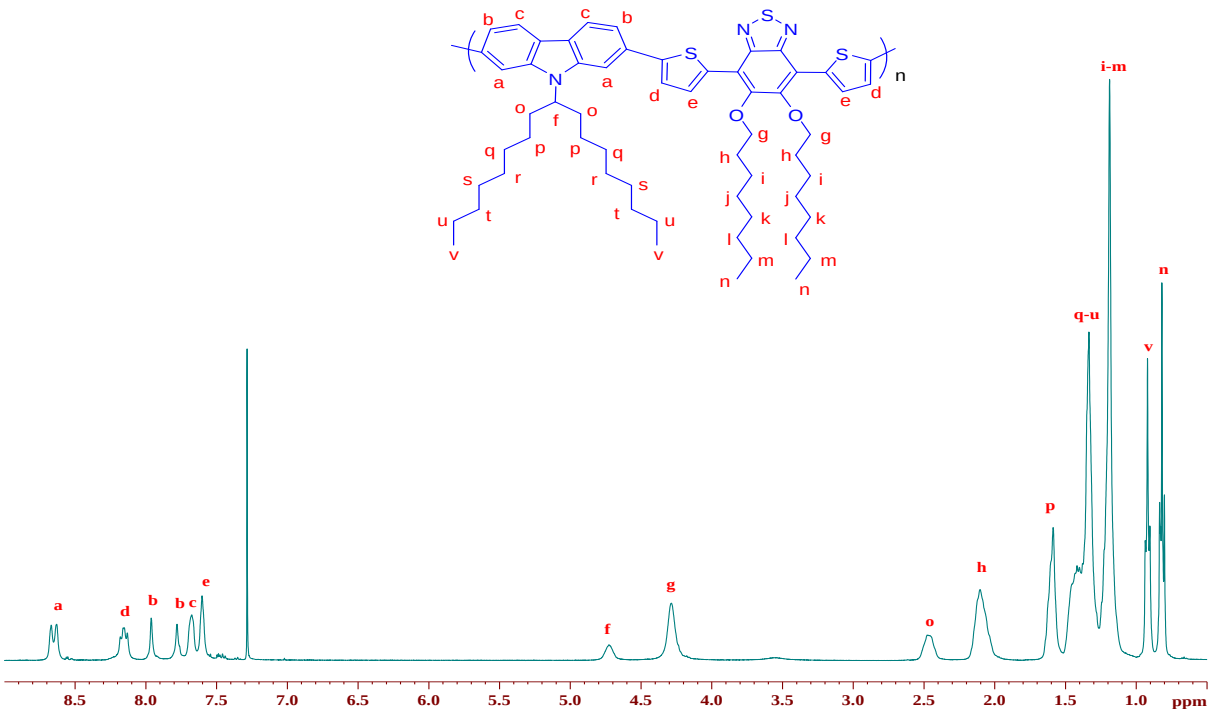

Figure 62: The proton NMR spectrum of P1.

The ^{1}H-NMR spectrum of **P2** are shown in Figure 63 . The two protons at positions a on the carbazole rings are shown as a broad singlet peak at 8.55 ppm. There is a broad multiplet peak at 7.75 ppm which represents four protons at positions b and c for carbazole

and **(DTBT-8)** units respectively. The protons at positions d of the acceptor unit are displayed at 7.65 ppm as a broad singlet peak. The alkyl proton peaks appear as nine different peaks from 4.60 ppm to 0.80 ppm.The broad peak at 4.60 ppm is due to the methine at the position e on the carbazole unit. The broad peak at 4.35 ppm corresponds to the protons at position f of the methylene attached to the oxygen atoms in the octyloxy chains of the **(BT)** unit. The peaks from 2.35 ppm to 0.80 ppm represent the rest protons of the alkyl chains connected to carbazole and benzothiadiazole units.

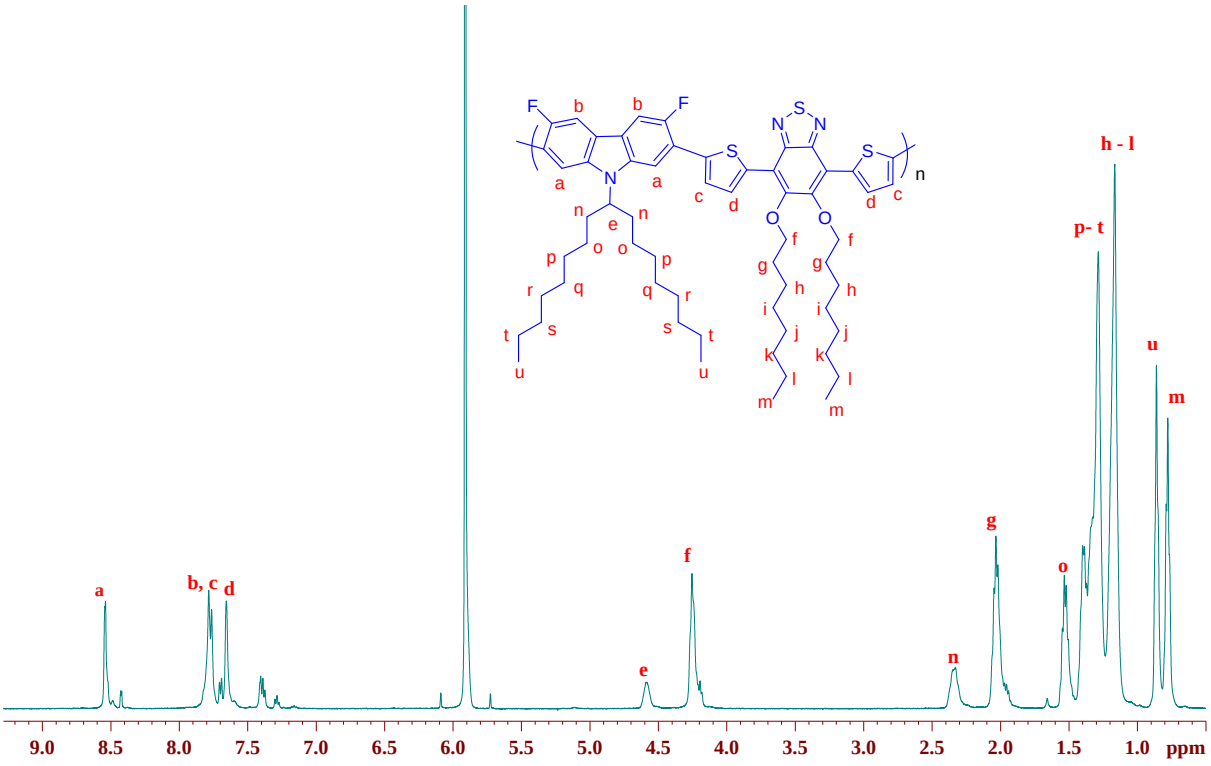

Figure 63: The proton NMR spectrum of P2

The ^{1}H-NMR spectrum of **P3** of the aromatic and aliphatic regions is shown in Figure 64. The spectrum of **P3** shows a broad singlet peak at 8.27 ppm which corresponds to the two protons at positions a on the fluorene rings, the broad singlet peak at 8.01 ppm corresponds to the two protons at position b, the broad multiplet at 7.8 ppm corresponds to the two protons on c position . The protons attached on the thiophene rings of the **(DTBT)** unit were displayed at 7.8 ppm, which corresponds to the protons at

positions d and e respectively. The two protons of benzothiadiazole unit **(BT)** at position f are shown as a broad singlet peak at 7.59 ppm . The alkyl protons of the alkyl chains connected to fluorene unit were shown from 2.12 ppm to 0.91 ppm. The ^{1}H NMR spectrum distinguish between the structures of the polymers **P1**-**P3**, where in the case of **P1** and **P2** carbazole based polymers peaks at 4.71 ppm where observed , while there is no peak in this region for polymer **P3** based on the fluorene unit.

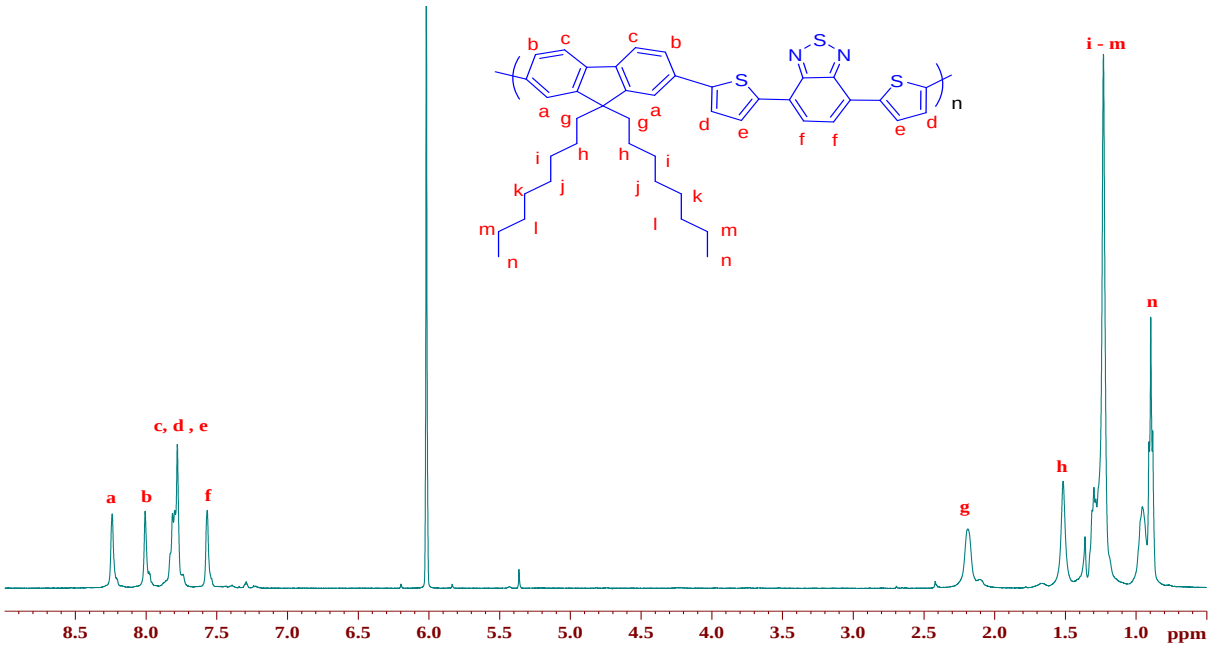

Figure 64: The proton NMR spectrum of P3

5.1.2.2 UV-Visible absorption spectroscopy analysis of (P1), (P2) and (P3)

The UV-Visible absorption spectra of the polymers **P1**-**P3** were measured in chloroform solution and in the solid state as thin films. The onset of absorption of the polymers in the solid state are used to determine the optical band gaps for all polymers.

The optical data for all polymers **P1-P3** are analyzed and compared to those of **PCDTBT** and summarized in Table 3**.**

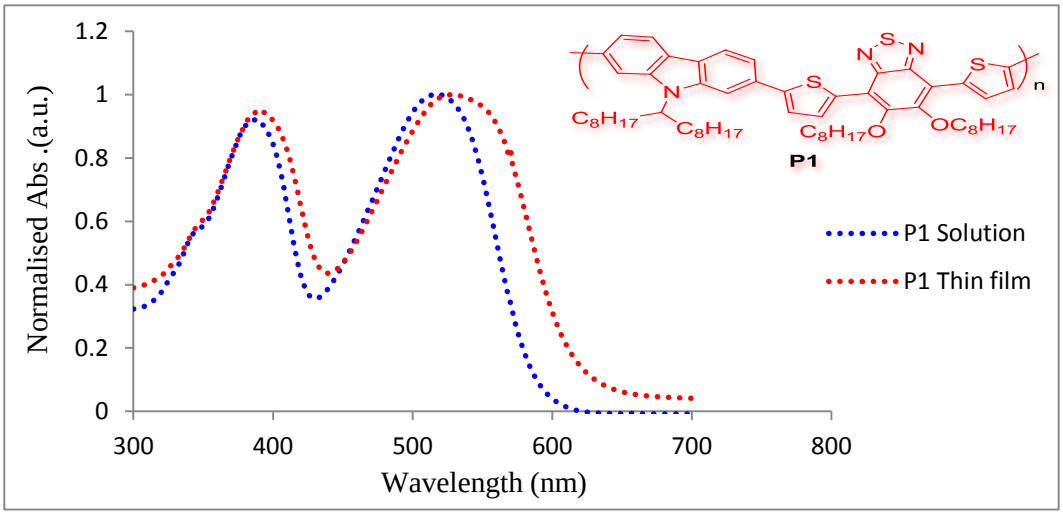

Figure 65: Normalised UV-Vis spectrum of P1 in $CHCl_3$ solution (blue dotted line), as a thin film (red dotted line).

The normalized UV-vis absorption spectra of polymer **P1** in $CHCl_3$ solution and solid state are shown in Figure 6**5** . The spectra shows two absorption bands for **P1** at $\lambda_{max\ 1}$ = 384 nm and $\lambda_{max\ 2}$ = 513 nm in chloroform solution, as well as the thin film exhibits two absorption bands in the solid state at $\lambda_{max\ 1}$ = 389 nm and $\lambda_{max\ 2}$ = 529 nm as shown in Figure 65 . It can be seen from the absorption spectrum that the absorption peak of the film of polymer **P1** at a longer wavelength is higher than that of solution indicating a red- shift by 16 nm and is broader due to the aggregation of polymer in solid state , Table 3 .

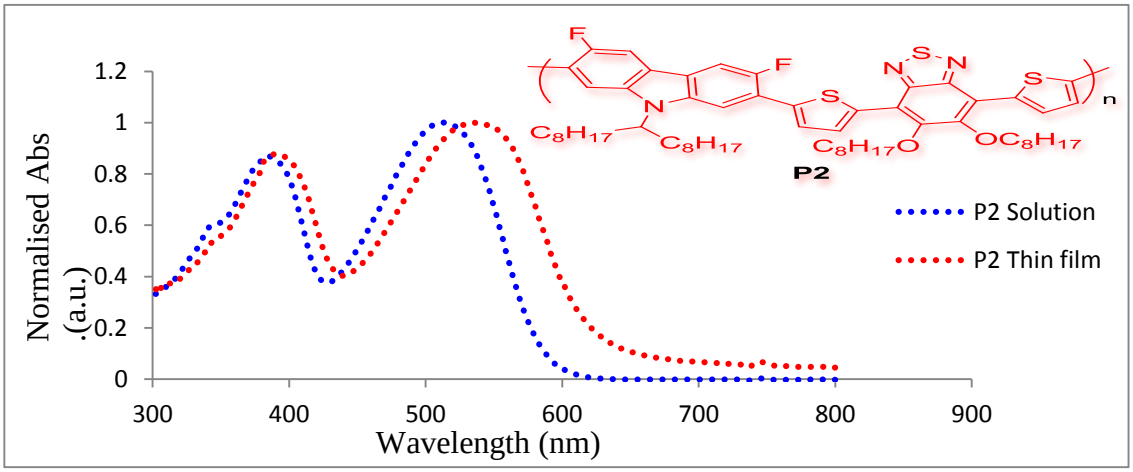

Figure 66: Normalised UV-Vis spectrum of P2 in $CHCl_3$ solution (blue dotted line) , as a thin film (red dotted line).

Figure 66 shows UV-Vis analysis of polymer **P2** in $CHCl_3$ solution and solid state. The spectra shows two absorption bands at λ_{max1} = 388 nm and $\lambda_{max\ 2}$ = 517 nm in chloroform solution, while in the solid state at $\lambda_{max\ 1}$ = 391 nm and $\lambda_{max\ 2}$ = 536 nm. In comparison with its solution absorption spectrum, the absorption peak of the polymer is at a longer wavelength than in the thin film and is obviously red-shifted by19 nm and is broader due to the aggregation of polymer in solid film making the polymer chains more planar and with extended electronic conjugation, Table 3**.**

The polymer **P3** was extracted in two fractions toluene and chloroform, so the UV-Vis analysis was done for both fractions. Figure 67 shows UV-Vis analyses of polymer **P3** for the toluene fraction in $CHCl_3$ solution and thin film. The absorption spectrum of **P3** in the toluene fraction shows two broad absorption peaks at λ_{max1} = 385 nm and $\lambda_{max\ 2}$ = 530 nm in chloroform solution. The absorption peaks of the thin film appear at λ_{max1} = 403 nm and $\lambda_{max\ 2}$ = 575 nm respectively indicating the aggregation of **P3** molecules in solid state. These red shifts from solution to solid state by about 18 and 45nm respectively.

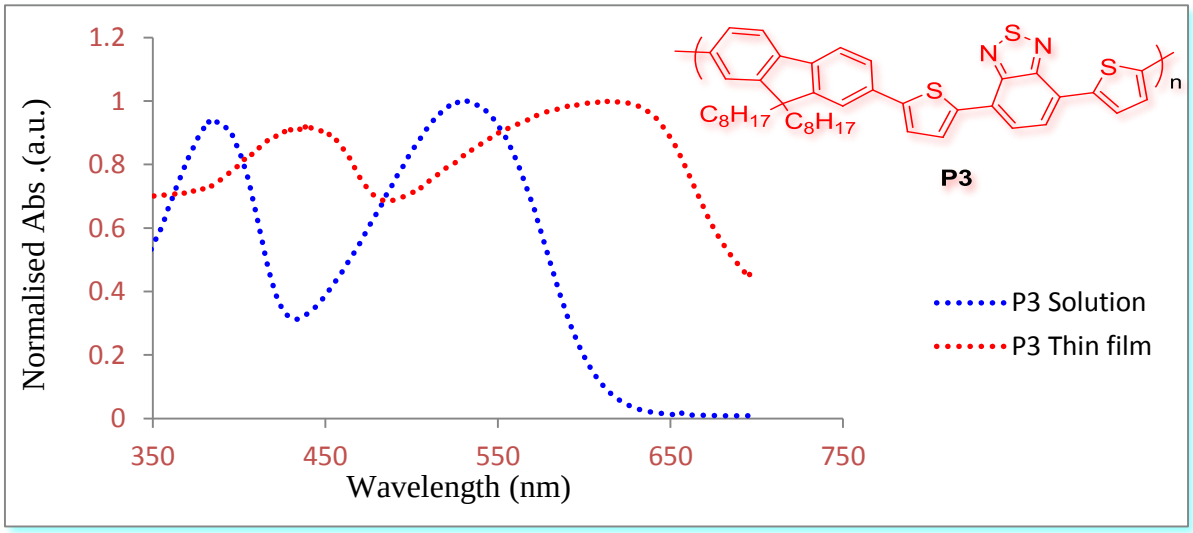

Figure 67: Normalised UV-Vis spectrum of toluene fraction for P3 in $CHCl_3$ solution (blue dotted line), as a thin film (red dotted line).

The UV-Vis analysis of the chloroform fraction of the polymer **P3** in solution and thin film is shown in Figure 68 . It shows two broad absorption peaks at λ_{max1} = 394 nm and $\lambda_{max\ 2}$ = 550 nm in solution and two broad absorption peaks at λ_{max1} = 408 nm and $\lambda_{max\ 2}$ = 591 nm in the thin film.

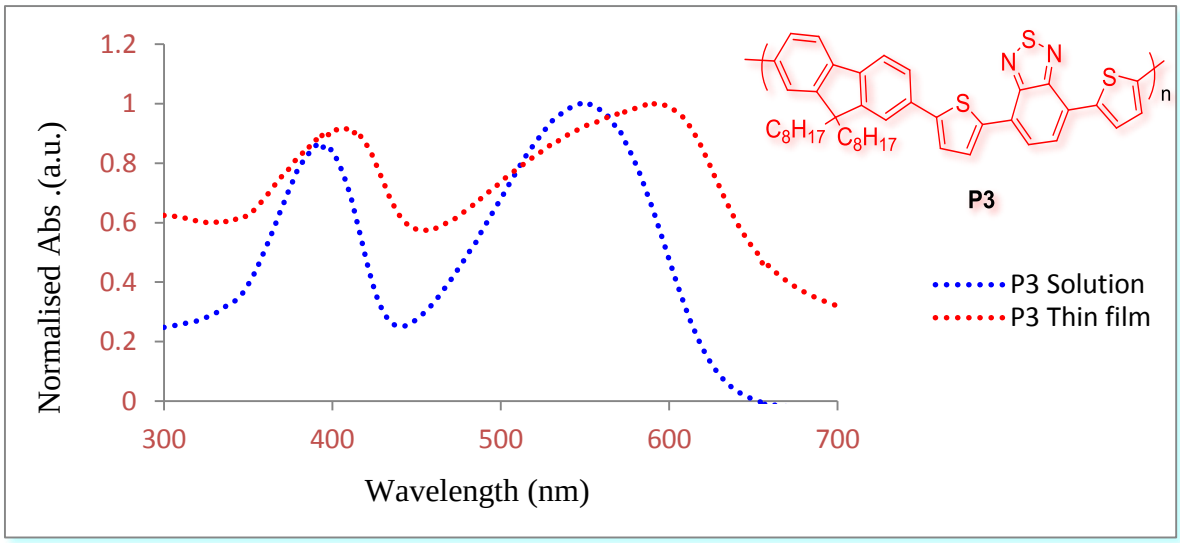

Figure 68: Normalised UV-Vis spectrum of chloroform fraction for P3 in $CHCl_3$ solution (blue dotted line), as a thin film (red dotted line).

In Figure 69 , the absorption peaks of the thin film from the chloroform fraction were compared with their analogue absorption peaks in the toluene fraction which show the same peak shapes, broad peaks and slightly red shifts of the sample from chloroform its absorption by about 5 and 16 nm respectively . These increases in the absorption values of the chloroform fraction can be attributed to the increase of the average molecular weight leading to more extended electronic conjugation and the ability of the polymer to form better aggregates in the solid state.

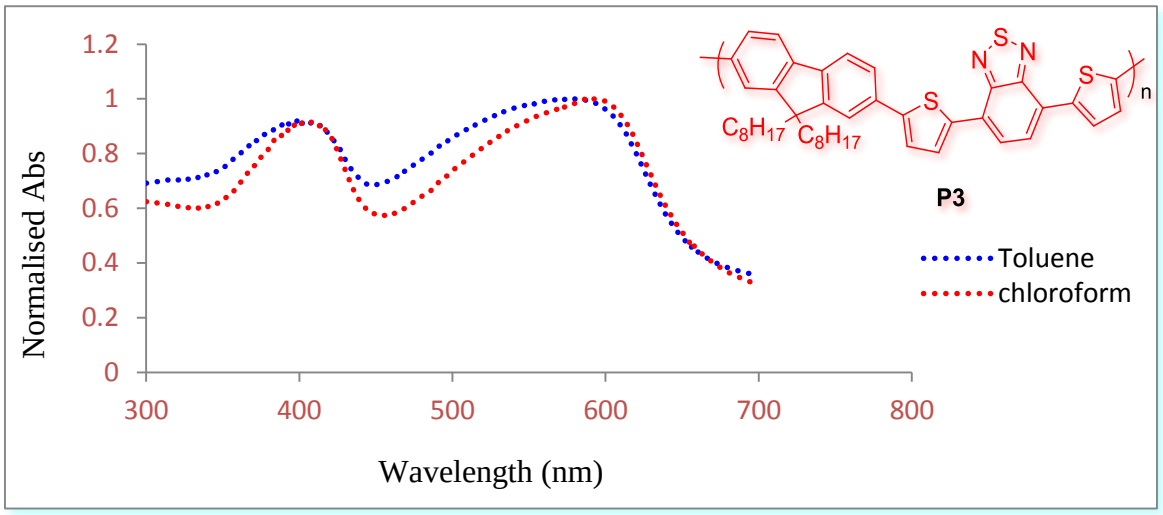

Figure 69: Normalised UV-Vis spectrum of P3 in thin film for toluene and chloroform fractions.

The normalized UV-vis absorption spectra of polymers **P1**, **P2** and **P3** in thin films are displayed in Figure 70. To compare and correlate the properties of these polymers, the chloroform fractions for both polymers were used due to their average molecular weights were close to each other (Table 2) . The $\lambda_{max\ 2}$ values of these polymers were 517, 536 and 591 nm respectively, indicating different values of absorption maxima, Table 3**.**

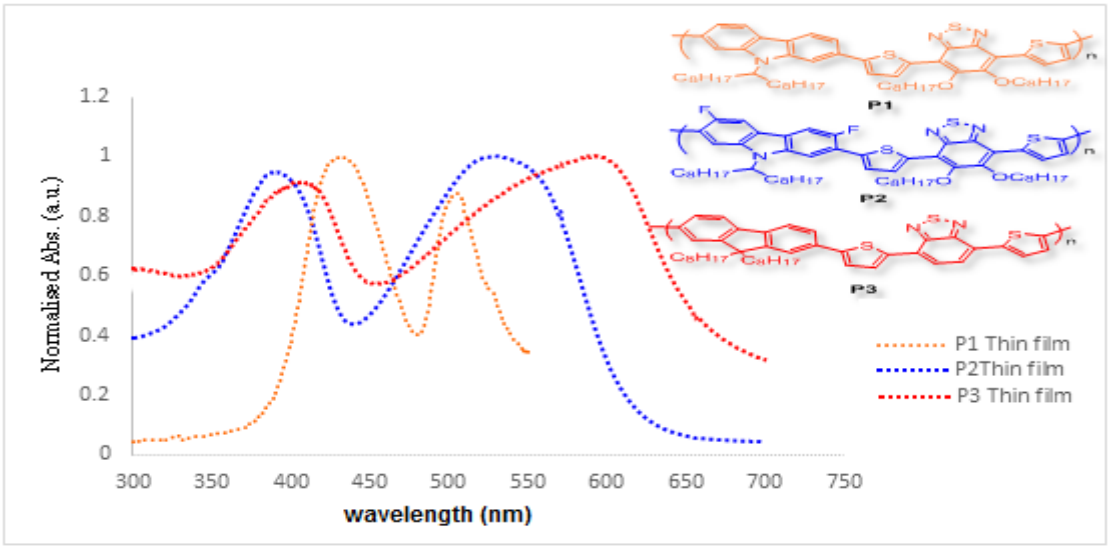

Figure 70: Normalised UV-Vis spectrums of P1 , P2 and P3 as thin film

It can be seen from Figure 70 that the absorption of polymer **P3** based on 9-9-dioctyl-fluorene repeat unit is a markedly higher wavelength than the corresponding polymers based on 2,7-linked carbazole units. Among these polymers, **P3** has the highest values of λ max, for both absorptions. It exhibits the highest (red - shift) λ_{max} = 591 nm with an absorption onset at 666 nm. From the onset of the absorption, the optical band gap energy of **P3** is determined to be 1.86 eV indicating it to be the narrowest band gap in comparison to **P1** and **P2**.

The high values of band gaps of polymers **P1** and **P2** based on carbazole repeat unit compared to that of **P3** can be attributed most probably to the reduced intramolecular charge transfer along polymer chains[95,128]. Moreover, the electron accepting properties of the benzothiadiazole repeat units could also be reduced by the electron donating properties of the octyloxy substituents attached to these repeat units in polymers **P1** and **P2**[95].

The normalized UV-vis absorption spectra of **P1** and **P2** and the values of λ max displayed in Figure 70 shows a more extended electronic conjugation in **P2**. The optical energy gap of polymers **P1** and **P2** as measured from their onsets of absorption in films indicate close band gap values of (2.01 for **P1**vs.1.98 eV for **P2**). The lower band gap of **P2** compared to that of **P1** could originate from fluorine- hydrogen interaction between the fluorine substituents at the 3.6-positions of carbazole repeat units and protons at the 4-positions of neighbouring thiophene repeat units along the polymer chains which could lead to a more planar structure and higher electronic delocalisation Figure 71. Such hydrogen - fluorine interactions were observed by Hursthouse [129] in the literature.

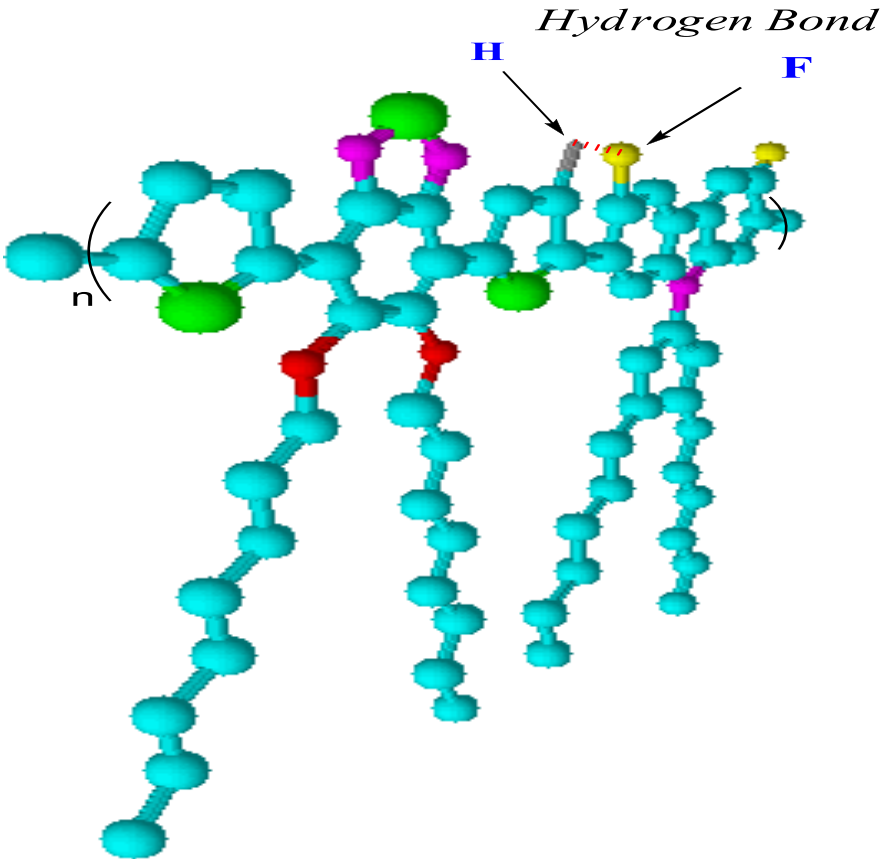

Figure 71: The H-F electrostatic interaction of P2 leading to more planar structure (chem Sketch - Drawing program)

Table 3 : UV-Vis data of P1, P2 , P3 and PCDTOBT

Polymers	Solution λ_{max} (nm)		Thin Film λ_{max} (nm)		Optical E_g
	λ_{max1}	λ_{max2}	λ_{max1}	λ_{max2}	(eV)
P1	384	513	389	529	2.01
P2	388	517	391	536	1.98
P3	394	550	408	591	1.86
PCDTBT	390	545	398	576	1.88

Absorption spectra of polymers **P1** , **P2** and **P3** as well as that of **PCDTBT** both in chloroform solutions and as thin films are summarised in Table 3. Comparison of the absorptions maxima of polymers **P1** and **P2** with that of **PCDTBT** indicates a blue shift of their absorptions by about 47 and 40 nm in thin films respectively. Although their band gaps values almost quite similar (2.01 for **P1** and 1.98 eV for **P2**), they exhibit higher values of band gaps than that of **PCDTBT**as measured from the onsets of their absorptions in films. The larger energy gaps and lower degree of electronic delocalisation of polymers **P1** and **P2** originate from reduced intramolecular charge transfer along polymer chains as result of the electron donating ability of octyloxy substituents on their benzothiadiazole repeat units. In addition, the intermolecular interaction between polymer chains in **PCDTBT** is much stronger than that of **P1** and **P2**; therefore **PCDTBT** shows a high degree of order produced by π-stacking of the polymer chains leading to a low band gap of 1.88 eV [27].

Comparison of the absorption peaks at the longer wavelength of polymer **P3** in solution and thin film with that of **PCDTBT** indicates a red shift of its absorption by about 5 and 15 nm in chloroform solutions and films respectively as shown in Table 3. The band gap of **P3** is lower than that of **PCDTBT** most probably result from the high intermolecular interaction between polymer chains in **P3** , leading to a high degree of order and low band gap of 1.86 eV .

5.1.2.3 Cyclic Voltammetry (CV) analysis

Cyclic voltammetry (CV) studies were performed on drop-cast polymer films in acetonitrile with tetrabutylammonium perchlorate as the electrolyte. The LUMO and HOMO levels were calculated from the onset reduction and oxidation. The electrochemical band gap (Eg) can be calculated from the difference between the

HOMO and LUMO levels. The electrochemical behaviour of **P1**, **P2** and **P3** were measured by cyclic voltammetry (CV) as shown in Figure 72. Both polymers **P1** and **P2** exhibit almost similar values of HOMO energy levels (-5.40 eV for **P1** and -5.39 eV for **P2**) despite the difference in the chemical structure of the donor units Table 4. The HOMO level of **P3** (-5.34 eV) is higher than those of **P1** and **P2** (-5.40 eV for **P1** and -5.39 eV for **P2**) even though it contains weak electron ability unit compared to that of carbazole unit. This could be due to the strong intramolecular charge transfer along the backbone of **P3**. It is worth noting that **P1** and **P2** have also comparable LUMO energy levels (-3.27 eV for **P1** and -3.29 eV for **P2**) which is most likely explained by the presence of the same acceptor repeat units. The higher LUMO values of **P1** and **P2** (-3.27 eV for **P1** and -3.29 eV for **P2**) when compared to that of **P3** (-3.44 eV) can be explained by a weakening of the electron accepting ability of benzothiadiazole moieties in **P1** and **P2** upon their substitution with electron releasing octyloxy substituents . It can be noted that the octyloxy substituent groups attached to the benzothiadiazole unit have a negative contribution to the electronic delocalisation along polymer backbone and reducing the electron accepting ability of the benzothiadiazole on **P1** and **P2** [95].

The electrochemical band gaps energies estimated from these electrochemical measurements indicates that **P3** has the smallest band gap energy (1.90 eV) while **P1** and **P2** have almost identical electrochemical band gap energies (2.13 eV for **P1** , 2.10 eV for **P2**) .The low LUMO level of **P3** leads to effective interaction between the donor and acceptor units and enriches the double bond character among the repeat units, making the HOMO and LUMO levels much closer with small band gaps as expected from theoretical studies.The very slight difference in band gap values of **P1** and **P2** is due to the

presence of an electrostatic interaction between fluorine substituents on the carbazole repeat units and hydrogens at the 4-position on the thiophene repeat units in **P2** (Figure 71) despite that the **P1** having a higher molecular weight than **P2** (Table 2). Moreover, polymer **P2** containing fluorine substituents on the carbazole repeat unit showed stronger intermolecular interactions and formed closer π–π^* stacking and more ordered packing in the solid state [94]. Interestingly, the electrochemical band gap values are slightly higher that the optical band gaps as expected due to exciton binding energy [29].

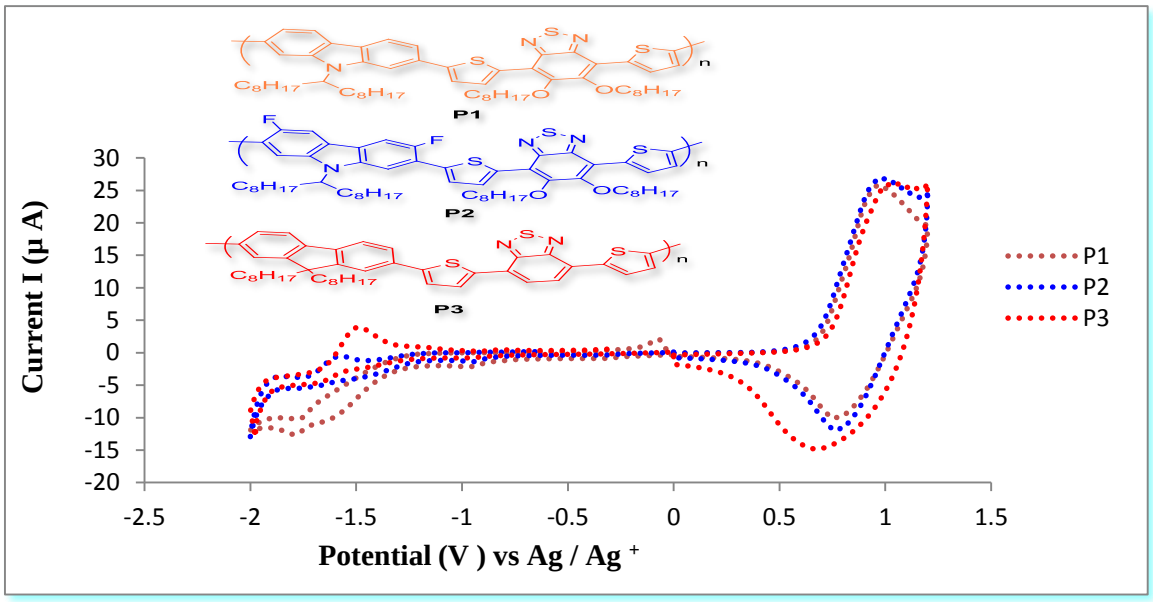

Figure 72: Cyclic voltammetry curves of P1, P2 and P3

A comparison of the electrochemical properties of **P1** and **P2** with copolymer **PCDTBT** reported by Leclerc [92] indicates that **PCDTBT** has lower electrochemical band gap energy (E_{elect} = 1.90 eV for **PCDTBT** ,E_{elect} = 2.13 eV for **P1** , E_{elect} = 2.10 eV for **P2**). Clearly, the effect of the electron releasing octyloxy substituents can be seen in **P1** and **P2** , which alter their electronic properties. **P3** shows similar value of electrochemical

band gap energy compared to that of **PCDTBT** (E_{elect} = 1.90 eV for **P3** and **PCDTBT**) even though they have different donor units . It is interesting to point out that these obtained results of band gaps provide an experimental evaluation of the contribution of intermolecular interactions to the band gap.

Table 4 : Photo-physical and electrochemical properties of P1, P2 and P3

Polymer	E_{op} (e V)	HOMO(eV)	LUMO (eV)	E_{elect} (eV)
P1	2.01	- 5.40	-3.27	2.13
P2	1.98	-5.39	-3.29	2.10
P3	1.86	-5.34	-3.44	1.90

5.1.2.4 Thermo-gravimetric Analysis (TGA)

The thermal stability of **P1**, **P2** and **P3** were studied using TGA and the curves of the thermal degradation of these polymers are shown in Figure 73 . It can be seen from the curves that all three polymers exhibit a high thermal stability up to 350 ° C which is high enough for the requirements of solar cell applications. **P1** shows two degradation steps, the first one occurs at 328 ˚C, the second main degradation step occurs at 468 ˚C , with a weight loss of 60% at 800 ° C. The polymer **P2** shows three degradation steps, the first step of degradation occurs at 332 ˚C, the second main degradation step occurs at 378 ˚C and the final degradation step at 528 ^{0}C, with a weight loss of 71.36 % at 800 ° C. **P3** shows two degradation steps, the first one occurs at 375 ˚C, the second main degradation step occurs at 623 ˚C , with a weight loss of 57.06 % at 800 ° C .The degradation and weight loss of polymers **P1**-**P3** beyond 500 ºC originate from the cleavage of alkyl chains attached to the carbazole and fluorene units . Moreover, **P1** and **P2** show degradation start earlier than **P3** owing to the loss of the two alkoxy groups

which are attached to the benzothiadiazole units **(BT)** . It can be seen that the polymer based on fluorene unit exhibit better thermal stability than polymers based on carbazole units.

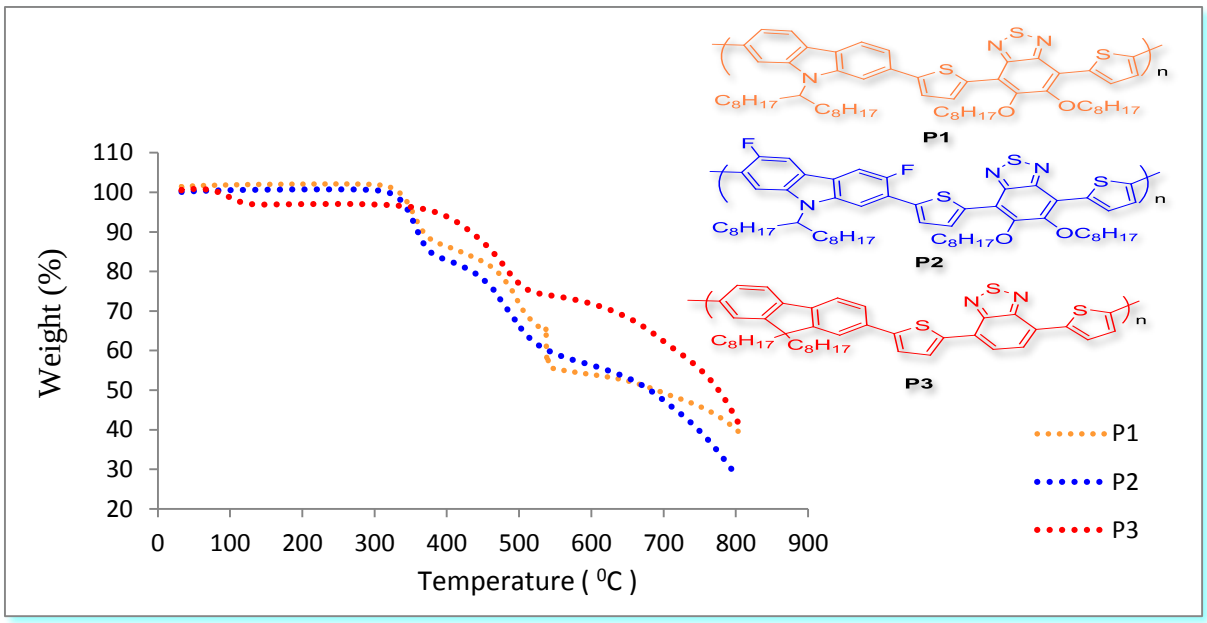

Figure 73: The TGA thermograms of P1-P3

5.2 The Bithiophene -Benzothiadazole-based Copolymers : (P4) (P5)

Polymers **P4**-**P5** were synthesised according to the Suzuki cross coupling reaction using carbazole bis- boronic esters. In polymer **P4**, the non-fluorinated carbazole unit is used as donor unit , while in polymer **P5** the donor unit is the 3,6-difluoro- substituted carbazole unit. In both polymers **P4** and **P5**, the acceptor unit is 4,7-di(2,2'-bithiophen-5-yl)-5,6-bis(octyloxy)benzo[c][1,2,5]thiadiazole **(DT2BT-8)** unit which contains two octyloxy substituents at the 5,6-positions of benzothiadiazole **(BT)** unit. The structures of the monomers used in preparation polymers **P4** and **P5** are shown in Figure 74 .

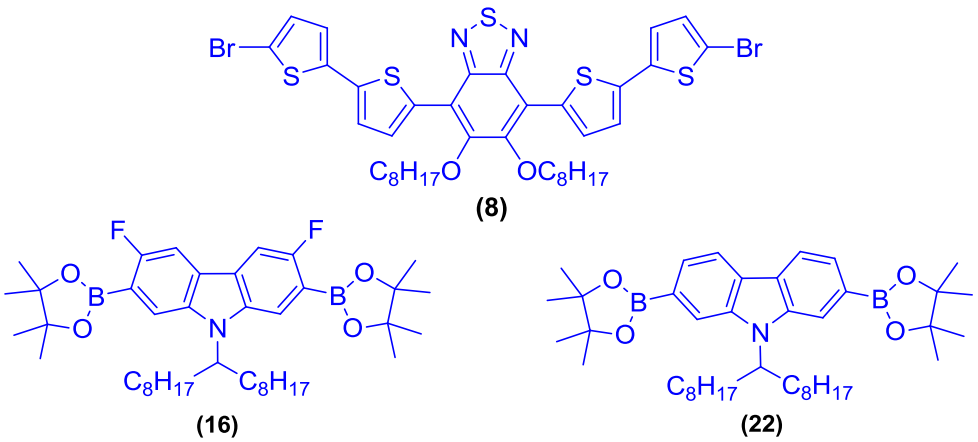

Figure 74: The structures of the monomers used in preparation polymers P4 and P5

5.2.1 Synthesis and Analysis of (P4) and (P5)

The polymerisation conditions for the preparation of polymers **P4** and **P5** are summarised in Table 5.

Table 5 : Summary of polymerisation conditions for polymers P4 and P5

Polymer	Polymerisation conditions					
	Solvent	Catalyst	Catalyst - ratio	base	Temp	Time
P4	Toluene	$Pd(OAc)_2$ +$P(o\text{-}tol)_3$	(1:2)	Et_4NOH	95 ^oC	4 h
P5	THF	$Pd(OAc)_2$ +$P(o\text{-}tol)_3$	(1:2)	$NaHCO_3$	95 ^oC	4 h

P4 was prepared from a Suzuki coupling reaction between 9-(heptadecan-9-yl)-2,7-bis(4,4,5,5-tetramethyl-1,3,2-dioxaborolan-2-yl)-9H-carbazole **(22)** and 4,7-di(2,2'-bithiophen-5-yl)-5,6-bis(octyloxy)benzo[c][1,2,5]thiadiazole **(DT2BT-8) (8)** to afford the polymer as a dark red powder in 60 % yield . The second target polymer **P5** was prepared by the reaction between 3,6-difluoro-9-(1-octyl-nonyl)-2,7-bis(4,4,5,5-tetramethyl-1,3,2-

dioxaborolan-2-yl)-9H-carbazole **(16)** and 4,7-di(2,2'-bithiophen-5-yl)-5,6-bis(octyloxy)benzo[c][1,2,5]thiadiazole **(DT2BT-8) (8)** to afford the polymer as a dark red powder with 73 % yield .The structures of the targets polymers **P4** and **P5** are presented in 75.

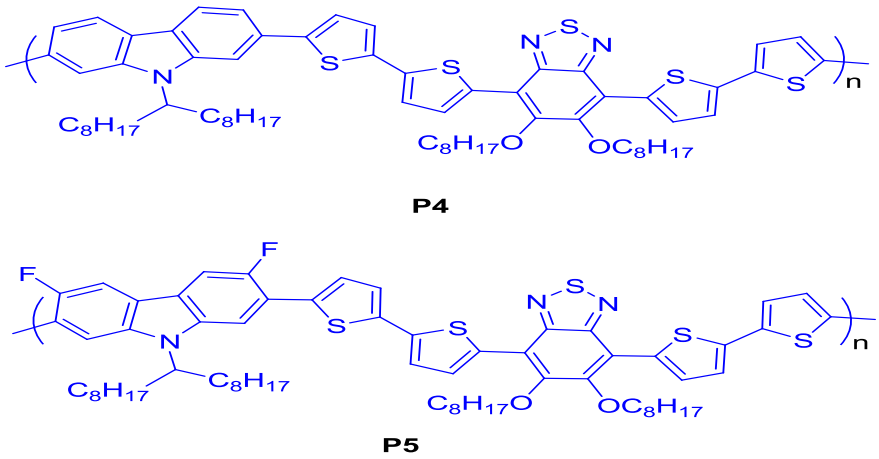

Figure 75: Structures of copolymers P4 and P5

The reaction mechanism for the preparation of polymers **P4** and **P5** follows the Suzuki coupling reaction mechanism described in Scheme 46.

The polymerisation process of **P4** and **P5** was performed in different conditions with respect to the solvents and bases used. The solvent used in **P4** was toluene and tetraethylammonium hydroxide (20 wt% in water) as a base at 95 ^{o}C. In contrast, the polymerisation of **P5** was carried out in different conditions using THF as solvent and $NaHCO_3$ as base. The polymerization process was left for 4 h for both polymers **P4** and **P5** and was stopped by adding the end-capping reagents (bromobenzene and phenyl boronic acid) to the polymer solutions, and also to increase the stability of the polymer in device operation. After similar work-up to that used for polymers **P1-P3**, polymers **P4** and **P5** were purified by Soxhlet extraction using methanol, acetone, hexane and toluene. Then,

the toluene fractions were precipitated in methanol to afford the purified polymers **P4**, **P5**.

The expected structures of polymers **P4** and **P5** were confirmed using elemental analysis, GPC and ^{1}H NMR. The elemental analysis technique was used to confirm complete replacement of bromine atoms with end-capping groups. All the GPC data and physical properties of polymers **P4** and **P5** are summarised in Table 6 , as derived from GPC .

Table 6 : Summary of physical analyses of polymers P4 and P5 , PD is the polydispersity of the polymer , DP is the degree of polymerisation

Polymer	Soxhlet Fraction	Yield		GPC		
		Mass/mg	%	MW	Mn	PD
P4	Toluene	310	60%	57.200	31.100	1.84
P5	Toluene	197	73%	16.800	6.000	2.80

5.2.2 Characterization of (P4) and (P5)

5.2.2.1 NMR Analysis

All the ^{1}H-NMR analyses for polymers **P4** and **P5** were performed in $C_2D_2Cl_4$ at 100 ˚C to avoid polymer aggregation. In Figure 76, the ^{1}H NMR spectrum of **P4** shows a broad singlet peak at 8.45 ppm which corresponds to the two protons at position a on the carbazole unit . The doublet peak at 8.01 ppm corresponds to the two protons at position b on the carbazole unit while the protons at position c were displayed as a broad singlet peak at 7.70 ppm. The spectrum clearly displays the aromatic environments for the **(DT2BT-8)** unit at 7.50 , 7.35 and 7.29 ppm. The two doublet peaks at 7.50 and 7.29 ppm correspond to the four protons at positions d and g on the thiophene rings on the **(DT2BT-**

8) unit . The protons at positions e and f are shown as a broad singlet peak at 7.35 ppm . The expected peaks for the alkyl protons appeared as nine different peaks from 4.60 ppm to 0.89 ppm.The broad peak at 4.60 ppm is due to the methine at the position h directly attached to the nitrogen atom on the carbazole unit.The broad peak at 4.26 ppm corresponds to the protons at position i on the carbon atoms attached to the oxygen atoms in the octyloxy chains of the benzothiadiazole units. The peaks from 2.35 ppm to 0.89 ppm represent the remaining alkyl protons of the alkyl chains connected to carbazole and benzothiadiazole units.

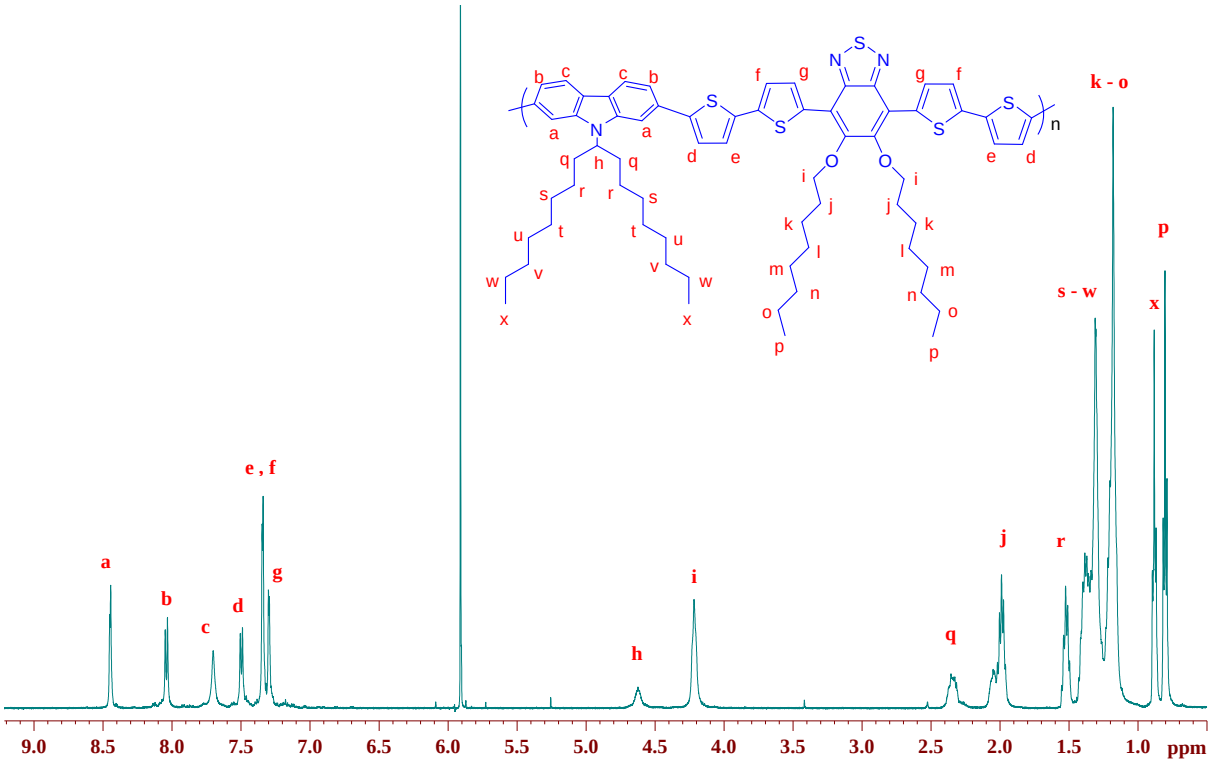

Figure 76: The ^{1}H NMR spectrum of P4 in $C_2D_4Cl_2$ at 100 ^{0}C.

Figure 77 shows the ^{1}H-NMR spectrum of **P5**. The two protons at positions a on the carbazole rings are shown as a broad singlet peak at 8.54 ppm. There are a broad multiple peaks at 7.75 ppm which represent four protons at position b of the carbazole unit and position c of the **(DT2BT-8)** unit respectively. The two protons at positions d of the

(DT2BT-8) unit are displayed at 7.50 ppm as as abroad singlet peak. The protons at positions e and f of the thiophene rings directly attached to the benzothiadiazole **(BT)** unit are shown at 7.45 ppm as a broad multiple peaks. The broad peak at 4.67 ppm is due to the methylene at the position g on the carbazole unit. The broad peak at 4.23 ppm corresponds to the protons at position h of the methine attached to the oxygen atoms in the octyloxy chains of the **(BT)** unit.The peaks from 2.31 ppm to 0.83 ppm represent the rest of the protons of the alkyl chains connected to carbazole and benzothiadiazole **(BT)** units.

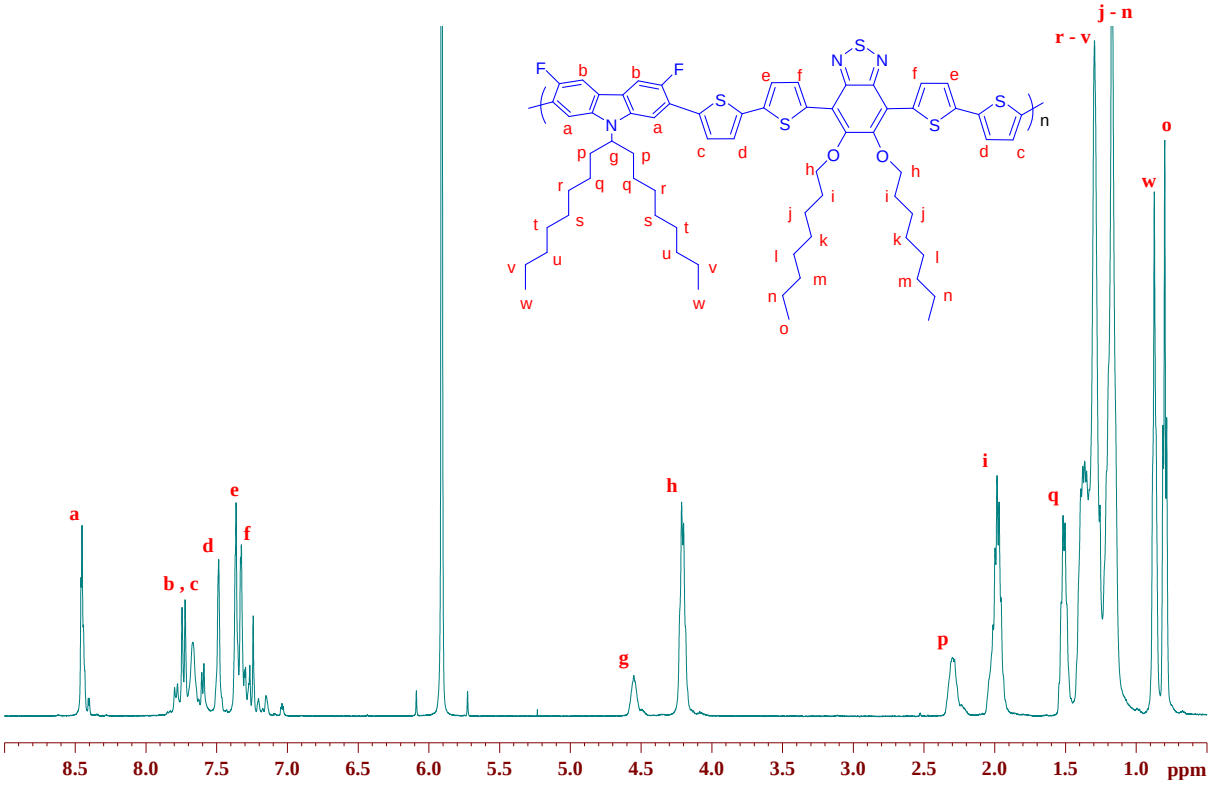

Figure 77: The ^{1}H NMR spectrum of P5 in $C_2D_4Cl_2$ at 100 ^{0}C.

5.2.2.2 UV-Visible absorption spectroscopy analysis of (P4) and (P5)

The UV-visible absorption spectra of polymers **P4** and **P5** were measured in chloroform solutions and in the solid state as thin films. The onset of absorption of the polymers in the solid state are used to determine the optical band gaps for all polymers.

The optical data for all polymers **P4** and **P5** are analyzed and compared to their analogous **P1** and **P2** containing one thiophene ring attached to each side of benzothiadiazole **(BT)** unit and summarized in Table 7.

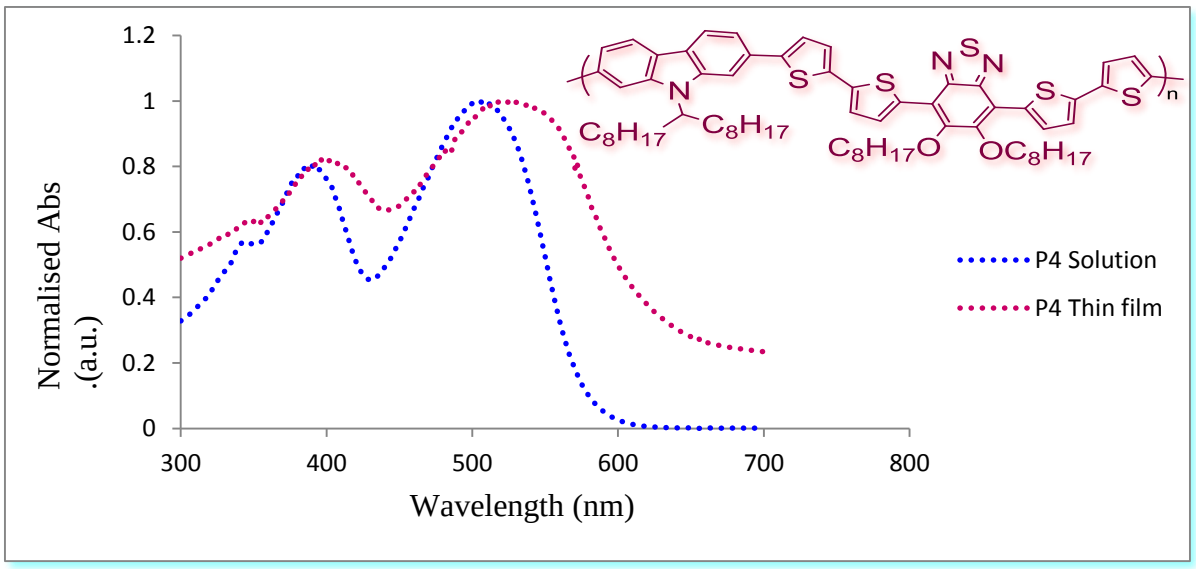

Figure 78: Normalised UV-Vis spectra of chloroform fraction for P4 in $CHCl_3$ solution (Dotted blue line), as a thin film (Dotted purple line).

The normalized UV-vis absorption spectra of polymer **P4** in $CHCl_3$ solution and thin film are shown in Figure 78 . The spectra show two absorption bands for **P4** at $\lambda_{max\ 1}$ = 390 nm and $\lambda_{max\ 2}$ = 506 nm in chloroform solution. The film exhibits two absorption bands at $\lambda_{max\ 1}$ = 396 nm and $\lambda_{max\ 2}$ = 523 nm .The absorption peak of polymer **P4** at the longer wavelength in the film has a slight red-shift of 17 nm compared with that in solution as summarized in Table 6 , indicating the presence of intermolecular interactions in the solid state and more planar confirmation of polymer chains.

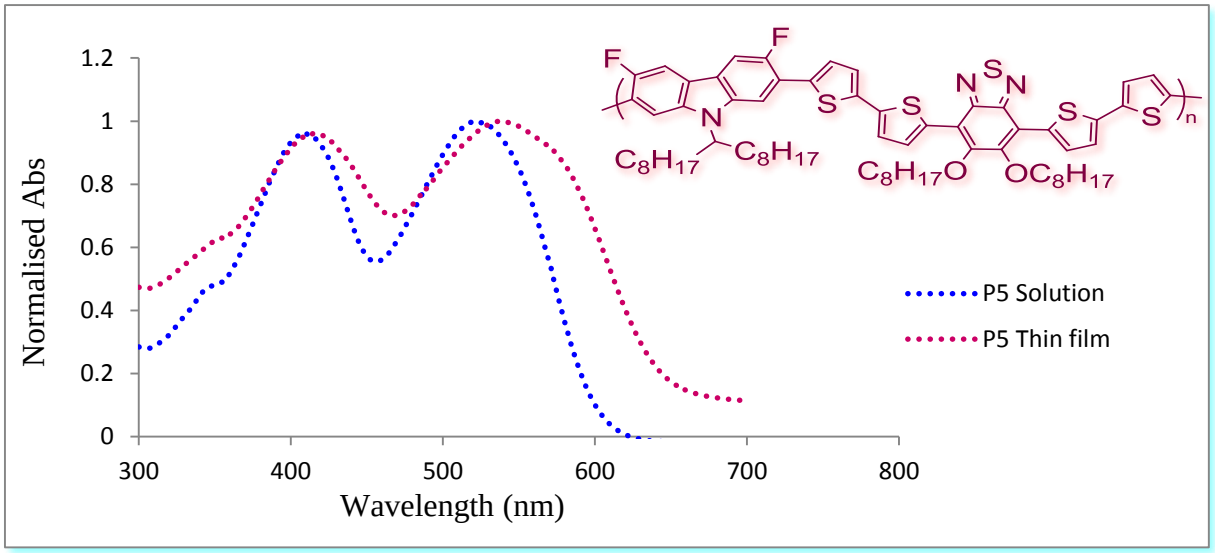

Figure 79: Normalised UV-Vis spectra of chloroform fraction for P5 in $CHCl_3$ solution (Dotted blue line), as a thin film (Dotted purple line).

UV-Vis spectra of polymer **P5** in $CHCl_3$ solution and in the solid state are shown in Figure 79. The spectra show two absorption bands at λ_{max1} = 408 nm and $\lambda_{max\ 2}$ = 522 nm in chloroform solution, while in solid they are at $\lambda_{max\ 1}$ = 415 nm and $\lambda_{max\ 2}$ = 538 nm . In comparison with its solution absorption one, the absorption peak in the thin film as at the longer wavelength for polymer **P5** is red-shifted by 16 nm and is broader due to the aggregation of polymer chains in the solid state.

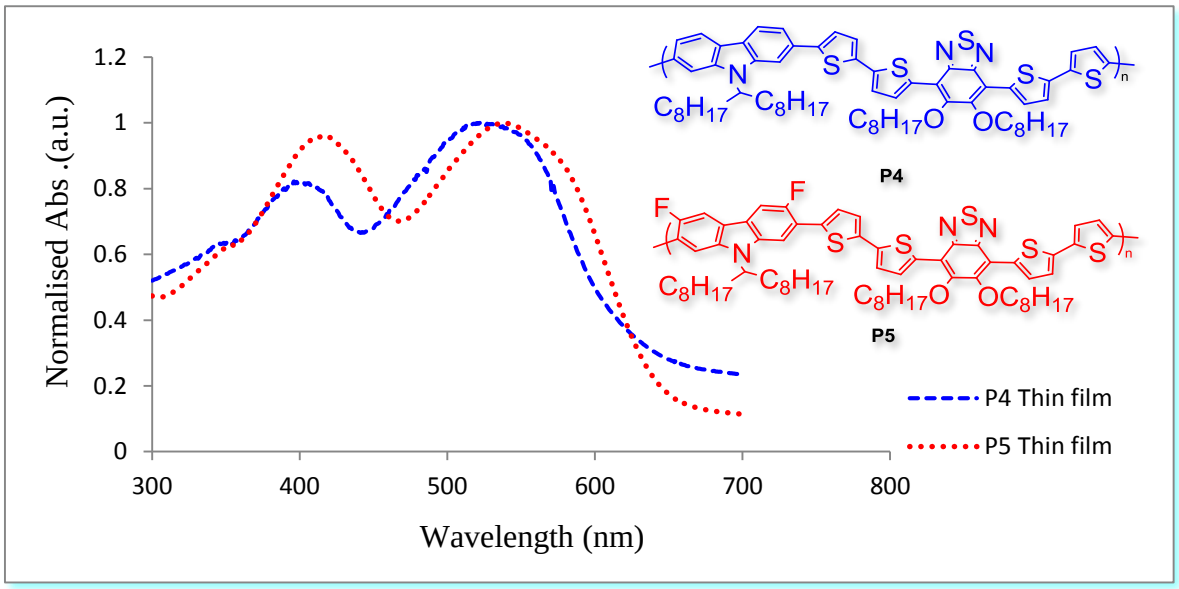

Figure 80: Normalised UV-Vis spectra of thin film for P4 (Square Dotted blue line) and P5 (Dotted red line).

The normalized UV-vis absorption spectra of films of **P4** and **P5** were compared and are displayed in Figure 80. Clearly, the absorption bands at both shorter and longer wavelengths of thin films of **P5** are at higher wavelengths when compared to their analogous bands in **P4** .The absorption spectra of **P4** in thin film shows two bands at 396 and 523 nm , while **P5** shows their analogous bands at 415 and 538 nm . The red shift in **P5** could be attributed to existence of the fluorine substituents on the carbazole unit where they are interacting with the hydrogen atoms on the neighbouring thiophene ring of the **(DT2BT-8)** unit , Figure 81 . Such interaction lead to form more planar polymer and increase the intramolecular charge transfer along the polymer backbone [129].

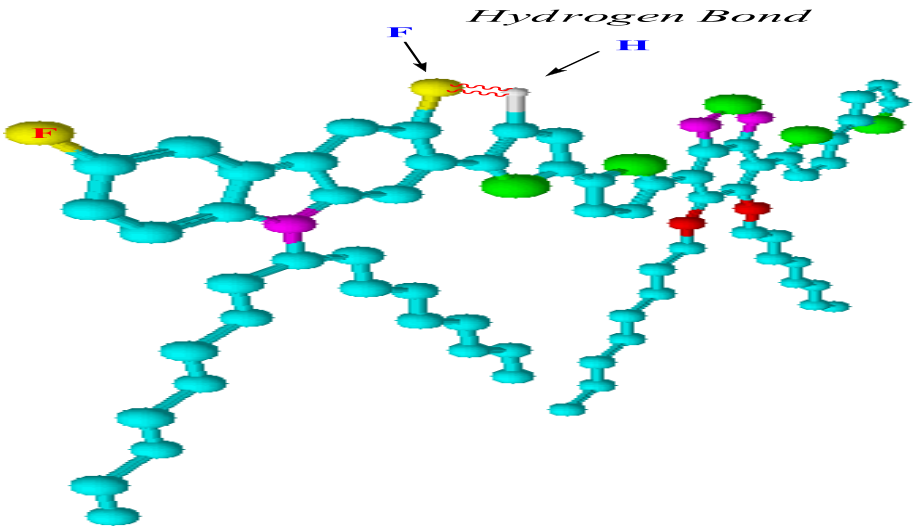

Figure 81: H-F electronic interaction of P5 leading to more planar structure (chem Sketch - Drawing program)

Figure 82 shows the normalized UV-vis absorption spectra of **P1** , **P2** and **P4** , **P5** .It can be seen that the absorption bands of **P4** and **P5** are red shifted compared to those of **P1** and **P2**. This is probably due to the introduction of extra thiophene repat units to the acceptor segment. Both polymers **P2** , **P5** containing substituted fluorine on the carbazole units show red shifts compared to those of **P1** and **P4** containing unsubstituted carbazole units as explained in Figure 81 .

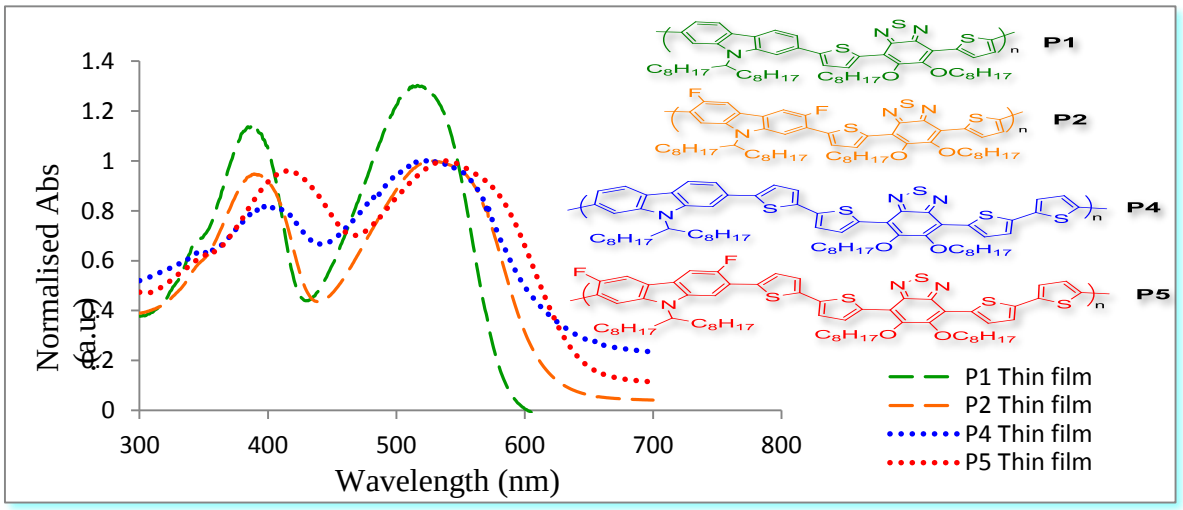

Figure 82: Normalised UV-Vis spectra of thin films for P1 (Dash green) , P2 (Dash orange) , P4 (Dotted blue) and P5 (Dotted red)

Table 7 : UV-Vis data of P1, P2 , P4 and P5

Polymers	Solution $\lambda_{max\ (nm)}$		Thin Film $\lambda_{max\ (nm)}$		Optical E_g
	λ_{max1}	λ_{max2}	λ_{max1}	λ_{max2}	(eV)
P1	384	513	390	529	2.01
P2	388	517	391	536	1.98
P4	390	505	396	537	1.97
P5	408	522	415	538	1.94

Absorption spectra of polymers **P4** and **P5** and their band gaps are summarised and compared with those of **P1** and **P2** as shown in Table 7. A comparison of the absorptions maxima of polymer **P4** in thin films with its analogue **P1** in both short and long wavelengths indicate red shifts of its absorption bands by 6 nm indicating electronic delocalization is more pronounced in **P4** .The optical energy gap of polymers **P4** as measured from its onset absorption in film also indicate lower value of 1.97 eV.

The absorption maxima of polymer **P5** containing fluorine substituents on the carbazole units was compared with its analogue **P2** in both short and long wavelength indicating red shifts of its absorptions bands by about 24 and 2 nm respectively. The optical energy gap of polymers **P5** as measured from its onset absorption in film also indicate lower value of 1.94 eV.

As can be seen from the Table 7, both polymers **P4** and **P5** exhibit lower values of band gaps compared to those of **P1** and **P2** ,indicating more electronic delocalization in the polymers backbone. This can be possibly attributed to both electronic and steric factors where the introduction of extra thiophene repeat units increases the electron donating

ability of the electron donating repeat units along the polymer backbone and consequently increases the intramolecular charge transfer along the polymer backbone[95].Furthermore the distance separating the solubilising substituents along the polymer backbone is also further increased, reducing their mutual steric interactions[95].

5.2.2.3 Cyclic Voltammetry (CV) analysis

Cyclic voltammetry (CV) studies were performed on drop-cast polymer films in acetonitrile with tetrabutylammonium perchlorate as the electrolyte. The LUMO and HOMO levels were calculated from the onset reduction and oxidation. The electrochemical band gap (Eg) can be calculated from the difference between the HOMO and LUMO levels.

The cyclic voltammetry curves of **P4** and **P5** are shown in Figure 83 and the results are summarized in Table 8. It is clear that **P4** has higher HOMO value when compared to that of **P5** (-5.20 eV for P4 and -5.50 eV for **P5**) .The deeper value of HOMO level of **P5** is because of the fluorene alternate repeat units are weaker electron donating groups than carbazole repeat units. In addition , the LUMO level of **P4** is higher than that of **P5** (-3.29 eV for **P4** and -3.47 eV for **P5**) even though having the same acceptor unit. It is interesting to note that **P4** has a lower electrochemical band gap energy by about 0.11 eV when compared to that of **P5** (E_{elect} = 1.91 eV for **P4** *vs* . E_{elect} = 2.02 eV for **P5**) . Interestingly, the electrochemical band gap values are slightly higher that their optical band gaps as expected due to exciton binding energy [29].

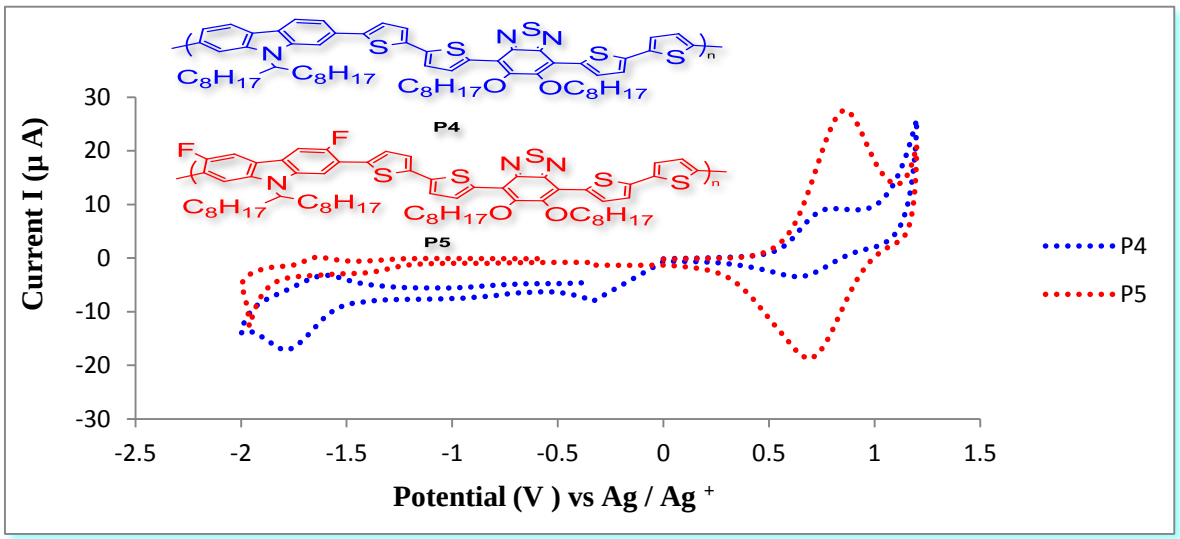

Figure 83: Cyclic voltammetry curves of P4, and P5.

A comparison of the HOMO level energy of **P4** with its analogous **P1** containing one thiophene ring indicates that **P4** has higher value relative to that of **P1** is most likely explained by the presence of more electron donating thiophene repeat units along its polymer backbone (-5.40 eV for **P1** *vs* . -5.20 eV for **P4**) . The LUMO level of polymer **P4** is comparable to that of **P1** (-3.29 eV for **P4** *vs.* - 3.27 eV for **P1**) As a result of the similarity between their acceptor units. The electrochemical band gap energy of **P4** shows a lower value than that of **P1** (E_{elect} = 1.91 eV for **P4** *vs* . E_{elect} = 2.13 eV for **P1**) . Again , this obtained value could be attributed to the presence of more electron donating thiophene repeat units along its polymer backbone which increases the length of conjugation and reduce the band gap energy.

A comparison of the HOMO energy level of **P5** with its analogous **P2** containing one thiophene ring indicates that **P5** has deeper value relative to that of **P2** (-5.5 eV for **P5** *vs* . -5.39 eV for **P2**) . Moreover, The LUMO level of polymer **P5** is deeper than that of **P2** (-3.47 eV for **P5** *vs.* - 3.29 eV for **P2**). The electrochemical band gap energy of **P5** is

slightly lower than that of **P2** (E_{elect} = 2.10 eV for **P2** *vs* . E_{elect} = 2.02 eV for **P5**) . Interestingly, it can be seen that the presence of more electron donating thiophene repeat units along polymer backbone in **P4** and **P5** has a contribution in reducing the band gap as expected due to an increase in the conjugation length along the polymer backbone.

Table 8 : Electrochemical properties of P1 , P2 and P4 , P5 .

Polymer	E_{op} (e V)	Homo (eV)	LUMO (eV)	E_{elect} (eV)
P1	2.01	- 5.40	-3.27	2.13
P2	1.98	-5.39	-3.29	2.10
P4	1.97	-5.20	-3.29	1.91
P5	1.94	-5.5	-3.47	2.02

5.2.2.4 Thermo-gravimetric Analysis (TGA)

The thermal stability of **P4** and **P5** were studied using TGA and the curves of the thermal degradation of these polymers are shown in Figure 84 . It can be seen from the curves that the two polymers exhibit a high thermal stability up to 340 ^{o} C which is high enough for the requirements of solar cell applications. Both polymers display similar thermal degradation patterns until 600 ^{0}C. **P4** shows three degradation steps, the first one occurs at 329 ˚C, the second degradation onset occurs at 462 ˚C the third degradation onset occurs at 540 ˚C , with a weight loss of 53 % at 800 ^{0}C. Polymer **P5** shows three degradation steps, the first degradation onset occurs at 332 ˚C, the second degradation onset occurs at 460 ˚C and the final degradation onset at 652 ˚C, with a weight loss of 66 % at 800 ˚C. The degradation and weight loss of polymers **P4** and **P5** beyond 600 ºC originated from the cleavage of alkyl chains attached to the carbazole units.

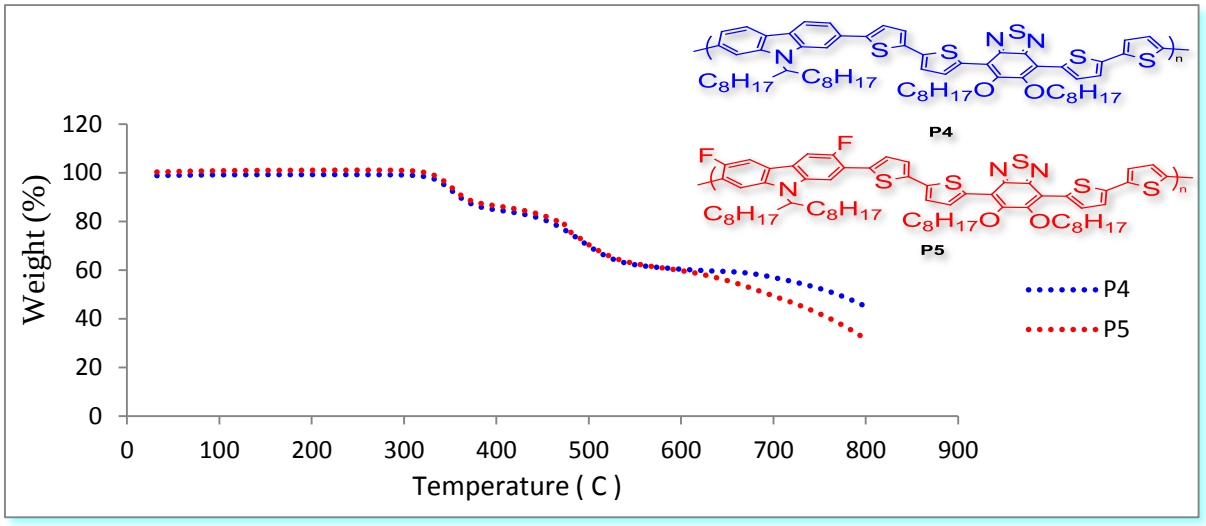

Figure 84: The TGA thermograms of P4 and P5

5.3 The Anthracene-based Copolymers: (P6) (P7)

Polymers **P6** and **P7** were synthesised according to Suzuki cross coupling reactions using anthracene derivatives as Suzuki boronic esters . In polymer **P6**, the 2,6- anthracene unit is used as donor unit , while in polymer **P7** the donor unit is 2,7- anthracene. In both polymers **P6** and **P7**, the acceptor unit is 4,7-di(2,2'-bithiophen-5-yl)-5,6-bis(octyloxy)benzo[c][1,2,5]thiadiazole **(DT2BT-8)** unit which contains two octyloxy substituents at the 5,6-positions of benzothiadiazole **(BT)** unit. The structures of the monomers used in the preparation of polymers **P6** and **P7** are shown in Figure 85 .

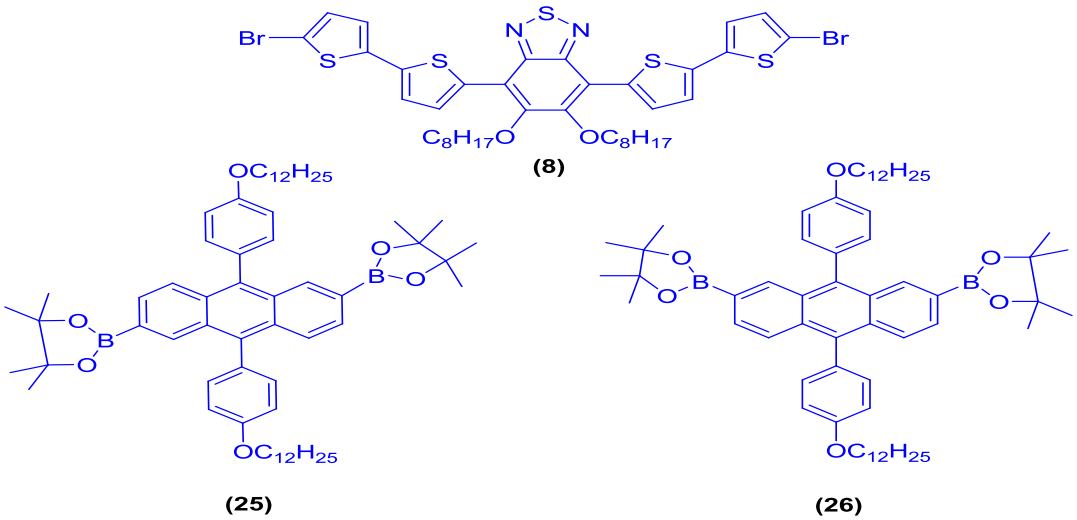

Figure 85: The structures of the monomers used in the preparation of polymers P6 and P7

5.3.1 Synthesis and Analysis of (P6) and (P7)

Polymers **P6** and **P7** were synthesised using Suzuki cross coupling reactions. The polymerisation conditions are summarised in Table 9.

Table 9 : Summary of polymerisation conditions for polymers P6 and P7

Polymer	Polymerisation conditions					
	Solvent	Catalyst	Catalyst-ratio	base	Temp	Time
P6	Toluene	$Pd(OAc)_2$ +$P(o\text{-}tol)_3$	(1:2)	Et_4NOH	95 ^oC	3 h
P7	Toluene	$Pd(OAc)_2$ +$P(o\text{-}tol)_3$	(1:2)	Et_4NOH	95 ^oC	3 h

Poly(9,10-bis(4-(dodecyloxy)phenyl)-anthracene-2,6-diyl-alt-(5,6-bis(octyloxy)-4,7-di(2,2'-bithiophen-5-yl)benzo[c][1,2,5] thiadiazole)-5,5-diyl] **P6** was prepared from a

Suzuki coupling reaction between 2,6-bis-(4,4,5,5-tetramethyl-[1,3,2]dioxaborolan-2-yl)-9,10-bis(4(dodecyloxy)phenyl) anthracene **(25)** and 4,7-di(2,2'-bithiophen-5-yl)-5,6-bis(octyloxy)benzo[c][1,2,5]thiadiazole **(DT2BT-8) (8)** to afford the polymer as a dark purple powder in 15 % yield . The second target polymer **P7** was carried out by the reaction 2,2'-(9,10-bis(4-(dodecyloxy)phenyl)anthracene-2,7-diyl)bis(4,4,5,5-tetramethyl-1,3,2-dioxaborolane) **(26)** and 4,7-di(2,2'-bithiophen-5-yl)-5,6-bis(octyloxy)benzo[c][1,2,5]thiadiazole **(DT2BT-8) (8)** to afford **P7** as a dark purple powder with 97 % yield. The structures of the target polymers **P6** and **P7** are presented in 86.

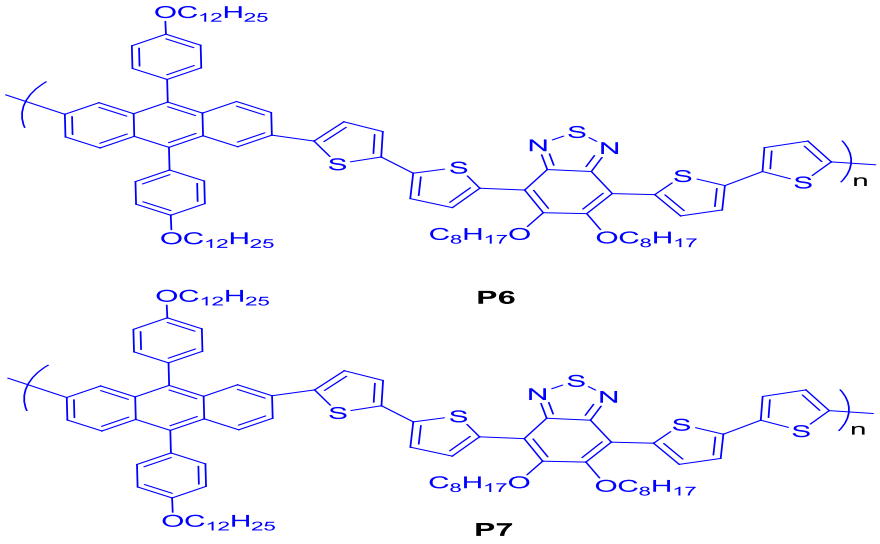

Figure 86: Structures of copolymers P6 and P7

The mechanism of the formation of polymers **P6** and **P7** follows the Suzuki coupling reaction mechanism that was described for the synthesis of **P1**-**P3** in Scheme 46.

The polymerisations were performed under argon and in a degassed system. The polymerisation process of **P6** and **P7** was performed in the same conditions. The solvent used in **P6** and **P7** was toluene and tetraethylammonium hydroxide (20 wt% in water) as a base at 95 ^{o}C . The polymerization time was 3 h for both polymers **P6** and **P7** and was stopped by adding the end-capping reagents (bromobenzene and phenyl boronic acid) to the polymer solutions, and also to increase the stability of the polymer in device operation.The purification of the polymer solutions **P6** and **P7** from catalytic traces was done by stirring with ammonia overnight to remove Pd nano-particles impurities which could affect the efficiency of the OPV devices [127]. Soxhlet extraction is another way to purify and fractionate the polymer from smaller molecules,oligomers and unreacted monomers. Polymers **P6** was purified by Soxhlet extraction using methanol, acetone, hexane , toluene and chloroform , while the purification of **P7** follows the same sequence until toluene. All solvents from methanol to hexane removed the palladium residues, small molecules and the low molecular weight polymer fractions. Then the purified polymers **P6** and **P7** were extracted with chloroform and toluene respectively.The expected structures of the polymers **P6** and **P7** were confirmed using elemental analysis, GPC and ^{1}H-NMR. The elemental analysis technique was used to confirm complete replacement of bromine atoms with end-capping groups. All the GPC data and physical properties of polymers **P6** and **P7** are summarised in table 10.

Table 10 : Summary of yields and GPC data of polymers P6 and P7.

Polymer	Soxhlet Fraction	Yield		GPC		
		Mass/mg	%	MW	Mn	PD
P6	Chloroform	44	15%	19.100	15.400	1.24
P7	Toluene	295	97%	69.000	33.000	2.09

5.3.2 Characterization of (P6) and (P7)

5.3.2.1 NMR Analysis

All the ^{1}H-NMR analyses for polymers **P6** and **P7** were performed in $C_2D_2Cl_4$ at 100 ˚C to avoid polymer aggregation especially in the aromatic region . In Figure 87 , the ^{1}H NMR spectrum of **P6** shows a broad singlet peak at 8.47 ppm which corresponds to the two protons at positions a on the anthracene unit, the two broad peaks at 7.95 and 7.80 ppm is related to the four protons at positions b and c on the anthracene unit . The protons at the positions d and e of thiophene rings are displayed as two doublet peaks at 7.60 and 7.65 ppm respectively. The doublet peak at 7.45 ppm can be assigned to the four protons at positions f and g of the thiophene directly attached to benzothiadiazole unit . The protons of the positions h to i of the attached phenyl group are shown as multi peaks from 7.3 to 7.1 ppm. The broad peak at 4.05 ppm corresponds to the protons at position j , j’ of the methylene attached to the oxygen atoms in the alkoxy chains of the anthracene and **(DT2BT-8)** units. The remaining aliphatic protons at the positions k - z and k’ – z’ were displayed from 1.99 ppm to 0.80 ppm.

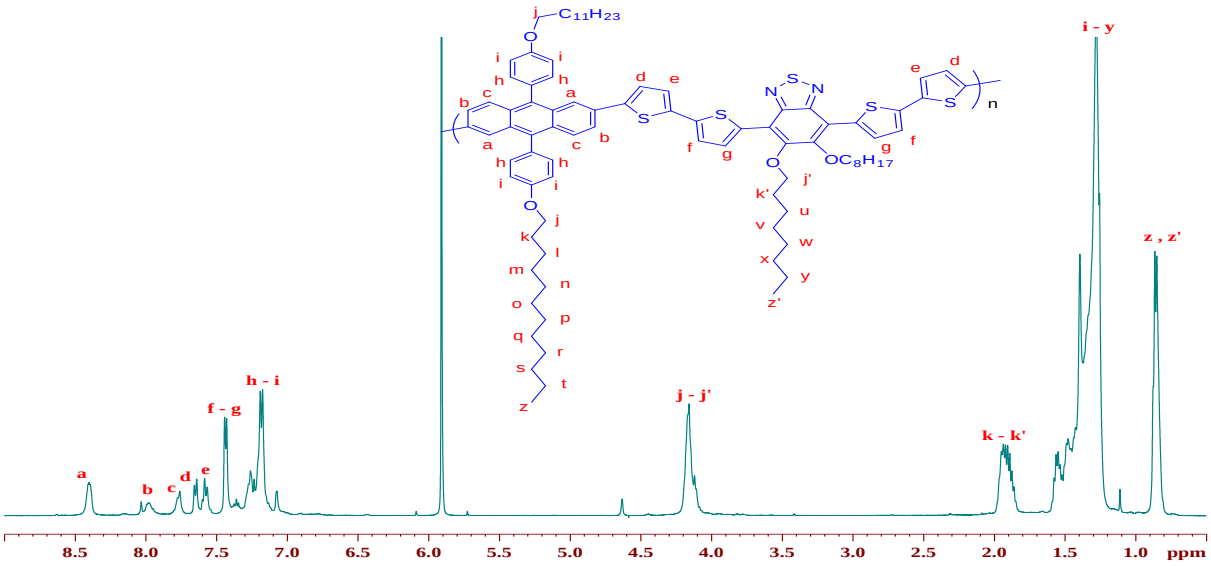

Figure 87: The proton NMR spectra of P6.

The ^{1}H NMR spectrum of **P7** reveals nine aromatic signals of anthracene and thiophene hydrogens as illustrated in Figure 88. The singlet peak at 8.42 ppm is related to the two protons at position a on the anthracene unit, the singlet peak at 8.0 ppm can be assigned to the two protons at positions b on the anthracene unit . The protons at the positions c are displayed as a doublet peak at 7.80 ppm . The protons at the position d and e of the thiophene directly attached to anthracene unit are shown as doublet peaks at 7.60 and 7.50 ppm respectively. The peak at 7.40 and 7.30 ppm correspond to the four protons at positions f and g of the thiophene ring attached to benzothiadiazole . The protons of the positions h h’ and i i’ of the attached phenyl groups are shown as multi peaks from 7.23 to 7.10 ppm. The broad peak at 4.16 ppm corresponds to the protons at position j , j’ and j’’ of the methylene attached to the oxygen atoms in the alkoxy chains of the anthracene and **(DT2BT-8)** units. The remaining aliphatic protons were displayed from 2.09 ppm to 0.80 ppm.

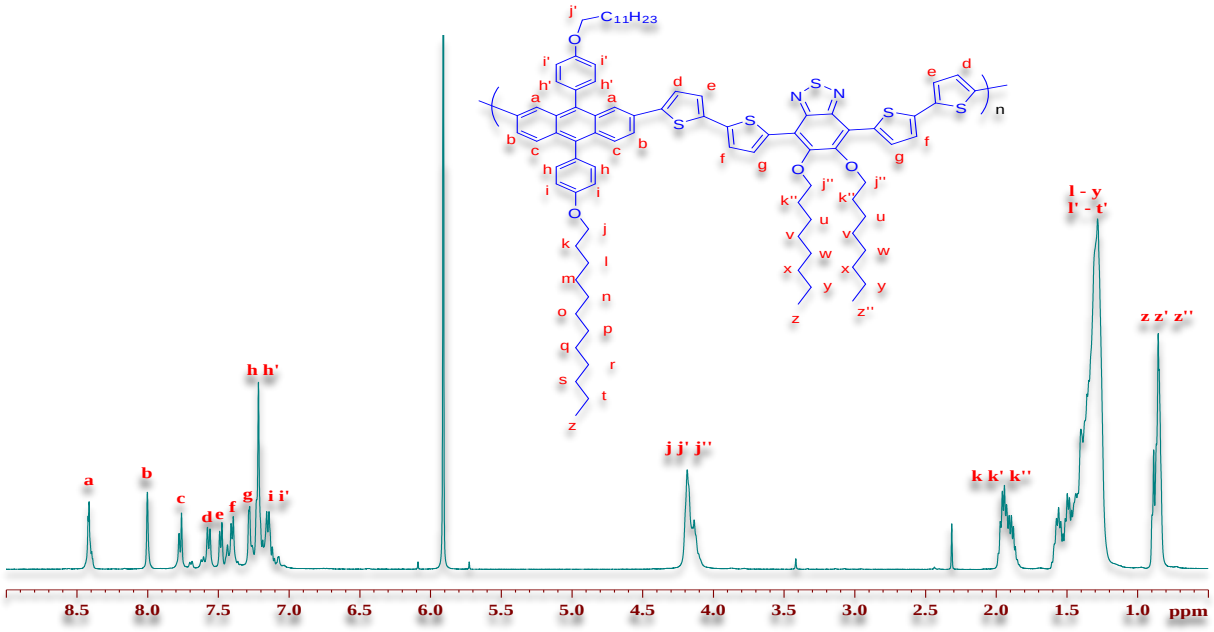

Figure 88: The proton NMR spectra of P7

5.3.2.2 UV-Visible absorption spectroscopy analysis(P6) and (P7)

The UV-Visible absorption spectra of polymers **P6** and **P7** were measured in chloroform solutions and in solid state as thin films. The onset of absorption of the polymers in the solid state are used to determine the optical band gaps for all polymers. The optical data for polymers **P6** and **P7** are summarized in Table 11.

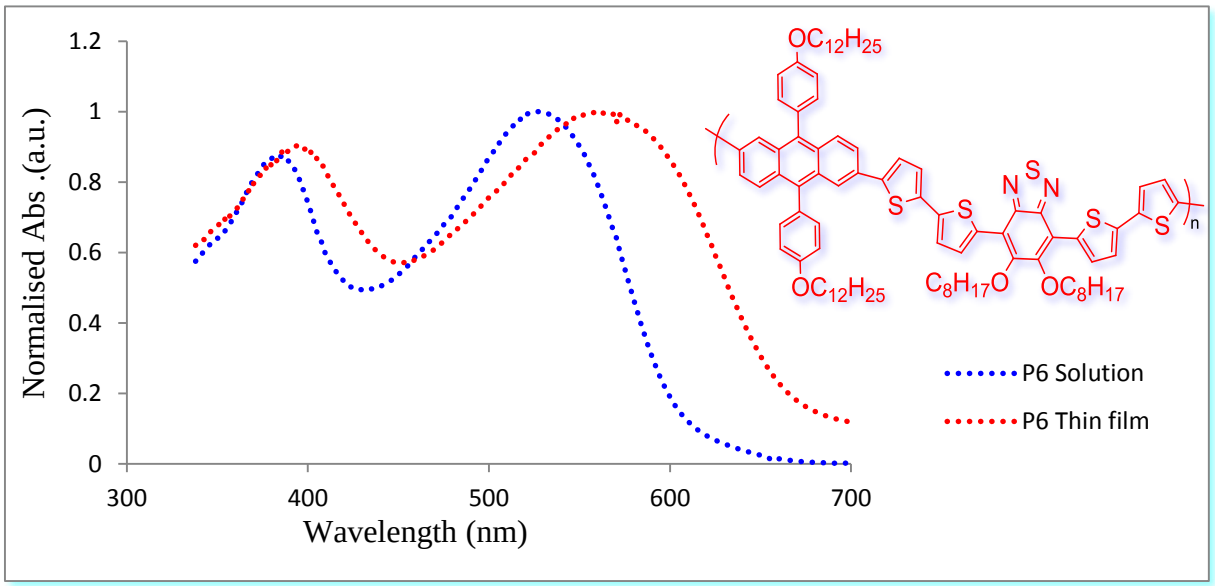

Figure 89: Normalised UV-Vis spectra of chloroform fraction for P6 in $CHCl_3$ solution (Dotted-blue line), as a thin film (Dotted-red line).

The normalized UV-vis absorption spectra of polymer **P6** in $CHCl_3$ solution and solid state are shown in Figure 89. The spectra show two absorption bands for **P6** at λmax_1 = 383 nm and λmax_2 = 529 nm in chloroform solution. The film exhibits two absorption bands at λmax_1 = 395 nm and λmax_2 = 562 nm .The absorption peaks of polymer **P6** are at the longer wavelength in the film has a red-shift of 33 nm compared with that in solution as summarized in Table 11 , indicating the presence of intermolecular interactions in the solid state .

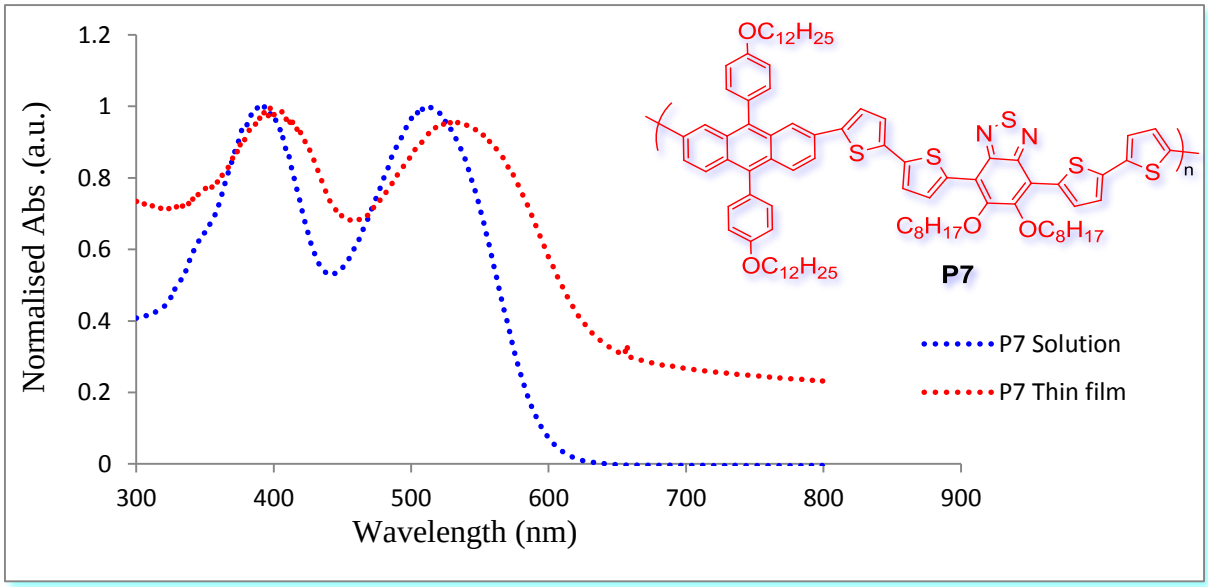

Figure 90: Normalised UV-Vis spectra of chloroform fraction for P7 in $CHCl_3$ solution (Dotted-blue line), as a thin film (Dotted-red line)

The normalized UV-vis absorption spectra of polymer **P7** in $CHCl_3$ solution and solid state are shown in Figure 90. The spectra show two absorption bands for **P7** at λmax_1 = 394 nm and λmax_2 = 511 nm in chloroform solution. The film exhibits two absorption bands at wavelength with λmax_1 = 398 nm and λmax_2 = 530 nm .The absorption peak of polymer **P7** at the longer wavelength in the film has a red-shift of 19 nm compared with that in

solution as summarized in Table 11, as result of the intermolecular interactions in the solid state .

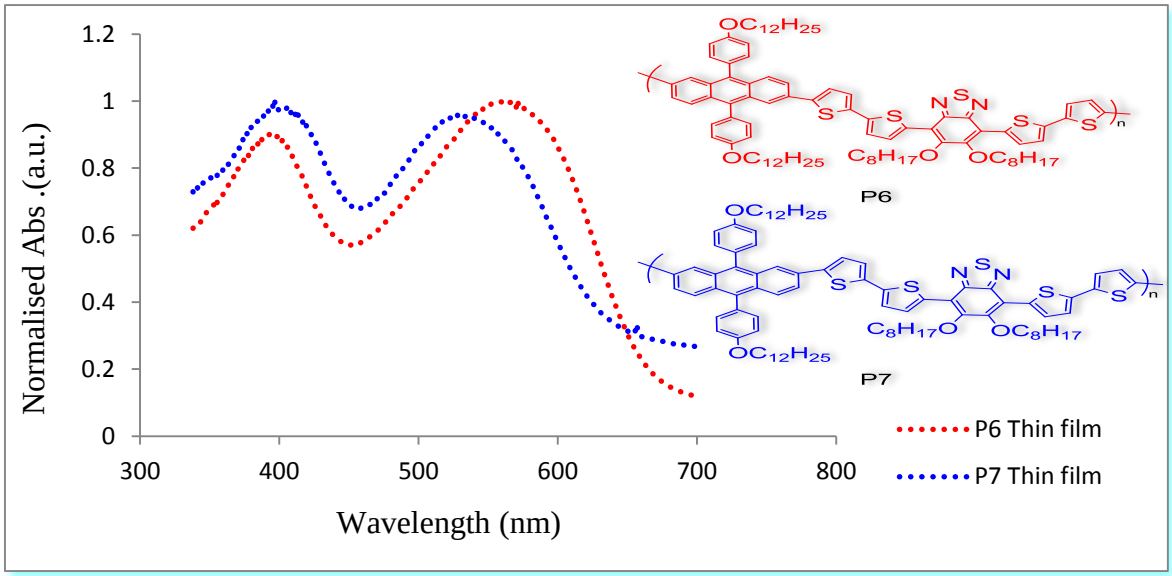

Figure 91: Normalised UV-Vis spectra of thin film for P6 (Dotted-blue line) and P7 (Dotted-red line).

Figure 91 shows the normalized UV-vis absorption spectra of **P6** and **P7** in thin films. It can be seen that the absorption bands of **P6** is extended compared to that of **P7**. The **P6** shows a red shift at longer wavelength by about 32 nm compared to its analogous **P7**. This can be attributed to the symmetrical structure of the polymer **P6** where the donor unit is linked at the positions 2,6-position,which leading to a more conjugated structure compare to the 2,7-linked anthracene polymer. Moreover, such symmetrical structure facilitates the order produced by π-stacking leading to more intermolecular interactions.

Table 11 : UV-Vis data of P6 and P7.

Polymers	Solution λ_{max} (nm)		Thin Film λ_{max} (nm)		λOnset.Abs	Optical E_g
	λ_{max1}	λ_{max2}	λ_{max1}	λ_{max2}	(nm)	(eV)
P6	383	529	359	562	666	1.87
P7	394	511	398	530	625	1.98

The absorption spectra of polymers **P6** and **P7** and their band gaps are summarised in Table 11 Both polymers show red shifts from solutions to thin film at longer wavelength by about (33 nm for **P6** *vs.* 19 nm for **P7**).The absorptions maxima of polymer **P6** containing symmetrical 2,6-anthracene unit as electron donor are at longer wavelength than that of its analogous **P7** by about 32 nm . The calculated absorption onsets of these polymers from their thin films at longer wavelengths show values of (666 nm for **P6** *vs.* 526 nm for **P7**) with optical energy band gaps of (1.87 eV for **P6** *vs.* 1.98 Ev for **P7**). These obtained results indicate that the 2,6-linked anthracene polymers exhibits higher electronic conjugation , intermolecular interactions and intramolecular charge transfer along polymer backbones when compared to that of 2,7-linked anthracene polymer. Again, the unsymmetrical structure of 2,7-linked anthracene polymers plays a crucial role on tuning and altering its electronic properties leading to chain twisting which in turn lead to a reduction in electron delocalisation along the polymer backbone.A comparison of the UV-Visible absorption spectra of polymers **P6** and **P7** with carbazole polymer **P4** containing **(DT2BT-8)** as accepting units indicating that **P6** shows higher values of λ_{max} in thin film with optical energy band gaps of (1.87 eV for **P6** *vs.* 1.98 Ev for **P4**) Table 12. This low value of band gap of **P6** can be attributed to the symmetrical structure of the polymer **P6** Moreover, such symmetrical structure facilitates the order produced by π-stacking

leading to more intermolecular interactions. In contrast, **P7** shows quite similar values of λ_{max} to those of **P4** and both polymers have the same value of the energy band gap 1.98 eV.

Polymers	Solution $\lambda_{max\ (nm)}$		Thin Film $\lambda_{max\ (nm)}$		Optical E_g
	λ_{max1}	λ_{max2}	λ_{max1}	λ_{max2}	(eV)
P4	390	505	396	523	
P6	383	529	359	562	1.87
P7	394	511	398	530	1.98

Table 12 : UV-Vis data of P6 , P7 and P4.

5.3.2.3 Cyclic Voltammetry (CV) analysis of P6 and P7

Cyclic voltammetry (CV) studies were performed on drop-cast polymer films in acetonitrile with tetrabutylammonium perchlorate as the electrolyte. The LUMO and HOMO levels were calculated from the onset of reduction and oxidation respectively. The electrochemical band gap (Eg) can be calculated from the difference between the HOMO and LUMO levels.

The cyclic voltammetry curves of **P6** and **P7** are shown in Figure 92 and 93 respectively. Their electronic properties are summarized in Table 13 . It is clear from the calculation carried out on the curve in Figure 92 that 2,6-linked anthracene copolymer **P6** has a HOMO energy level at (-5.35 eV), while its LUMO energy level is at (-3.11 eV) showing an electrochemical energy band gap around (2.24 eV) . The electrochemical band gap

value of **P6** is higher than its optical band gap (E_{opt} = 1.87 eV) by about (0.37 eV) as expected due to exciton binding energy.

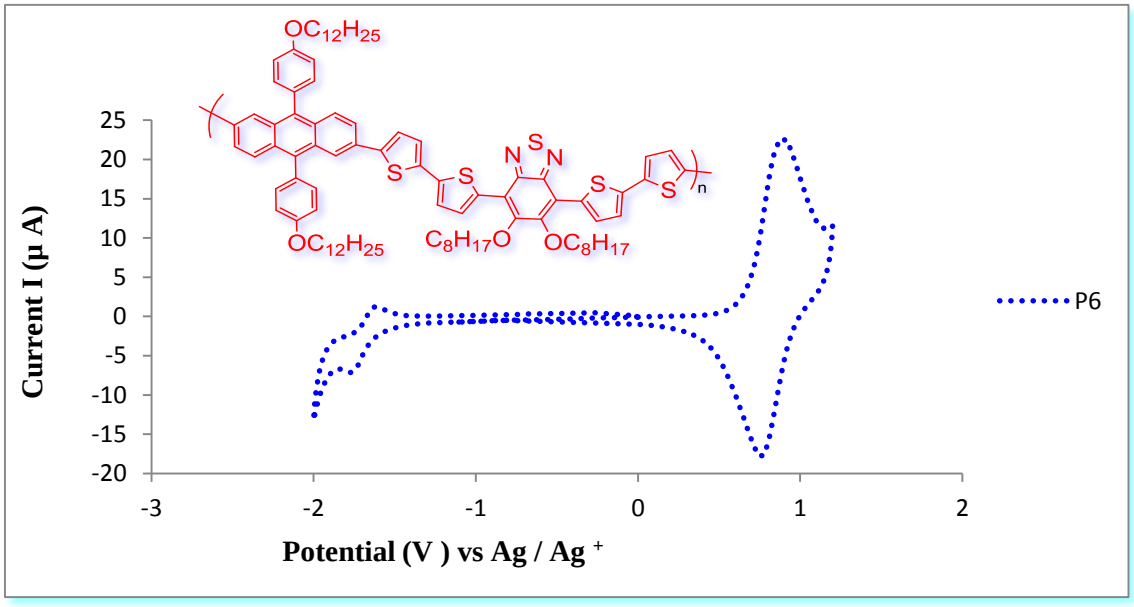

Figure 92: Cyclic voltammetry curve of P6.

Figure 93 shows the cyclic voltammetry curve of 2,7-linked anthracene copolymer **P7**.The HOMO and LUMO energy levels are (-5.50 eV and -3.15 eV) respectively.The electrochemical energy band gap calculated from the difference between its HOMO and LUMO levels is estimated around (2.35 eV). Again, its electrochemical band gap value is higher than its optical band gap (E_{opt} = 1.98 eV) due to exciton binding energy.

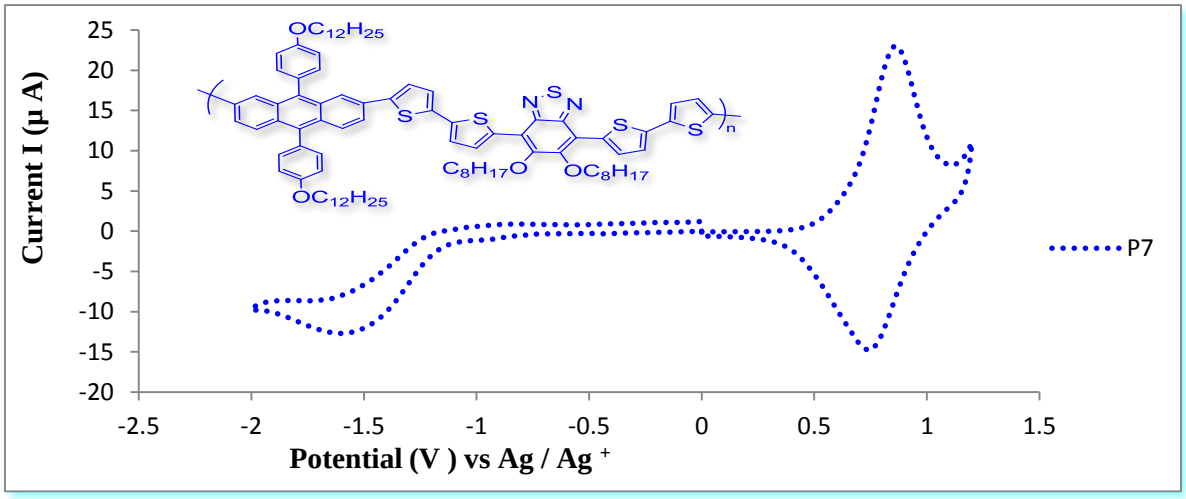

Figure 93: Cyclic voltammetry curve of P7.

A comparison of the HOMO level of **P6** with its analogous 2,7-linked anthracene copolymer **P7** indicates that **P7** has deeper HOMO energy level (-5.35 eV for **P6** *vs.* -5.5 eV for **P7**).Their LUMO energy levels are almost identical due to having the same acceptor unit (-3.11 eV for **P6** *vs.* -3.15 eV for **P7**). A comparison of the electrochemical band gap of 2,6- linked anthracene copolymer **P6** with its analogous 2,7- linked anthracene copolymer **P7** indicates that **P6** has lower electrochemical energy band gap (Eelect= 2.24 eV for **P6** vs Eelect= 2.35 eV for **P7**).

The deeper HOMO energy level of 2,7-linked anthracene polymers **P7** compared to that of its analogous 2,6-linked anthracene copolymer **P6** is probably due to steric hindrance in the unsymmetrical structure of 2,7-anthracene unit which reduce the electron delocalisation, intermolecular interactions and the intramolecular charge transfer along the polymer backbone.

Table 13 : Electrochemical properties of P6 and P7.

Polymer	E_{op} (e V)	Homo (eV)	LUMO (eV)	E_{elect} (eV)
P6	1.87	- 5.35	-3.11	2.24
P7	1.98	-5.50	-3.15	2.35

5.3.2.4 Thermo-gravimetric Analysis (TGA)

The thermal stability of **P6** and **P7** were studied using TGA and the curves of the thermal degradation of these polymers are shown in Figure 94. It can be seen from the curves that the two polymers exhibit a high thermal stability up to 330 ^{o} C which is high enough for the requirements of solar cell applications. Both polymers **P6** and **P7** display similar thermal degradation patterns until 570 ^{0}C. **P6** shows two degradation onsets steps, the first one occurs at 330 ˚C, the second degradation onset occurs at 441˚C, with a weight loss of 69 % at 800 ^{0}C . Polymer **P7** also shows two degradation steps, the first step occurs at 356 ˚C, the second at 428 ˚C, with a weight loss of 54.5 % at 800 ^{0}C. The degradation and weight loss of polymers **P4** and **P5** beyond 600 ºC originated from the cleavage of alkyl chains attached to the anthracene and **(DT2BT-8)** units on polymer chains.

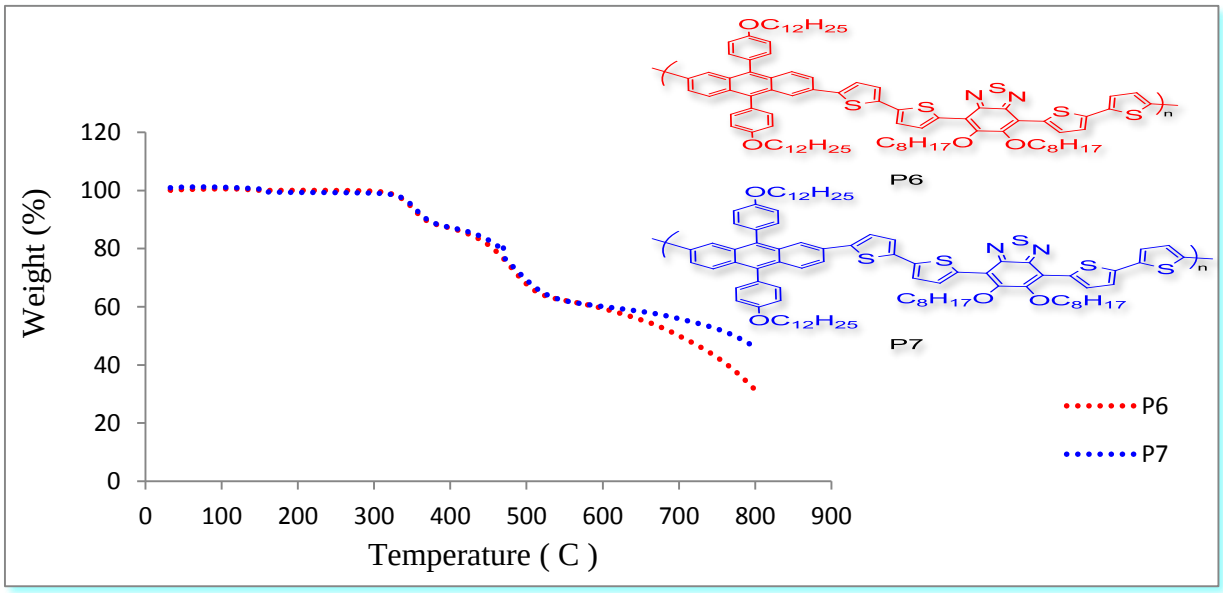

Figure 94: The TGA thermgram of P6 and P7

5.4 Fluorene- carbazole based block copolymers : (P8)

Designing and improving organic solar cells to accomplish several features at once ; absorb sunlight, separate the excited states is a big challenge. Moreover , control of the energy levels of the HOMO and LUMO is highly desirable to attain the ideal performance in BHJ devices. Organic block copolymers are a promising way for efficient charge separation due to their self-assembly properties in nano-morphology.

Among polymers **P1**- **P7**, **P1** and **P3** achieved good results in BHJ solar cell applications, so they are great candidates to absorbs a large portion of sunlight extending to 700 nm due to their extended absorption range from 350 to 700 nm. **P1** and its blend with PCBM achieved power conversion efficiencie of 4.22 % in BHJ solar cells , while **P3** exhibit the highest efficiency among these polymers by about 5.41 %. Moreover, these polymers exhibit fine – tuned LUMO levels, which allow for an efficient electron transfer between these polymer [91]Figure 95 .

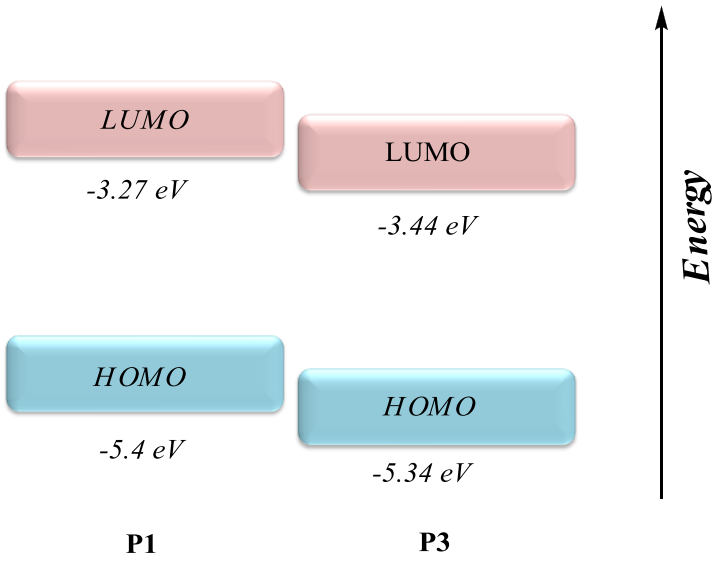

Figure 95: Diagram showing the HOMO and LUMO energy levels of P1 and P3 to prepare P8

It was then thought that making a block copolymer using blocks from both polymers **P1** with **P3** could achieve a polymer with good absorption spectral coverage between 300 and 700 nm , good phase separation and tuning energy levels .Such a block copolymer would have **P1** blocks as the electron donor segments and **P3** blocks as acceptor blocks. The polymer would hence be used as the active layer in PV devices without the need to use fullerene as additives. Polymer **P8** was synthesised according to Suzuki cross coupling reaction with using fluorene and carbazole units as boronic esters and unsubstituted 4,7-dithien-2-yl-2,1,3-benzothiadiazole **(DTBT)** , 5,6-dioctyl-4,7-di(thiophen-2-yl)benzo[c][1,2,5]thiadiazole **(DTBT- 8)** units .The structures of the monomers used to prepare the block copolymer **P8** are shown in Figure 96.

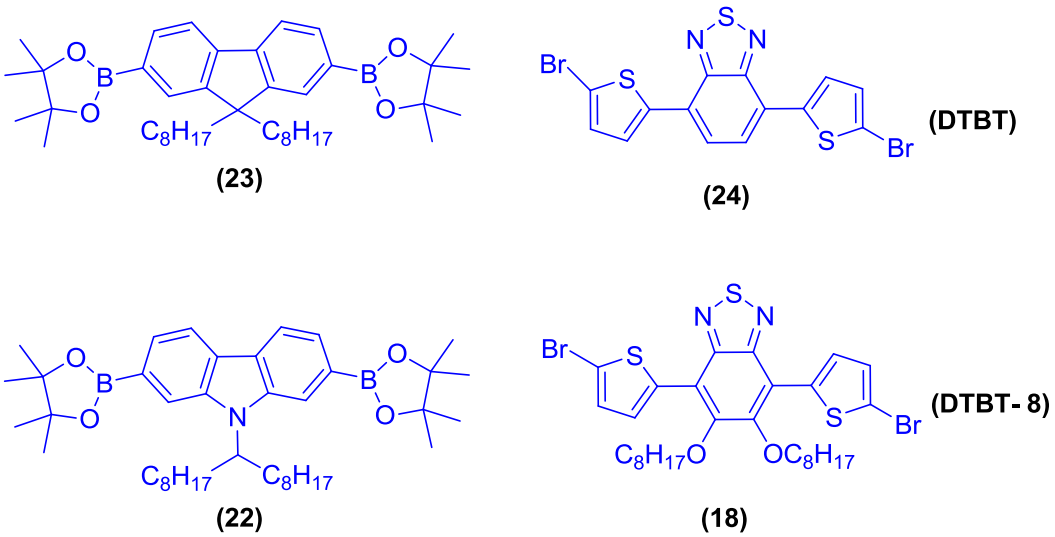

Figure 96: The structures of the monomers used in the preparation of block copolymer P8

5.4.1 Synthesis and Analysis of (P8)

Polymer **P8** was synthesised using Suzuki cross coupling reaction. The polymerisation conditions are summarised in Table 14

Table 14 : Summary of polymerisation condition for block copolymer P8

Polymer	1^{O} block monomers	Time of 1^{0} plymerisation	2^{O} block monomers	Time of 2^{0} plymerisation	Monomers ratio	Catlyst -ratio
P8	23 & 24	3 h	22 & 18	48 h	1:1:1:1	1:2

Poly[4-(5-(9,9-dioctyl-7-(5-(7-(thiophen-2-yl)benzo[c][1,2,5]thiadiazol-4-yl)thiophen-2-yl)-9H-fluoren-2-yl)thiophen-2-yl)-7-(5-(9-(heptadecan-9-yl)-9H-carbazol-2-yl)thiophen-2-yl)-5,6-bis(octyloxy)benzo[c][1,2,5]thiadiazole] **P8** was prepared from a Suzuki coupling reaction between 9,9-Dioctylfluorene-2,7-diboronic acid bis(1,3-propanediol) ester **(23)** and 4,7-bis(5-bromothiophen-2-yl)-benzo[c][1,2,5]thiadiazole **(DTBT) (24)** using dry toluene as solvent and Et_4NOH as base. Both polymarisations were done in the presence of $Pd(OAc)_2$ and $P(o\text{-}tol)_3$ as catalyst with ratio (1:2) respectively. The first polymerisation of **(23)** and **(24)** was done for 3 hours at 90 ^{0}C until the solution became more viscous. Then, the mixture was cooled to room temperature and 9-(heptadecan-9-yl)-2,7-bis-(4,4,5,5-tetramethyl-[1,3,2]dioxaborolan-2-yl)-9H-carbazole **(22)** and 4,7-bis(5-bromothiophen-2-yl)-5,6-bis(octyloxy)benzo-[c][1,2,5]-thiadiazole **(DTBT-8) (18)** were added and heated to 90 °C for 48 h.The ratio between monomers in the first block and second block was (1:1:1:1) . The polymerisation was stopped by adding the end-capping reagents (bromobenzene and phenyl boronic acid) to the polymer solutions. The structures of the target polymer **P8** is presented in Figure 97.

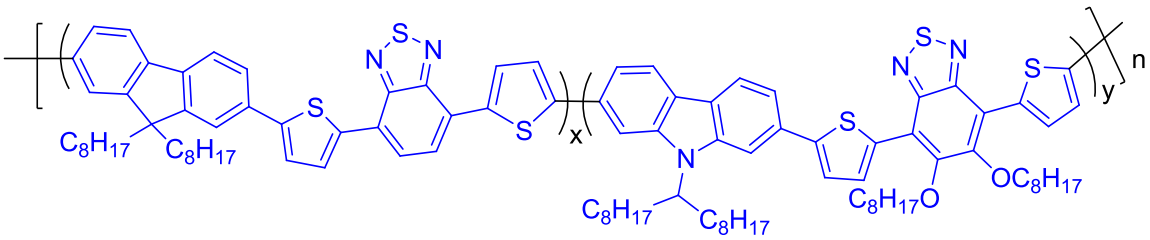

P8

Figure 97: Structure of block cocopolymer P8

The reaction mechanism for preparation polymer **P8** follows the Suzuki coupling reaction mechanism that was described for the synthesis of **P1- P3** in Scheme 46.

The purification of polymer **P8** from catalytic traces was done by stirring with ammonia overnight. Soxhlet extraction was used to purify and fractionate the polymer from smaller molecules, oligomers and unreacted monomers. **P8** was also purified by Soxhlet extraction using methanol, acetone , hexane , toluene and chloroform. The toluene and chloroform fractions were concentrated to about 50 mL and then poured into methanol (200mL). Then the purified polymer in toluene and chloroform fractions were separated and precipitated to afford as purple powders with 43 % yield in toluene and 20 % in chloroform.

The expected structure of the **P8** was confirmed using elemental analysis, GPC and ^{1}H-NMR. The elemental analysis technique was used to confirm complete replacement of bromine atoms with end-capping groups. All the GPC data and physical properties of polymer **P8** are summarised in Table 15 , as derived from GPC .

Table 15 : Yields and GPC data of fractions of polymer P8

Polymer	Soxhlet Fraction	Yield		GPC		
		Mass/mg	%	MW	Mn	PD

P8	Toluene	160	43%	14.600	8.700	1.68
	Chloroform	77	20%	30.100	18.800	1.59

5.4.2 Characterization of (P8)

5.4.2.1 NMR Analysis

The ^{1}H-NMR analysis for the block copolymer **P8** was performed in $C_2D_2Cl_4$ at 100 ˚C to avoid polymer aggregation especially in the aromatic region. In Figure 98 , the ^{1}H NMR spectrum of toluene fraction of **P8** shows a broad peak at 8.65 ppm which corresponds to the two protons at position a on the fluorene unit, the two broad peaks at 8.15 and 7.90 ppm related to the four protons at positions b and c on the fluorene unit . The protons at the positions d , e and f of the carbazole unit are displayed multi peaks at 7.75. The multi peaks from 7.10 to 7.25 ppm can be assigned to the eight protons at positions g , h , j and k of the thiophene rings . The two protons at the position i on the benzothiadiazole are shown at 7.55 ppm . The broad peak at 4.75 ppm corresponds to the methine at the position l on the carbazole unit. The broad peak at 4.30 ppm corresponds to the protons at position m of the methylene attached to the oxygen atoms in the octyloxy chains of the benzothiadiazole **(BT)** unit.The peaks from 2.49 ppm to 0.83 ppm represent the rest protons of the alkyl chains connected to carbazole , fluorene and benzothiadiazole **(BT)** units.

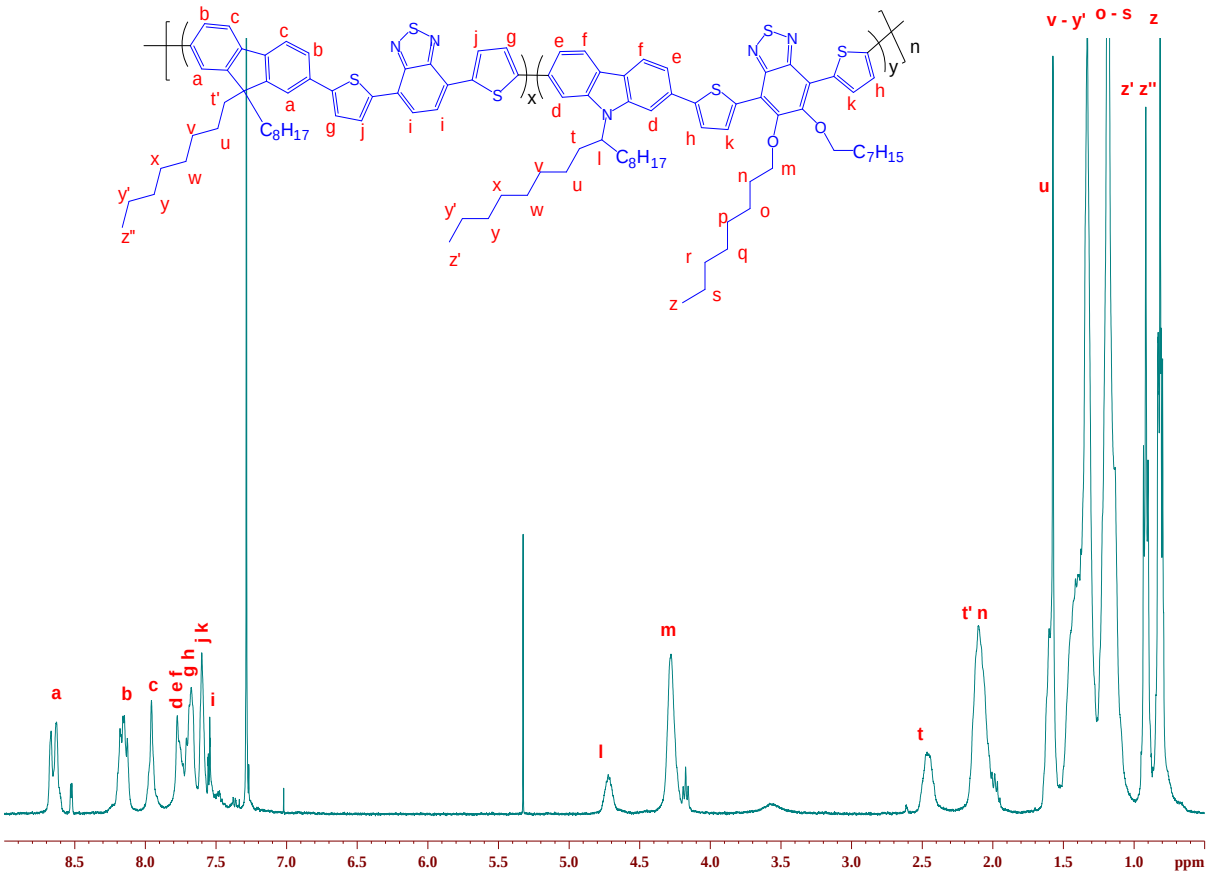

Figure 98: The proton NMR spectra of P8.

5.4.2.1 UV-Visible absorption spectroscopy analysis of (P8)

The UV-Visible absorption spectra of **P8** were measured in chloroform solution and in solid state as thin films. The onset of absorption of the polymer in the solid state are used to determine the optical band gap for the polymer. The optical data for all fractions of polymer **P8** are analyzed and compared to **P1** and **P3** , as summarized in Table 16.

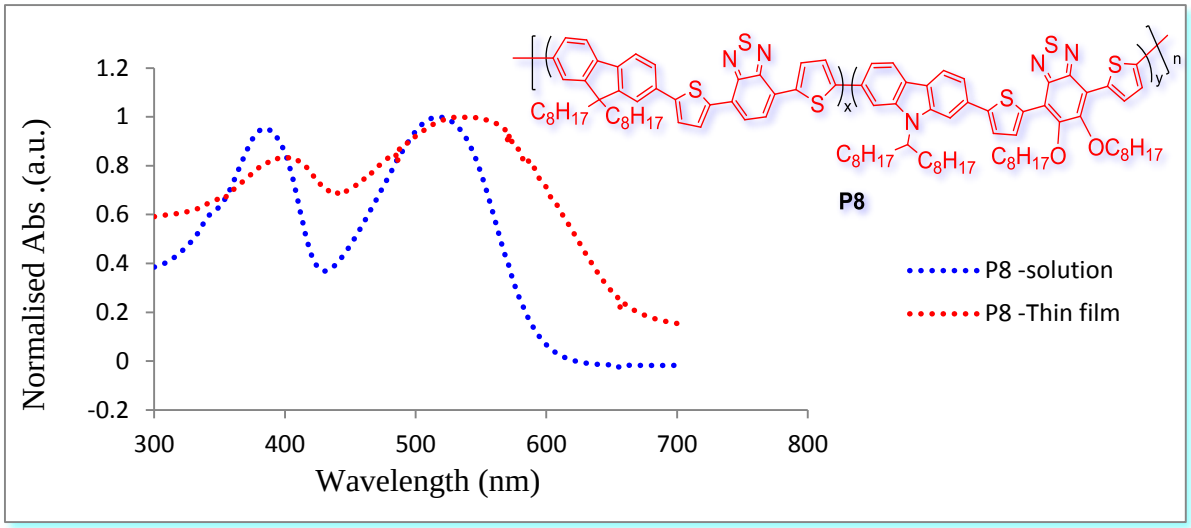

Figure 99: Normalised UV-Vis spectra of toluene fraction for P8 in $CHCl_3$ solution (Dotted-blue line), as a thin film (Dotted-red line)

Figure 99 shows UV-Vis analysis of polymer **P8** for toluene fraction in $CHCl_3$ solution and thin film. The absorption spectrum of **P8** in toluene fraction shows two broad absorption peaks at λ_{max1} = 384 nm and $\lambda_{max\ 2}$ = 518 nm in chloroform solution. The thin film shows a red-shift and exhibits two bands at 402 and 532 nm .

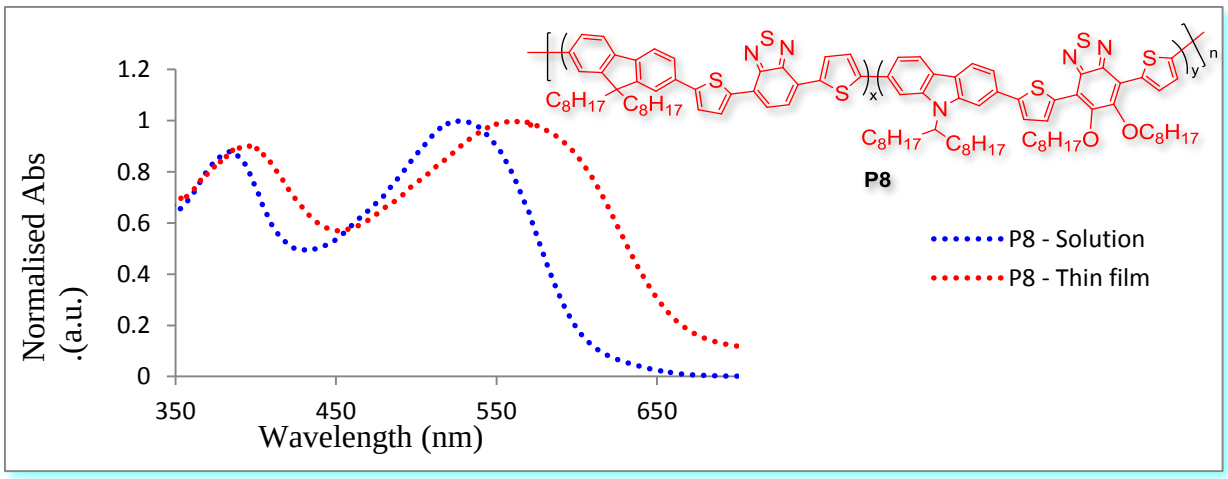

Figure 100: Normalised UV-Vis spectra of chloroform fraction for P8 in $CHCl_3$ solution (Dotted-blue line), as a thin film (Dotted-red line)

The UV-Vis analysis of polymer **P8** of chloroform fraction in solution and thin film is shown in Figure 100 . The absorption spectrum of **P8** shows two broad absorption peaks at

λ_{max1} = 389 nm and $\lambda_{max\ 2}$ = 534 nm in chloroform solution. The UV-Vis analysis of **P8** in thin film shows two broad absorption peaks at λ_{max1} = 392 nm and $\lambda_{max\ 2}$ = 544 nm .

Figure 101 shows the absorption peak in thin films for both fractions toluene and chloroform. Both polymers absorb the light between 300 to 700 nm. It can be seen from Figure 101 that there are shift in the λ max values between solutions and solid state thin films which are assumed to be due to aggregation as in thin films polymers have more planar structure than in solution. Also the freedom of movement of polymer chains in solution leads to polymer chain twisting and so lead to lower conjugation. Although the absorption of the chloroform fraction at long wavelength is higher than that of toluene by about 12 nm , the toluene fraction shows broad band compare to that of chloroform.

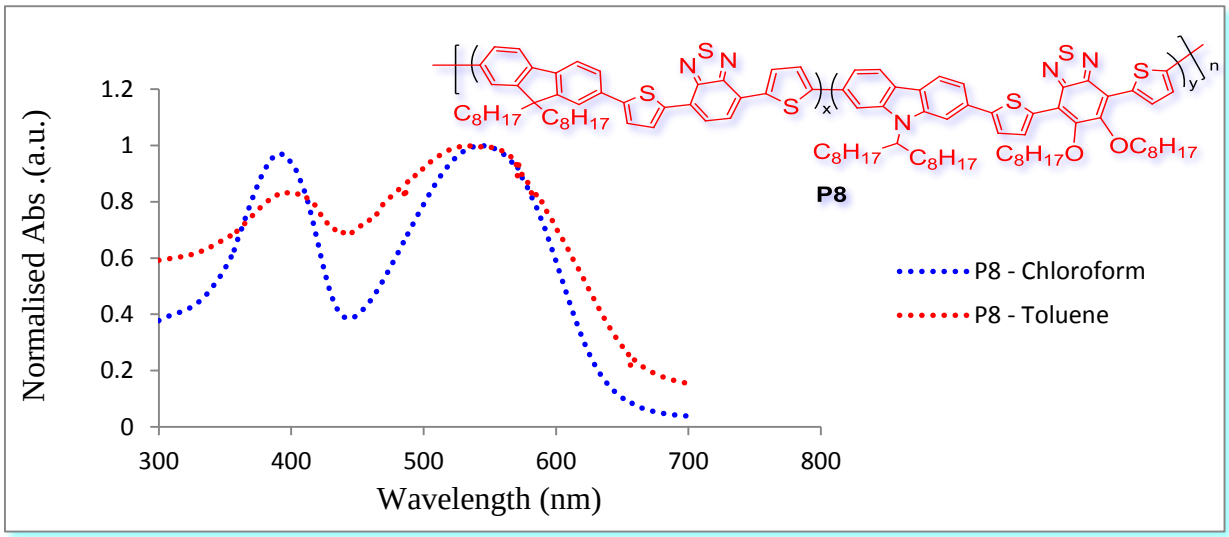

Figure 101: Normalised UV-Vis spectra of P8 in thin film for toluene and chloroform fractions.

The UV-Vis analysis of polymer **P8** in thin film was also compared to its blocks polymer **P1** and **P3** as shown in Figure 102. The absorption band at longer wavelength of **P8** is located between **P1** and **P3** bands. Even thought the bands shape of **P3** and **P8** are very similar and much broader than that of **P1**, **P3** displays the highest red – shift among these

polymers due to the high intermolecular interaction between polymer chains in **P3**, leading to a high degree of order.

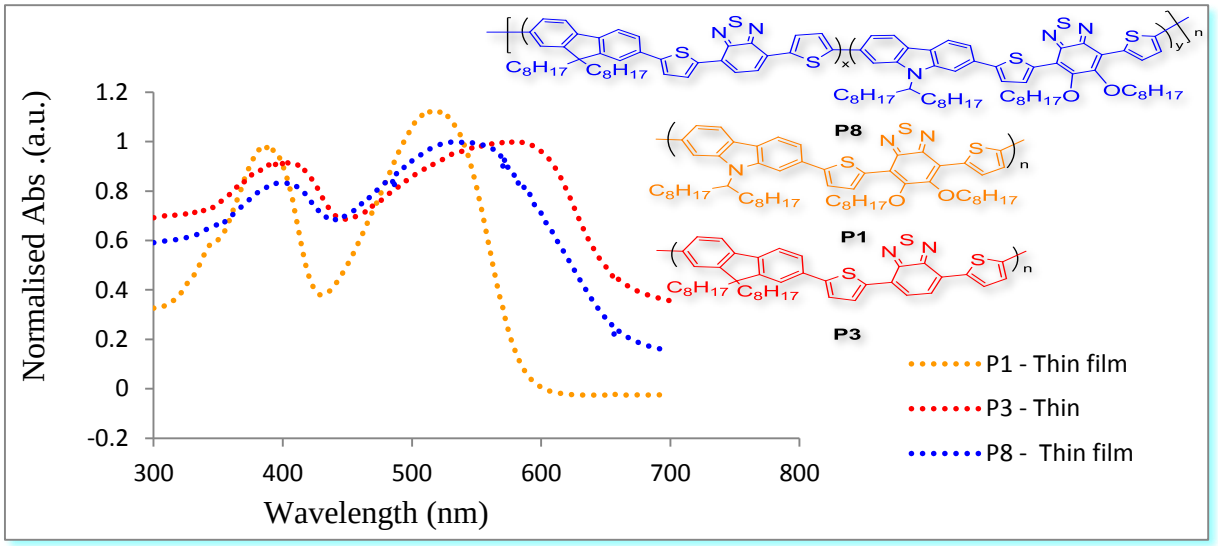

Figure102: Normalised UV-Vis spectra of P8 comparing to its blocks P1 and P3 in thin film

The absorption spectra of polymers **P8** and its blocks **P1** and **P3** in chloroform solutions and as thin films are summarised in Table 16.

Table 16 : UV-Vis data of P1 , P3 and P8

Polymers	Solution λ_{max} (nm)		Thin Film λ_{max} (nm)		λOnset.Abs	Optical E_g
	λ_{max1}	λ_{max2}	λ_{max1}	λ_{max2}	(nm)	(eV)
P1	384	513	390	529	616	2.01
P3	394	550	408	591	666	1.86
P8 - Tol	384	518	402	532	663	1.87
P8 - Chlo	389	534	392	544	645	1.92

Comparison of the absorptions maxima in thin films of polymer **P8** in both fractions with that of **P1** indicate red- shifts in **P8**. The red – shift of **P8** in toluene fraction was slightly smaller by about 3 nm while in chloroform fraction was 15 nm. Noticeably, blue – shifts at longer wavelength in thin films can be observed for **P8** when comparing with **P3** by about 59 and 47 nm for toluene and chloroform fractions respectively.

Although the λ_{max2} at 544 nm of chloroform in **P8** is higher than that of toluene at 532 nm , the absorption onset of toluene fraction is higher than that of chloroform fraction by about 18 nm. This increase most probably result from the broad band of the toluene fraction which is also lead to reduce the band gap from 1.92 eV for chloroform to 1.87 eV for toluene as shown in Figure 101 .

The band gap values in all **P8** fractions are lower than that of **P1** , while these value are markedly higher than the band gap of **P3** .This can be attributed to the intermolecular interaction between polymer chains in **P3** is much stronger than that of **P8** ,which leads to a high degree of order in the polymer chains, leading to a low band gap. Moreover, the pendent octyloxy and octyl substituents groups attached to the **P8** backbone reduce and hinder the intermolecular interaction between polymer chains.

5.4.2.3 Cyclic Voltammetry (CV) analysis of P8

Cyclic voltammetry (CV) studies were performed on drop-cast polymer films in acetonitrile with tetrabutylammonium perchlorate as the electrolyte. The LUMO and HOMO levels were calculated from the onset of reduction and oxidation respectively. The electrochemical band gap (Eg) can be calculated from the difference between the HOMO and LUMO levels. The cyclic voltammetry curves of toluene and chloroform fractions for **P8** are shown in Figure 103 and its electrochemical properties are summarized in Table 17. Both fractions of **P8** show almost the same value of the

oxidation and reduction potential as well as their HOMO energy levels are exactly identical (- 5.35 eV). Moreover, their LUMO energy levels are very close (-3.22 eV for toluene fraction *vs* . -3.23 eV for chloroform fraction) , which leads to have approximately comparable values of electrochemical band gaps (E_{elect} = 2.13 eV *vs*. E_{elect} = 2.12 eV) for toluene and chloroform respectively.

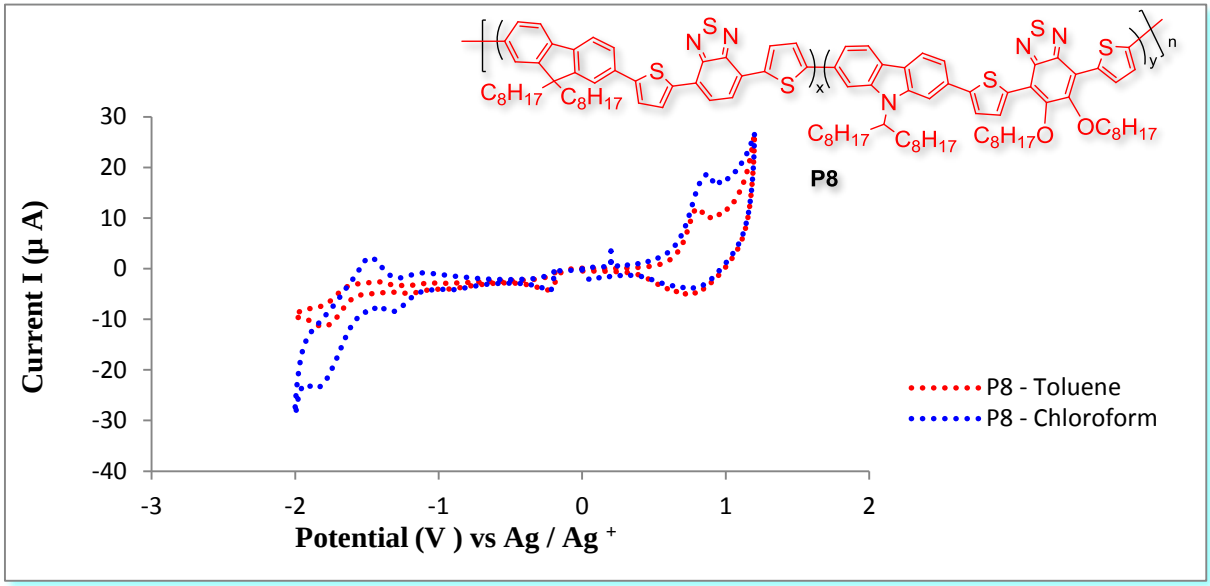

Figure 103: Cyclic voltammetry curves in toluene and chloroform fractions of P8.

P8 is a di-block copolymer between **P1** and **P3** .The electrochemical studies of **P1** and **P3** were done based on the toluene fraction ; therefore the toluene fraction of **P8** is investigated and compared with its analogous toluene fractions of **P1** and **P3**. As it can be seen from (Table13) that **P8** and **P3** have comparable HOMO energy levels (- 5.35 eV for **P8** *vs*. - 5.34 eV for **P3**) while the LUMO level of **P8** is higher than that of P3 (- 3.22 eV for **P8** *vs*. - 3.44 eV for **P3**).The electrochemical band gap of **P8** is higher than that of **P3** (E_{elect} = 2.13 eV for **P8** *vs*. E_{elect} = 1.90 eV for **P3**). This low value by about 0.23 eV of **P8** band gap could be due to the pendent octyloxy and octyl substituents groups attached to the **P8** backbone, which reduce the planarity of the polymer backbone due to steric

hindrance. Moreover, such bulky groups will reduce and hinder the intermolecular interaction between polymer chains in the solid state of **P8** leading to reduce the band gap when compared with **P3** which does not have octyloxy substituents groups in the acceptor unit.

A comparison of the HOMO's energy levels of **P8** with its analogous in **P1** indicates that **P1** has deeper HOMO energy level than **P8** (-5.40 eV for **P1** *vs.* -5.35 eV for **P8**) while their LUMO's level are comparable (- 3.29 eV for **P1** *vs.* - 3.22 eV for **P8**). The electrochemical band gap estimated from their HOMO's and LUMO's are exactly the same (E_{elect} = 2.13 eV for **P8** and **P1**). Noticeably, it can be said that the presence of the octyloxy substituent groups attached to the benzothiadiazole in both polymers **P8** and **P1** play a crucial role to some extent to minimize the electronic delocalisation along polymer backbone and reducing the electron accepting ability of the benzothiadiazole unit on **P1** and **P8** .

Table 17 : Photo-physical and electrochemical properties of P1, P2 and P3.

Polymer	E_{op} (e V)	Homo (eV)	LUMO (eV)	E_{elect} (eV)
P1	2.01	- 5.40	-3.27	2.13
P3	1.86	-5.34	-3.44	1.90
P8	1.87	-5.35	-3.22	2.13

5.4.2.4 Thermo-gravimetric Analysis (TGA) (P8)

The thermal stability of **P1** , **P3** and **P8** were studied using TGA and the curves of the thermal degradation of these polymers are shown in Figure 104 . It can be seen from the curves that **P8** exhibits a high thermal stability up to 330 ^{o} C which is high enough for the requirements of solar cell applications. Polymer **P8** display similar thermal

degradation patterns to that of **P1** until 441^{0}C. **P8** shows two degradation steps, the first one occurs at 335 ˚C, the second degradation onset occurs at 438 ˚C , with a weight loss of 56.6 % at 800 ^{0}C .The degradation and weight loss of polymers **P8** beyond 500 ºC originated from the cleavage of alkyl chains attached to the fluorene , carbazole units and **(DTBT- 8)** units.

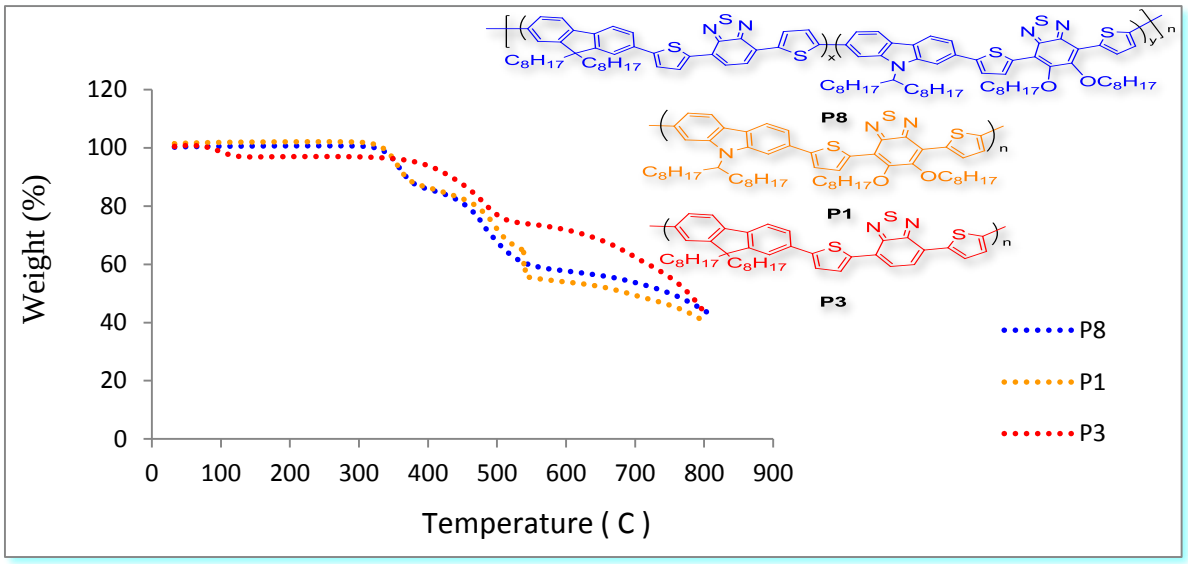

Figure 104: The TGA thermgram of P8 , P1 and P3

5.4.3 Morphology study

5.4.3.1 AFM study of P8

The morphology of the active layer is known to be a critical and direct pathway to improve the performance of bulk heterojunction solar cells based on a mixture of donor and acceptor components in blends used as active layers [68]. Creating nanoscale morphology network of a mixture of the donor and acceptor units is essential to accomplish a large interfacial area to insure quantitative charge separation. During the mixing of donor and acceptor components in the active layer, the homogeneous intermixing between donor and acceptor phases is essential. The use of block copolymers could lead to self organizing of

polymer blocks and the contact surface between these blocks is minimized by aggregating into domains. Therefore, Atomic force microscopy , AFM , was used to study the behaviour and the morphology of the block co-polymer **P8**. It is also an occasion to determine whether **P8** is a block-copolymer rather than a mixture of polymers **P1** and **P3**. If copolymer **P8** is simply a mixture of polymers **P1** and **P3** , this should results in phase segregation of the two polymers leading to visible and distinct domains of the films of **P8**.

The AFM technique used in the study of films of **P8** is non- contact mode (tapping mode). The toluene and chloroform co-polymer fractions of **P8** were studied to investigate the morphological differences between these fractions. Moreover, the atomic force microscopy (AFM) was employed to find out the effect of solvent chosen for spin casting in morphology structure and its ability to dissolve all components .

Height – 10nm Range from Min-Max for all (-5nm to 5nm)

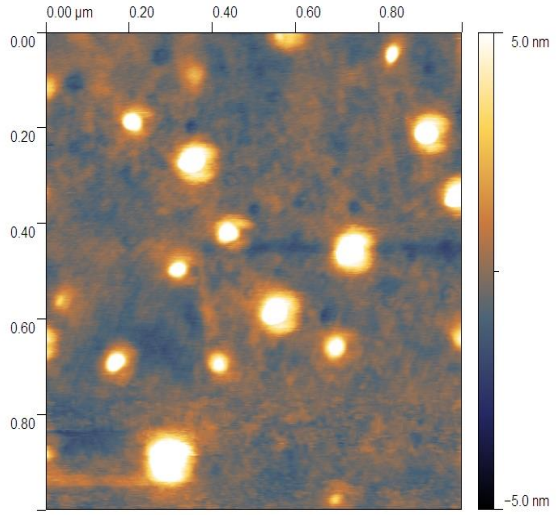

P8– Toluene

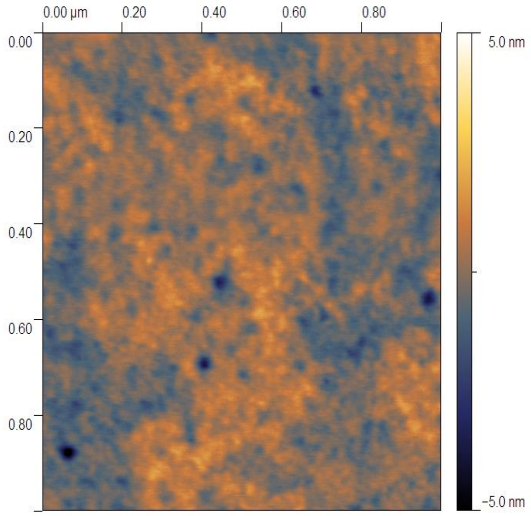

P8 – Chloroform

Phase – 10 degres Range from Min-Max for all (-5deg to 5deg)

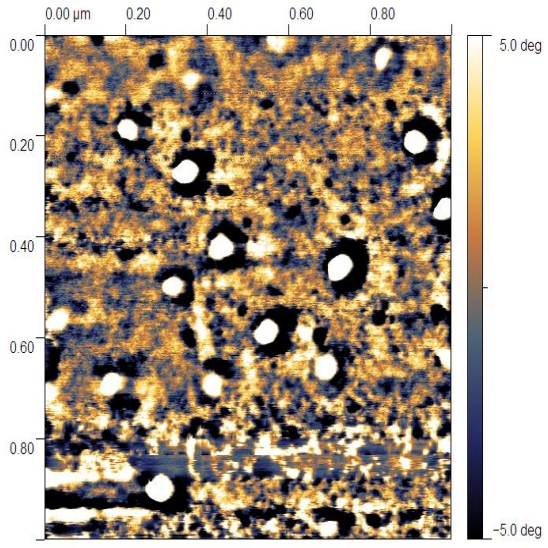

P8 – Toluene

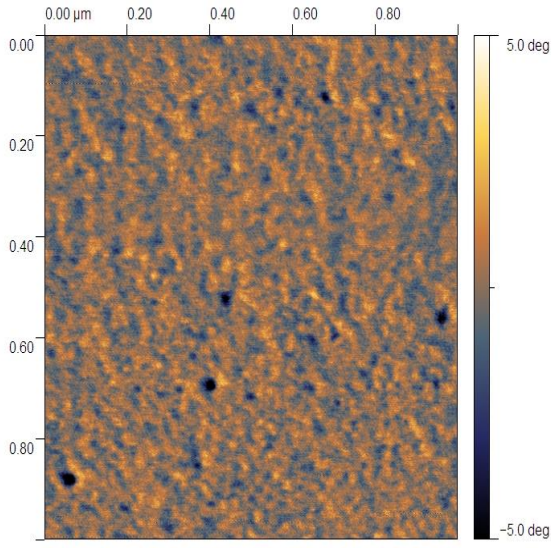

P8 - Chloroform

Figure 105: AFM images (height and phase) of P8 fractions , showing the morphology on a micrometer scale.

Figures 105 shows atomic force microscopy (AFM) phase images (height and phase) for toluene and chloroform fractions of the co-polymer **P8** at room temperature . The images in Figure 105 confirm very different surface morphologies and also there is an obvious contrast between the toluene and chloroform and their ability to dissolve all the components. The AFM image shows that the toluene fraction has some aggregates and bigger domains than chloroform fraction .This aggregates could be due to low solubility of the first block **P3** in toluene which contains just two alkyl groups attached to the fluorene unit. In contrast to toluene fraction, chloroform fraction , as shown in Figure 105, exhibits smooth height surface with less aggregates than toluene fraction. Also the AFM image shows that chloroform dissolve the all components better than toluene. These observations more pronounced can be seen clearly in the two bottom images. It can be concluded that the solvent has an effect on morphology structure and it was found that chloroform was better solvent for these components making this fraction could be better for device studies.

5.5 Attempts to prepare poly (3-hexylthiophene) - based block copolymers (P9)

Poly(3-hexylthiophene) (P3HT's) have been extensively studied as a candidate material for photovoltaic applications because of their good environmental stability , solubility and processability . This polymer is used as (p-type conjugated polymer) or electron donor in

a blend with [6,6]-phenyl-C61-butyric acid methyl ester, PCBM) as (n-type molecule) or electron acceptor [111] . The photovoltaic device based on P3HT/ PCBM achieve PCEs approaching 5.2% [130]. However, thin films of P3HT/PCBM exhibits microphase separation over time, giving large crystalline aggregates of PCBM that reduce device performance[110]. One approach to overcome this issue is to synthesise block co-polymers that contain polymers blocks where they are known to self-assemble in nanoscale morphologies. Poly(3-hexylthiophene) (P3HT – Br) containing one proton and one bromine atom as end groups was targetted in order to it use as a block in donor/ acceptor block copolymers. The polymer **P9** (P3HT – Br) was targetted and the polymer end group analysis undertaken using matrix-assisted laser desorption / ionization mass spectrometry (MALDI-MS). The monomers used in preparing this polymer are 2,5-dibromo-3-hexylthiophene **(20)** and 2-bromo-3-hexylthiophene **(21)** shown in Figure 106.

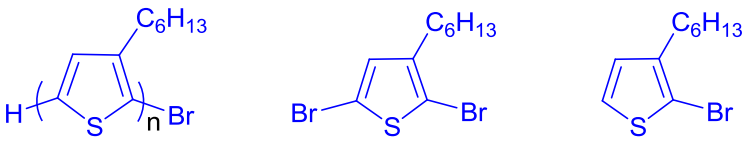

P9 **(20)** **(21)**

Figure 106: P9 and monomers used to prepare it.

In order to use this polymer as a block in a donor/ acceptor block copolymer it is required to have 95% of H / Br end groups in order to produce diblock copolymers in high yield. Due to the arduous polymer synthesis and purification of (P3HT – Br) **P9** containing one proton and one bromine atom as end groups different methods were investigated in order to determine which method will give high yield of H/Br end groups. The methods chosen to prepare polymer **P9** are discussed below.

5.5.1 Method 1: Time of Polymerization is 2h.

Poly(3-hexythiophene) (Br-P3HT) **(P9)** was prepared according to the procedure by Antoun [131]. The polymerisation process was carried out in THF using metal-catalyzed polymerization of 2,5-dibromo-3-hexylthiophene **(20)** , i-PrMgCl.LiCl as Grignard reagent and Ni(dppp)Cl_2 as catalyst Scheme (47) .

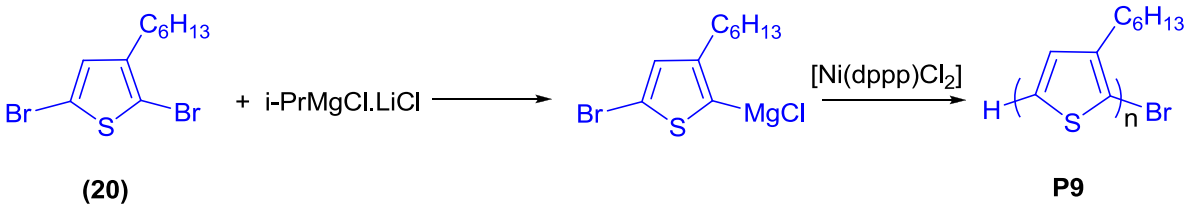

(20) **P9**

Scheme 47 : Preparing of P9

The polymerisation was done at room temperature for 2 h . The purification was done by precipitation of the polymer in methanol , then it was separated using a centrifuge. The precipitated polymer was extracted using Soxhlet extraction with methanol, hexane and toluene. The polymer was obtained from the toluene fraction to afford **P9** as dark red powder (300 mg , yield 40 %).

5.5.1.1 Characterization of P9 (*method 1*).

5.5.1.1.1 Gel Permeation Chromatography studies of P9

All the GPC data and physical properties of polymer **P9** are summarised in Table 18 .

Table 18 : Yield and GPC data of polymer P9.

Polymer	Soxhlet Fraction	Yield		GPC		
		Mass/mg	%	MW	Mn	PD

P9	Toluene	300	40%	32,500	24, 900	1.30

5.5.1.1.2 MALDI-MS of P9

MALDI-MS was used to characterize the polymer end groups and the data of polymer **P9** indicated that 75% of polymer chains had hydrogen end-groups with only 25% having the required structure with one hydrogen atom on one side and one bromine atom on the other Table 19.

Table 19 : MALDI-MS data analysis of P9

Polymer	% H/Br End group	Mw	% H/H End group	Mw
P9	25%	3568	75%	3650

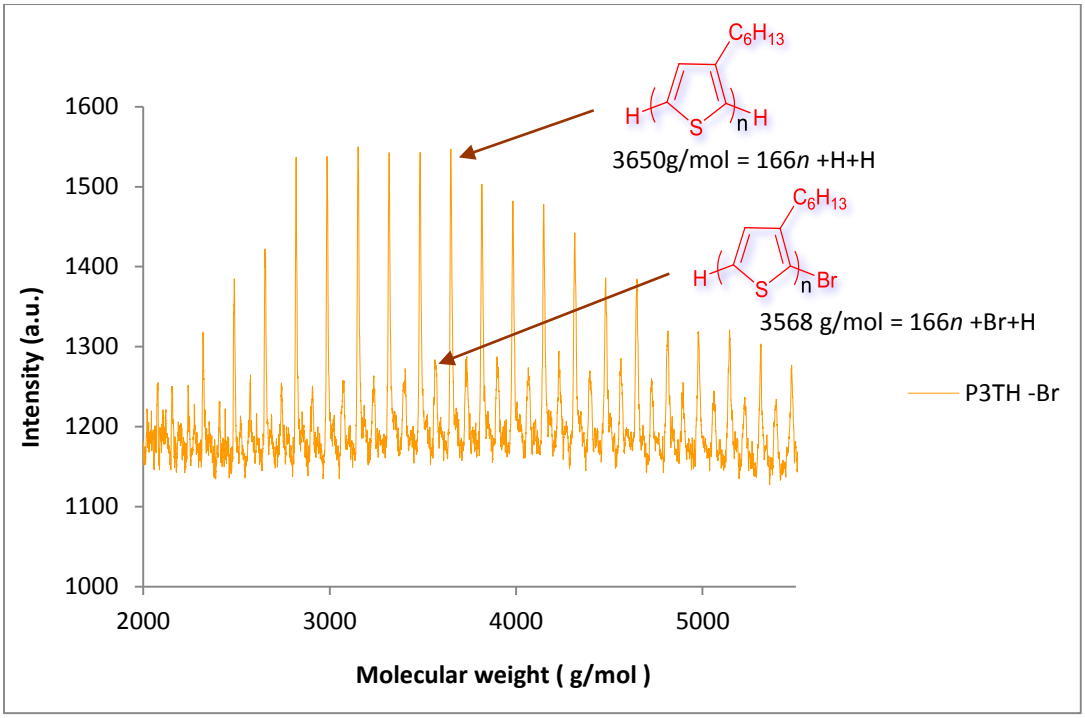

Figure 107: Mass spectroscopy (MALDI-MS) for P9 .

The data analysis from MALDI-MS in Figure 107 confirms the structure of the repeat unit of Poly(3-hexythiophene) system. It is clear that MALDI-MS displays two major types of signal peaks per repeat unit . The difference between each type of end group was calculated to be 166 g/mol , which confirms the repeat unit mass of poly(3-hexylthiophene) = 166 g/mol) [132]. The data analysis reveals that the mass of each peak can be accurately expressed by (166 *n*+H+H) and (166 *n*+Br+H) where *n* is equal to the number of repeat units. From the above information [132], it can be concluded that this polymer sample has only two major types of end group configurations. The peak corresponds to (166 *n*+H+H) corresponds to polymer chains that are terminated by hydrogen atoms at both the 2- and the 5-positions, herein referred to as H/H with number of repeat units *n* =21 [132]. The peak corresponding to (166 *n*+Br+H) refers to polymer chains terminated by a bromine atom on one end and a hydrogen atom on the other end

(referred to as H/Br) with number of repeat units *n* =21 [132]. Figure 107 shows that the formed polymer is a mixture polymer with 25 % (H/Br) and 75 % (H/H) end groups. To attain polymers with 100 % H/Br the i-PrMgCl.LiCl has to be completely consumed in the reaction to form active Grignard monomer [114]. The polymerisation time could affect the formation of active Grignard monomer; therefore the polymerisation time was left overnight as discussed in next method.

5.5.1.1.3 NMR Analysis

The ^{1}H-NMR analyses for the polymer **P9** were performed in $CDCl_3$ at 100 ˚C. In Figure 108 , the ^{1}H NMR spectrum of **P9** reveals one aromatic signal at 7.02 ppm, which is related to the proton at position a of the thiophene ring. The two protons at the position b of the the methylene directly attached to the thiophene ring are displayed at 2.8 ppm . The two protons at position c are shown as multi peaks at 1.7 ppm . The peaks from 1.55 ppm to 1.40 ppm represents the protons at positions d , e and f respectively. The CH_3 group is shown at position g as triplet peak at 0.90 ppm . The single environment in the aromatic region proves the regioregularity of **P9**.

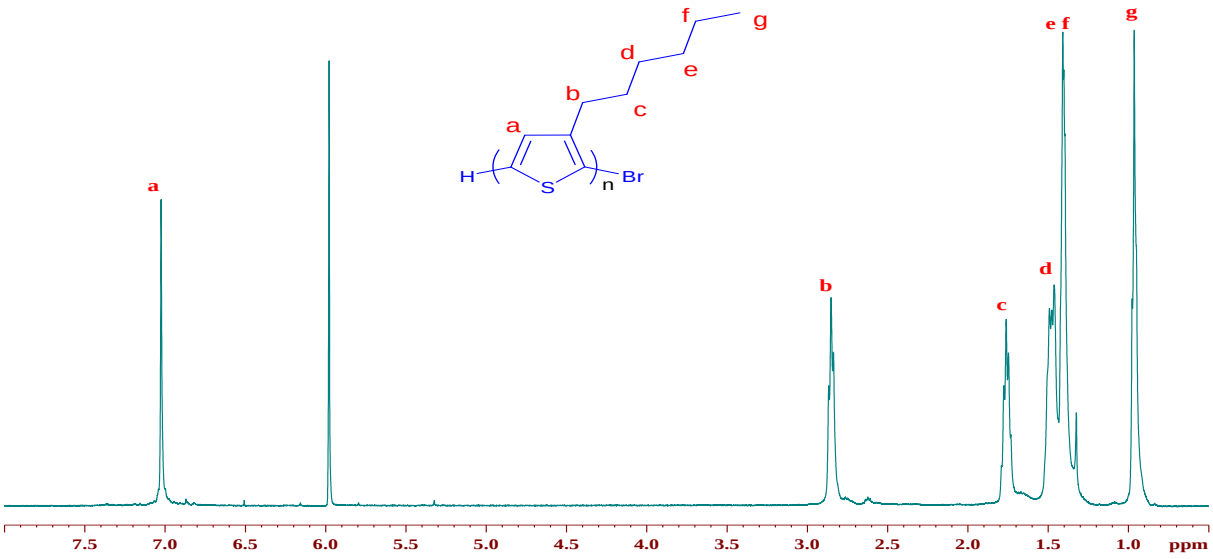

Figure 108: The proton NMR spectra of P9.

5.5.2 Method 2: Time of Polymerization is 24h.

Poly(3-hexythiophene) (Br-P3HT) **(P9)** was prepared according to the procedure by Antoun, et al [131]. The polymerisation process was carried out in THF using metal-catalyzed polymerization of 2,5-dibromo-3-hexylthiophene **(20)** , i-PrMgCl.LiCl as Grignard reagent and Ni(dppp)Cl_2 as catalyst**.** The polymerisation was done at room temperature for 24h. The purification was done by precipitation of the polymer in methanol, then it was separated using a centrifuge. The precipitated polymer was extracted using Soxhlet extraction with methanol, hexane, toluene and chloroform. The polymer was obtained from the toluene and chloroform fractions to afford **P9** as dark red powder (6%, 7%) respectively.

5.5.2.1 Characterization of P9 (method 2).

5.5.2.1.1 Gel Permeation Chromatography studies of P9

All the GPC data and physical properties of polymer **P9** are summarised in Table 20

Table 20 : Yield and GPC data of polymer P9.

Polymer	Soxhlet Fraction	Yield		GPC		
		Mass/mg	%	MW	Mn	PD
P9	Toluene	100	6%	28.200	20.500	1.37
	Chloroform	130	7%	46.000	35.000	1.31

5.5.2.1.2 MALDI-MS of P9

MALDI-MS was used to characterize the polymer end groups and the data of polymer **P9** are summarised in table 21.

Table 21 : MALDI-MS data analysis of P9

Polymer	% H/Br End group	Mw	% H/H End group	Mw
P9	25%	4490	75%	4570

The data analysis from MALDI-MS in Table 21 illustrates that the polymer was formed with 25 % (H/Br) and 75 % (H/H) end groups as shown in Figure 109**.**

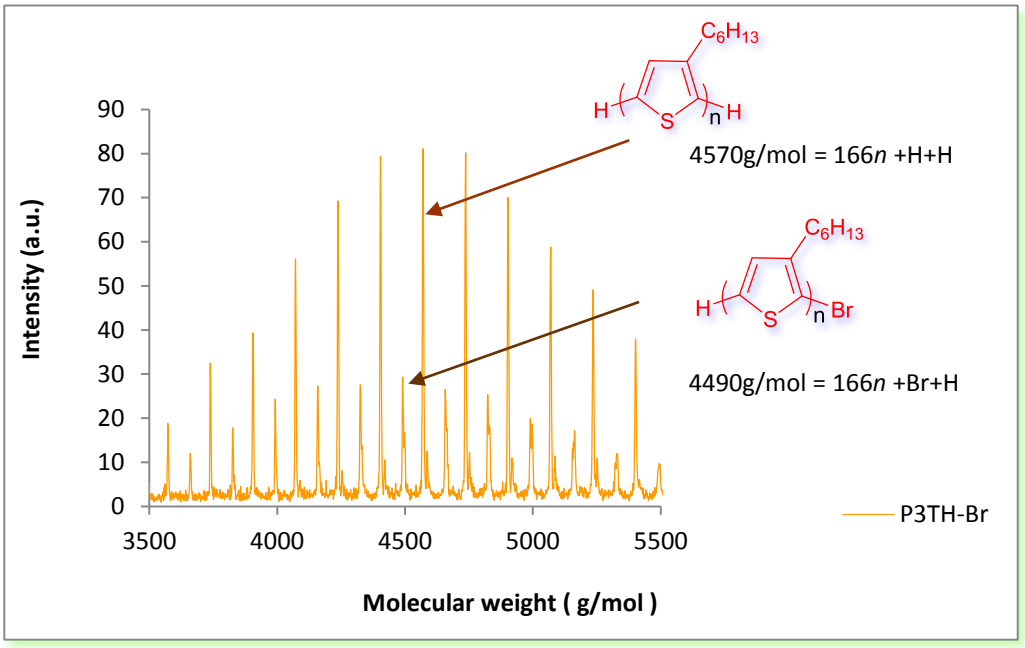

Figure 109: Mass spectroscopy (MALDI-MS) for P9 .

It is clear from Figure 109 that there are two types of end groups signals , which after calculation revealed that they are of type H/H and H/Br with the H/H end group signal

intensity being the strongest and the number of repeat units *n* =27. The intensity of end group signal H/H with 75 % and H/Br with 25% end groups indicates that the polymerisation time does not affect the yield of the end groups.

5.5.3 Method 3: via the *McCullough* method.

Poly(3-hexythiophene) (Br-P3HT) **(9)** was prepared according to the procedure by McCullough [113]. The polymerisation process was carried out in THF using 2-bromo-3-hexylthiophene (21), diisopropylamine, *n*-BuLi and [Ni(dppp)Cl_2] as catalyst. The polymerisation was done at room temperature for 30 min. The purification was done by precipitate the polymer in methanol , then the precipitated polymer was extracted using Soxhlet extraction with with methanol, hexane, dichloromethane, and THF. The polymer was obtained in THF to afford **P9** as red powder (430 mg, 18 % yield).

5.5.3.1 Characterization of P9 McCullough method.

5.5.3.1.1 MALDI-MS of P9

MALDI-MS was used to characterize the polymer end group and the data of polymer **P9** are summarised in Table 22.

Table 22 : MALDI-MS data analysis of P9

Polymer	% H/Br End group	Mw	% H/H End group	Mw
P9	52%	4902	48%	4980

The data analysis from MALDI-MS in Table 22 illustrates that the polymer was formed with 52% (H/Br) and 48 % (H/H) end groups as shown in Figure 110.

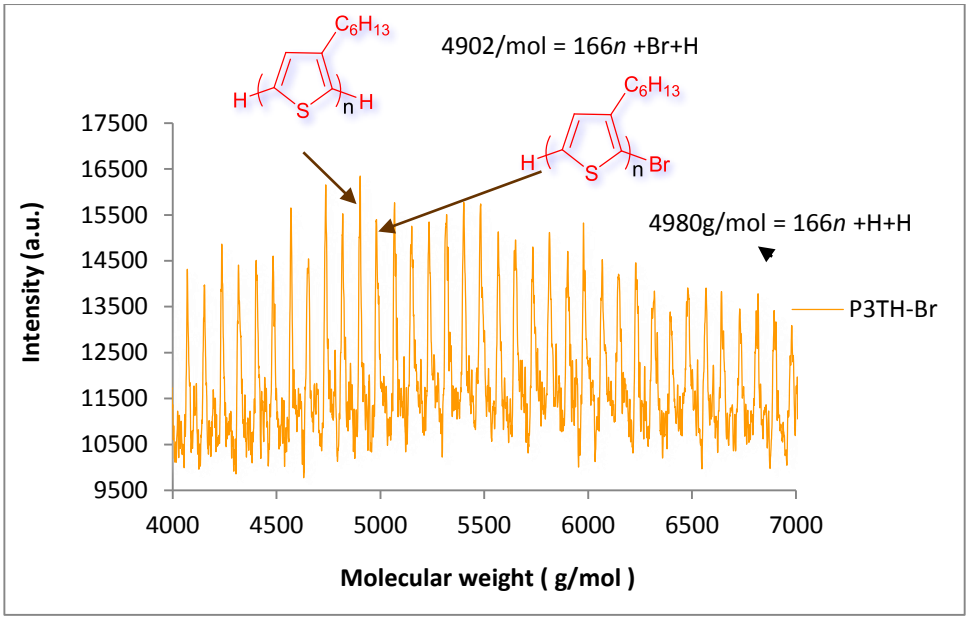

Figure 110: Mass spectroscopy (MALDI-MS) for P9 .

It can be seen from Figure 110 that there are two types of end groups signals , which revealed that they are of type H/H and H/Br with number of repeat units *n* = 29.Morover, the curve shows that the H/H end group signal intensity being the strongest. The peak corresponds to (166 *n* +H+Br) represents the polymer chains terminated by a bromine a tom with 52 % H/Br . The peak corresponds to (166 *n* +H+H) refers to polymer chains that are terminated by hydrogen atoms in both side with 48 % H/H .

5.5.4 Method 4: via the McCullough method.

This method follows the same procedure in the method 3 with an excess of diisopropylamine (DIPA) to insure the formation lithium diisopropylamine (LDA) where it is used to lithiate 2-bromo-3-hexylthiophene **(21)** and follow the same procedure in method 3 . The purification was done by precipitating the polymer in methanol , then the precipitated polymer was extracted using Soxhlet extraction with with methanol, hexane,

dichloromethane. The polymer **P9** was obtained in DCM as red powder (100 mg, 4 % yield),

5.5.4.1 Characterization of P9 McCullough method 4.

5.5.4.1.1 MALDI-MS of P9

MALDI-MS was used to characterize the polymer end group and the data of polymer P9 are summarised in table 23.

Table 23 : MALDI-MS data analysis of P9

Polymer	% H/Br End group	Mw	% H/H End group	Mw
P9	35%	3737	65%	3651

The data analysis from MALDI-MS in Table 23 shows that the polymer was formed with 35 % (H/Br) and 65 % (H/H) end groups as shown in Figure 111.

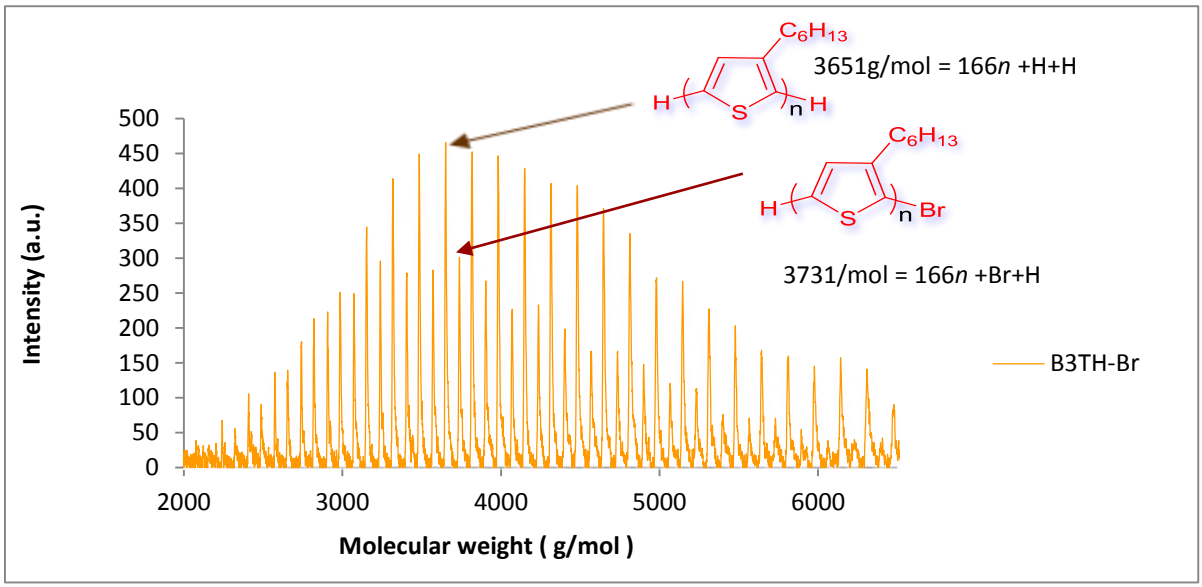

Figure 111: Mass spectroscopy (MALDI-MS) for P9 .

Figure 111 shows the MALDI-MS of P9 , indicating the structure of the repeat unit of Poly(3-Hexythiophene) system. It can be seen that MALDI-MS displays two major types of signal peaks per repeat units where the difference between each type of end group was calculated to be 166 g/mol , which confirms the repeat unit mass of poly(3-hexylthiophene) = 166 g/mol). The peak corresponds to (166 *n*+H+H) corresponds to polymer chains that are terminated by hydrogen atoms at both the 2- and the 5-positions .The peak corresponding to (166 *n*+Br+H) refers to polymer chains terminated by a bromine atom on one end and a hydrogen atom on the other end . Figure 52 shows that the formed polymer is a mixture polymer with 45 % (H/Br) and 65 % (H/H) end groups. It can be concluded that this polymer sample has only two major types of end group configurations (H/Br) and (H/H) with a number repeat unit *n* = 22 . a comparison of this peak with that of Figure 51 indicates that (H/Br) peak intensity in Figure 52 shows some improvement due to using an access of diisopropylamine (DIPA).However; this yield of (H/Br) is still not enough to react as active monomer in Suzuki polymerisation.

5.5.5 Method 5

Poly(3-hexythiophene) (Br-P3HT) **(9)** was prepared according to the procedure by by Lohwasser [114].

This polymerisation was done in THF using 2,5-dibromo-3-hexylthiophene **(20)** .Then t-BuMgCl was added with a syringe for 20 h to form the active Grignard monomer . The polymerisation was catalysed using Ni(dppp)Cl_2 and was left for165 mins. The polymerization was quenched with 5N HCl. The polymer was precipitated in methanol and purified by Soxhlet extraction. The polymer was obtained in chloroform as red powder (15 mg, 1.3 % yield).

5.5.5.1 Characterization of P9 method 5.

5.5.5.1.1 MALDI-MS of P9

MALDI-MS was used to characterize the polymer end group and the data of polymer **P9** are summarised in Table 24.

Table 24 : MALDI-MS data analysis of P9

Polymer	% H/Br End group	% H/H End group	Mw
P9	2%	98%	1574

The data analysis from MALDI-MS in Table 24 indicates that the polymer was formed with high yield of (H/H) end group as shown in Figure 112.

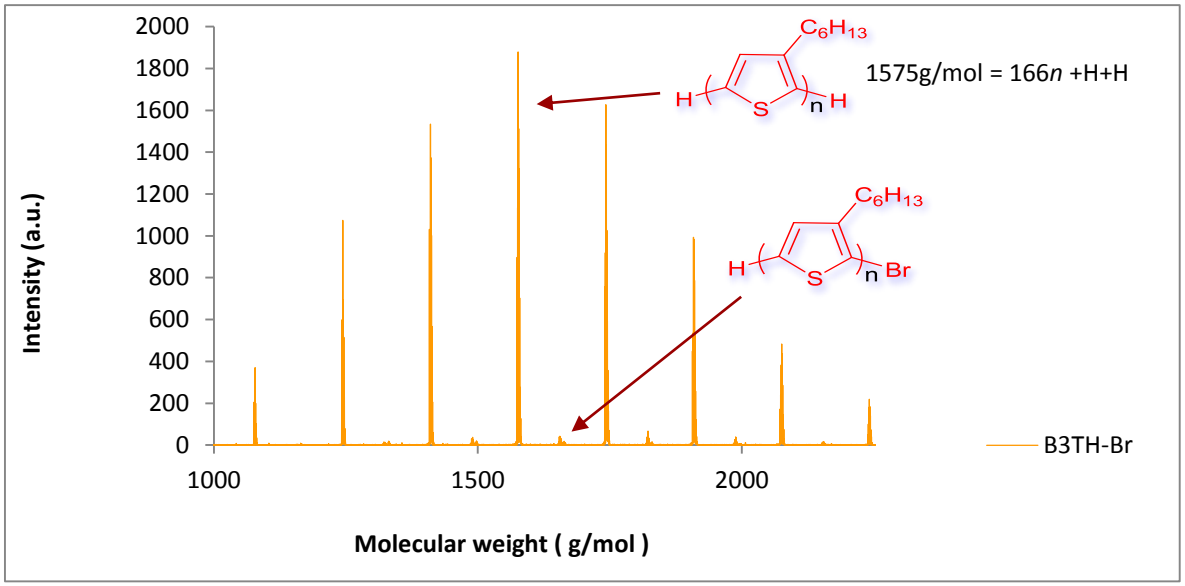

Figure 112: Mass spectroscopy (MALDI-MS) for P9 .

Figure 112 shows the MALDI-MS of **P9** . It can be seen that MALDI-MS displays two major types of signal peaks per repeat units where the difference between each type of end group was calculated to be 166 g/mol , which confirms the repeat unit mass of poly(3-hexylthiophene) = 166 g/mol). The peak corresponds to (166 *n*+H+H) corresponds to

polymer chains that are terminated by hydrogen atoms at both the 2- and the 5-positions a number repeat unit $n = 9$ .The peak corresponding to (166 n+Br+H) is very small which refers to polymer chains terminated by a bromine atom on one end and a hydrogen atom on the other end .

It can be concluded that the preparation P3TH with high yield 90% and more of H/Br end groups was not obtained using the previous methods which rather leads to form a mixture of H/H and H/Br end groups. Among those methods, the McCullough method is the best approach to obtain a high yield 50 % of homogeneous H/Br end groups. Although McCullough and Yokozawa reported that the P3TH with homogeneous H/Br end groups can be easily obtained, Lohwasser and several groups observed formation of a mixture of H/H and H/Br end groups [114]. Lohwasser and co-workers investigated the parameters that affect the nature of the resulting polymers [114]. They found that the formation of the active Grignard monomer from dihalides is a crucial step and controlling this step is an important to attain homogeneous H/Br end groups [114]. Moreover , the polymerisation time has to be taken in account during polymerisation process [114]. The syntheses of **P9** with high yield of homogeneous H/Br end group was a difficult step in this project , therefore; making diblock copolymers of **P9** with **P1** , **P3** and **P4** was then not completed.

5.6 Photovoltaic device characterization

The polymers photovoltaic properties of **P1**, **P3** , **P4** and **P6** were studied in the department of Physics and Astronomy at The University of Sheffield by the Lidzey group. Photovoltaic devices were made using blends of polymers **P1**, **P3** , **P4** and **P6** with Phenyl-C70-butyric acid methyl ester (PC70BM) as electron acceptor in heterojunction photovoltaic devices . PC70BM was used in weight/weight ratios of 1 : 2, 1 : 3 and 1 : 4 in order to optimise devices performance . The structure of the devices of **P1**, **P3** , **P4** and

P6 were made on a series of ITO/PEDOT:PSS/polymer:PC70BM/Ca/Al. Polymer solar cell devices were fabricated onto pre-patterned indium tin oxide (ITO) glass . The ITO electrodes were spin- coated by 20 – 30 nm layer of PEDOT:PSS , which was annealed in order to remove any trace of moisture. Then, the polymer / PCBM layer was spin-coated on the top of the coated substrate using solvents that would not dissolve the PEDOT:PSS layer. 5 nm of Ca was then evaporated on top of the active layer, followed by 100 nm of Al to complete the PV cells. The photovoltaic properties of **P1**, **P3**, **P4** and **P6** are summarised in Table 25, and the rest of the polymers studied are still under investigation.

Table 25 : Photovoltaic properties of polymers P1, P3, P4 and P6 .

Polymer	Polymer / PCBM (Weight ratio)	Solvent	Active Layer thickness/nm	Annealing temp/ ^{0}C	V_{oc} /V	I_{sc} (mA cm^{-2})	FF (%)	PCE (%)
P1	1/4	DCB[a]	93	80	0.76	6.92	42.8	2.25
	1/4	$CHCl_3$	72	80	0.82	8.36	48.8	3.34
	1/2	CB[b]	100	120	0.74	7.28	39.5	2.13
	1/3	CB	100	120	0.76	8.14	38.7	2.39
	1/4	CB	72	80	0.82	8.39	48.6	3.35
	1/4	CB	72	***120***	***0.96***	***9.38***	***46.9***	***4.22***
P3	1/4	$CHCl_3$	70	NA	1.03	9.66	54.74	***5.41***
P4	1/4	DCB	81	80	0.80	8.29	40.2	2.67
	1/4	CB	87	80	0.82	7.14	47.4	2.77
	1/2	$CHCl_3$	60	110	0.88	7.60	49.5	3.31
	1/3	$CHCl_3$	59	110	0.90	8.68	51.7	4.04
	1/4	$CHCl_3$	61	***110***	***0.90***	***8.44***	***54.2***	***4.12***
P6	1/3			125	0.71	10.49	55.88	***4.17***

[a] DCB = dichlorobenzene . [b] CB = chlorobenzene .

It can be seen from Table 25 that a series of weight/weight ratios 1 : 2, 1 : 3 and 1 : 4 of polymers : PC70BM were used to optimise the devices performance. In terms of photovoltaic response , the blend ratio between the polymer and the PCBM in solar cell devices is of great importance where it is found that the optimum ratio depends on the type of polymer mixed. In the case of **P1**, **P3** and **P4** , It can be noticed that the most efficient devices and the highest efficiency were obtained when a blending ratio was 1 : 4 or (20:80 wt%) between the two constituents (polymers : $PC_{70}BM$) while **P6** the highest efficiency was that in which weight/weight ratios of polymer : $PC_{70}BM$ of 1 : 3 was used [95]. Table 25 shows the bulk heterojunctions device parameters , open circuit voltage (V_{oc}) , short circuit photocurrent (I_{SC}) and fill factor (FF) of **P1** and **P3** of (polymers : $PC_{70}BM$) in terms of their dependence on the blending ratio [68]. It can be seen that the open circuit voltage (V_{oc}) , short circuit photocurrent (I_{SC}) , fill factor (FF) and also the power conversion efficiency were still increasing up to reach the highest efficiency upon using 80 % of C_{70} ($PC_{70}BM$). This increasing in short circuit photocurrent (I_{SC}) can be attributed to the improved charge transport[68] . On the other hand, **P6** reveals that 4.17 % power conversion efficiency was obtained for device in which w /w ratio of **P6** : $PC_{70}BM$ of 1 : 3 was used [87] .

Choosing of spin casting solvent is a decisive factor in generating homogenous morphology and improving efficiency. In bulk heterojunctions morphology , the solvent should have the ability to dissolve all components to form homogenous blend films of polymer and PCBM. Such homogenous blend film will prevent formation of large scale of phase separation , which cause macroscale phase segregation in the system. The data shown in Table 25 investigates the impact of solvents used to spin - cast the active layers.

For **P3** and **P4** , using chloroform gave the highest efficiency as the best solvent to use while **P1** gave the best result upon the use of chlorobenzene .

Annealing of devices is a critical factor to controlling the morphology of the polymer/ PCBM blends and increasing the power conversion efficiency due to improve nanocrystalline nature as a result of phase-separation and self assembly of polymer chains. Moreover, it was found that such annealing would force the film morphology to self organize through the transition from amorphous to crystalline state which increases charge mobility and facilitates charge extraction [67,95]. In addition , thermal annealing of bulk heterojunction blends was found to remove residual casting solvent, which also improve the device efficiency [95]. Therefore , It can be seen from **Table 21** that **P1** , **P4** and **P6** were annealed at different temperatures and their performances displayed the best power conversion efficiency when devices were annealed at high temperatures , 120 , 110 and 125 ^{0} C for **P1** , **P4** and **P6** respectively [95]. **P1** displayed the highest efficiency 4.22 % when the device was annealed at 80 ^{0} C , while polymers **P4** and P6 provided the best efficiencies when their devices were annealed at 110 and 125 ^{0}C respectively.

The difference between the HOMO energy level of the polymer electron donor and the LUMO energy level of the acceptor is proportional to the magntude of the open circuit voltage of the solar cell. Among these polymers, **P3** displayed the highest open circuit voltage with a value of V*oc* = 1.03 V Table 25 , which be explained by its deeper HOMO level when compared to those of **P1** , **P4** and **P6**. A comparison of the open circuit voltages (V*oc*) of **P4** to that of **P1** indicates that **P1** has higher (V*oc*) value than **P4** (V*oc* = 0.96 for **P1** *vs*. V*oc* = 0.90 for **P4**) as result of the deeper HOMO level of **P1** (-5.40 eV for **P1** *vs*. - 5.20 eV for **P4**) . The lower value (Voc) for **P6** compared to that of **P1** (V*oc* = 0.71 for **P6** *vs*. V*oc* = 0.96 for **P1**) could be due to the higher HOMO level of **P6** (-

5.35 eV for **P6** *vs*. - 5.40 eV for **P1**) .The charge transport and extraction has great importance in the operation of solar cell . Table 25 shows the parameters that determine these steps, The short-circuit current densities (I_{SC}) and fill-factor (FF). 2,6-Linked anthracene based polymers **(P6)** shows the highest values of short circuit current (Isc) and open circuit voltage (Isc = 10. 49 mA cm^{-2} , FF = 55.88 %) compared to that of **P1** , **P3** and **P4**. However, it shows the lowest value of power conversion efficiency (PCE) of 4.17 % when compared to those of **P1** , **P3** and **P4** . The short-circuit current densities (I_{SC}) and fill-factor (FF) values for devices using polymer **P3** (Isc = 9. 66 mA cm^{-2}, FF = 54.74 %) were higher than those of **P1** and **P4** (Isc = 9. 38 mA cm^{-2} , FF = 46.9% for **P1** and (Isc = 8. 44 mA cm^{-2}, FF = 54.2 % for **P4**) . These findings illustrate that the charge transport and extraction from devices using polymer **P3** are more efficient than in the case of devices using **P1** and **P4**. These low values of short-circuit current densities (I_{SC}) and fill-factor (FF) for **P1** and **P4** perhaps as a result the creation of a micro/nanostructure that effects efficient exciton dissociation and extraction of photo-generated electrons and holes [95] .Among the polymers shown in Table 25 , it can be seen that fluorene based polymer **P3** shows the highest power conversion efficiency PCE up to 5.41 % . Polymer **P1** is based on carbazole units as donor units and **(DTBT- 8)** as acceptor units and shows a power conversion efficiency (PCE) ranging from 2.13 - 4.22 %. The highest value of the power conversion efficiency (PCE) 4.22 % was obtained in chlorobenzene for **P1**. Polymer **P4** which is also based on carbazole units as donor units and **(DT2BT- 8)** as acceptor units display a power conversion efficiency PCE ranging from 2.67 - 4.12 % with the highest power conversion efficiency (PCE) 4.12 % obtained using chloroform as casting solvent which provided a high value of open circuit voltage (V*oc* = 0.90 V). On the other hand , **P6** which consists of 2,6-linked anthracene based polymers shows the lowest value of a power conversion efficiency (PCE) 4.17 % even

though it has a high value of short-circuit current densities (I_{SC}) . This low value of the PCE in **P6** compared to those of **P1** , **P3** and **P4** could be due the presence of more solubilising groups on the polymer backbone where a higher fraction of the polymer is composed of non-conjugated substituents. These solubilising groups are found to reduce the charge carrier mobility in the polymer and limit the efficiency of charge-carrier extraction [95]. Moreover, such solubilising groups influence the efficient intermolecular interaction between the polymer chains which in turn reduce the band gap and the power conversion efficiency PCE .

Chapter 6: Conclusion and Future Work

A series of low band gap polymers for use in bulk heterojunction organic solar cell applications were prepared successfully *via* Suzuki cross coupling reaction. The carbazole, fluorene–thiophene based copolymers (**P1**, **P2** , **P3**) were prepared and their electronic properties investigated and compared with each other and with their analogous PCDTBT polymer. The electronic properties of these polymers show that **(P3)** containing fluorene unit as electron donor and unsubstituted 4,7-dithien-2-yl-2,1,3-benzothiadiazole **(DTBT)** as acceptor unit has the narrowest optical and electrochemical band gaps due to the high degree of electronic delocalisation along polymer chains originating from the high intramolecular interaction between the polymer chains. Moreover ; the absence of substituted octyloxy groups on the **(DTBT)** unit increase the electron accepting ability of the acceptor unit. The electronic properties of these polymers show that **(P3)** when compared to PCDTBT has lower optical and electrochemical band gaps. The photophysical properties of **P1** and **P2** containing carbazole unit and 5,6-dioctyl-4,7-di(thiophen-2-yl)benzo[c][1,2,5]thiadiazole **(DTBT- 8)** as acceptor unit were almost similar. However, their band gaps are higher than those of **P3** and PCDTBT due to the effect of octyloxy groups on the electron acceptor ability of benzothiadiazole unit. The optical and electrochemical band gaps of **P2** are slightly lower than those of **P1** due to the electrostatic interaction between the hydrogens at the 4-position on thiophene rings and the fluorine substituents on the neighbouring carbazole repeat units.The molecular weights of copolymer **P1** and **P2** were higher than those of **P3** due to the presence of two octyloxy groups on the benzothiadiazole unit **(BT)** , which make these copolymers more soluble.

Extension of the conjugation length in the polymer chains would improve the absorption and electronic properties of the polymers. Therefore, a series of copolymers **P4** and **P5** were prepared successfully *via* Suzuki cross coupling reaction. These two polymers contain 4,7-di(2,2'-bithiophen-5-yl)-5,6-bis(octyloxy)benzo[c][1,2,5]thiadiazole **(DT2BT-8)** unit as acceptor unit while the donor units are 2,7-Linked carbazole units for **P4** and 2,7-linked -3,6-difluoro carbazole units for **P5**. it is remarkable that extending the conjugation length of these polymers with two extra unsubstituted thiophene rings was found to alter their electronic properties. They **(P4, P5)** show lower optical band gap energies in the range (1.94 – 1.98 eV) when compared to those of **P1** and **P2**. This results confirm that extending of the electronic conjugation along polymer backbones upon introduction of sterically less demanding repeat units such as thiophene reduce the band gaps of the resulting polymers.

A series of new donor-acceptor 2,6- and 2,7 - anthracene based copolymers **P6** and **P7** were prepared successfully. The optical band gaps of these polymers are in the range (1.87 – 1.98 eV) while their electrochemical band gaps range from 2.24 eV to 2.35 eV . The 2,6-anthracene copolymer **P6** shows the lowest band gap values whether optical or electrochemical. This results can be attributed to the chemical structure of these polymers where the 2,6 - anthracene based copolymer **P6** is more planar and more symmetrical. On the other hand, the steric hindrance in the chemical structure of 2.7- anthracene based polymer **P7** due to the alkoxy groups make the polymer structure less symmetric and induces a slight amount of chain twisting which leads to reducing the electron delocalisatoin along the copolymer backbones and increases its band gap.

The proportion of a donor / acceptor block copolymer was also investigated in this thesis in order to make self-assemble active layers in PV cells that eliminate the problem of

phase seperation when using PCBM as an acceptor. A block copolymer **P8** is a di- block copolymer consists of two blocks **P1** and **P3** which was prepared successfully *via* Suzuki cross coupling reaction and its photophysical properties and morphology were studied. The polymer shows an optical band gap 1.87 eV while the electrochemical band gap was 2.13 eV . The AFM studies illustrates that the polymer shows less aggregates than toluene fraction which means that the chloroform fraction could be better for device studies.

Polyhexylthiophene **P9** with a hydrogen and bromine end groups was prepared *via* McCullough method and the suggested method by Lohwasser [114].The end groups of this polymer was investigated using matrix-assisted laser desorption / ionization mass spectrometry (MALDI-MS. In all these methods, the polymer **P9** was prepared in a mixture of H/H and H/Br end groups. Formation of the active Grignard monomer and the time of polymerization could affect the end group to attain homogeneous H/Br end groups. Obtaining **P9** with high yield of homogeneous H/Br end group was a arduous step in this project , therefore; making diblock copolymers of **P9** with **P1** , **P3** and **P4** was then abandoned.

The photovoltaic studies results obtained of these series of copolymers indicate that **P3** has the highest power conversion efficiency (5.41 %), then **P1** , **P6** and **P4** with power conversion efficiencies of 4.22, 4.17 and 4.12 % respectively.

Future work should include physical studies to investigate the performance of **P2** , **P5** , **P7** and P8 with blends of fullerene derivatives in solar cell devices. The fluorene copolymer **P3** shows a great promising result for use in organic solar cell devices. Therefore, investigation of fluorene unit with variety of acceptors units could lead to important new classes of donor-acceptor polymers with a great potential in solar cells devices.Also carbazole and anthracene copolymers show promising results in organic solar cell devices

in this project. Therefore, it is worth to investigate variety of carbazole and anthracene derivatives with substituents of short alkyl chains to enhance the solubility and achieve an efficient intermolecular interaction with a high degree of order produced by π-stacking between polymer chains. This approach might alter the photophysical and electrochemical properties of the polymer leading to reduce the band gap and increase the efficiency . In addition , the future work should pay attention for preparing block copolymers as a great tool to improve the nanomorphlogy structure. Future studies are required to improve and explore effective and easy methods to prepare polyhexylthiophene **P9** to attain a high yield of homogeneous H/Br end group. Moreover, using of different polymarization conditions to increase the homogeneous H/Br end group yield should be further investigated.

References

(1) (a) Smol, J. *Nature* **2012**, *483*(b)

(2) Benett., P.; *Earth: The Incredible Recycling Machine*; Wayland (Publishers) Ltd: East Sussex, 1993.

(3) Green, M. A.; Emery, K.; Bucher, K.; King, D. L.; Igari, S. *Progress in Photovoltaics* **1997**, *5*, 265.

(4) Chapin, D. M.; Fuller, C. S.; Pearson, G. L. *Journal of Applied Physics* **1954**, *25*, 676.

(5) Zhao, J. H.; Wang, A. H.; Green, M. A.; Ferrazza, F. *Applied Physics Letters* **1998**, *73*, 1991.

(6) Brabec, C. J.; Padinger, F.; Sariciftci, N. S.; Hummelen, J. C. *Journal of Applied Physics* **1999**, *85*, 6866.

(7) Bundgaard, E.; Krebs, F. C. **2007**, - *91*, 954.

(8) Pron, A.; Rannou, P. *progress in polymer science* **2002**, *27*, 135.

(9) (a) Chiang, C. K.; Fincher, C. R.; Park, Y. W.; Heeger, A. J.; Shirakawa, H.; Louis, E. J.; Gau, S. C.; Macdiarmid, A. G. *Physical Review Letters* **1977**, *39*, 1098(b) Friend, R. H. *Pure and Applied Chemistry* **2001**, *73*, 425.

(10) Anne, D. C.; Roger, C. H.; Eric, C.; Laurence, V.; Henri, C. *Polymer International* **2010**, *59* 1452.

(11) Shirakawa, H.; Louis, E. J.; Macdiarmid, A. G.; Chiang, C. K.; Heeger, A. J. *Journal of the Chemical Society-Chemical Communications* **1977**, 578.

(12) Saxena, V.; Malhotra, B. D. *Current Applied Physics* **2003**, *3*, 293.

(13) F, D., Kleist.; N, R., Byrd. *Journal of Polymer Science Part A-1: Polymer Chemistry*

1969, *7*, 3419.

(14) Heeger, A. J. *Chemical Society Reviews* **2010**, *39*, 2354.

(15) Jain, S. C.; Willander, M.; Kumar, V. *Semiconductors and Semimetals* **2007**, *81*, 188.

(16) Bakhshi, A. K.; Bhalla, G. *Journal of Scientific & Industrial Research* **2004**, *63*, 715.

(17) (a) Spanggaard, H.; Krebs, F. C. *Solar Energy Materials and Solar Cells* **2004**, *83*, 125(b) Bayliss, N. S. *Journal of Chemical Physics* **1948**, *16*, 287(c) Bayliss, N. S. *Quarterly Reviews* **1952**, *6*, 319(d) Kuhn, H. *Helvetica Chimica Acta* **1948**, *31*, 1441(e) Hoffmann, R. A. *Chem. Int. Ed* **1987**, *26*, 846.

(18) (a) Henderson, R. L.; Ashcroft, N. W. *Physical Review A* **1976**, *13*, 859(b) van Mullekom, H. A. M.; Vekemans, J. A. J. M.; Havinga, E. E.; Meijer, E. W. *Materials Science and Engineering* **2001**, *32*, 1.

(19) Marks, R. N.; Halls, J. J. M.; Bradley, D. D. C.; Friend, R. H.; Holmes, A. B. *Journal of Physics-Condensed Matter* **1994**, *6*, 1379.

(20) Bansi, D. M. *Handbook of Polymers in Electronics*; Rapra Technology Limited: Exeter, 2002.

(21) (a) Chiang, C. K.; Druy, M. A.; Gau, S. C.; Heeger, A. J.; Louis, E. J.; Macdiarmid, A. G.; Park, Y. W.; Shirakawa, H. *Journal of the American Chemical Society* **1978**, *100*, 1013(b) Jain, S. C.; Willander, M.; Kumar, V. *Semiconductors and Semimetals* **2007**, *81*, 1.

(22) Coropceanu, V.; Cornil, J.; da Silva Filho, D. A.; Olivier, Y.; Silbey, R.; Brédas, J.-L. *Chemical Reviews* **2007**, *107*, 926.

(23) Seeger, K.; Gill, W. D.; Clarke, T. C.; Street, G. B. *Solid State Communications* **1978**, *28*, 873.

(24) Kaneto, K. *Thin Solid Films* **2001**, *393*, 249

(25) Jeyadey, S.; Conwell, E. M. *Physical Review B* **1987**, *36*, 3284.

(26) Kumar, D.; Sharma, R. C. *European Polymer Journal* **1998**, *34*, 1053.

(27) Roncali, J. *Macromol. Rapid Commun* **2007**, *28*, 1761.

(28) Allen, J., Bard.; Larry, R. F. *Electrochemical Methods : Fundamentals and Applications*; John Wiley & Sons: NewYork, 1944.

(29) Wu, P.-T.; Kim, F. S.; Champion, R. D.; Jenekhe, S. A. *Macromolecules* **2008**, *41*, 7021.

(30) Neugebauer, H.; Kvarnstrom, C.; Brabec, C.; Sariciftci, N. S.; Kiebooms, R.; Wudl, F.; Luzzati, S. *Journal of Chemical Physics* **1999**, *110*, 12108.

(31) Chochos, C. L.; Choulis, S. A. *Progress in Polymer Science* **2011**, *36*, 1326.

(32) Roncali, J. *Chemical Reviews* **1997**, *97*, 173.

(33) Kroon, R.; Lenes, M.; Hummelen, J. C.; Blom, P. W. M.; De Boer, B. *Polymer Reviews* **2008**, *48*, 531.

(34) Winder, C.; Sariciftci, N. S. *Journal of Materials Chemistry* **2004**, *14*, 1077.

(35) Cheng, Y.-J.; Yang, S.-H.; Hsu, C.-S. *Chemical Reviews* **2009**, *109*, 5868.

(36) Bundgaard, E.; Krebs, F. C. *Solar Energy Materials and Solar Cells* **2007**, *91*, 954.

(37) Roncali, J.; Garreau, R.; Yassar, A.; Marque, P.; Garnier, F.; Lemaire, M. *Journal of Physical Chemistry* **1987**, *91*, 6706.

(38) (a) Lambert, T. L.; Ferraris, J. P. *Journal of the Chemical Society-Chemical Communications* **1991**, 752(b) Ferraris, J. P.; Lambert, T. L. *Journal of the Chemical Society-Chemical Communications* **1991**, 1268.

(39) Kertesz, M.; Choi, C. H.; Yang, S. *Chemical Reviews* **2005**, *105*, 3448.

(40) Jen, K. Y.; Maxfield, M.; Shacklette, L. W.; Elsenbaumer, R. L. *Journal of the Chemical Society-Chemical Communications* **1987**, 309.

(41) Wudl, F.; Kobayashi, M.; Heeger, A. J. *Journal of Organic Chemistry* **1984**, *49*, 3382.

(42) (a) Bredas, J. L.; Heeger, A. J.; Wudl, F. *Journal of Chemical Physics* **1986**, *85*, 4673(b) Hoogmartens, I.; Adriaensens, P.; Vanderzande, D.; Gelan, J.; Quattrocchi, C.; Lazzaroni, R.; Bredas, J. L. *Macromolecules* **1992**, *25*, 7347.

(43) Roncali, J.; Thobiegautier, C. *Advanced Materials* **1994**, *6*, 846.

(44) Patra, A.; Wijsboom, Y. H.; Leitus, G.; Bendikov, M. *Chemistry of Materials* **2011**, *23*, 896.

(45) Chanrasekhar, P. *Conducting Polymers, Fundamentals and Applications*; Kluwer Academic Publishers: Norell, MA, , 1999.

(46) Sakamoto, J.; Rehahn, M.; Schlüter, D., 2010.

(47) Miyaura, N.; Suzuki, A. *Journal of the Chemical Society, Chemical Communications* **1979**, 866.

(48) (a) Casado, A. L.; Espinet, P.; Gallego, A. M. *Journal of the American Chemical Society* **2000**, *122*, 11771(b) Lee, A. S. Y.; Dai, W. C. *Tetrahedron* **1997**, *53*, 859.

(49) Green, M. A.; Emery, K.; King, D. L.; Igari, S.; Warta, W. *Progress in Photovoltaics* **2003**, *11*, 347.

(50) Jain, S. C.; Willander, M.; Kumar, V. In *Semiconductors and Semimetals*; S.C. Jain, M. W., Kumar, V., Eds.; Elsevier, 2007; Vol. Volume 81.

(51) Carsten , D.; Vladimir, D. *REPORTS ONPROGRESS INPHYSICS* **2010**, *73*.

(52) P. B. Miranda; D. Moses; Heeger, A. J. *Physical Review A* **2001**, *64*.

(53) Ameri, T.; Dennler, G.; Lungenschmied, C.; Brabec, C. J. *Energy & Environmental Science* **2009**, *2*, 347.

(54) (a) Choong, V.; Park, Y.; Gao, Y.; Wehrmeister, T.; Mullen, K.; Hsieh, B. R.; Tang, C. W. *Applied Physics Letters* **1996**, *69*, 1492(b) Ghosh, A. K.; Feng, T.

Journal of Applied Physics **1978**, *49*, 5982(c) Halls, J. J. M.; Pichler, K.; Friend, R. H.; Moratti, S. C.; Holmes, A. B. *Applied Physics Letters* **1996**, *68*, 3120.

(55) Deibel, C.; Strobel, T.; Dyakonov, V. *Advanced Materials* **2010**, *22*, 4097.

(56) Gregg, B. A.; Hanna, M. C. *Journal of Applied Physics* **2003**, *93*, 3605.

(57) Clarke, T. M.; Durrant, J. R. *Chemical Reviews* **2010**, *110*, 6736.

(58) Nunzi, J. M. *Comptes Rendus Physique* **2002**, *3*, 523.

(59) Bradley, D. D. C.; Grell, M.; Long, X.; Mellor, H.; Grice, A.; Inbasekaran, M.; Woo, E. P. *Optical Probes of Conjugated Polymers* **1997**, *3145*, 254.

(60) Jousselme, B.; Blanchard, P.; Levillain, E.; Delaunay, J.; Allain, M.; Richomme, P.; Rondeau, D.; Gallego-Planas, N.; Roncali, J. *Journal of the American Chemical Society* **2003**, *125*, 1363.

(61) Hoppe, H.; Sariciftci, N. S. *Journal of Materials Research* **2004**, *19*, 1924.

(62) Jean; Nunzi, M. *PHOTONIQUE MOLECULAIRE* **2002**, *3*.

(63) Zhou, H.; Yang, L.; You, W. *Macromolecules* **2012**, *45*, 607.

(64) Benanti, T.; Venkataraman, D. *Photosynthesis Research* **2006**, *87*, 73.

(65) (a) Shaheen, S. E.; Brabec, C. J.; Sariciftci, N. S.; Padinger, F.; Fromherz, T.; Hummelen, J. C. *Applied Physics Letters* **2001**, *78*, 841(b) Brabec, C. J. *Solar Energy Materials and Solar Cells* **2004**, *83*, 273.

(66) Brabec, C. J.; Gowrisanker, S.; Halls, J. J. M.; Laird, D.; Jia, S.; Williams, S. P. **2010**, - *22*.

(67) Yang, X.; Loos, J. *Macromolecules* **2007**, *40*, 1353.

(68) Hoppe, H.; Sariciftci, N. S. *Journal of Materials Chemistry* **2006**, *16*, 45.

(69) Brabec, C. J. *Solar Energy Materials and Solar Cells* **2004**, *83*, 273.

(70) Thompson, B. C.; Fréchet, J. M. J. *Angewandte Chemie International Edition* **2008**, *47*, 58.

(71) Yu, G.; Gao, J.; Hummelen, J. C.; Wudl, F.; Heeger, A. J. *Science* **1995**, *270*, 1789.

(72) Qin, R.; Bo, Z. *Macromolecular Rapid Communications* **2012**, *33*, 87.

(73) Blouin, N.; Leclerc, M. *Accounts of Chemical Research* **2008**, *41*, 1110.

(74) Morin, J.-F.; Leclerc, M.; Adès, D.; Siove, A. *Macromolecular Rapid Communications* **2005**, *26*, 761.

(75) Blouin, N.; Leclerc, M. *Accounts of Chemical Research* **2008**, *41*, 1110.

(76) Boudreault, P.-L. T.; Beaupre, S.; Leclerc, M. *Polymer Chemistry* **2010**, *1*, 127.

(77) Li, J. L.; Dierschke, F.; Wu, J. S.; Grimsdale, A. C.; Mullen, K. *Journal of Materials Chemistry* **2006**, *16*, 96.

(78) Yi, H.; Johnson, R. G.; Iraqi, A.; Mohamad, D.; Royce, R.; Lidzey, D. G. *Macromolecular Rapid Communications* **2008**, *29*, 1804.

(79) Mario, L.; Jean , M. *Design and Synthesis of Conjugated Polymers*; Wiley: Weinheim, 2010.

(80) Beaupre, S.; Boudreault, P.-L. T.; Leclerc, M. *Advanced Materials* **2010**, *22*, E6.

(81) Kitazawa, D.; Watanabe, N.; Yamamoto, S.; Tsukamoto, J. *Applied Physics Letters* **2009**, *95*.

(82) Gevorgyan, S. A.; Krebs, F. C. **2009**.

(83) PASQUALE, O., bologna, 2012.

(84) Marsden, J. A.; Haley, M. M. In *Metal-Catalyzed Cross-Coupling Reactions*; Wiley: Germany, 2008.

(85) Glenis, S.; Horowitz, G.; Tourillon, G.; Garnier, F. *Thin Solid Films* **1984**, *111*, 93.

(86) Kallmann., H. P.; Pope., M. *J. Chem. Phys* **1959**, *30*.

(87) Almeataq, M. S.; Yi, H.; Al-Faifi, S.; Alghamdi, A. A. B.; Iraqi, A.; Scarratt, N. W.; Wang, T.; Lidzey, D. G. **2013**.

(88) Park, J.-H.; Chung, D. S.; Lee, D. H.; Kong, H.; Jung, I. H.; Park, M.-J.; Cho, N. S.; Park, C. E.; Shim, H.-K. *Chemical Communications* **2010**, *46*, 1863.

(89) Ding, P.; Chu, C.-C.; Zou, Y.; Xiao, D.; Pan, C.; Hsu, C.-S. *Journal of Applied Polymer Science* **2012**, *123*, 99.

(90) Zhou, E.; Yamakawa, S.; Zhang, Y.; Tajima, K.; Yang, C.; Hashimoto, K. *Journal of Materials Chemistry* **2009**, *19*, 7730.

(91) Zou, Y.; Gendron, D.; Badrou-Aïch, R. d.; Najari, A.; Tao, Y.; Leclerc, M. *Macromolecules* **2009**, *42*, 2891.

(92) Blouin, N.; Michaud, A.; Leclerc, M. *Adv. Mater. (Weinheim, Ger.)* **2007**, *19*, 2295.

(93) Qin, R.; Li, W.; Li, C.; Du, C.; Veit, C.; Schleiermacher, H.-F.; Andersson, M.; Bo, Z.; Liu, Z.; Inganäs, O.; Wuerfel, U.; Zhang, F. *Journal of the American Chemical Society* **2009**, *131*, 14612.

(94) Du, C.; Li, W.; Duan, Y.; Li, C.; Dong, H.; Zhu, J.; Hu, W.; Bo, Z. *Polymer Chemistry* **2013**, *4*, 2773.

(95) Yi, H.; Al-Faifi, S.; Iraqi, A.; Watters, D. C.; Kingsley, J.; Lidzey, D. G. *Journal of Materials Chemistry* **2011**, *21*, 13649.

(96) Liu, C.; Cai, W.; Guan, X.; Duan, C.; Xue, Q.; Ying, L.; Huang, F.; Cao, Y. *Polymer Chemistry* **2013**, *4*, 3949.

(97) de Cuendias, A.; Hiorns, R. C.; Cloutet, E.; Vignau, L.; Cramail, H. **2010**, - *59*.

(98) McNeill, C. R.; Halls, J. J. M.; Wilson, R.; Whiting, G. L.; Berkebile, S.; Ramsey, M. G.; Friend, R. H.; Greenham, N. C. **2008**, - *18*.

(99) Mori, D.; Benten, H.; Kosaka, J.; Ohkita, H.; Ito, S.; Miyake, K. *ACS Applied Materials & Interfaces* **2011**, *3*, 2924.

(100) Erjun, Z.; Junzi, C.; Qingshuo, W.; Keisuke, T.; Chunhe, Y.; Kazuhito, H. *Angewandte Chemie International Edition* **2011**, *50*, 2799.

(101) Zhang, F. L.; Mammo, W.; Andersson, L. M.; Admassie, S.; Andersson, M. R.; Inganas, L.; Ingands, O. *Advanced Materials* **2006**, *18*, 2169.

(102) Sessler, J. L.; Callaway, W. B.; Dudek, S. P.; Date, R. W.; Bruce, D. W. *Inorganic Chemistry* **2004**, *43*, 6650.

(103) Helgesen, M.; Gevorgyan, S. A.; Krebs, F. C.; Janssen, R. A. J. *Chem. Mater.* **2009**, *21*, 4669.

(104) Bouffard, J.; Swager, T. M. *Macromolecules (Washington, DC, U. S.)* **2008**, *41*, 5559.

(105) Feng, A.-H.; Chen, J.-Y.; Yang, L.-M.; Lee, G.-H.; Wang, Y.; Luh, T.-Y. *J. Org. Chem.* **2001**, *66*, 7922.

(106) Yamato, T.; Hideshima, C.; Suehiro, K.; Tashiro, M.; Prakash, G. K. S.; Olah, G. A. *J. Org. Chem.* **1991**, *56*, 6248.

(107) Sonntag, M.; Strohriegl, P. *Chem. Mater.* **2004**, *16*, 4736.

(108) Brunner, K.; van Dijken, A.; Borner, H.; Bastiaansen, J.; Kiggen, N. M. M.; Langeveld, B. M. W. *Journal of the American Chemical Society* **2004**, *126*, 6035.

(109) Urien, M.; Erothu, H.; Cloutet, E.; Hiorns, R. C.; Vignau, L.; Cramail, H. *Macromolecules* **2008**, *41*, 7033.

(110) Hammer, B. A. G.; Bokel, F. A.; Hayward, R. C.; Emrick, T. *Chemistry of Materials* **2011**, *23*, 4250.

(111) Li, J.-C.; Kim, S.-J.; Lee, S.-H.; Lee, Y.-S.; Zong, K.; Yu, S.-C. *Macromolecular Research* **2009**, *17*, 356.

(112) Antoun, T.; Iraqi, A.; Kergoat, L.; Miozzo, L.; Yassar, A. *Macromolecular Chemistry and Physics* **2011**, *212*, 1129.

(113) Liu, J. S.; McCullough, R. D. *Macromolecules* **2002**, *35*, 9882.

(114) Lohwasser, R. H.; Thelakkat, M. *Macromolecules* **2011**, *44*, 3388.

(115) Zhang, D. M.; Tessier, C. A.; Youngs, W. J. *Chem. Mater.* **1999**, *11*, 3050.

(116) Bui, T.-T.; Thiebaut, O.; Grelet, E.; Achard, M.-F.; Garreau-de Bonneval, B.; Ching, K. I. M.-C. *European Journal of Inorganic Chemistry* **2011**, 2663.

(117) Ding, P.; Chu, C.-C.; Liu, B.; Peng, B.; Zou, Y.; He, Y.; Zhou, K.; Hsu, C.-S. *Macromolecular Chemistry and Physics* **2010**, *211*, 2555.

(118) Santos , L. S.; Rosso , G. B.; Pilli, R. A.; Eberlin, M. N. *J. Org. Chem* **2007**, *72*.

(119) Xi, M.; Bent, B. E. *Journal of the American Chemical Society* **1993**, *115*, 7426.

(120) Sperotto, E.; van Klink, G. P. M.; van Koten, G.; de Vries, J. G. *Dalton Transactions* **2010**, *39*, 10338.

(121) Kun, H.; Yi, H.; Johnson, R.; Iraqi, A. *Polymers for Advanced Technologies* **2008**, *19*, 299.

(122) Brédas, J. L. *The Journal of Chemical Physics* **1985**, *82*, 3808.

(123) Suzuki, A. *Pure and Applied Chemistry* **1985**, *57*, 1749.

(124) Tamao, K.; Sumitani, K.; Kumada, M. *Journal of the American Chemical Society* **1972**, *94*, 4374.

(125) Babudri, F. C., D.; Farinola, G. M.; Naso, F *European Journal of Organic Chemistry* **2002**, .

(126) Chen; Yang, L.-M. *The Journal of Organic Chemistry* **2007**, *72*, 6324.

(127) (a) Krebs, F. C.; Nyberg, R. B.; Jørgensen, M. *Chemistry of Materials* **2004**, *16*, 1313(b) Nielsen, K. T.; Bechgaard, K.; Krebs, F. C. *Macromolecules* **2005**, *38*, 658.

(128) Alghamdi, A. A. B.; Watters, D. C.; Yi, H.; Al-Faifi, S.; Almeataq, M. S.; Coles, D.; Kingsley, J.; Lidzey, D. G.; Iraqi, A. *Journal of Materials Chemistry A* **2013**, *1*, 5165.

(129) Crouch, D. J.; Skabara, P. J.; Lohr, J. E.; McDouall, J. J. W.; Heeney, M.; McCulloch, I.; Sparrowe, D.; Shkunov, M.; Coles, S. J.; Horton, P. N.; Hursthouse, M. B. *Chemistry of Materials* **2005**, *17*, 6567.

(130) Ma, W. L.; Yang, C. Y.; Gong, X.; Lee, K.; Heeger, A. *J. Advanced Functional Materials* **2005**, *15*, 1617.

(131) Antoun, T.; Iraqi, A.; Kergoat, L.; Miozzo, L.; Yassar, A. *Macromolecular Chemistry and Physics* **2011**, *212*, 1136.

(132) Liu, J. S.; Loewe, R. S.; McCullough, R. D. *Macromolecules* **1999**, *32*, 5777.